National Library of Canada
Acquisitions and Bibliographic Services Branch
395 Wellington Street
Ottawa, Ontario
K1A 0N4

Bibliothèque nationale du Canada
Direction des acquisitions et des services bibliographiques
395, rue Wellington
Ottawa (Ontario)
K1A 0N4

Your file Votre référence

Our file Notre référence

NOTICE

The quality of this microform is heavily dependent upon the quality of the original thesis submitted for microfilming. Every effort has been made to ensure the highest quality of reproduction possible.

If pages are missing, contact the university which granted the degree.

Some pages may have indistinct print especially if the original pages were typed with a poor typewriter ribbon or if the university sent us an inferior photocopy.

Reproduction in full or in part of this microform is governed by the Canadian Copyright Act, R.S.C. 1970, c. C-30, and subsequent amendments.

AVIS

La qualité de cette microforme dépend grandement de la qualité de la thèse soumise au microfilmage. Nous avons tout fait pour assurer une qualité supérieure de reproduction.

S'il manque des pages, veuillez communiquer avec l'université qui a conféré le grade.

La qualité d'impression de certaines pages peut laisser à désirer, surtout si les pages originales ont été dactylographiées à l'aide d'un ruban usé ou si l'université nous a fait parvenir une photocopie de qualité inférieure.

La reproduction, même partielle, de cette microforme est soumise à la Loi canadienne sur le droit d'auteur, SRC 1970, c. C-30, et ses amendements subséquents.

Canada

UNIVERSITY OF ALBERTA

Chain Pillar Design in Longwall Mining for Bump-prone Seams

By

Yuan Pen

A THESIS

SUBMITTED TO THE FACULTY OF GRADUATE STUDIES AND RESEARCH
IN PARTIAL FULFILLMENT OF THE REQUIREMENTS FOR THE DEGREE OF

Doctor of Philosophy

IN

Mining Engineering

Department of Mining, Metallurgical and Petroleum Engineering

EDMONTON, ALBERTA

FALL, 1994

National Library of Canada
Acquisitions and Bibliographic Services Branch
395 Wellington Street
Ottawa, Ontario
K1A 0N4

Bibliothèque nationale du Canada
Direction des acquisitions et des services bibliographiques
395, rue Wellington
Ottawa (Ontario)
K1A 0N4

Your file Votre référence

Our file Notre référence

The author has granted an irrevocable non-exclusive licence allowing the National Library of Canada to reproduce, loan, distribute or sell copies of his/her thesis by any means and in any form or format, making this thesis available to interested persons.

L'auteur a accordé une licence irrévocable et non exclusive permettant à la Bibliothèque nationale du Canada de reproduire, prêter, distribuer ou vendre des copies de sa thèse de quelque manière et sous quelque forme que ce soit pour mettre des exemplaires de cette thèse à la disposition des personnes intéressées.

The author retains ownership of the copyright in his/her thesis. Neither the thesis nor substantial extracts from it may be printed or otherwise reproduced without his/her permission.

L'auteur conserve la propriété du droit d'auteur qui protège sa thèse. Ni la thèse ni des extraits substantiels de celle-ci ne doivent être imprimés ou autrement reproduits sans son autorisation.

ISBN 0-315-95246-6

Canada

UNIVERSITY OF ALBERTA

RELEASE FORM

NAME OF AUTHOR: Yuan Pen

TITLE OF THESIS: Chain Pillar Design in Longwall Mining for Bump-prone Seams

DEGREE FOR WHICH THESIS WAS SUBMITTED: Doctor of Philosophy

YEAR THIS DEGREE GRANTED: 1994

Permission is hereby granted to the UNIVERSITY OF ALBERTA LIBRARY to reproduce single copies of this thesis and to lend or sell such copies for private, scholarly or scientific research purposes only.

The author reserves all other publication right and other rights with the copyright in the thesis, and except as hereinbefore provided neither the thesis nor any substantial portion thereof may be printed or otherwise reproduced in any material form without the author's written permission.

(SIGNED) 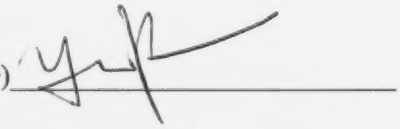

PERMANENT ADDRESS:

c/o Dept. of Mining, Metallurgical and Petroleum Eng.
University of Alberta
Edmonton, Alberta
Canada T6G 2G6

Date May 26, 1994

UNIVERSITY OF ALBERTA

FACULTY OF GRADUATE STUDIES AND RESEARCH

The undersigned certify that they have read, and recommend to the Faculty of Graduate Studies and Research, for acceptance, a thesis entitled:

Chain Pillar Design in Longwall Mining for Bump-prone Seams

by Yuan Pen in partial fulfillment of the requirements for the degree of Doctor of Philosophy in Mining Engineering

Professor Jerry M. Whiting

Professor Ken Barron

Professor Loverne R. Plitt

Associate Professor David Chan

Assistant Professor W. Simon Tortike

Professor M. D. G. Salamon

Date May 13, 1994

Dedicated to

Jia and Mum for their love and inspiration.

ABSTRACT

Pillar bumps have long been hazards in room and pillar mines around the world. With mines going deeper, pillar bumps also pose a threat to the personnel and equipment in longwall mining. One of the pillar bump mechanisms states that two parameters control the occurrence of pillar bumps; these are the post-failure pillar stiffness and the local mine stiffness (LMS). The magnitudes of the two parameters control whether there is violent or controlled failure. Although the mechanism was proposed in the late 1960s, the application of the mechanism to general mining practice is still far away. One of the reasons for this is that it is difficult to determine LMS in complex mining configurations with non-linear material properties.

In an effort to solve this problem, LMS for a specific pillar was defined and a non-linear three dimensional boundary element program based on the displacement discontinuity theory was modified, by the integration of Starfield's "perturbation method", to calculate LMS. The change of LMS with the advance of the longwall face, the various chain pillar configurations, varied coal behavior, and the different surrounding rock properties were investigated by a parametric numerical analysis. To estimate the post-failure stiffness, the post-failure stiffness data from laboratory and field were collected and studied, from which an upper boundary estimation of the post-failure stiffness was derived.

Based on the results of the numerical analysis on LMS and the post-failure stiffness study, a design methodology for longwall chain pillars under the bump-prone conditions was proposed. The application of the methodology was demonstrated by a case history back analysis, which included an interpretation of the field data, a numerical simulation of the field case, and a stability evaluation based on the proposed LMS concept.

The results obtained from the parametric studies and case history simulation showed that the modified program worked well, and LMS of specific locations can be monitored throughout the mining simulation. The calculated change of LMS combined with the post-failure stiffness estimation can give an indication of when, where and whether there will be violent pillar bumps during the panel recovery. The chain pillar design can be evaluated and modified accordingly. Eventually, this will improve the safety and lead to a more reasonable design for longwall mining.

ACKNOWLEDGMENTS

The author expresses his sincere gratitude and appreciation for the keen interest, guidance, encouragement and support shown by his supervisor, Dr. K. Barron. Dr. Barron inspired the author's interest and led the author into the field of pillar design and stability evaluation. He strongly supported the work by ensuring the funding and many other resources, and making available his extraordinarily broad and diverse experience whenever necessary.

The author owes a special debt to Kunming Institute of Technology and the Provincial Government of Yunnan, The People's Republic of China, for providing the author the opportunity and partial funding to persue a P.h D. in Canada.

Special thanks to the staff in the geotechnical group of Pittsburgh Research Center, U.S.B.M, especially the group leader, Anthony T. Iannacchione, engineers, Dr. Christopher Mark, Keith Heasley, and Alan A. Campoli, who provided the valuable field data, the original version of the MULSIM/NL computer program and necessary information.

The author expresses his grateful appreciation to the kindness and assistance from Dr. R.K. Zipf, Jr., Denver Research Center, U.S.B.M., who made the latest version of MULSIM/NL available and provided insights and advice about the program and its modification.

The author is also grateful to the technicians and colleagues in the Department of Mining, Metallurgical & Petroleum Engineering, in particular, Doug Both for providing assistance to the author in general and specific computer and graphic configurations; Xiaoqin Chen, Dr. Samuel Frimpong, Yongzhen Xie, Dr. Yunjian Wu, and Suishen Wang, for their discussion, encouragement and great companionship.

The support of the secretarial staff at the Department of Mining, Metallurgical & Petroleum Engineering, especially Mesdames Erika Auton and Key Whiting is highly appreciated.

Above all, the author is deeply in debt to his wife Yan, his son, Jia and his mother, Chaolan, for their unfailing support, sacrifice and tolerance.

TABLE OF CONTENTS

Chapter page

Chapter 1: INTRODUCTION 1

1.1 Problem definition 1

1.1.1 Longwall mining 1

1.1.2 Pillar bumps in longwall mining 3

1.1.2.1 Pillar bump definition 4

1.1.2.2 Factors contributing to pillar bumps 5

1.1.3 Chain pillar design 5

1.1.4 Summary 6

1.2 Objectives of research 7

1.2.1 Research methodology 8

1.2.2 Scope and limits of the research 8

Chapter 2: PILLAR DESIGN 9

2.1 Geological factors 10

2.2 Pillar strength 10

2.2.1 Coal mass uniaxial compressive strength 10

2.2.2 Pillar strength formulas 11

2.2.3 Analytical methods 13

2.3 Loads applied to longwall pillars 15

2.3.1 Development loads 16

2.3.1.1 Tributary area theory 16

2.3.1.2 Deflection theory 16

2.3.1.3 Numerical solutions 17

2.3.1.4 Summary and conclusions 17

2.3.2 Abutment loads 17

2.4 Chain pillar design 19

2.4.1 Calculation of abutment loads 19

2.4.1.1 Analytical approaches 20

2.4.1.2 Numerical methods 22

2.4.2 Summary and conclusions 24

2.5 Yield pillar design 24

Chapter 3: PILLAR STABILITY 26

3.1 Pillar behavior 26

3.1.1 Stability theory 28

3.1.2 Evaluation of pillar bumps 31

3.1.2.1 Definition of stiffness 31

3.1.2.2 Determination of local mine stiffness 36

3.1.2.3 Determination of post-failure pillar stiffness 38

3.2 Conclusions 41

Chapter 4: PRELIMINARY STUDIES 42

4.1 Introduction 42

4.2 Introduction to MULSIM/NL 43

4.3 Assumptions and limitations of MULSIM/NL 48

4.3.1 Elastic strata 48

4.3.2 Effect of confinement 48

4.4 Structure of MULSIM/NL and its modification 48

4.4.1 Zipf's modification 49

4.4.2 Definition of the local mine stiffness 49

4.4.3 Implementation of local mine stiffness calculation 52

4.5 Verification of the program 53

4.6 Conclusion 57

Chapter 5: EXAMINATION OF LOCAL MINE STIFFNESS 58

5.1 Introduction 58

5.2 Elastic model 58

5.3 Non-elastic models 61

5.3.1 Effect of pillar location 62

5.3.2 Effect of the modulus ratio of strata to coal 67

5.3.3 Effect of the strain softening of coal 68

5.3.4 Summary 79

5.3.5 Comparison of different chain pillar configurations 70

5.4 Pillar post-failure stiffness determination 73

5.5 Conclusions 75

5.6 Pillar design methodology 76

Chapter 6: FIELD STUDY 78

6.1 Introduction 78

6.2 Geology of the VP No. 3 mine 78

6.3 Site monitoring program 80

6.4 Interpretation of the field data 84

6.4.1 Vertical stress change 84

6.4.2 Vertical closure 91

6.4.3 Pillar dilation 95

6.4.4 Horizontal stress change 99

6.5 Summary of the analysis 101

Chapter 7: FIELD SIMULATION 103

7.1 Fitting criteria 103

7.2 Model setup 104

7.2.1 Mine model mesh 104

7.2.2 Model fitting and modification 106

7.3 Comparison of the model with the observed results 110

7.3.1 Development 7 110

7.3.2 Development 8 114

7.3.3 Summary 117

7.4 Local mine stiffness analysis 117

7.4.1 Development 7 118

7.4.2 Development 8 120

7.4.3 Comparison of the two developments 122

7.5 Conclusions 122

Chapter 8: SUMMARY, CONCLUSIONS AND RECOMMENDATIONS FOR FURTHER RESEARCH 124

8.1 Summary and conclusions 124

8.2 Recommendations for further research 127

REFERENCES 129

Appendix A: CONCEPT OF DISPLACEMENT DISCONTINUITY THEORY 136

A.1 Assumptions 136

A.2 Definitions 136

A.3 Boundary conditions 137

A.4 Mathematical solution 138

A.5 Discretizing the seam 139

A.6 Application of boundary conditions 142

Appendix B: PROGRAM INPUT PARAMETERS AND OUTPUT FOR THE MODELS 143

B.1 Test elastic model 143

B.2 Model with four entries and three rows of equal size of pillars 151

B.3 Model with AYY pillar configuration 159

B.4 Development 7 model 164

B.5 Development 8 model 172

Appendix C: CHANGES OF AVERAGE VERTICAL PILLAR STRESS, STRAIN AND LOCAL MINE STIFFNESS WITH THE MINING STEPS 180

Appendix D: STRESS AND CLOSURE DISTRIBUTIONS FOR SELECTED MODELS 197

Appendix E: POST-FAILURE STIFFNESS COMPILATIONS 214

E.1 Das's data (1986) 214

E.2 Seedsman's data (1991) 214

E.3 Heerden's data (1975) 216

E.4 Cook's data (1971) 216

E.5 Wagner's data (1974) 217

E.6 Wang's data (1976) 217

E.7 Pittsburgh Research Center (Iannacchione, 1988) 217

E.8 Crouch's data (1973) 218

Appendix F: THREE DIMENSIONAL PRESENTATION OF THE VERTICAL STRESS AND CLOSURE DISTRIBUTIONS FOR DEVELOPMENT 7 AND DEVELOPMENT 8 MODELS AT SELECTED MINING STEPS 219

LIST OF TABLES

Table Page

Table 2.1 Empirical pillar strength equations. 12

Table 4.1 The structure of material array EPROP (after Zipf, 1992). 47

Table 4.2 Influence coefficient matrix c_{ij} obtained by Salamon (1970). 54

Table 4.3 Influence coefficient matrix c_{ij} obtained by author. 54

Table 4.4 Material parameters array EPROP for Salamon's example. 56

Table 5.1 Material parameters array EPROP for elastic model. 60

Table 5.2 Material parameters array EPROP for strain softening coal. 62

Table 6.1 Physical properties of the roof, coal and floor of study areas (specimen testing). 80

Table 7.1 The material parameters array EPROP of the modified model. 109

LIST OF FIGURES

Figure Page

Figure 1.1 Typical longwall mining layout (after Peng, 1986).....2

Figure 1.2 Typical retreating longwall section (after Peng, 1986). 3

Figure 1.3 Abutment pressures around a longwall panel (after Peng 1986).....4

Figure 2.1 Pillar design flow chart.....9

Figure 2.2 Comparison of the pillar strength formulas (after Peng, 1986).....12

Figure 2.3 Four stages of longwall mining advance (afer Mark 1987).....18

Figure 2.4 Typical loading curve of a pillar in longwall panel.....19

Figure 2.5 Stress distribution and load deficiency in the gob (after Wilson, 1972) 20

Figure 3.1 Typical uniaxial compressive testing curve for rocks. 27

Figure 3.2 Conventional compression test in laboratory with a stiffer testing machine ...27

Figure 3.3 Schematic representation of pillar loading in the field and loading a rock specimen in a conventional test machine.....30

Figure 3.4 Condition for stability in case of two pillars (after Salamon, 1970). 34

Figure 3.5 Field and laboratory data of the pillar post-failure stiffness.....40

Figure 4.1 Boundary elements of seam plane in surrounding rock mass.....44

Figure 4.2 Material models available in MULSIM/NL program (after Zipf, 1992).....46

Figure 4.3 Structure of MULSIM/NL and Zipf's addition of local mine stiffness calculation at a selected point (after Zipf, 1992).....50

Figure 4.4 The flow chart of the modified MULSIM/NL for LMS calculation of a pillar.51

Figure 4.5 Salamon's infinitely long strip pillars case (1970) 53

Figure 4.6 Model for Salamon's example case with fine mesh element 5×5 m and coarse mesh block 25×25 m.(d = 20 m, L = 115 m, D = 125, 250, 375, 500, 625, and 750 m). 55

Figure 4.7 Comparison of the modified MULSIM/NL's results with analytical solutions.57

Figure 5.1 Testing elastic longwall panel layout and mining sequence.....58

Figure 5.2 Linear relation of the perturbation displacement magnitude and resulting stress.....59

Figure 5.3 Local mine stiffness change with the advance of longwall face. 60

Figure 5.4 Non-elastic model with equal size of chain pillars.....61

Figure 5.5 Changes of stress, strain and local mine stiffness with the face advance within pillar columns.....63

Figure 5.6 Changes of stress, strain and local mine stiffness with the face advance cross pillar rows. 65

Figure 5.7 Change of local mine stiffness with overburden (pillar rc position). 66

Figure 5.8 Relation between local mine stiffness and rock/coal modulus ratio. 67

Figure 5.9 Three different strain softening models.....68

Figure 5.10 Effect of the softening behavior of coal on the local mine stiffness. 69

Figure 5.11 Fine meshes of the three chain pillar configurations.....71

Figure 5.12 Local mine stiffness change for three pillar configurations. 72

Figure 5.13 Upper boundary fitting of the field and laboratory data of the pillar post-failure stiffness.....74

Figure 6.1 Mine map of No. 3 mine 79

Figure 6.2 Generalized stratigraphic column for study area. 80

Figure 6.3 Plan of development 7 and instrument array. 82

Figure 6.4 Plan of development 8 and instrument array. 82

Figure 6.5 Correlation of the absolute longwall face position to time 83

Figure 6.6 Vertical stress change of the abutment pillar (development 7, A-A line). 85

Figure 6.7 Vertical stress change of the cross section A-A of development 7. 86

Figure 6.8 Vertical stress change of the abutment pillar (development 8, A-A line). 89

Figure 6.9 Vertical stress change of the cross section A-A of development 8. 90

Figure 6.10 Closure in entries at development 7. 92

Figure 6.11 Closure in entries at development 8. 93

Figure 6.12 Lateral deformation of the abutment pillar (development 7, A-A line). 96

Figure 6.13 Lateral deformation of the abutment pillar (development 8, A-A line). 97

Figure 6.14 Horizontal stress change into the tailgate side of the abutment pillars. 100

Figure 7.1 Coarse and fine mesh of the model for development 7. 105

Figure 7.2 Coarse and fine mesh of the model for development 8. 105

Figure 7.3 Plane view of the fine mesh for a square pillar with different strength properties based on the location of the element to a free surface. 107

Figure 7.4 The comparison of the modified model with Heasley's model. 108

Figure 7.5 3D vertical stress and closure for development 7 model at mining step 3. 112

Figure 7.6 Cross section view of vertical stress at line A-A of the development 7 model. 113

Figure 7.7 Closure of entries at cross section A-A of the development 7 model. 113

Figure 7.8 3D vertical stress and closure for development 8 model at mining step 9. 115

Figure 7.9 Cross section view of vertical stress at line A-A of the development 8 model. 116

Figure 7.10 Closure of entries at cross section A-A of the development 8 model. 116

Figure 7.11 Simulation result for development 7 model. 118

Figure 7.12 Simulation result of development 8 model.....121

Figure C.1.1 Pillar stress, strain and local mine stiffness change with mining step number, model with three rows of equal size pillars, 500 ft overburden. Strata modulus E = 145000 psi, seam modulus Es = 290000 psi, E/Es = 0.5. (Brittle).....181

Figure C.1.2 Pillar stress, strain and local mine stiffness change with mining step number, model with three rows of equal size pillars, 500 ft overburden. Strata modulus E = 145000 psi, seam modulus Es = 290000 psi, E/Es = 0.5. (Brittle).....182

Figure C.1.3 Pillar stress, strain and local mine stiffness change with mining step number, model with three rows of equal size pillars, 500 ft overburden. Strata modulus E = 145000 psi, seam modulus Es = 290000 psi, E/Es = 0.5. (Brittle).....183

Figure C.2.1 Pillar stress, strain and local mine stiffness change with mining step number, model with three rows of equal size pillars, 750 ft overburden. Strata modulus E = 145000 psi, seam modulus Es = 290000 psi, E/Es = 0.5. (Brittle).....184

Figure C.2.2 Pillar stress, strain and local mine stiffness change with mining step number, model with three rows of equal size pillars, 750 ft overburden. Strata modulus E = 145000 psi, seam modulus Es = 290000 psi, E/Es = 0.5. (Brittle).....185

Figure C.2.3 Pillar stress, strain and local mine stiffness change with mining step number, model with three rows of equal size pillars, 750 ft overburden. Strata modulus E = 145000 psi, seam modulus Es = 290000 psi, E/Es = 0.5. (Brittle).....186

Figure C.3.1 Pillar stress, strain and local mine stiffness change with mining step number, model with three rows of equal size pillars, 1000 ft overburden. Strata modulus E = 145000 psi, seam modulus Es = 290000 psi, E/Es = 0.5. (Brittle).....187

Figure C.3.2 Pillar stress, strain and local mine stiffness change with mining step number, model with three rows of equal size pillars, 1000 ft overburden. Strata modulus E = 145000 psi, seam modulus Es = 290000 psi, E/Es = 0.5. (Brittle).....188

Figure C.3.3 Pillar stress, strain and local mine stiffness change with mining step number, model with three rows of equal size pillars, 1000 ft overburden. Strata modulus E = 45000 psi, seam modulus Es = 290000 psi, E/Es = 0.5. (Brittle).....189

Figure C.4 Pillar stress, strain and local mine stiffness change with mining step number, model with three rows of equal size pillars, 750 ft overburden. Strata modulus E = 725000 psi, seam modulus Es = 290000 psi, E/Es = 2.5 . (Brittle).....190

Figure C.5 Pillar stress, strain and local mine stiffness change with mining step number, model with three rows of equal size pillars, 1000 ft overburden. Strata modulus E = 725000 psi, seam modulus Es = 290000 psi, E/Es = 2.5. (Brittle).....191

Figure C.6 Pillar stress, strain and local mine stiffness change with mining step number, model with three rows of equal size pillars, 750 ft overburden. Strata modulus E = 290000 psi, seam modulus Es = 290000 psi, E/Es = 1.(Brittle).....192

Figure C.7 Pillar stress, strain and local mine stiffness change with mining step number, model with three rows of equal size pillars, 750 ft overburden. Strata modulus E = 145000 psi, seam modulus Es = 290000 psi. (More brittle). 193

Figure C.8 Pillar stress, strain and local mine stiffness change with mining step number, model with three rows of equal size pillars, 1000 ft overburden. Strata modulus E = 145000 psi, seam modulus Es = 290000 psi. (More brittle). 194

Figure C.9 Pillar stress, strain and local mine stiffness change with mining step number, model with three rows of equal size pillars, 750 ft overburden. Strata modulus E = 145000 psi, seam modulus Es = 290000 psi. (Soft).....195

Figure C.10 Pillar stress, strain and local mine stiffness change with mining step number, model with three rows of equal size pillars, 1000 ft overburden. Strata modulus E = 145000 psi, seam modulus Es = 290000 psi. (Soft).....196

Figure D.1 Vertical stress in the fine mesh zone through the selected mining steps for the two entries elastic model (500 ft overburden). 198

Figure D.2 Vertical closure in the fine mesh zone through the selected mining steps for the two entries elastic model (500 ft overburden).....199

Figure D.3 Vertical stress in the fine mesh zone through the selected mining steps for the four entries with three rows of equal size pillars model (500 ft overburden, strain softening seam, brittle).....200

Figure D.4 Vertical closure in the fine mesh zone through the selected mining steps for the four entries with three rows of equal size pillars model (500 ft overburden, strain softening seam, brittle).....201

Figure D.5 Vertical stress in the fine mesh zone through the selected mining steps for the four entries with three rows of equal size pillars model (750 ft overburden, strain softening seam, brittle).....202

Figure D.6 Vertical closure in the fine mesh zone through the selected mining steps for the four entries with three rows of equal size pillars model (750 ft overburden, strain softening seam, brittle).....203

Figure D.7 Vertical stress in the fine mesh zone through the selected mining steps for the four entries with three rows of equal size pillars model (1000 ft overburden, strain softening seam, brittle).....204

Figure D.8 Vertical closure in the fine mesh zone through the selected mining steps for the four entries with three rows of equal size pillars model (1000 ft overburden, strain softening seam, brittle).....205

Figure D.9 Vertical stress in the fine mesh zone through the selected mining steps for the four entries with central abutment pillar (YAY) model (750 ft overburden, strain softening seam, brittle).....206

Figure D.10 Vertical closure in the fine mesh zone through the selected mining steps for the four entries with central abutment pillar (YAY) model (750 ft overburden, strain softening seam, brittle).....207

Figure D.11 Vertical stress in the fine mesh zone through the selected mining steps for the four entries with central abutment pillar (YAY) model (1000 ft overburden, strain softening seam, brittle).....208

Figure D.12 Vertical closure in the fine mesh zone through the selected mining steps for the four entries with central abutment pillar (YAY) model (1000 ft overburden, strain softening seam, brittle).....209

Figure D.13 Vertical stress in the fine mesh zone through the selected mining steps for development 7 model (strain softening seam, 1900 ft overburden).....210

Figure D.14 Vertical closure in the fine mesh zone through the selected mining steps for development 7 model (strain softening seam, 1900 ft overburden).....211

Figure D.15 Vertical stress in the fine mesh zone through the selected mining steps for development 8 model (strain softening seam, 2000 ft overburden).....212

Figure D.16 Vertical closure in the fine mesh zone through the selected mining steps for development 8 model (strain softening seam, 2000 ft overburden).....213

Figure F.1 Vertical stress and closure at mining step 2 for development 7.....220

Figure F.2 Vertical stress and closure at mining step 3 for development 7.....221

Figure F.3 Vertical stress and closure at mining step 4 for development 7.....222

Figure F.4 Vertical stress and closure at mining step 5 for development 7.....223

Figure F.5 Vertical stress and closure at mining step 6 for development 7.....224

Figure F.6 Vertical stress and closure at mining step 9 for development 7.....225

Figure F.7 Vertical stress and closure at mining step 13 for development 7.....226

Figure F.8 Vertical stress and closure at mining step 1 for development 8.....227

Figure F.9 Vertical stress and closure at mining step 3 for development 8.....228

Figure F.10 Vertical stress and closure at mining step 5 for development 8.....229

Figure F.11 Vertical stress and closure at mining step 6 for development 8.....230

Figure F.12 Vertical stress and closure at mining step 9 for development 8.....231

Figure F.13 Vertical stress and closure at mining step 11 for development 8.....232

Figure F.14 Vertical stress and closure at mining step 12 for development 8.....233

Figure F.15 Vertical stress and closure at mining step 13 for development 8.....234

NOMENCLATURE

A, B	pillar formula constants
a, b, c, d, e	influence functions
A_{ii}	co-factor of the element $k_i+\lambda_i$ in the determinant det(K + Λ)
C	central pillar position in a pillar column
c_{ij}	influence coefficients, they are the elements of the influence matrix
D	cubic coal block side dimension, down pillar position in a pillar column, panel length
d	width of a room and a pillar
det	determinant
$det(K+\Lambda)_i$	determinant of [K + Λ] when λ_i is assigned to be zero
E	Young's modulus for strata
E_c	Young's modulus for coal
E_f	final modulus, Young's modulus for floor
E_h	hardening modulus
E_i	initial modulus, Young's modulus for immediate roof
E_m	Young's modulus for main roof
E_p	plastic modulus, post-failure stiffness for pillar
E_s	Young's modulus for seam
E_t	tangent modulus
F	front abutment factor

G	shear modulus for strata
G_s	shear modulus for seam
h	cubic coal block side dimension, seam depth
H	pillar height, seam depth
k	stiffness of the spring, triaxial stress factor, Gaddy factor, stiffness of spring
k_i	local mine stiffness relative to the location of pillar i
L	panel length, panel width
L_d	development load
L_f	first front abutment load
L_{ff}	second front abutment load
L_p	pillar length
L_s	first side abutment load
L_{ss}	second side abutment load
n	gob height factor
p_i	pillar force acting on a geometrically similar but weightless and unstressed rock mass
P_r	loads on the specimen
P_s	loads on the spring
q	original hydrostatic stress
S	displacements at the one end of the spring, pillar cross section area
S_c	convergence vector at the i-th pillar location induced by the pillar forces $p_1, p_2, ..., p_i, ..., p_n$

s_{ci}	convergence caused by pillar force p_i
S_x, S_y, S_z	relative displacements (closure and rides)
t	thickness of seam
u, v, w	displacements
U	upper pillar position in a pillar column
W	panel width, virtual work
W	pillar width
w_c	crosscut width
w_e	entry width
W_p	pillar width
W_r	work done by the specimen
W_s	work done by the spring
x	distance from pillar rib to the location in the pillar
γ	displacements at the one end of the spring, unit weight
μ	Poisson's ratio
λ	post-failure stiffness for rock specimen
β	shear angle
σ	stress level
$f'(s)$	post-failure stiffness of rock specimen
$f(s)$	deformation curve for rock specimen
ε_0	offset strain
σ_0	offset stress

σ_1 , σ_3	maximum and minimum principle stresses
σ_I	mass strength of a cubic coal block
Δc	uniform perturbation closure (or displacement)
λ_c	critical stiffness which is the smallest eigenvalue of strata stiffness matrix [K]
σ_c	uniaxial compressive strength
σ_c	uniaxial compressive strength of coal mass
γ_i	convergence element
λ_i	post-failure stiffness for pillar i
$f_i'(s_i)$	post-failure stiffness of the pillars
$f_i(s_i)$	deformation curve of pillar i
λ_{ii}	post-failure stiffness of the pillars
λ_m	is the minimum slope of the force-convergence curves of the pillars
ε_p	peak strain
σ_p	peak stress
σ_p	pillar strength
Δp_i	resultant load changes in element i
ΔP_i	load increments
ΔP_r	force change in rock
ΔP_s	force change in spring
ε_r	residual strain
σ_r	residual stress

ΔS	displacement increment
ΔS_i	accompanying displacements
σ_v	final stress
σ_x, τ_x, τ_y	stresses on a plane
$[\Lambda]$	pillar stiffness matrix which is an n×n diagonal matrix
[C]	influence matrix which is a n×n matrix
[K]	strata stiffness matrix which is the inverse of [C]
$\{\Gamma\}$	convergence vector caused by the excavation in the stressed rock mass without supporting pillars
{P}	pillar force vector
{S}	total convergence vector
$\{S_c\}$	convergence vector caused by pillar force vector

SUBSCRIPTS

+	upper seam plane
-	lower seam plane
c	central pillar position in a pillar row
d	down pillar position in a pillar column, development
e	part of the convergence caused by pillar forces on a geometrically similar but weightless and unstressed rock mass
f	first front abutment
ff	second front abutment
i j	pillar identification numbers

l	left pillar position in a pillar row
m	middle pillar position in a pillar column
r	right pillar position in a pillar row
s	first side abutment
ss	second side abutment
u	upper pillar position in a pillar column

SUPERSCRIPTS

t	transposition
-1	inverse
α, β	pillar formula constants

ABBREVIATIONS

2D, 3D	two and three dimensions
ALPS	analysis of longwall pillar stability
AYY	headgate abutment-yield-yield chain pillar configuration
EPROP	material property array used in MULSIM/NL
LMS	local mine stiffness
MULSIM/NL	a non-linear three dimension displacement discontinuity boundary element program developed by US Bureau of Mines
YAY	yield-abutment-yield chain pillar configuration
YYA	yield-yield-tailgate abutment chain pillar configuration

SYMBOLS

<···>	row vector
{×}	column vector
[···]	matrix

Chapter 1

INTRODUCTION

1.1 Problem definition

The introduction of longwall mining into the coal mines in North America since the 1960's has greatly increased the amount of coal production, while at the same time the pillar bump problems which were very common in some coal fields with the conventional room-and-pillar mining method have been relieved to a great extent (Mark, 1989). The advantage of the high production and improved safety standard for the longwall mining method has been attracting more and more attention from mines around the world, especially in the USA.

However, studies indicated that there still are pillar stability problems even with longwall mining (Campoli, 1987 and 1989). This is because the available longwall design methods were basically based on the traditional ultimate strength design concept, and the stability of the chain pillars in the post-failure period were not addressed in these methods. Clearly, these kinds of design approaches are not satisfactory when the bump-prone coal beds are encountered. Therefore, unless the consideration of the post-failure behavior of the chain pillars is included in the pillar design process, the dangers of unexpected accidents, such as pillars violently bursting into the entries, still pose a threat to the safety of the personnel and equipment close to the entries.

1.1.1 Longwall mining

Longwall mining is used in relatively flat lying, thin tabular seams. In this method a long face is established across a panel between sets of entries, and the face is retreated or advanced by narrow cuts along the face which is protected by mechanical powered supports. The roof behind the face is allowed to cave into the extracted area known as the gob. Figure 1.1 shows a sketch of a typical longwall mining panels.

Usually a series of longwall panels are developed in parallel and are mined in succession. The panels are separated by chain pillars to protect the entries on either side of each panel, as illustrated in figure 1.2.

The entries on one side of the panel are used for fresh air intake, and the transportation of men, supplies and mined coal out or into the face; these entries are called head entries. The entries on the other side of the panel are used as the return air path and are called tail entries.

Head and tail entries are the life line for longwall mining. They have to be kept open for transportation and ventilation purposes until the face passes. Therefore, the successful operation of longwall and face advance depends on the status of the entries. The entries are protected by the chain pillars. The ground control problems for entries, such as roof fall, floor heave, and excessive closure are all related to the integrity of the chain pillars. Consequently, the behavior of the entries is mainly controlled by the stability of the chain pillars.

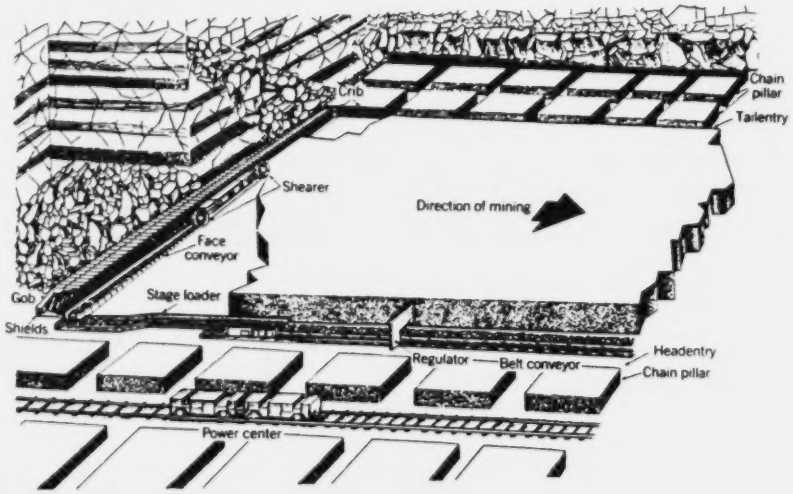

Figure 1.1

Typical longwall mining layout (after Peng, 1986).

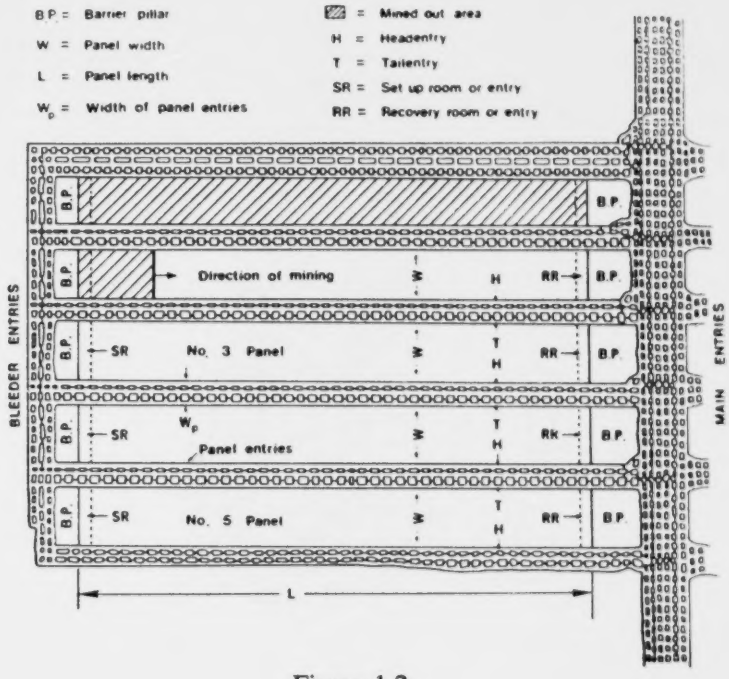

Figure 1.2

Typical retreating longwall section (after Peng, 1986).

1.1.2 Pillar bumps in longwall mining

Figure 1.3 illustrates the stress redistribution around the panel caused by longwall mining. Analysis shows (Hsiung, 1984) that during advance of the longwall face, stress builds up on the coal at the face and at the two sides of the panel. The stress build-ups can be 1 to 6 times more than the overburden pressure. The increased pressure zones at the face and in the side coal are called the front abutment pressure and side abutment pressure respectively. The peaks of the abutment pressure migrate into the coal when the exterior coal yields or fractures.

The side abutment pressure is supported by the chain pillars along the panel sides. The chain pillars at the T-junction of tail entry and the face are especially vulnerable to the complex and severe abutment pressure because of superposition of the front abutment pressure and the side abutment pressure. For the bump-prone coal beds, which are identified as the coal beds with strong and brittle coal, overburden greater than 500 ft, and

strong roof and floor (Peng, 1986 and Iannacchione, 1990), very often the chain pillars at or near the T-junction burst violently into the entry; this may involve several cubic feet to hundreds of cubic feet of coal. This violent pillar failure is called pillar bump.

Pillar bumps are very serious hazards in longwall mining, because they are violent and usually unpredictable. Bumps occurring in the longwall mining have injured personnel, damaged equipment and delayed the longwall operation. Pillar bumps often occur in the tail entries, this may lead to the collapse of the entry roof and eventually close the entries. Sometimes the risk of pillar bumps is so serious that the whole mining section has to be abandoned.

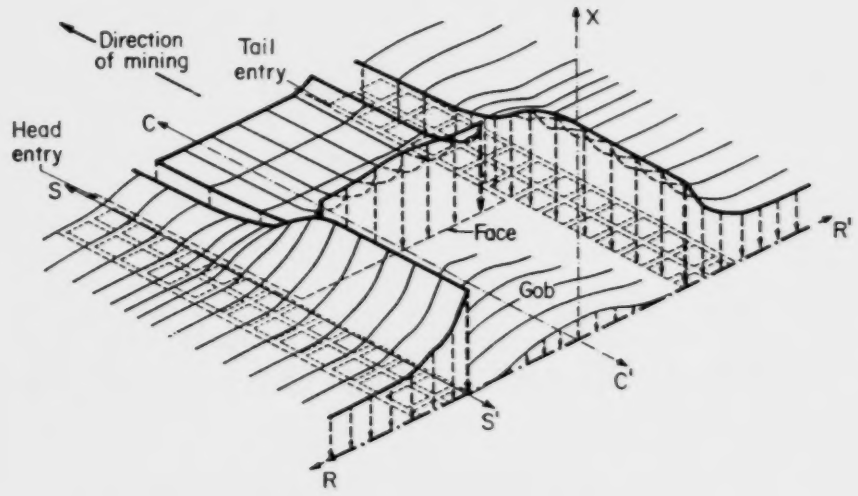

Abutment pressures around a longwall panel (after Peng, 1986)

1.1.2.1 Pillar bump definition

A pillar bump is defined as an instantaneous release of high stressed pillar rib material which is propelled into a mine opening (Haramy, 1988). Pillar bumps have transient and violent features, but usually there is no gas involved in a pillar bump. When a pillar bursts, its load-bearing capacity is totally or partially lost and the load is immediately transferred to the adjacent pillars. This may lead to the bumping of the adjacent pillar and to the so-called "Domino bump failure" in which the collapse of the whole mining section occurs.

The noticeable feature of a pillar bump from a pillar yielding is the visible loss of contact between the pillar and the roof after the bump. It was repeatedly reported that, after a pillar bump, there were gaps formed between the pillar top and the roof, showing that the contact between pillar and roof was partially or totally lost (Campoli, 1987 and 1990). This is the clear evidence that a part of the pillar has been ejected out from the pillar when a pillar bump occurs.

1.1.2.2 Factors contributing to pillar bumps

A pillar bump is believed to occur when the maximum designed load is surpassed and the stiffness of the surrounding strata (or local mine stiffness) is less than the post-failure stiffness of the pillar. The term "local mine stiffness" is the ratio between the force change on the pillar and the roof/floor convergence at that pillar location; this is further defined and mathematically expressed in section 3.1.2.1, page 31. The following factors also contribute to pillar bumps:

(1) Overburden is directly linked to pillar bumps. The pillar bumps occur when the overburden is beyond 500 ft. The severity and frequency of pillar bumps increases with the depth of mining. The majority of coal mine bumps in US. occur in mining operations with over 2000 ft overburden (Haramy, 1988).

(2) Geological characteristics of coal beds and surrounding rocks contribute to pillar bumps. It was reported that bumps usually occur in the coal beds with stiff roof and floor or with faults and igneous dikes in the surrounding rocks (Iannacchione, 1991).

(3) Mining configurations and sequence are also related to pillar bumps. Room-and pillar mining has more bumps than longwall mining (Holland, 1955), which indicates that geometric factors and mining sequence play a role in the bump events.

1.1.3 Chain pillar design

The design requirements for the chain pillars separating the panels are primarily that they should maintain the stability of the head and tail entries throughout all the mining phases necessary for complete panel recovery. At the same time there are economic incentives to minimize the size of these chain pillars to ensure the maximum resource

recovery. Chain pillars must be designed to support the side abutment load induced by mining development and panel recovery, and to protect the panel entries from excessive displacement of the roof and floor. Hence, the dimensioning of the chain pillars is a major factor in longwall design.

There can be two basic and different approaches to chain pillar design; these are "stiff" pillar design and "yield" pillar design.

In the stiff pillar design approach, the pillars are designed to support the abutment load and to support the roof so that there is no significant movement in the roof until the panels are finished. Consequently, the strength of the pillars must be greater than the expected maximum abutment load imposed upon them during the mining period. Usually the failure mode is not considered, although gradual yielding is intuitively assumed. Therefore, if the pillars are undersized or after their service lives end, they will fail, shedding the load elsewhere. These failures may be relatively gentle or they may be violent - such violent failures are known as "pillar bumps".

In yield pillar design, the pillars are designed to yield (fail gently) to the abutment load, shedding their excess load onto nearby abutments and the caved material in the gob. This leads to a stress-released zone created around the entry and protects the entry from excessive loading. Hence they are designed intentionally to be undersized and the post failure behavior of the pillars needs to be considered. Again this may lead to a gentle failure or violent failure depending on the post-failure loading and unloading characteristics of the strata and pillars.

For longwall mining, more and more mines are using a combination of the stiff and yield pillars to obtain safer and more economical design. Usually, there are rows of abutment pillars sided with the rows of the yield pillars. The abutment pillars are designed to support the side abutment loads until the longwall face has passed. The yield pillars are designed to yield to the development load to release the stress on the nearby entries, and also to perform as buffer zones between entries and the stiff abutment pillars if violent failures of the abutment pillars occur.

1.1.4 Summary

Currently, chain pillar design is mainly based on the ultimate strength, which may suitable for the room and pillar mining in shallow overburden conditions. With the

mining going deeper, more and more mines are encountering pillar bump problems. Although the introduction of longwall mining into North America has significantly improved the situation, pillar bumps in the tail entry still constitute a threat to the stability of the tail entry, as well as to the personnel and equipment. This illustrates the lack of understanding of pillar behavior in design of chain pillars for longwall mining.

On the other hand, for better ground control, chain pillars are encouraged to fail after the second face passes or once they are isolated in the gob area. Therefore pillar bumps, under some circumstances, may be unavoidable. In this situation, the timing and the location of the pillar bumps will be critical for the safety considerations. The best design of chain pillar should include the evaluation of the timing and mode of the potential pillar failures.

1.2 Objectives of research

The main contribution of this thesis would be to improve chain pillar design for longwall coal mining under bump-prone conditions. To accomplish this, studies have to be pursued in the following areas:

(1) To examine the available stiff and yield pillar design methods and to investigate how to introduce bump evaluation into pillar design.

(2) To investigate the methods and concepts used to define the pillar stiffness and the local mine stiffness, and to integrate those concepts into a boundary element program;

(3) To investigate the response of the local mine stiffness to the longwall face advance, mine geometry, coal behavior and properties of the roof and floor rocks;

(4) To use the developed stiffness concepts to simulate real mining situations and to investigate the possibility of using local mine stiffness to predict and control pillar bumps in longwall mining.

(5) If possible, to provide practical chain pillar design guidelines for longwall coal mining which will eliminate the risk of bumps or, at least, to confine the location of pillar bumps to the gob area.

1.2.1 Research Methodology

The research will be based on a non-linear three dimensional boundary element program developed by US. Bureau of Mines, and the local mine stiffness concept proposed by Salamon (1970). Disturbing methods proposed by Starfield (1968) will be integrated into the boundary element program to determine the local mine stiffness.

The main focus is on implementing the local mine stiffness concept into chain pillar design. To accomplish this goal, literature on the local mine stiffness, pillar stiffness measurements and analytical and numerical analyses of mine stiffness are reviewed and analyzed. The local mine stiffness and pillar stiffness will be defined according to the results of this analysis.

The calculated local mine stiffness will be compared to an analytical solution derived by Salamon (1970) to check the validity of the modified program. Then, the program will be applied to the longwall retreat mining situation in V.P. No. 3 mine. The simulation results from the computer program will be compared to the field data from that mine to evaluate applicability of the program.

1.2.2 Scope and limits of the research

Research scope is to examine the effect of the ratio of the modulus of the coal and the strata, the softening behavior of coal, the face advance, the location of the pillar in the panel layout and the change of chain pillar layout on the local mine stiffness by performing a parametric three dimensional boundary element computer simulation for longwall mining in tabular seam beds. The study also includes a review of the chain pillar design methods and the pillar strength and behavior, a geotechnical interpretation of the field data from US Bureau of Mines, a demonstration simulation of the case history of V.P. No. 3 mine, and a derivation of post-failure pillar stiffness.

Numerical simulation is carried out with focus on the behavior of pillars and roof in bump-prone strata conditions, especially in coal beds with a strong roof and floor. Therefore, the behavior of the surrounding rock can be assumed to be elastic. Inelasticity is allowed to occur only in the vicinity of the openings, i.e. in the seam. The seam can be specified to be elastic or non-elastic, such as strain softening. The time dependent behavior of the seam is not considered.

Chapter 2

PILLAR DESIGN

Design of longwall chain pillars basically follows the traditional pillar design procedures as shown in figure 2.1.

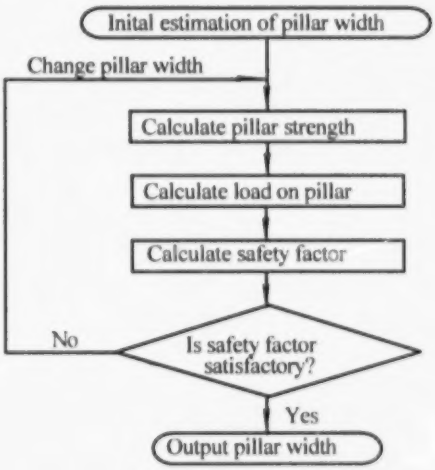

Figure 2.1

Pillar design flow chart.

The initial pillar dimensions are usually given by experience and economic considerations. Then, the pillar strength and the load on the specific size of pillars are estimated by assuming some kind of loading mechanism and strength formula. According to the role a pillar is designed to play, these procedures are repeated until a satisfactory safety factor is obtained. Usually, uncertainty in quantifying the strength and loads of pillars and in determination of pillar creep behavior is compromised by choosing a high safety factor.

Chain pillars in longwall mining are designed to protect head entry and tail entries during panel recovery and are expected to yield after the face of the second panel has passed. Before calculation of pillar strength and pillar load, it is necessary to investigate geological factors which may affect the pillar design process.

2.1 Geological factors

Geological factors include topographic difference, stratigraphic thickness of roof, physical properties of roof, floor and coal, and any possible faults or defects in the roof. Topography will affect the direction and magnitude of stresses; stratigraphic thickness may affect the transfer of overburden load to the seam. Weak roof and floor may cause roof fall or floor heave problems. For the strong roof and floor, the main concern is the stability of the pillars and caving of the gob. Because the bump-prone coal beds are identified as the coal beds with strong roof and floor (Campoli, 1990, Haramy, 1988 and Iannacchione, 1991), the review will focus on the pillar design under strong roof and floor conditions. Failure will be restricted to the coal beds, and not in the roof or floor.

2.2 Pillar strength

2.2.1 Coal mass uniaxial compressive strength

It has been established by the years of experience from experiments on specimens in the laboratory and field, that the coal mass strength is lower than the strength determined by laboratory testing on small specimens, because the in-situ coal contains more flaws or fractures than the laboratory size specimens. This size-determined relationship can be represented by the Hustrulid's equation below (Hustrulid, 1976):

$$\sigma_1 = \frac{k}{\sqrt{h}} \tag{2.1}$$

where σ_1 is the mass strength of a cubical coal block with dimension h. k is the Gaddy Factor and is defined by (Gaddy, 1956) as:

$$k = \sigma_c \sqrt{D} \tag{2.2}$$

where σ_c is the uniaxial compressive strength of coal specimens tested in the laboratory having a cube side dimension D.

Equation (2.1) indicates that strength of the coal block decreases with the increase of block dimension. However, a significant development made by Bieniawski (1968) revealed that there is a critical dimension beyond which the strength of the coal block remains constant. Bieniawski later defined the critical dimension as critical size for the

specific coal. Therefore, if the dimension of the coal block is greater than the critical size, the critical size should be used instead of the actual dimension h in equation (2.1). For North American coal, the critical size was identified to be 36 in. (0.9 m) (Bieniawski, 1992).

Equations (2.1) and (2.2) illustrate that the in-situ strength of coal or coal measure rock can be estimated by testing small cubic specimens, provided that the information of the critical size is available

2.2.2 Pillar strength formulas

The above equations give the mass strength of a cubical coal block. For a pillar, its strength is also affected by the pillar geometry characterized by the width/height ratio. Generally, the strength of a pillar increases with the increase of its width/height ratio because of the confining pressure build-up towards the pillar core. There are a number of strength formulas developed throughout the years which tried to combine both the size effect and the shape effect on pillar strength (Obert and Duvall, 1967, Holland, 1964, Gaddy, 1956, Holland, 1973, Salamon and Munro, 1967, and Bieniawski, 1967). They can be generalized as:

$$\sigma_p = \sigma_1 (A + B\frac{W^\alpha}{H^\beta}) \qquad (2.3)$$

where σ_p is the pillar strength; σ_1 is the in-situ compressive strength of a cubical block to be determined by equation 2.1; W and H are the width and the height of the pillar; A, B , α and β are constants and are given in Table 2.1. in respect to the different formulas.

Generally, the formulas are reliable for small pillar design because all of them are derived from the studies of the field data and laboratory data in the shallow mines where the pillar dimension is relatively small. The application of the formulas to the thick overburden pillar design are usually not encouraged because of the lack of data with width/height ratio beyond 5 in the derivation of the formulas. With more and more longwalls operating under the deep cover, where pillars with width/height ratio over 9 are very common, there is need to develop new design approaches which can cope with the wide pillars with a width/height ratio beyond 9.

Table 2.1 Empirical pillar strength equations.

Formulas	A	B	α	β	Safety Factor	Applicable W/H range
Obert-Duvall/Wang	0.778	0.222	1.00	1.00	1.5-2.0	≤8
Bieniawski	0.640	0.360	1.00	1.00	1.5-2.0	≤10
Holland-Gaddy	0.000	6.000	0.50	1.00	1.8-2.2	≤5
Holland	0.000	1.000	0.50	0.50	2.0	≤5
Salamon-Munro	0.000	1.732	0.46	0.66	1.31-1.88	≤5

A comparison of the different formulas was made by Bieniawski (1992), as shown in figure 2.2. It is clear that Holland-Gaddy formula is most conservative; the other four formulas are very similar when width/height ratio is less than 5. Bieniawski formula is most unconservative beyond the range of width/height ratio 5. The experience of application of these formulas have proved all the formulas worked well for pillars with

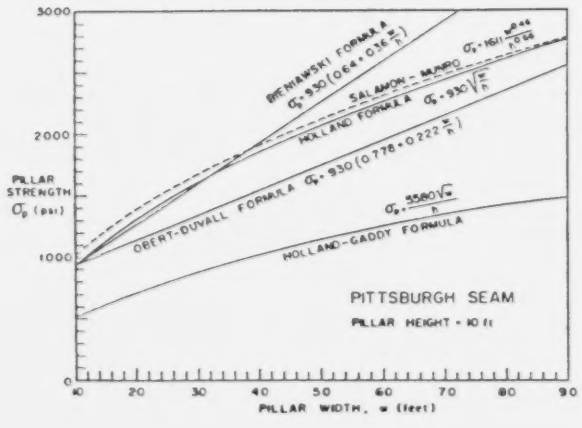

Figure 2.2

Comparison of the pillar strength formulas (after Bieniawski, 1992).

low width/height ratio but will underestimate pillar strength for wider pillars unless some corrections were made (Salamon, 1985, Madden, 1991, Wagner, 1984, and Bieniawski, 1984). It was also noticed by Babcock (1984 and 1990) that although the constraint conditions at the pillar ends affects the confining pressure build-up toward the pillar core, they are ignored by these formulas. Therefore, when unusual pillar end conditions exist (such as very soft thin layer existing between pillar ends and the floor or roof), the strength values calculated by the pillar formulas have to be adjusted to include the extreme end constraint condition.

2.2.3 Analytical methods

All the strength formulas above assume or imply the uniform loading and uniform stress across the pillars. This is good approximation for small pillars, but very often a chain pillar in longwall layout is very wide and is not uniformly loaded. Failure is initiated first at the critically stressed part of the pillar and then propagates to full collapse. Several analytical models have been developed to address this aspect in which the "confined elastic core" pillar model proposed by Wilson (1972, 1977, and 1982) is most comprehensive.

(1) Wilson model

Wilson hypothesized that a pillar, flanked on both sides by gobs, consists of an elastic core surrounded by exterior yield (fractured) zone. The linear Mohr-Coulomb criterion is used as the failure criterion for intact coal:

$$\sigma_1 = k\sigma_3 + \sigma_0 \qquad (2.4)$$

where σ_1 and σ_3 are the maximum and minimum principle stress respectively; σ_0 is the uniaxial compressive strength of the coal mass; k is called the "triaxial stress factor" and can be measured experimentally. Wilson stated that for coal measures, k = 4 and $\sigma_0 = \sigma_c/3$ where σ_c is the uniaxial compressive strength of a coal specimen.

The stress in the yield zone is guided by the equation:

$$\sigma_1 = k\sigma_3 \qquad (2.5)$$

The boundary between the yield zone and the elastic zone is defined by assuming that the horizontal stress σ_3 reaches the original hydrostatic stress $q = \gamma H$ at the boundary in

the two equations. Airy's solution is used to relate the horizontal stress to the distance x from the pillar rib to the location in the pillar where the stress is sought. According to the derived relations in the model, the horizontal stress in the yield zone increases exponentially with distance x until it reaches the original horizontal stress level. Based on the equation (2.5), the vertical stress also increases exponentially with x. The vertical stress in elastic zone is also assumed to be an exponential function of x, to facilitate the calculation. In the extreme case, the boundary reaches the center of the pillar. Therefore, the pillar strength is the integration of the vertical stress over the pillar width.

The confined core model revealed that the stress in the pillar is not uniformly distributed and that the failure starts from exterior of the pillar. It also explained why wide pillars can sustain higher stress than the narrow pillars because the failed exterior zone will provide the constraint to the elastic core in the middle of the pillar, thus increasing the loading capacity of the pillar core.

However the confined core model also has some serious drawbacks which were summarized by Salamon (1992) as:

a. The deformation characteristics of the strata and the pillar are not considered;

b. The choice of the generated horizontal stress stopping at the original stress level has no rational basis;

c. The load transfer and the residual strength of the failed slices do not satisfy physical laws;

d. The restraint of the pillar edge cannot be zero.

In addition, he also pointed out that Wilson's model will predict excessively high stress in the pillar core because the horizontal stress increases exponentially with the distance to the pillar edge in the model. He then suggested that strain-softening behavior has to be taken into account to improve the model.

(2) Barron model

Some of the problems of the confined core model were overcome by "Barron model" which was first proposed by Barron (1983 and 1984) and later revised by Barron and Pen (1992).

In the Barron model, the Hoek-Brown failure criterion is used instead of the Mohr-Coulomb criterion. A pseudoductile failure mechanism is introduced into the pillar model which leads to the existence of an additional pseudoductile zone between the fracture zone and elastic core. In this pseudoductile zone (or yield zone), the horizontal stress increases linearly instead of exponentially with the distance to the pillar edge, which prevents one overestimating the pillar strength for a wider pillar. The boundary of the fractured zone and yield zone is defined by the intersection of the linear Mohr-Coulomb equation and non-linear Hoek-Brown equation, which eliminates the boundary assumption in Wilson's model.

There are two extreme failure modes for the model. In one case, the yield boundary is extended to the pillar center which is called "ultimate yield". In the other case, the fracture boundary reaches the pillar center, which is called "ultimate fracture". The pillar strength will be the integration of the vertical stress over distance x in the fracture zone and the yield zone, or in the fracture zone only, depending on the failure modes. However, although the pseudoductile failure mechanism was proved to exist in hard rock under extremely high stress, there is only some indirect evidence of pseudoductile failure of coal in the pillar core (Barron, 1988). Therefore, direct physical evidence is still needed for Barron's model.

2.3 Loads applied to longwall pillars

Generally, a coal seam is sandwiched between the relatively stronger roof and floor rocks which are loaded by the overburden. Stress is uniformly distributed in the coal seam and the host rocks. When mining activity starts, the equilibrium is destroyed and the stress in the coal and rocks is redistributed. Traditional retreat longwall mining development includes driving the panel entries from main entries. When the panel entries are developed to the designed length, the bleeder entry is driven to connect them. The panel entries consist of two, three or four entries depending on the requirements of ventilation, transportation and mining law. Once the development is finished, the extraction begins with the face moving from bleeder entries towards the main entries. According to Mark (1987), the loads on longwall pillars can be divided into two parts: development loads which are present when longwall development has just finished, and abutment loads which arrive during panel extraction.

2.3.1 Development loads

Development loads are the loads added to the chain pillars when the panel entries are finished, due to the weight of the overburden directly above the pillars and entries. The two major approaches to calculate development loads are tributary area theory and elastic deflection theory. Most early researchers (Wilson, 1972, King and Whittaker, 1971) used the "tributary area theory" to calculate development loads, which is commonly used in calculation of loads in room and pillar mining.

2.3.1.1 Tributary area theory

Tributary area theory assumes that pillars support all of the overlying ground tributary to their locations. It follows that the average pillar stress is given as:

$$\sigma_p = \gamma h \frac{(w_e + W_p)(w_c + L_p)}{W_p L_p} \qquad (2.6)$$

where w_e and w_c are entry width and cross cut width; W_p and L_p are pillar width and pillar length respectively; γ is the unit weight of the overburden and h is the overburden height.

It is assumed in this formula that the distribution of pillars and rooms are uniform and extended to infinity in all directions. In reality, pillars and rooms are surrounded by the intact strata. Therefore, the result is conservative and is the upper bound of the pillar load.

2.3.1.2 Deflection theory

Coates (1965) noted that the tributary area theory ignores the geometrical parameters such as the span of the mining zone with respect to its depth for horizontal workings, and the deformation characteristics of the materials. Based on the elastic solution of the deflection of a point on a circular hole in a plate due to an applied uniaxial stress, Coates developed pillar loading formulas that take into account the pillar location in the panel and the modulus of surrounding rock and pillars. The application of the Coate's formulas indicated that they fit the field results better than the tributary theory, but because of the

complexity of the formulas, their application is still not as popular as that of the tributary area theory.

2.3.1.3 Numerical solutions

Theoretically, the above equations can only be applied to situations in which pillars and mining zones are in uniform distribution. For a more complex distribution of pillars and mining zones, especially for situations in which there is more than one material in the overburden or materials behave in a non-elastic manner, numerical solutions based on the finite element method or boundary element method are needed to solve the problems. In a case study, Mark (1987) compared the results from tributary area theory with those from finite element modeling. He stated that the accuracy of the tributary theory decreases with the increment of the extraction ratio and that, for estimation of the development load, tributary area theory gives an acceptable solution which is within 10% of the modeling results for two dimensional extraction ratios up to 50% (Mark, 1987). With the development of computer software and the challenge of the more difficult mining conditions, application of numerical solutions based on the computer modeling seems unavoidable.

2.3.1.4 Summary and conclusions

Development loads are relatively easy to calculate because, at the development stage, the panel usually can be treated as a two-dimensional case. The tributary equation only gives the upper bound of the development loads because of the assumption mentioned above. Coates' equation provides a more realistic estimate if pillar locations in the panel and the interaction of pillars and the surrounding strata have to be taken into account. But both equations cannot handle three-dimensional cases. Numerical solutions are more versatile and accurate, provided that the input parameters can be obtained with reasonable confidence.

2.3.2 Abutment loads

When coal in a longwall panel is extracted, the load on the coal is transferred to the side pillars. According to Peng and Chiang (1984), the abutment load is first detected at a distance of about one times the overburden depth away from the face. With the advance of the face inby and outby the side pillars, the loads on side pillars increase from the

development load towards a maximum load. During the whole process of panel extraction, the side pillars may go through the full loading process, including critical failure or yield and post failure unloading. Therefore, determination of the time when maximum load is reached and the magnitude of the maximum load is crucial to the longwall pillar design.

Mark (1987) identified two critical abutment loads:

(1) Front abutment loads, which are the loads applied on the chain pillars when the distance of the face to the pillars is zero;

(2) Side abutment loads, which are the loads when the face has passed the pillar by a sufficient distance.

Because, for chain pillars, the mining process includes coal extraction from the panels at the both sides of the chain pillars, front abutment loads and side abutment loads on the chain pillars can be further divided into the head gate front abutment loads L_f and the first side abutment loads L_s(which are the one side abutment loads), as well as the tailgate front abutment loads L_{ff} and the second side abutment loads L_{ss} (which are the two side abutment loads) according to the face positions of the first or the second panel recovery as shown in figure 2.3.

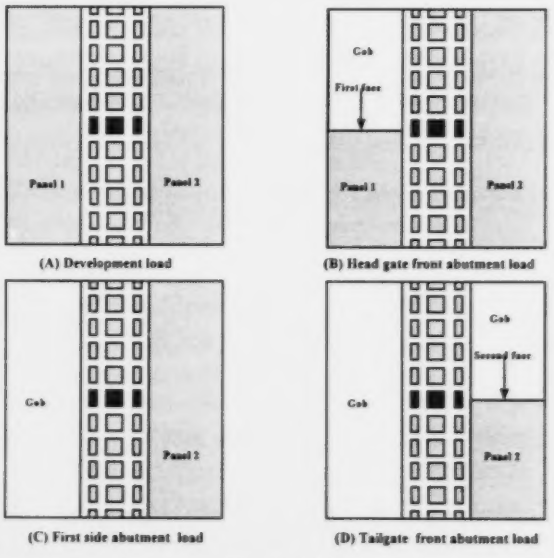

Figure 2.3

Four stages of longwall mining advance.

In retreat longwall mining, the tail entry has to be kept in good condition until the face of the second panel has passed. It means that the chain pillars have to be designed at least to remain stable through the arrivals of the development loads L_d, the first side abutment loads (L_f and L_s) and the tailgate front abutment loads L_{ff}. An idealized loading curve of a chain pillar with respect to the face positions is plotted in figure 2.4. The minus and plus sign in the figure represent the face is inby and outby the pillars respectively.

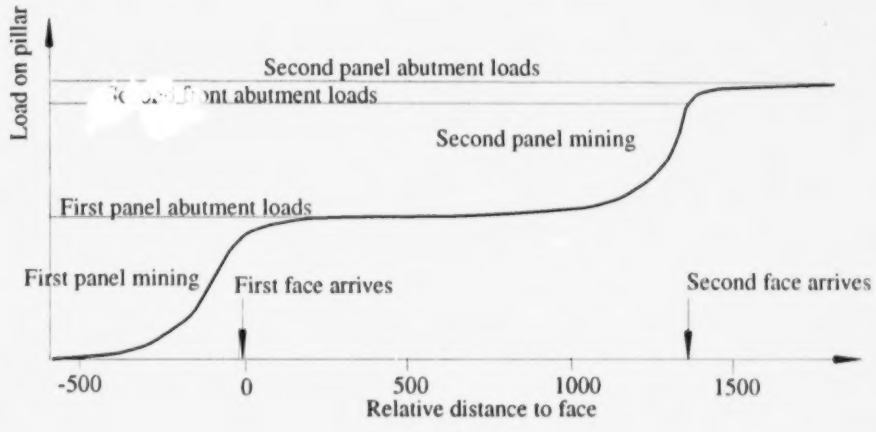

Figure 2.4

Typical loading curve of a pillar in longwall panel.

For best ground control, chain pillars are encouraged to gradually fail after the second front abutment loads arrive. This will lead to smooth caving behind the face and decrease the pillar bump danger. However, the traditional pillar design only uses side abutment load as a design base because of the difficulty in calculating the front abutment loads and a conservative design attitude.

2.4 Chain pillar design

Once the pillar strength is calculated by the methods discussed above, the abutment loads applied on the pillar have to be decided before the safety factor can be evaluated.

2.4.1 Calculation of abutment loads

There are a number of approaches available for calculating side abutment loads. They can be classified into analytical and numerical approaches.

2.4.1.1 Analytical approaches

(1) Wilson's approach

Wilson used a "stress balance" approach to approximate the stress distribution in the waste area and in the pillar rib (Wilson, 1972 and Wilson, 1982). He stated that "As the total aggregate downward force remains that of the cover load, any stress rise over the ribside must be compensated for by an equivalent stress reduction over the waste, and vice versa" (Wilson, 1983). Based on studies in Great Britain, he concluded that if the cover depth is H, the load carried on the waste increases linearly, from zero at the rib to the cover load some distance (0.3H) away from rib. The total load on the pillar is the distributed cover load plus the load deficiency in the waste. Clearly, unless some assumptions are made, Wilson's approach cannot calculate the pillar load when the longwall face is close to or in the line with the pillar.

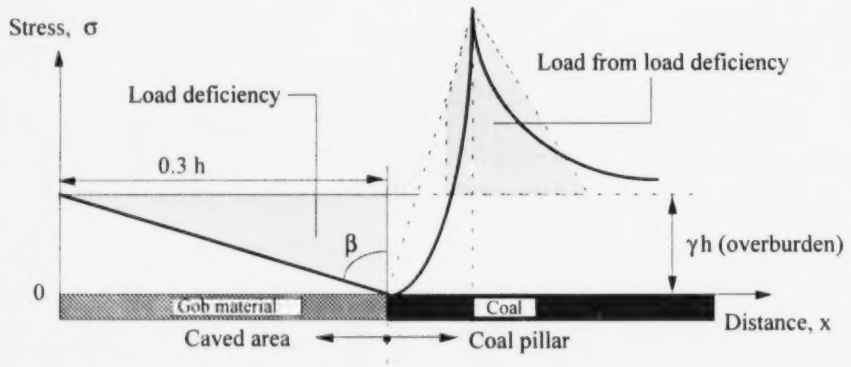

Figure 2.5

Stress distribution and load deficiency in the gob (after Wilson, 1972).

King and Whittaker (King, 1983) also presented an approach which is based on a different concept but has very similar result to that of Wilson. The angle of β in Wilson's figure (figure 2.5) was defined by King as the "shear angle" which they claimed to be equal to the angle of draw. The angle was assumed to be a meaningful physical parameter which defines the wedge loading on the gob. The load of the remaining overhanging sections are transferred to the pillars. Although they stated that for typical British coal, the shear angle is about 30° or should be equal to the angle of draw, they

provide no physical explanation for the shear angle, nor the method presented to obtain its value.

This situation was improved by the concept presented by Choi and McCain (Choi, 1980). Based on the surface subsidence measurement and numerical simulation, Choi and McCain defined a "complete displacement zone" resting on the gob within which no further rock movement occurred even when an adjacent panel is mined. The complete displacement zone is defined by a "negative angle of draw" which is equivalent to King's shear angle β and can be measured by determining the transition point on the subsidence profile. Only the protruding area outside of the complete displacement zone applies the abutment load on the pillars.

All analytical methods assume or imply a linear stress build-up toward the center of the gob area which is a simplification of the real situation. Because the initially loose material in the gob experiences the whole compacting process, theoretically, one would expect that the stress build-up is in a nonlinear form, such as a power or exponential function. However, to assume a nonlinear stress in gob will complicate the analytical calculation.

The shear angle concept simplified the abutment load calculation. However, there were cases in which no apparent transition points on the measured subsidence profiles can be positively identified to define the angle (Mark, 1987). Mark also admitted that rather than a measurable physical characteristic of gob, the shear angle is perhaps only an approximation for facilitating the side abutment calculation.

(2) ALPS method

Mark and Bieniawski (Mark, 1989) proposed a semi-empirical and semi-analytical chain pillar design method which can calculate the front abutment. The shear angle concept is used to define the side abutment load and Bieniawski's empirical pillar strength formula is used to estimate pillar strength. The distinct feature of the method is that Mark introduced the "front abutment factor", F, from which the front abutment L_f can be estimated as:

$$L_f = F \cdot L_s \qquad (2.7)$$

where L_s is the side abutment which can be calculated by the overhanging region defined by the shear angle concept; F is the front abutment factor, which is less than one

and has to be determined by either field measurement or empirical estimation; L_f is the front abutment load.

Mark recommended that F to be 0.5 and 0.7 for the headgate front abutment and tailgate front abutment respectively. Because different strata conditions may affect F, he suggested that F has to be corrected by the field observation or measurement. Although the introduction of the front abutment factor solved the problem of front abutment calculation in analytical approaches, the claim of a linear relation between the front abutment and the side abutment is unconvincing. Unless it is verified by the field measurement or, at least, by numerical modeling, the risk of overestimating or underestimating the front abutment still exists.

2.4.1.2 Numerical methods

In numerical analysis, the region of interest (usually a part of a mining panel) is divided into a numbers of small elements. A pillar may consists of many elements. The strength of the pillar is dependent on the whole behavioral picture of the elements. The elements behave according to the assigned constitutive law which can be elastic or elastic-plastic, depending on the nature of the material. The range of a purely elastic response is limited by a failure criterion. The obtained stress is compared to the possible maximum stress to give a quantitative description of the state of the element.

(1) Limit design method

Pariseau (1975) demonstrated that assigning elastic-perfect plastic and elastic-perfect brittle properties to the elements will provide the upper bound and lower bound to pillar stability. In the first case, once a material fails, it cannot sustain additional load but the deformation is still continuous, which corresponds to plastic flow. The additional load has to be supported by the inner core of pillar; in the second case, a material failure leads to total loss of its bearing capacity. All the load is transferred to the inner pillar core and deformation is discontinuous, which corresponds to brittle fracture. A local safety factor, which is the ratio of the maximum shear stress possible to the actual maximum shear stress for the Coulomb failure criterion, was used to represent the extent of the failure. The local failure usually is tolerable provided the failure is restricted to only part of the pillar. The pillar instability or collapse was manifested as unarrested plastic flow (yielding) or unarrested spalling (brittle fracture) through the pillar.

(2) Peng and Hsiung method

From an extensive three-dimensional finite element analysis, Hsiung and Peng (Hsiung, 1984) studied the influence of various parameters on the coal pillar behavior in longwall mining. The safety factor is the ratio of uniaxial strength to the equivalent vertical stress on the pillar, adjusted by the reduction of the intact area in the pillar. The studied parameters included Young's modulus and thickness of immediate roof, main roof, floor and coal, overburden, in-situ horizontal stress, uniaxial compressive strength of coal, panel width and length, entry width and pillar width. After eliminating the insignificant effect of the in-situ horizontal stress, the thickness of the strata and the entry width, they obtained a quantified relationship by statistically correlating the parameters with each other as:

$$\log W_p = -4.676\times10^{-3}\frac{E_i}{E_j} - 4.04\times10^{-3}\frac{E_m}{E_c} - 3.33\times10^{-2}\log\left(\frac{E_f}{E_c}\right) - 0.0789\log\sigma_c + 0.5144\log h + 0.0494\log\left(\frac{L}{2}\right) + 0.1941\log W \quad (2.8)$$

where W_p - width of a square chain pillar;

E_i, E_c, E_m, and E_f - Young's modulus of the immediate roof, coal, main roof and floor;

σ_c - uniaxial compressive strength of coal mass;

h - seam depth;

L - panel length;

W - panel width.

This formula is very impressive because, although it was derived from numerical analysis, it came out as a very simple formula. It was also specifically derived for longwall chain pillar design. But because in their simulation, the panel entry system was confined to three entries with two columns of equal size square pillars, and the height and the internal friction of coal were not varied, the formula can only applied to a similar entry system. There is also not much information on how the head gate pillars behave during the second face extraction, which is the main concern for pillar bumps.

Furthermore, there is a lack of sensitivity analysis about the parameters involved in the equation. A complete criticism of the formula was presented by Mark (1987).

2.4.2 Summary and conclusions

Traditional designs using empirical strength formulas are based on the ultimate strength of a pillar. It assumes that once the ultimate strength is reached, the load on pillars will drop to zero.

All the empirical or analytical approaches (except ALPS) just calculate the side abutment loads because calculation of front abutment loads needs three dimensional analysis. Therefore, without field measurements or some kind of assumption, only numerical methods can provide satisfactory solutions when a detailed study of the pillar loading process is required. Furthermore, both the empirical and analytical design approaches cannot consider the interaction between pillars and the interaction between pillars and surrounding strata..

Empirical pillar strength formulas have been used successfully for pillars with low width/height ratio because they are derived directly from the experiments and observations of this type of specimen and pillars. They are suitable for small pillars in shallow seams. They will provide a conservative strength estimate for wider pillars with width/height ratios beyond 5.

For wider pillars, which are very common in mining of deep seam beds, analytical approaches may provide a better strength estimate because the non-uniform stress distribution in pillars and different failure mechanisms are addressed in these analytical approaches. However, all analytical approaches have their own assumptions which are difficult to prove or verify in the field. Therefore, their applications are not always satisfactory.

Numerical approaches seem to be the most suitable if the interactions between pillars and between roof and pillars need to be considered or the three dimensional case has to be dealt with, because the effect of interaction of pillars with roof and floor is naturally included in 2D or 3D numerical analysis. Progressive failure can also be easily handled in numerical approaches. The major problem with a numerical approach is the difficulty in quantifying the input parameters. Therefore, there is always some kind of back analysis or fitting process needed in the numerical analysis.

2.5 Yield pillar design

Yield pillars in longwall mining are mainly used to redistribute stress in the entry-pillar system so as to protect the adjacent area from excessive stress concentration, and to shield personnel and equipment from the nearby abutment pillar bumping. Yield pillars have been used successfully in entry development and longwall mining (Carr, 1984) in which yield pillars eliminated massive floor heave. Other applications of yield pillars include the design of yield pillars to minimize surface subsidence and to reduce the pillar interaction in multiple seams mining. It was reported that yield pillars led to a cleaner caving line along the tailentry, which reduced danger of pillar bumps. A finite element analysis also revealed that yield pillars created a stress released zone in the adjacent area, which eliminated the yield zone in the entry floor (Tsang, 1989), but at the same time, they also increase the tensile stress in the entry roof. They concluded that yield pillars can be applied to most geological conditions, especially a weak floor condition, as long as the roof is properly considered.

The requirements for a yield pillar is that it yields totally but in a stable manner and transfers the load to the adjacent area. Therefore, the size of the yield pillars should be designed to be small enough to totally yield long before the maximum load arrives; the failure of the yield pillar should be stable, which means the post-failure stiffness and the adjacent roof stability have to be included in the design. Mark recommended that yield pillars should be designed to yield at the development load (Mark 1987). Although it is insisted that for yield pillars, the stiffness of the pillars and strata should be checked to avoid pillar bursts (Seedsman, 1991), there are no valid and effective ways yet to include the stiffness check into pillar design practice because of the complexity of determination of both pillar stiffness and strata stiffness.

Chapter 3

PILLAR STABILITY

All the pillar strength formulas assume that, once the strength of the pillar is reached, the pillar fails, and the load on the pillar immediately sheds to the remaining pillars or rib, and the pillar loses its function. Therefore, only the maximum load of the pillar needs to be considered in the design process. Realizing that for most cases in mining, pillar failures are unavoidable and some times are even preferred, many researchers started to look further into the post-failure region in pillar design. Obviously, from the safety point of view, a pillar which fails gradually after the peak load is more favorable than a pillar which fails violently at the peak load. The design methods evolved to not only consider the pillar strength, but also to consider the behavior of the pillar when its strength is passed, i.e., to consider the failure modes of the pillars. In this respect, the post-failure mechanism proposed by Cook in the 1960s (1965) and the controlled failure concept provided by Salamon (1970) are most important to the design of pillars.

3.1 Pillar behavior

A pillar loaded between the roof and floor in the field is very similar to a specimen loaded in a conventional test machine. Therefore, to a great extent, pillar behavior can be investigated by a laboratory test on a small specimen. Prior to the 1960's, uniaxial compressive tests on laboratory-scale specimens usually generated a typical stress-strain curve as shown in figure 3.1. Testing terminated violently with sudden failure of specimen when the ultimate compressive strength was passed.

In the 1960s, researchers (Cook, 1965, Starfield and Wawersik, 1970) realized that the testing machine formed a part of system which included both specimen and loading frame. Testing results would be affected not only by the specimen, but also by the characteristics of the test machine. Later, similar tests were performed using the so-called "stiff" test machine and the complete stress-strain curve was obtained, as shown in figure 3.2. It is shown in this curve that after the ultimate compressive strength of the specimen is passed, the specimen gradually sheds load capacity and fails smoothly.

The obtaining of the total stress-strain curve marked a significant advance in rock mechanics. It not only illustrates why there are many pillars in the field obviously having

failed but still standing and holding substantial loads, but also leads to the development of pillar stability theory which explains why some pillars fail violently and others gently.

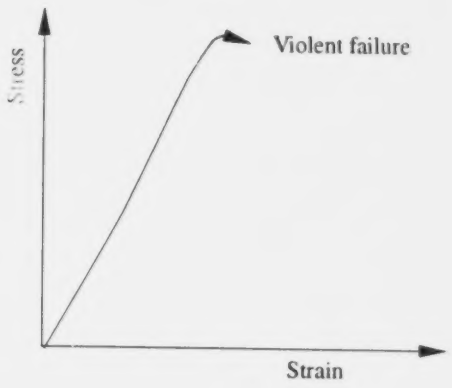

Figure 3.1

Typical uniaxial compressive testing curve for rocks.

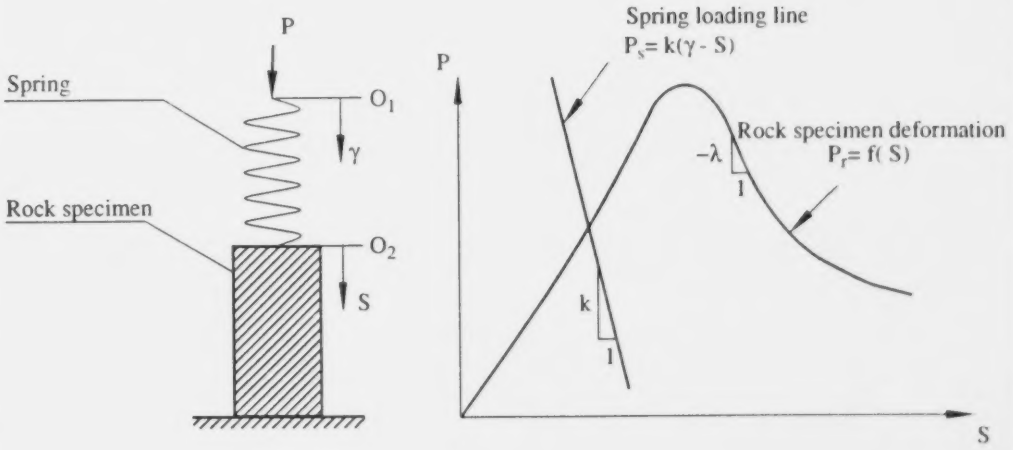

Figure 3.2

Conventional compression test in laboratory with a stiff testing machine.

3.1.1 Stability theory

The mechanism of pillar bumps was first proposed by Cook in his historical paper (Cook, 1965) and was later theoretically summarized by Salamon (1970). According to the theory, the mine structure is stable if the virtual work done on the structure is positive, regardless of the displacement experienced by pillars, i.e.

$$W = \frac{1}{2}\sum \Delta P_i \Delta S_i > 0 \tag{3.1}$$

where ΔP_i are small load increments to be imposed on various points in a structure; ΔS_i are the accompanying displacements at these points; W is the virtual work done on the structure by the imposed load increments. The equation simply states that the applied work by the external force on the specimen cannot be more than that can be absorbed by the specimen.

The stability problem for a mine structure can be simplified into that of a system in which a specimen (pillar) is loaded in a conventional testing machine (strata) as illustrated in figure 3.2. The load-displacement characteristics of the specimen and the machine (which is simplified as a spring) are expressed as:

$$P_r = f(S) \tag{3.2}$$

and

$$P_s = k(\gamma - S) \tag{3.3}$$

where subscripts r and s refer to the rock specimen and spring (machine); γ and S are displacements at the two ends of the spring and k is the stiffness of the spring, which is defined as the slope of the load-displacement curve of the spring; P_r and P_s are the loads on the specimen and the spring respectively.

For equilibrium, the net force at the spring-rock interface must be zero. Suppose a small external force is applied at interface of the rock specimen and the spring, causing the displacement ΔS. From equations (3.2)and (3.3), the force changes in the rock and the spring will be

$$\Delta P_r = \lambda \Delta S \tag{3.4}$$

and

$$\Delta P_s = -k\Delta S \tag{3.5}$$

where λ is the slope of the load-displacement curve for specimen and is defined as the stiffness of the rock specimen.

The criterion for stability is that the work W_s done by the spring over the displacement ΔS should be less than the work W_r to be done by the specimen over the same displacement. Otherwise, the specimen will not be able to absorb the energy supplied by the spring and the equilibrium cannot be maintained. Therefore, the stability condition is

$$W_s - W_r < 0 \tag{3.6}$$

or

$$\begin{aligned} W_r - W_s &= \frac{1}{2}\Delta P_s \Delta S - \frac{1}{2}\Delta P_s \Delta S \\ &= \frac{1}{2}(k+\lambda)\Delta S^2 > 0 \end{aligned} \tag{3.7}$$

which is equivalent to the equation (3.1). Obviously

$$k + \lambda > 0 \tag{3.8}$$

will satisfy the stability condition.

For the specimen-spring system, before the ultimate strength is reached, the stiffness of the machine and the specimen are positive. Equation (3.8) is always satisfied. The system is stable. After the ultimate compressive strength is passed, the stiffness of the specimen becomes negative. If $k < |\lambda|$, equation (3.8) is violated, the specimen fails violently, which corresponds to the soft test machine case. If $k > |\lambda|$, there is no violation of equation (3.8); therefore, the specimen fails smoothly, which corresponds to the stiff machine case.

As shown in figure 3.3, mine pillars are loaded as a result of mining-induced displacements of the country rock which are resisted by the pillar rock. Therefore, for the i-th pillar in the mine, country rock and pillar equilibrium is stable if

$$k_i + \lambda_i > 0 \tag{3.9}$$

where the local mine stiffness k_i replaces the spring stiffness k and pillar stiffness λ_i replaces the specimen stiffness λ. Clearly the strata stiffness is defined here as "local mine stiffness" because the stiffness not only depends on the strata's stiffness, but also depends on the stiffness of all the other pillars, i.e. to the pillar i, the loading system (spring) is the combination of the strata and the other pillars in the panel. In the elastic range, pillar stiffness λ_i is positive. Hence the stable condition of equation (3.9) is always satisfied. In the post-failure range, λ_i becomes negative and instability will occur whenever $|\lambda_i|$ is greater than k_i. If equation (3.9) is satisfied by all pillars in the mine, the structure is stable.

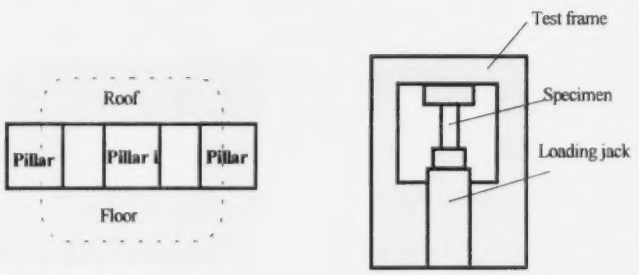

Figure 3.3

Schematic representation of pillar loading in the field and loading a rock specimen in a conventional test machine.

Therefore, pillar behavior is controlled by its ultimate strength, its post-failure stiffness and the local mine stiffness. After its ultimate strength is passed, these stiffnesses will control whether the pillar failure is smooth (controlled failure) or violent (pillar bump).

3.1.2 Evaluation of pillar bumps

It is clear that if the post-failure pillar stiffness and local mine stiffness can be obtained and the stress level in the pillars can be estimated, the stability of these pillars can be evaluated, based upon the above theory.

The stress level has to be continuously monitored to evaluate the stability of pillars. It can be estimated by analytical or numerical methods, but the determination of the post-failure pillar stiffness and the local mine stiffness in a mining layout is difficult because the stiffness not only depends on the material's physical properties, but also depends on the other factors such as the geometry and configuration of the pillars.

3.1.2.1 Definition of stiffness

Stiffness is defined as the total force needed to generate an unit displacement. In the stability analysis of mine structures, terms frequently mentioned are mine stiffness (or strata stiffness, regional stiffness), critical stiffness, local mine stiffness, and pillar stiffness.

(1) Strata stiffness

Salamon (1967) demonstrated that, assuming that the strata surrounding the mine openings are linear elastic and that non-elastic behavior is confined to the pillars, the total convergence of the roof and floor of the excavation can be determined by the superposition of two convergence distributions expressed as

$$\{S\} = \{\Gamma\} + \{S_e\} \tag{3.10}$$

where $\{S\}$ is the total convergence vector; $\{\Gamma\}=<\gamma_1, \gamma_2, ..., \gamma_i, ..., \gamma_n>^t$ is the convergence vector caused by the excavation in the stressed rock mass without supporting pillars and $\{S_e\}=<s_{e1}, s_{e2}, ..., s_{ei}, ..., s_{en},>^t$ is the convergence vector caused by the pillar force vector $\{P\}=<p_1, p_2, ..., p_i, ..., p_n>^t$ acting on a geometrically similar but weightless and unstressed rock mass. $\{S_e\}$ is defined as

$$\{S_e\} = [C]\{P\} \tag{3.11}$$

in which s_{ci} is the convergence at the i-th pillar location induced by the pillar forces $p_1, p_2, ..., p_i, ..., p_n$. [C] is a n×n matrix and is called the influence matrix. Its elements c_{ij} are called influence coefficients which are determined by the elastic properties of the strata and geometry of the excavation. They are independent of the properties of the pillars. The physical meaning of the influence coefficient c_{ij} is the amount of convergence generated at the pillar position i by an unit load applied at pillar location j, without considering the contribution by other pillars. Therefore, the equation (3.11) is just the summation of all such contributions.

Combining equation (3.10) and equation (3.11), the loading line of the strata can be obtained as:

$$\begin{aligned} \{P\} &= [C]^{-1}(\{\Gamma\} - \{S\}) \\ &= [K](\{\Gamma\} - \{S\}) \end{aligned} \tag{3.12}$$

where [K] is the inverse of [C] and is called the strata stiffness matrix. This equation is very similar to equation (3.3) for a spring.

The force-convergence relation of pillar i can be expressed as

$$p_i = f_i(s_i) \tag{3.13}$$

The matrix of the force changes with respect to the pillars is

$$\{\Delta P_i\} = [\Lambda]\{\Delta S\} \tag{3.14}$$

where [Λ] is an n×n diagonal matrix with elements $\lambda_{ii} = \lambda_i = f_i'(s_i)$, which are the post-failure stiffnesses of the pillars.

The matrix of force change with respect to the strata can be obtained from Equation (3.12). Note in derivation, $\Delta\gamma_i = 0$:

$$\{\Delta P_s\} = -[K]\{\Delta S\} \tag{3.15}$$

The virtual work will be

$$W = \frac{1}{2}\{S\}^t([K]+[\Lambda])\{S\} \tag{3.16}$$

According to virtual work theory, the mining layout is stable if the virtual work represented by equation (3.16) is positive. This is assured if all principle minors of det(K + Λ) are positive. Therefore, the condition for stability can be written as

$$[K+\Lambda] > 0 \tag{3.17}$$

As long as the equation above holds, the so-called "perfect stability" can be maintained which means that through the mining of the layout, violent failure will not occur, regardless of the magnitude of convergence experienced by the pillars.

The necessary conditions for equation (3.17) to be true are:

a. the all diagonal terms of the matrix [K+Λ] are positive, i.e.

$$k_{ii} + \lambda_i > 0 \tag{3.18}$$

b. the determent of [K+Λ] is positive, i.e.

$$\left|[K+\Lambda]\right| > 0 \tag{3.19}$$

Violation of any one of the two conditions will lead to instability. This can be demonstrated by an example opening of two pillars proposed by Salamon (1970).

The system is stable if $k_{11} + \lambda_1 > 0$, $k_{22} + \lambda_2 > 0$ and $\det([K + \Lambda]) > 0$ are satisfied.

Let $\det([K + \Lambda]) = (k_{11} + \lambda_1)(k_{22} + \lambda_2) - k_{12}k_{21} = 0$ and let $k_{12}k_{21} = c^2$, then

$$(k_{11} + \lambda_1)(k_{22} + \lambda_2) = c^2$$

Comparing hyperbolic curve $\lambda_1\lambda_2 = 1$ and noting that $(k_{11} + \lambda_1) > 0$ and $(k_{22} + \lambda_2) > 0$, the hyperbolic boundary of the shaded area represented in figure 3.4 was obtained. Therefore, the conditions $k_{ii} + \lambda_i > 0$ and $\det([K + \Lambda]) > 0$ uniquely define the stable area, which is represented by the shaded area in figure 3.4. In the n dimension case, the shaded surface of the area intersects the every axis of λ_i once and defines the boundary of the stable area.

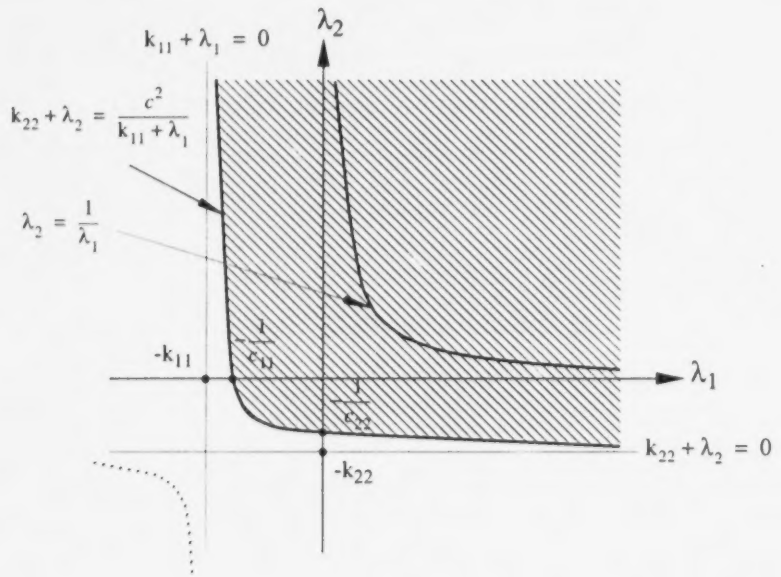

Figure 3.4

Condition for stability in case of two pillars (after Salamon, 1970).

Note, although the condition $k_{ii} + \lambda_i > 0$ is just one of the necessary conditions for stability, if the non-diagonal terms of [K] are very small and can be neglected, which is usually the case for a lot of practical situations, it can be used as the sufficient condition for stability evaluation (Salamon, 1970).

(2) Critical stiffness

Salamon proved that it is a sufficient condition for stability to have:

$$\lambda_m > \lambda_c < 0 \tag{3.20}$$

where λ_m is the minimum slope of the force-convergence curves of the pillars; λ_c is the smallest eigenvalue of strata stiffness matrix [K] and is called the critical stiffness of the layout. Note that the critical stiffness is also independent of pillar properties because it was derived directly from [K].

(3) Local mine stiffness

Starfield and Wawersik (Starfield, 1968) proposed that stability of the mining excavation can be tested by replacing the i-th pillar with a jack. As the jack is retracted a short distance, the relation between force and convergence change for the pillar is

$$\Delta p_i = -k_i \Delta s_i \tag{3.21}$$

where k_i is called "local stiffness" or "local mine stiffness". It will be shown that, although the "strata stiffness" and "critical stiffness" are independent of the pillar behavior, the local stiffness will depend on the behavior of the other pillars in the panel. The relation between local mine stiffness and strata stiffness is obtained by Salamon as follows:

It is clear when

$$k_i + \lambda_i = 0 \tag{3.22}$$

the panel is unstable. If λ_i in equation (3.20) is replaced with $-k_i$ and assuming that all other values of λ_i are known, then:

$$k_i = \frac{\det\left([(K+\Lambda)]\right)_i}{A_{ii}} \tag{3.23}$$

where A_{ii} is the co-factor of the element $k_i+\lambda_i$ in the determinant $\det(K + \Lambda)$. The term $\det(K+\Lambda)_i$ denotes the determinant of $[K + \Lambda]$ when λ_i is assigned to be zero. The equation (3.23) indicates that, unlike the strata stiffness which is independent of the pillar properties, the local stiffness at i-th pillar location will depend on stiffness of the other pillars in the layout.

For the example of two pillars, the unstable condition is:

$$\begin{vmatrix} k_{11}+\lambda_1 & k_{12} \\ k_{21} & k_{22}+\lambda_2 \end{vmatrix} = 0 \tag{3.24}$$

To obtain the local mine stiffness at the pillar position 2, let $\lambda_2 + k_2 = 0$, where k_2 denotes the local stiffness at pillar position 2, then

$$\begin{vmatrix} k_{11}+\lambda_1 & k_{12} \\ k_{21} & k_{22}-k_2 \end{vmatrix} = 0 \qquad (3.25)$$

i.e.

$$k_2 = k_{22} - \frac{k_{12}k_{21}}{k_{11}+\lambda_1} \qquad (3.26)$$

It is clear from the above derivation that the local mine stiffness k_2 at the location of pillar 2 not only depends on the strata stiffness [K], but also depends on the stiffness λ_1 of the pillar 1 which may or may not be in the post-failure state.

3.1.2.2 Determination of local mine stiffness

There are several factors which might control the local mine stiffness. They are the moduli of roof and floor rocks, the mine geometry and the stress-strain relationship for coal.

For a specified condition, usually, local mine stiffness is determined by the so-called "perturbation method" proposed by Starfield and Wawersik (Starfield, 1968). In this method a pillar in the field is replaced by an imaginary hydraulic jack under equilibrium. A small uniformly distributed load or a uniform displacement increment is to be imposed at the interface of roof and pillars by the jack, and the accompanying displacements or loads on jack are determined analytically or numerically. The slope of the jack's load-displacement curve is defined as the local mine stiffness for that particular pillar position. This method can be easily integrated into an analytical or numerical analysis. For tabular ore bodies like coal beds with the complex mining configurations, this can be best achieved by using computer programs in boundary element analysis (Brady, 1980, Ozbay, 1989, and Zipf, 1992).

Starfield and Wawersik (Starfield, 1968) numerically calculated the local mine stiffness of a panel with five rows of rib pillars separating the panel into six rooms. The host rock and the pillar were assumed to deform linear-elastically. Pillars and rooms were assumed to be infinitely long so that the plane strain condition is satisfied and a two dimension boundary element analysis could be performed. The unit displacement disturbance was applied for calculation of the stiffness. It was found that the local

stiffness at a particular pillar location decreases with increasing number of rooms in the panel. But it seems there is critical value of number of rooms beyond which a further increase gives little reduction in stiffness.

With a similar method but with the unit load disturbance, Salamon (1970) analytically calculated the critical stiffness of a similar panel layout. The analysis showed that the critical stiffness of the panel decreases with the increasing of pillar number (or room number) in the layout. He concluded that, as the number of the pillars in the panel is increased, it becomes progressively more difficult to maintain the perfect stability of the panel; this means that local instability might be inevitable when the number of the pillars in the panel reaches a certain limit, except by having $\lambda_1 > 0$.

By keeping the extraction ratio constant, Brady (1980) found that the local mine stiffness decreases with the increase of room width and pillar width. The two dimensional boundary element method with unit uniformly distributed load disturbance over the width of a pillar was used in his analysis. The convergence at the pillar position was taken as the average convergence over the pillar width in order to calculate the local stiffness.

Ozbay performed a parametric study on a similar two dimensional rib pillar-panel configuration by using a displacement discontinuity computer program (Ozbay, 1989). The unit uniformly distributed displacement disturbance was applied over the width of a pillar to calculate stiffness. He reported that if the extraction ratio is kept constant, the critical stiffness of strata decreases rapidly with the increasing span/height ratio L/H ; the critical stiffness approaches the value of zero asymptotically with the increase of the mining span; this indicates that for the shallow coal beds, any failure of pillars will lead to unstable failure if the pillars have strain softening behavior. The critical stiffness was also found to decrease with increasing extraction ratio, but this decrease becomes insignificant when the number of the pillars in the panel is greater than 5.

Recently the results of a three dimensional boundary element analysis were reported by Zipf (1992). The results showed that the local mine stiffness does not change with the location in the panel layout. No matter which location it refers to in the panel layout, the local mine stiffness decreases with the face advance initially but recovers and approaches the same constant value later. The magnitude of the local mine stiffness is dominated by the modulus of the surrounding strata. He concluded that the actual gate road pillar geometry and the position of an element within the panel have no influence on the calculation of the local mine stiffness. But he noticed that the element size and strain

level may have a considerable influence on the local mine stiffness. Zipf's results are significant because the effect of the advance of a longwall face on the local mine stiffness was considered for the first time in the analysis. However, even a pillar may cover more than 100 elements, a unit displacement was only applied to a single element in his study. Therefore, the application of these results is limited because the obtained local mine stiffness corresponds to a single element of that pillar, instead of the whole pillar.

Instead of numerically calculating the stiffness, some researchers used beam theory to estimate the roof stiffness. A laminated beam model under plain strain conditions, proposed by Salamon (1989), was used by Seedsman to calculate the roof stiffness (Seedsman and Hornby, 1991). His results showed that roof stiffness reached a minimum at the center of the panel and increased with the decreasing distance to the rib. The magnitude of the roof stiffness depends on the normalized beam thickness and the stiffness of the rib material. Roof stiffness at the panel center decreases with decrease of both the beam thickness and the rib stiffness. When the rib stiffness is very small, the change of the roof stiffness with the position in the panel becomes insignificant. Obviously, the stiffness determined by beam theory will depends on the thickness of the beam which usually is difficult to determine. Therefore, the stiffness varies significantly with the choice of beam thickness.

3.1.2.3 Determination of post-failure pillar stiffness

The most reliable method to determine the pillar stiffness would be to directly load the pillar to failure in the field and obtain the load-deformation curve for the pillar. Such measurements have been made by Bieniawski (1968), Cook (1971), Wagner (1974) and Heerden (1975), but these direct measurements can only be made on small size pillars (1 - 4 m) because of the limitations of equipment and cost.

Cook (1967) was the first to point out that a pillar in the field can be tested to obtain meaningful post-failure information as long as the end constraint and the stiffness of the loading equipment are carefully considered. He also presented a basic design for such a test. Based on this design, Bieniawski (1968) started a field pillar testing program in South Africa. Unfortunately, no post-failure information was obtained because of the low stiffness of the loading equipment.

With improved loading equipment, Cook (1971) conducted a demonstration field test in which field pillars were loaded to failure by numbers of hydraulic jacks, and the

complete deformation-load curves of the field pillars were obtained. The pillars had the cross-sections of up to 1.5 square meter.

Wagner (1974) conducted the first comprehensive field tests on pillars ranging from 0.6 to 2.0 m side length and width/height ratios from 0.6 to 2.2. The elastic modulus was found to be independent of the size or shape of the pillars, but the post-failure slope was found to be affected remarkably by the pillar width/height ratio. In fact, the post-failure slope decreases with the increasing width/height ratio, which indicates that the post-failure behavior is a structural or system property rather than an inherent material property.

Heerden (1975) reported the results from similar field testing. Pillars with cross-section 1.4 by 1.4 meter square and width/height ratios up to 3.5 were loaded to failure. The results agree very well with those obtained by Wager.

Wang (1976) obtained the post-failure slope of a field pillar in the Pocahontas No.3 seam, U.S.A., by monitoring the stress change in the pillar and the convergence around the pillar. The loading was increased by sequencially reducing the pillar size by mining.

Because of the difficulty in measuring the post-failure stiffness of squat pillars, efforts have also been made to relate laboratory specimen data to the limited field data and then to extrapolate this data to the larger size of pillars (Brady, 1980 and Ozbay, 1989). However, the extrapolation may be misleading and may lead to erroneous conclusions. For example, Ozbay concluded that a pillar with width/height ratio greater than 5 would have been excluded from bump failure, but it has been reported that even the pillars with a width-height ratio greater than 8 experienced bump failures (Babcock, 1984 and Campoli, 1990).

Starfield's test on marble specimens ranging from 0.5 to 2 width/height ratio also demonstrated that the post-failure slope decreases with increasing width/height ratio (Starfield, 1968).

Das (1986) reported a very interesting laboratory testing result from 54 mm diameter coal specimens in India. Coal specimens from four seam beds were tested. The result showed that the post-failure slope decreases as the width/height ratio increases. The post-failure slope is seen to become zero around a width/height ratio of 10 and becomes positive with further increase in width/height ratio, which indicates that at high width/height ratio the coal specimen initially loses strength after failure but then gradually

recovers strength with continuing straining. The specimens with width/height ratio 13.5 were seemingly unbreakable. The work by Das is significant because the width/height ratio reaches as high as 13.5, whereas most previously reported tests never went beyond 5. It is believed that the recovering of the strength is due to the repacking of the broken pieces of the specimen under high compression. However, this needs further investigation because the height of the specimen in his tests with width/height ratios 10 to 13.5 reached 4-5 mm which is already close to the grain size of the coal. Therefore, whether the repacking can occur in field condition is still not clear.

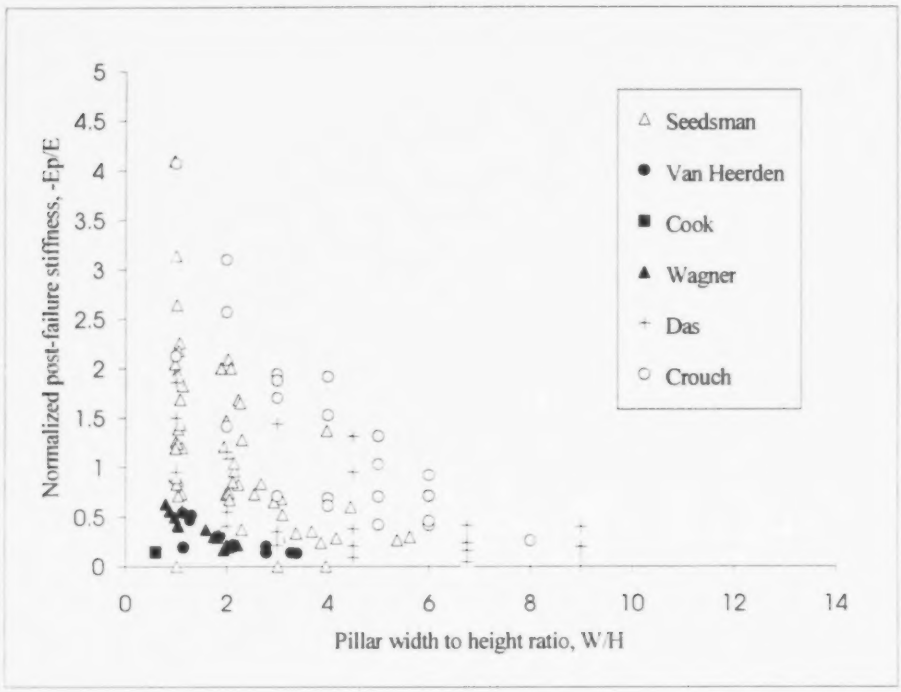

Figure 3.5

Field and laboratory data of the pillar post-failure stiffness.

A similar test was also conducted by Seedsman (1991) in Australia. The specimens were from a coal seam with width/height ratio up to about 6. The results were very similar to those obtained by Das. The post-failure slope is seen to become zero at around width/height ratio of 9.

The data from the researchers mentioned above is presented in figure 3.5. It is worth noting that most of the data are from the experiments on specimens with width/height ratio less than 5.

3.2 Conclusions

Currently, chain pillar design is mainly based on the ultimate strength consideration and the pillar bump problem is not considered, or is neglected in the design. This may either lead to an oversized pillar, which is a waste of the resources, or a yield pillar which is bump-prone.

Most analyses have been restricted to the two dimensional room-and-pillar cases and the longwall face advance has not been considered in those cases. Therefore, the application of these results is limited.

Although the local mine stiffness theory has been well established for a long time, there are only limited applications of this theory to practical mining problems, especially in three dimensional longwall cases. In this area, the most comprehensive work has been done by Zipf (1992). A three dimensional boundary program was used in his study. However, some of the conclusions he drew are questionable. One of these conclusions states that the moduli of roof and floor rock materials have a dominant effect on the local mine stiffness, but stress-strain properties of coal and mine geometry have almost no effect on the local mine stiffness. Based on this conclusion, mines with a strong roof and floor condition would have less bump problems than mines with a weak roof and floor, but from field investigations, coal mine bumps usually occur in the mines with coal beds sandwiched between strong roofs and floors (Campoli, 1990, Haramy, 1988 and Iannacchione, 1991). Because of this contradiction, Zipf further concluded that the local mine stiffness approach cannot be used to evaluate bump failure. Therefore, there is controversy in the application of the local mine stiffness concept to solve the pillar bump problem. Further study and clarification are clearly needed.

Chapter 4

PRELIMINARY STUDIES

4.1 Introduction

According to the theory proposed by Salamon (1970), the magnitudes of the local mine stiffness and pillar post-failure stiffness define the stable or violent failure of the pillar. While the post-failure stiffness of a pillar may change with the deformation of the pillar, the local mine stiffness may also change if the configuration of the panel changes significantly during the mining. Because in longwall mining the chain pillars usually have the same shape and size, they will behave similarly in pre-failure and post failure regions; this implies a constant minimum post-failure stiffness for all the pillars in the panel. The occurrence of pillar bumps for different pillars in the panel might totally depend on the difference in local mine stiffness for these pillars. Therefore, the examination of the difference and change of the local mine stiffness with the change of the panel configuration, pillar behavior and coal excavation is very important in evaluation of pillar stability in longwall mining.

From Salamon's derivation, the local mine stiffness depends on the strata modulus, which is constant for a specific strata, pillar configuration and the behavior of the pillars in the panel. In a longwall panel, although the chain pillars usually are not excavated, a large area of coal in the panel, which supports the overburden, is extracted gradually. Therefore, it is expected that the extraction of the coal, which is represented by the advance of the longwall face, will have significant effect on the local mine stiffness.

A typical longwall model would consist of a current panel with an excavated panel on the one side which is gob, and an intact panel on the other side. The panel should be long enough to eliminate the effect of the model ends on the stress and displacement calculation for the chain pillars in the middle of the panel. Because of the tabular characteristics of coal beds and the three dimensional characteristics of longwall face advance, the displacement discontinuity boundary element program developed by US Bureau of Mines (Zipf, 1992) was chosen to simulate longwall mining and to perform the local mine stiffness calculation.

4.2 Introduction to MULSIM/NL

MULSIM/NL is a three dimensional displacement discontinuity boundary element computer program which is specifically suitable for analyzing the stress and displacement of tabular, multiple seams in elastic and homogeneous surrounding rock.

The basis of the program is the analytical solution of the problem of constant discontinuity in displacement over a square source plane area in the infinite solid elastic medium given by Rongved (1957). This solution was first introduced by Salamon (1967) into the mining problems of flat seams as the "face element" method. The solution is presented by Sinha (1979) as :

$$\begin{aligned} \sigma_z &= aS_z \\ \tau_x &= bS_x + cS_y \\ \tau_y &= dS_x + eS_y \end{aligned} \tag{4.1}$$

where a, b, c, d, and e are influence functions depending on the material properties of the host medium and the spatial coordinates (Starfield, 1972); S_x, S_y and S_z are constant displacement discontinuities applied on a square source element and σ_z, τ_x, τ_y are the induced stresses over the square field elements. Here S_x, S_y and S_z are relative movements between upper layer $z = 0_+$ and lower layer $z = 0_-$ of the square element and are defined by:

$$\begin{aligned} S_x &= u_- - u_+ \\ S_y &= v_- - v_+ \\ S_z &= w_- - w_+ \end{aligned} \tag{4.2}$$

where u, v and w are the displacements of the element; positive and minus subscripts represent the upper layer and lower layer of the element respectively as shown in figure 4.1. S_z is usually referred to as convergence or closure. S_x and S_y are referred to as rides. For conciseness, the relative displacements S_x, S_y and S_z will simply be referred to in the following sections as displacements or closure unless otherwise specified. The derivation of equation (4.1) is attached in appendix A.

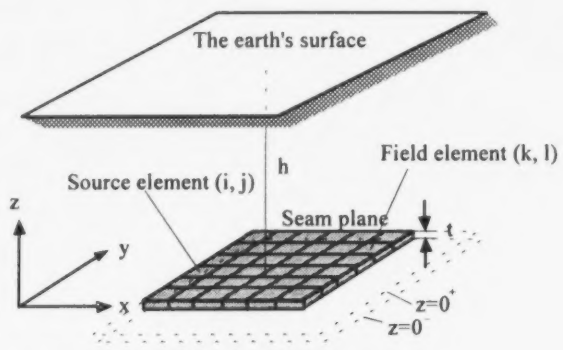

Figure 4.1

Boundary elements of seam plane in surrounding rock mass.

To solve the displacement discontinuity problem in a seam, the tabular seam is divided into N square elements as shown in figure 4.1 and the displacement discontinuities are taken to be constant over each element. Equation (4.1) indicates that displacements discontinuities (S_x, S_y and S_z) occurring at the field square element lk, will lead to the corresponding stress changes (σ_z, τ_x, τ_y) occurring in the source element ij. The effects of the N square field elements on the source element ij are summed according to the equations (4.1) from 1 to N. This leads to a system of 3N equations with 6N unknowns. The 3N additional equations needed to solve this problem are generated from the following boundary conditions.

(1) For the mined-out elements or open elements, the element stresses are zero and the boundary conditions are:

$$\begin{aligned} \sigma_z &= 0 \\ \tau_x &= 0 \\ \tau_y &= 0 \end{aligned} \qquad (4.3)$$

(2) For the intact linear elastic elements, the element stresses are equal to the induced stresses and the boundary conditions are:

$$\sigma_z = E_s \frac{S_z}{t}$$
$$\tau_x = G_s \frac{S_x}{t} \qquad (4.4)$$
$$\tau_y = G_s \frac{S_y}{t}$$

where E_s and G_s are the Young's modulus and shear modulus of the elements and t is the element thickness. Equation (4.4) represents the linear elastic boundary condition. It is straight forward to implement other non-linear elastic elements into the boundary conditions which can simulate the strain hardening or strain softening behavior of the elements.

In MULSIM/NL six types of elements can be used. They are linear elastic, strain softening and elastic-plastic elements for coal, and linear elastic, strain hardening and bi-linear hardening elements for the gob material, from which 26 types of materials can be simulated. The six models are presented in figure 4.2. In these models, the strain softening model for coal is especially important because the coal is generally recognized as strain softening material. The strain softening of pillar elements poses the potential danger of the pillar bumps, as illustrated by the stiffness theory mentioned previously.

The MULSIM/NL uses a 26 by 10 array called EPROP to store parameters used by the six stress-strain material models. The program permits the use of up to 26 different materials, labeled A though Z which can be any one of the six models in figure 4.2. EPROP uses its columns 1 to 6 to store the material parameters. The columns 7 to 10 are vacant for future development. Table 4.1 shows the required parameters and their location in EPROP for the six material models.

The shear modulus is given by the equation:

$$G = \frac{E}{2(1+\mu)} \qquad (4.5)$$

It is assumed in MULSIM/NL that equation (4.5) holds for all the models no matter what the stress range in the models. This is a simplification for the non-linear materials

due to the lack of the knowledge of the shear modulus for these materials. Nevertheless, the value of G will have no effect on the resulting stresses and displacements if the seam is horizontal.

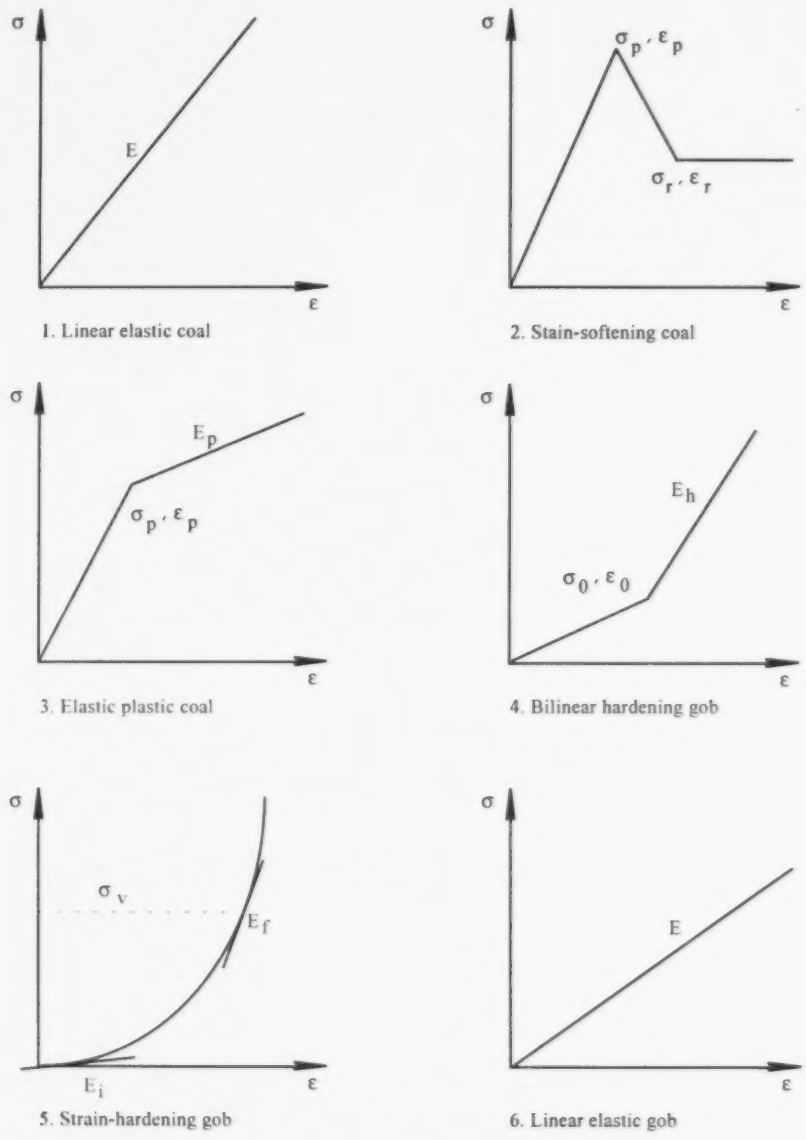

Figure 4.2

Material models available in MULSIM/NL program (after Zipf, 1992).

Table 4.1 The structure of material array EPROP (after Zipf, 1992).

Model	1	2	3	4	5	6
1	Linear elastic coal	Young's modulus (E)	Shear modulus (G)	NAp	NAp	NAp
2	Strain softening coal	Peak stress (σ_p)	Peak strain (ε_p)	Residual stress (σ_r)	Residual strain (ε_r)	Poisson's ratio (μ)
3	Elastic-plastic coal	Peak stress (σ_p)	Peak strain (ε_p)	Plastic modulus(E_p)	Poisson's ratio (μ)	NAp
4	Bilinear hardening gob	Offset stress (σ_0)	Offset strain (ε_0)	Hardening modulus(E_h)	Poisson's ratio (μ)	Gob height factor (n)
5	Strain hardening gob	Initial modulus(E_i)	Final modulus(E_f)	Final stress (σ_v)	Gob height factor (n)	Poisson's ratio (μ)
6	Linear elastic gob	Young's modulus (E)	Shear modulus(G)	Gob height factor (n)	NAp	NAp

NAp - Not applicable.

The gob height factor (n) has value of 1 to 6 and is used to reduce the gob material modulus in compensation for the effect of the possible fracturing and collapse of the gob roof.

The Gauss-Seidel iteration scheme is used to solve the system. An additional restriction is applied which requires the maximum closure of the element to be no greater than the seam thickness. The maximum of 50 by 50 coarse mesh blocks can be used in MULSIM/NL, from which 30 by 50 coarse mesh blocks can be further divided into 150 by 150 fine mesh elements to give the detailed results.

Multiple seam layers and multiple mining steps can be handled in MULSIM/NL simulation. The longwall face advance can be conveniently simulated by using the MULSIM/NL's multiple mining step simulation feature. The local mine stiffness evaluation can also be easily incorporated into the program because of this feature.

4.3 Assumptions and limitations of MULSIM/NL

There are some important assumptions and limitions about MULSIM/NL which should be borne in mind, whenever the program is used.

4.3.1 Elastic strata

The basic analytical solution assumes the surrounding strata are linear elastic; inelasticity is restricted to the seam bed. As mentioned before, bump-prone coal beds are identified as beds with a stiff roof and floor. Therefore, the elastic assumption of the stiff roof and floor would be reasonable in this study. The failure and yielding of the elastic roof or floor cannot be simulated in the study, but the effect of the roof failure and collapse in the gob area can be compensated for by assigning a reduced modulus to the gob material. As generally accepted, coal is apparently not an elastic material. Assuming inelastic behavior of the coal pillars and coal beds would be logical.

4.3.2 Effect of confinement

The displacement discontinuity theory assumes the thickness of the beds is negligible compared to the transverse dimension. This leads to the absence of horizontal stress between the "in seam" elements. Although it will unlikely affect the general distribution of the stress and displacement , the stress and displacement calculation for an individual pillar may not be correct without considering the horizontal confining stress between the elements of the pillar. Fortunately, an artificial way of assigning different material properties to the pillar elements, according to the distance from the pillar periphery to the pillar core can be applied to simulate the effect of confining pressure. However, the assignment of different material properties increases the complexity of the model.

4.4 Structure of MULSIM/NL and its modification

The MULSIM/NL program can be used directly to simulate multiple longwall mining sequences, but the calculation of the local mine stiffness cannot be done without modification to integrate the Starfield's perturbation method into the program. The perturbation method requires that, for a specific pillar in an equilibrium state with the strata, a unit deformation can be applied at the interface of the pillar and the strata and the resulting load change on the pillar can be obtained.

A simplified flowchart of MULSIM/NL is shown in figure 4.3. MULSIM/NL first reads the input model control parameters and calculates influence coefficient matrix. For every mining step, after it reads coarse and fine mesh patterns and initializes the stress and displacement arrays, the program iterates for the equilibrium. When the equilibrium is reached, the stresses and displacements for every element are stored.

4.4.1 Zipf's modification

Zipf (1992) demonstrated that an unit deformation can be applied on a element which may represent a pillar or a part of the pillar in MULSIM/NL program. The local mine stiffness was defined by the ratio of the associated load on the perturbed element over the perturbing deformation. His modification is also presented in figure 4.3.

Zipf simply added a LMS loop which specifies the increase of displacement for a LMS element after the first equilibrium of every mining step was established, and then iterates for the new equilibrium. It is obvious that Zipf's modification can calculate the local stiffness for a selected element, which results in the local mine stiffness for an individual element, but not for a pillar if the pillar consists of a numbers of elements, which is usually the case for the most of the longwall mining simulations. It is also believed that Zipf's element perturbation method may be one of the reasons why the local mine stiffness he obtained is not sensitive to the change in the pillar configuration and the location in the panel.

4.4.2 Definition of the local mine stiffness

The intent of this research is to derive the local mine stiffness for pillars, which can be compared with the available field measured or derived pillar post-failure stiffness, so as to examine the possibility of applying local mine stiffness to control pillar bumps and to improve the chain pillar design in longwall mining under the bump-prone coal bed condition. Therefore, all elements of a pillar should be perturbed by a constant uniform deformation across the pillar section. The local mine stiffness is defined as the ratio of the uniform strain perturbation over the average associated stress difference on the pillar. However, for easy comparison with material modulus, the local mine stiffness is redefined as the ratio of the average associated stress difference on the pillar over the uniform strain perturbation, which has the units of modulus, i.e.:

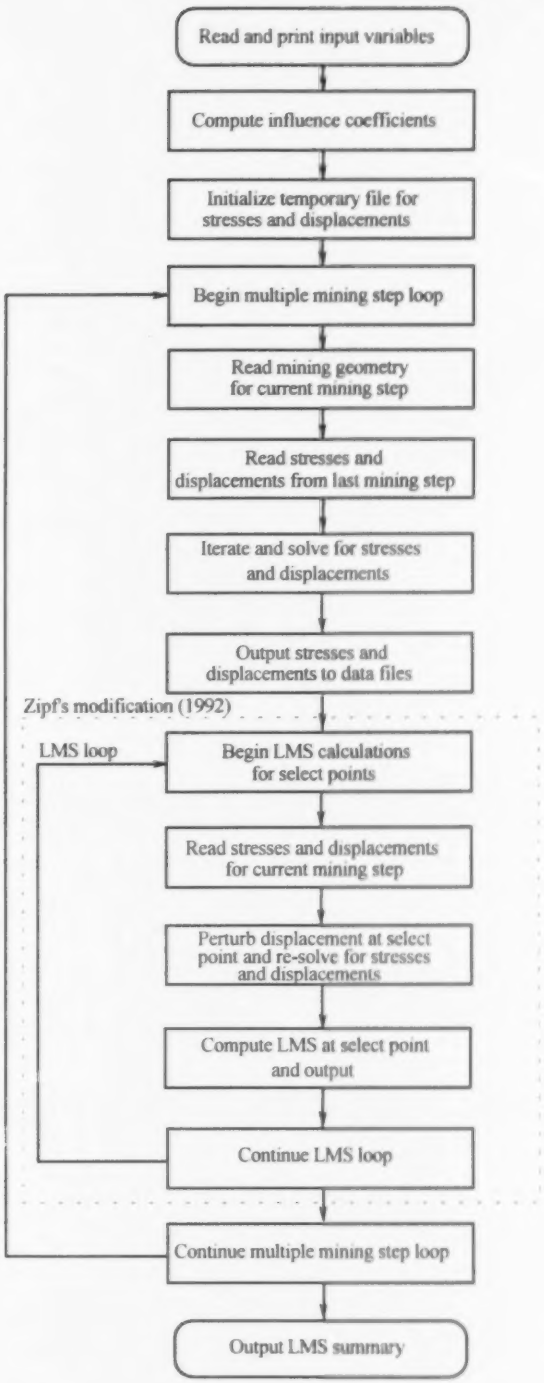
Read and print input variables
Compute influence coefficients
Initialize temporary file for stresses and displacements
Begin multiple mining step loop
Read mining geometry for current mining step
Read stresses and displacements from last mining step
Iterate and solve for stresses and displacements
Output stresses and displacements to data files
Zipf's modification (1992)
LMS loop
Begin LMS calculations for select points
Read stresses and displacements for current mining step
Perturb displacement at select point and re-solve for stresses and displacements
Compute LMS at select point and output
Continue LMS loop
Continue multiple mining step loop
Output LMS summary

Figure 4.3

Structure of MULSIM/NL and Zipf's addition of local mine stiffness calculation at a selected point (after Zipf, 1992).

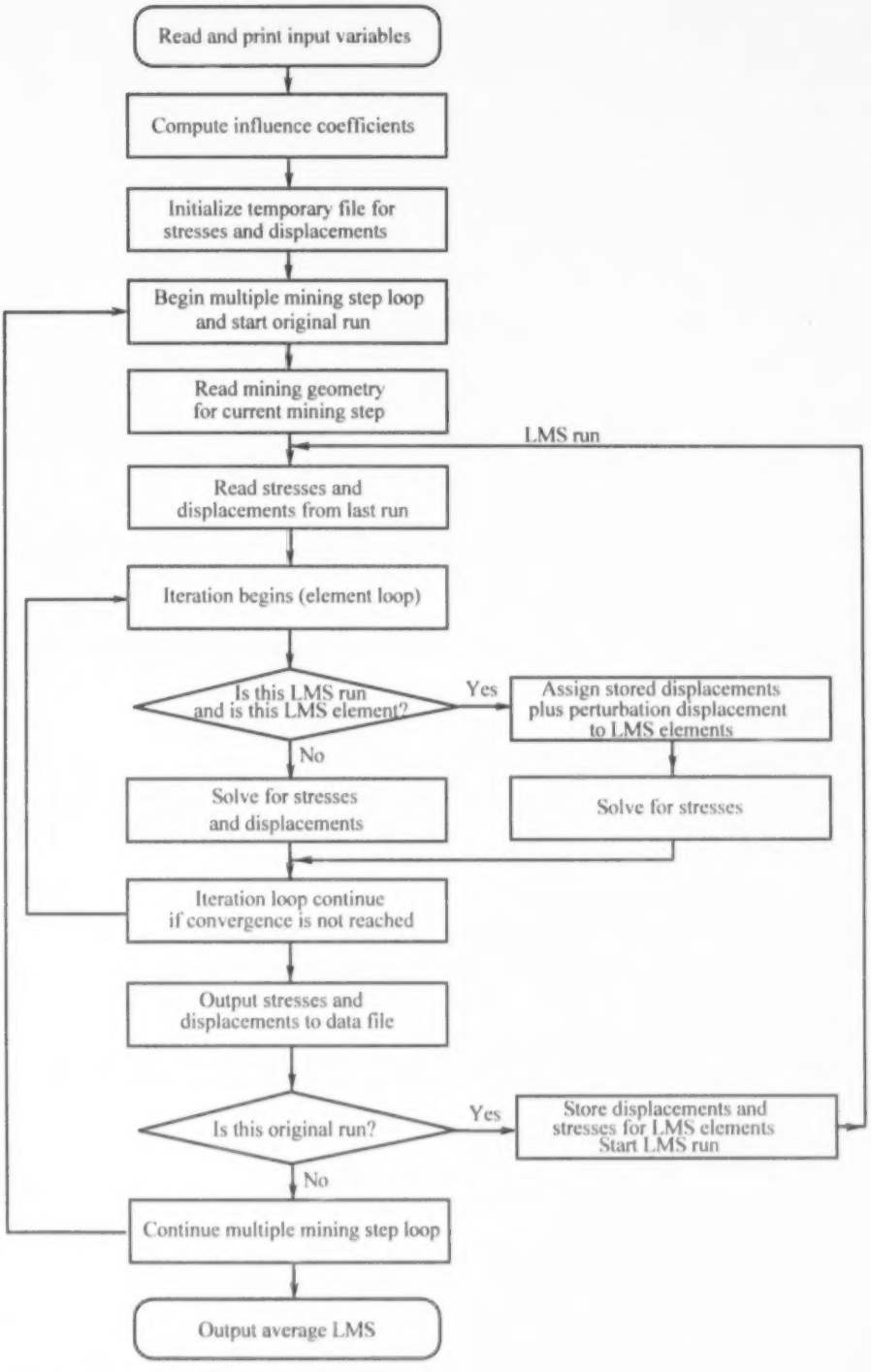
Read and print input variables
Compute influence coefficients
Initialize temporary file for stresses and displacements
Begin multiple mining step loop and start original run
Read mining geometry for current mining step
LMS run
Read stresses and displacements from last run
Iteration begins (element loop)
Is this LMS run and is this LMS element?
Yes
Assign stored displacements plus perturbation displacement to LMS elements
No
Solve for stresses and displacements
Solve for stresses
Iteration loop continue if convergence is not reached
Output stresses and displacements to data file
Is this original run?
Yes
Store displacements and stresses for LMS elements Start LMS run
No
Continue multiple mining step loop
Output average LMS

Figure 4.4

The flow chart of the modified MULSIM/NL for LMS calculation of a pillar.

$$LMS = \frac{\sum_{i=1}^{n} \Delta p_i}{\frac{S}{\frac{\Delta c}{H}}} \qquad (4.6)$$

where LMS represents the local mine stiffness of a pillar which consists of n square elements; Δc is the uniform perturbation closure applied on the pillar elements; Δp_i are the associated load changes of the pillar elements; H and S are the pillar height and pillar cross section area respectively.

4.4.3 Implementation of local mine stiffness calculation

In a similar manner to Zipf's point perturbation method, the MULSIM/NL program was modified by the author to perturb all elements of a pillar so as to obtain the averaged local mine stiffness for the pillar. Note the modified program can handle pillars with shapes other than a square shape. The flow chart of the modified program is also presented in figure 4.4 to compare with that of Zipf.

To implement Starfield's perturbation method, the multiple mining simulation capacity was modified to provide the necessary displacement disturbance after the first equilibrium was reached; the 10th column of the element material property matrix EPROP, which is not used by MULSIM/NL, was employed to specify the pillar elements on which the perturbation is to be applied. Those elements are referred as the local mine stiffness elements, or LMS elements.

The program first solves for the displacements and stresses for a model under the first equilibrium for the original boundary conditions. The displacements of the specific pillar elements (i.e. the LMS elements) are stored in a temporary array for use in the next run of the program. Then the exciting uniform displacement is added to the stored LMS element displacements. The resulting pillar element displacements, combined with the original boundary conditions, are applied as the new boundary conditions to the model and the program restarts as the LMS run, solving for the new equilibrium.

After the new equilibrium is reached, the associated stress difference on the pillar from the displacement perturbation was averaged over the elements of the pillar, and

then divided by the perturbation strain (perturbation displacement divided by the pillar height) to obtain the local mine stiffness. Note that for convenience, the final output of local mine stiffness for the pillar was defined by the ratio of the average stress difference over the perturbation strain as shown by equation (4.6), instead of the load difference over the perturbation displacement. The process is repeated for each mining step. The local mine stiffness changes during longwall face advance are obtained.

4.5 Verification of the program

Although the implementation of the local mine stiffness into the MULSIM/NL program is straight forward, a simple case analyzed by Salamon (1970) is chosen to check the validity of the modified program. A mining panel with five infinite long strip pillars and six rooms is shown in figure 4.5. Assuming plain strain conditions, Salamon provided the analytical solutions of the influence matrix, the inverse of which is the strata stiffness. Ozbey (1989) demonstrated that "influence matrix can be obtained by numerical techniques using boundary-element computer program: the elements occupying the jth pillar area are excited by a field force P_j on the assumption that there are no other pillars present in the layout. The convergence induced at all the pillar locations are first divided by P_j and then recorded as the jth column of the influence coefficient matrix. The other elements of the influence coefficient matrix are determined by a repetition of the same procedure at other pillar locations in the layout".

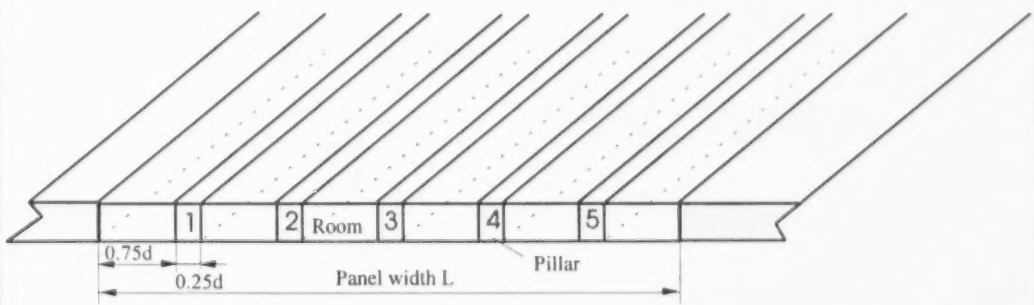

Figure 4.5

Salamon's infinitely long strip pillars case (1970)

First, the method proposed by Ozbey is verified by applying a two-dimensional boundary program (Hoek, 1980) to Salamon's case shown in figure 4.5. The panel

consists of five infinitely long rib pillars under the infinite depth which can be treated as a two dimension case. Assuming plain strain conditions, Salamon analytically derived the influence coefficient matrix with respect to the five strip pillars (1970). The result is presented in table 4.2.

Table 4.2 Influence coefficient matrix c_{ij} obtained by Salamon (1970).

j th\ ith	1	2	3	4	5
1	1.2270	0.4497	0.2870	0.1928	0.1152
2	0.4517	1.3980	0.5474	0.3362	0.1933
3	0.2880	0.5478	1.4392	0.5447	0.2880
4	0.1933	0.3362	0.5474	1.3980	0.4517
5	0.1152	0.1928	0.2870	0.4497	1.2270

Table 4.3 Influence coefficient matrix c_{ij} obtained by author.

j th\ ith	1	2	3	4	5
1	1.254	0.433	0.299	0.187	0.112
2	0.448	1.418	0.522	0.336	0.187
3	0.261	0.522	1.455	0.522	0.261
4	0.187	0.336	0.522	1.418	0.448
5	0.112	0.187	0.276	0.433	1.254

The dimensions d and L in figure 4.5 are specified as 20 m and 115 m. The Young's modulus and Poisson's ratio are 7000 MPa and 0.25, respectively. The unit perturbation load is applied twice at the pillar locations 1 to 5 respectively, and the associated deformation differences at the five pillar locations were recorded. Note when there is only one pillar in the layout, the local mine stiffness is equivalent to the strata stiffness for the

pillar location. The obtained influence coefficient matrix is presented in table 4.2. The influence coefficients in tables 4.2 and 4.3 are normalized with respect to the factor $\Omega = 4(1 - \mu^2)/E$, where μ and E are the Poisson's ratio and Young's modulus (in GPa) of the strata respectively. Comparing Salamon's table 4.2 with table 4.3 shows that there is only an insignificant difference between the two tables. This confirmed that Ozbey's numerical method works well.

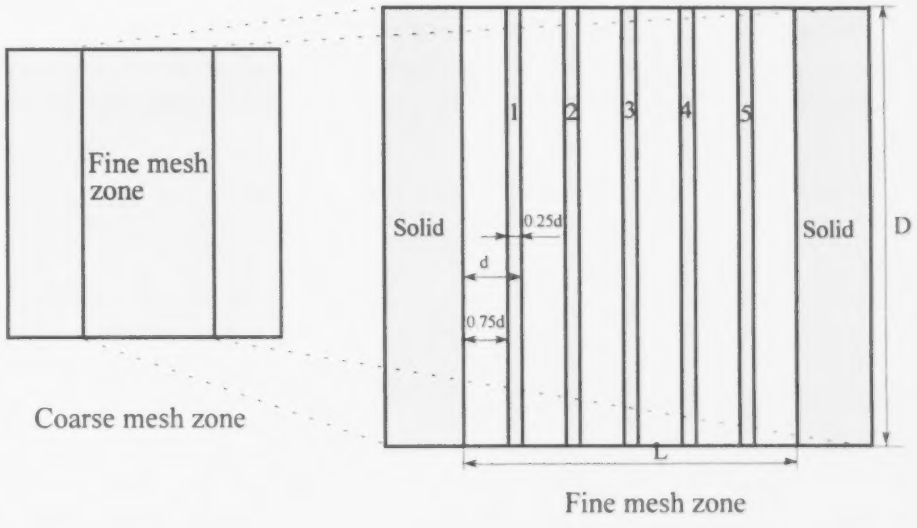

Figure 4.6

Model for Salamon's example case with fine mesh element 5×5 m and coarse mesh block 25×25 m.(d = 20 m, L = 115 m, D = 125, 250, 375, 500, 625, and 750 m).

Clearly, the only difference of the local mine stiffness calculation in the modified MULSIM/NL program from the Ozbey's method is that the exciting source in the modified MULSIM/NL program is the displacement, instead of the force. Although the force exciting is easier to implement into the boundary program than the displacement exciting, the latter was chosen because (1) the unit displacement disturbance across the pillar is more likely to occur than the unit force disturbance across the pillar in the wide pillar cases, due to the yielding of the part of the pillar; (2) most of the available measured post-failure pillar stiffness data were measured with a uniform deformation condition. Therefore, the results from the displacement excitation are believed to be closer to what occurs in the field. There is no difference between force perturbation and displacement perturbation theoretically if only element perturbation is used. However,

because the stress and strain of the perturbation pillar are not uniform for the multi-elements perturbation as the author proposed, a small discrepancy may occur in the results from the two perturbation methods (Salamon, 1970).

Salamon's case was further tested by applying the modified MULSIM/NL to calculate the influence coefficient matrix. The coarse mesh and fine mesh of the model are presented in figure 4.6. The material parameters are presented in table 4.4. Both the strata and the pillars are assumed to be the same material and are linear elastic (labeled by A), but the 10th column of the material array for pillar is assigned a positive value which indicates that the pillar elements (labeled by B) are to be excited for LMS calculation.

Table 4.4 Material parameters array EPROP for Salamon's example.

Model	1	2	3	4	5	6	10	Comment
1	Linear elastic coal	7500 (psi)	2800 (psi)				0	Strata, seam and pillar (A)
1	Linear elastic coal	7500 (psi)	2800 (psi)				1	Pillar element to be excited (B)

The five strip pillars are excited separately. The length of the panel is varied. It is expected that with the increase of the panel length, the influence coefficients obtained by the modified program for the three dimensional case would approach Salamon's two-dimensional solutions, because of the approximation to the plain strain condition when the panel length is extended. For simplification, only the influence coefficients c_{ii} at the five pillar locations were calculated and are compared in figure 4.7 with the diagonal terms of the influence matrix obtained analytically by Salamon in table 4.2.

The calculated local stiffness is compared to the analytical results given by Salamon (1970). Figure 4.7 shows the normalized influence coefficients obtained from the model as the length of the panel increases. It appears that, as the panel length increases, the model results converge to a specific shape curve which is similar to Salamon's analytical solution for an infinitely long panel. However, the model results apparently slightly over shoot Salamon's result. This difference is believed to come from three sources: (1) the difference between the plain strain condition for Salamon's model and the three dimensions condition for MULSIM/NL model. The effect of the boundary of the limited length panel for the three dimension model may affect the result; (2) MULSIM/NL's

inherent treatment of the uncoupled boundary stresses is liable to overestimate the displacement (Sinha, 1979); (3) the numerical error arising from the discretizing the seam plane and the approximate iteration scheme of MULSIM/NL.

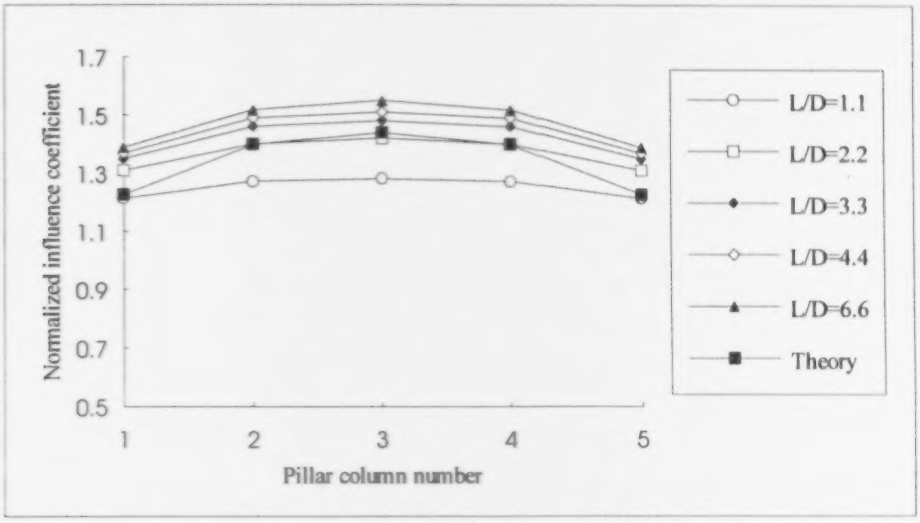

Figure 4.7

Comparison of the modified MULSIM/NL's results with analytical solutions.

Nevertheless, figure 4.7 still shows that the program gives reasonable convergence to the solution with the increase of the panel length. The legitimacy of the program is further demonstrated by the longwall simulation exercises in the next chapter.

4.6 Conclusion

The Starfield's perturbation concept was used to determine the local mine stiffness. The numerical method proposed by Ozbey (1989) was tested against the theoretical solution derived from a five strip pillar model proposed by Salamon (1970). The results show that very good agreement with Salamon's results was obtained by the perturbation method. The perturbation method was implemented into the MULSIM/NL program. The application of the program to Salamon's two-dimensional model show a reasonable agreement and convergence, while a slight overshooting of displacement discrepancy was also noticed.

Chapter 5

EXAMINATION OF LOCAL MINE STIFFNESS

5.1 Introduction

It is expected that the change of the longwall layout will affect the local mine stiffness. To investigate the significance of the effect of the longwall layout, an elastic model is set up in which the strata, pillar and gob material are all assumed to be elastic. Assuming elastic properties will eliminate the effects of the other factors such as pillar strain softening and gob hardening on the local mine stiffness.

The effect of the elastic moduli of the strata and the seam, softening behavior of coal, location in the panel, overburden and pillar configuration will be further examined by building non-elastic models with different pillar configurations and different overburdens.

5.2 Elastic model

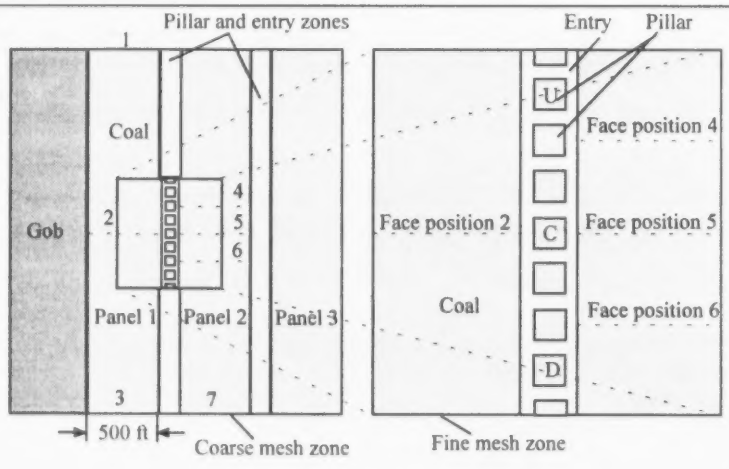

Figure 5.1

Testing elastic longwall panel layout and mining sequence.

The modified program has been further tested by application to a simplified longwall model shown in figure 5.1. The model is totally elastic. The surrounding rock, coal seam and gob are all assumed to be linear elastic with an overburden of 500 ft (150 m). The

Young's modulus and Poisson's ratio for strata are 900000 psi (6205.5 MPa) and 0.25. The elastic properties for the in seam materials are shown in table 5.1. The more detailed input parameters, mesh configurations and output are included in appendix B.1

The coarse mesh (50×50 ft (15×15 m) block size) covered four longwall panels, one of which is already mined out and filled with linear elastic gob material. The thickness of the seam is specified as 6 ft. The panel width and length are 500 ft (150 m) and 2500 ft (750 m) respectively. The fine mesh zone (10×10 ft (3×3 m) element size) covered 800 ft by 800 ft (240 m by 240 m) area of the coarse mesh zone with one row of chain pillars in the middle. The pillar has square shape with a width of 80 ft (24 m).

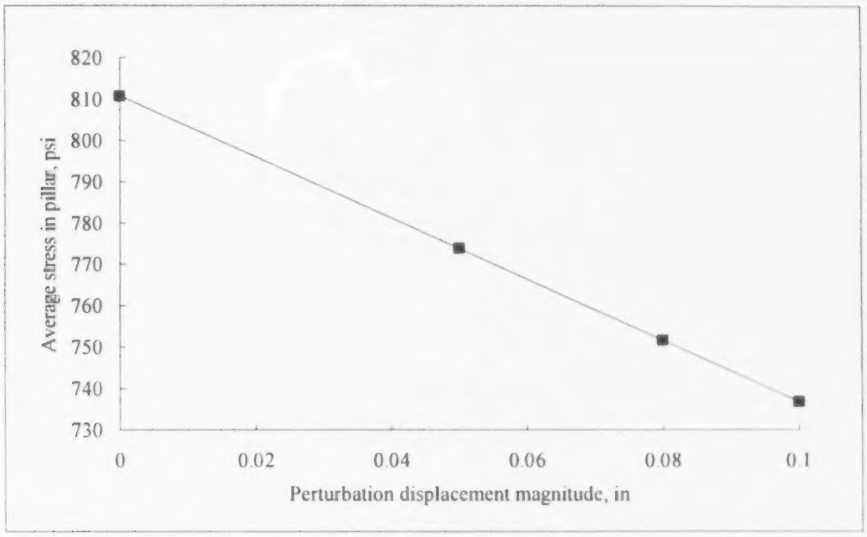

Figure 5.2

Linear relation of the perturbation displacement magnitude and resulting stress.

The local mine stiffness at pillar C is first checked to ensure the accuracy of the program. It is expected that with the linear property of the strata and seam, the local mine stiffness value at the pillar location should not be affected by the perturbation magnitude, i.e., the relation of the perturbation displacement to the resulting stress in the pillar should be linear, no matter what magnitude of the perturbation displacement is used.

Figure 5.2 demonstrated that a linear relation exists between the perturbation displacement and the resulting stress in the pillar. This further verified that the implemented local stiffness calculation works correctly.

Table 5.1 Material parameters array EPROP for elastic model.

Model	1	2	3	4	5	6	10	Comment
1	Linear elastic coal	500000 (psi)	217000 (psi)				0	Seam (A)
6	Linear elastic gob	5000 (psi)	1790 (psi)	1			0	Gob (B)
1	linear elastic coal	275000 (psi)	119000 (psi)				0	Pillar and entry zone (C)
1	Linear elastic coal	500000 (psi)	217000 (psi)				1	LMS element (E)

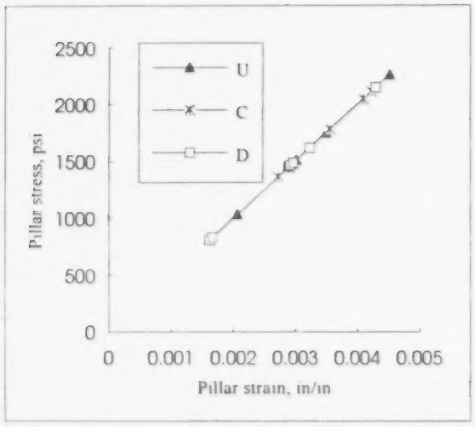

(A) Averaged stress-strain relation.

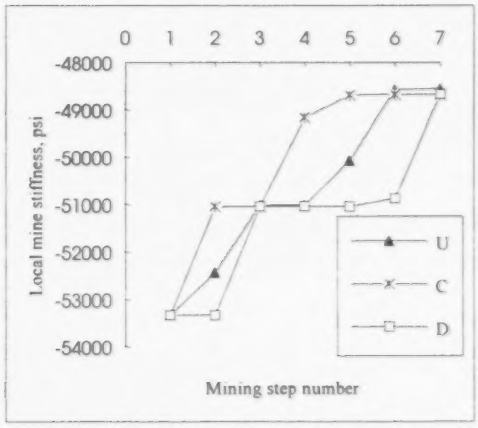

(B) Local mine stiffness vs mining step number.

Figure 5.3

Local mine stiffness change with the advance of longwall face.

The change of local mine stiffness at the middle pillar locations U, C and D is calculated through the seven mining steps and represented in figure 5.3. The recovery of two panels adjacent to the chain pillars is simulated by seven consecutive mining steps. The changes of normal stress and closure with the face advance are presented in the appendix D (figure D.1 and D.2).

It is obvious from figure 5.3 that the local mine stiffness decreases with the advance of the longwall face. The greatest change of the local stiffness coincides with the position where the face is close to or in the line with the test pillar location during the mining of the first and the second panels. This indicates that the critical condition for pillars to bump occurs when face is very close or in the line with the pillar. Because this model remains elastic through the mining simulation, the change in local mine stiffness represents the effect of geometry change, i.e., longwall face advance.

5.3 Non-elastic models

A more detailed study has been carried out to determine if other factors, i.e. the ratio of the surrounding rock modulus to the coal modulus, the non-linear behavior of the coal, the location in the panel and the configuration of the chain pillars, will affect the changes in the local mine stiffness.

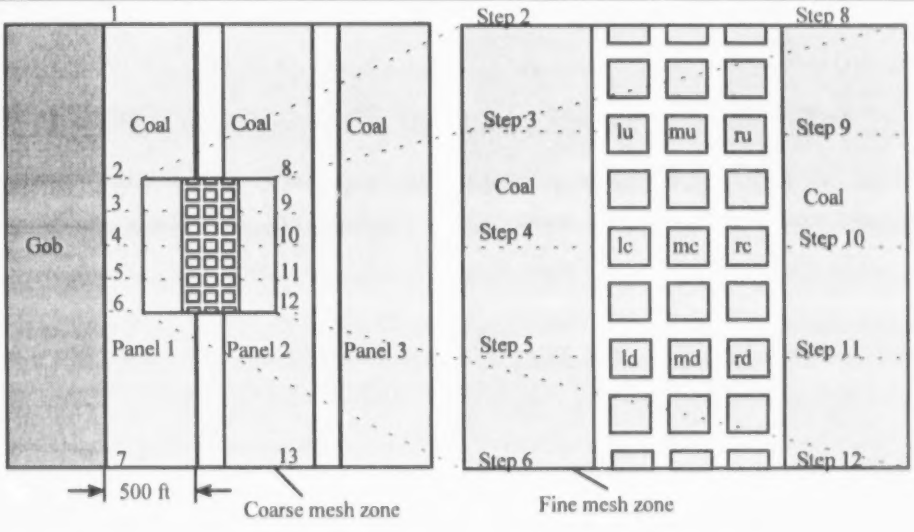

Figure 5.4

Non-elastic model with equal size of chain pillars.

A model with four entries and three columns of chain pillars was setup. The coarse mesh is similar to the elastic model, but the fine mesh is varied to represent different pillar configurations. The fine mesh configuration of the non-elastic model is presented in figure 5.4, which has three rows of chain pillars with equal size of 80×80 ft (24×24 m).

The detailed fine and coarse meshes, input parameters and output for the model is shown in the appendix B.2. The rock and gob remain elastic with Young's modulus 145000 psi (999.8 MPa) and 2900 psi (20 MPa) and Poisson's ratio 0.25 and 0.3 respectively. The coal in the coarse mesh is also assumed to be elastic. However, the coal in the fine mesh area is specified as strain-softening material. The in seam material parameters are presented in table 5.2.

Table 5.2 Material parameters array EPROP for strain softening coal.

Model	1	2	3	4	5	6	10	Comment
2	Strain softening coal	2900 (psi)	0.01	1450	0.015	0.3	0	Seam and pillar in fine mesh (A)
6	Linear elastic gob	2900 (psi)	1160 (psi)	1			0	Gob (B)
2	Strain softening coal	1800 (psi)	0.01	899 (psi)	0.015	0.32	0	Pillar and entry zone (C)
1	Linear elastic coal	290000 (psi)	116000 (psi)				0	Seam in coarse mesh (D)
2	Strain softening coal	2900 (psi)	0.01	1450 (psi)	0.015	0.3	1	LMS element (E)

The residual stress is varied, while the residual strain is maintained, to simulate different post-failure coal stiffness. The overburden is varied to investigate the change of the local mine stiffness with different failure stages. The pillar configuration is also varied to investigate the effect of pillar configuration on the local mine stiffness. The detailed mesh configuration and input parameters are included in appendix B.3. For all models, the mining is simulated in 13 consecutive mining steps as shown in figure 5.4. The stress and closure changes with the face advance are included in appendix D, which clearly show that the stress initially builds up around the boundary of the pillars and gradually migrates into the core part of the coal until the pillars have totally yielded.

5.3.1 Effect of pillar location

The local mine stiffness at nine locations in figure 5.4 were monitored throughout 13 mining steps. These locations are labeled by two characters. The first character l, m or r represents column position (left, middle and right) of chain pillars, and the second letter u, c or d represents position within the same pillar column (up, central and down) as labeled in figure 5.4. For example, pillar position lc represents the pillar position in the center of the left pillar column. These positions are chosen to investigate if the local mine stiffness is affected by the location in the panel. Within the fine mesh, the face advances 200 ft (60 m) for every mining step.

(1) Within pillar columns

It was expected that because of the great length of the longwall panels and the similarity of the loading history of the pillars along the chain pillar direction, the local mine stiffness should not be affected by the location along the chain pillars in the panel, except those locations which were very close to the two ends of the panel.

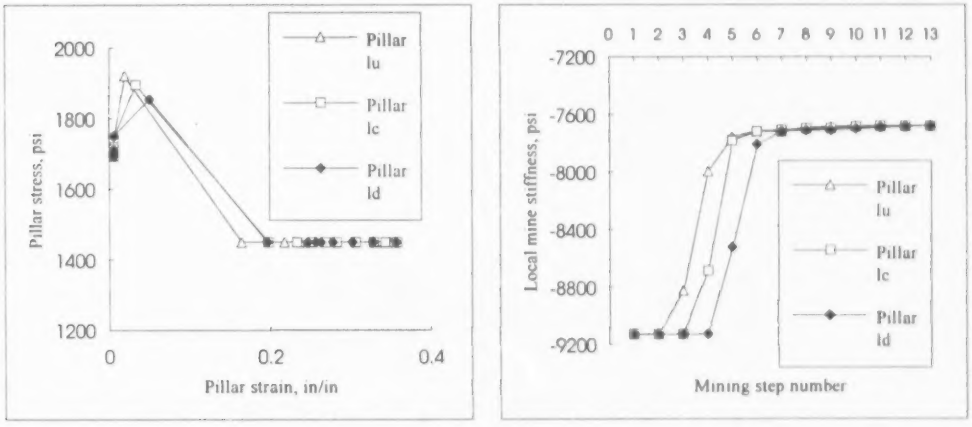

(A) Averaged stress-strain relation.

(B) Local mines stiffness vs mining step number.

Figure 5.5

Changes of stress, strain and local mine stiffness with the face advance within pillar columns.

The change of stress, strain of the nine pillars and the change of the local mine stiffness of the nine pillar locations with the face advance are presented in figures C.1 to

C.10 of appendix C. Figure 5.5 shows the reaction of the three pillars within the left pillar column with 750 ft (225 m) overburden. The change of the stress, strain and local mine stiffness for pillar lu, lc and ld are very similar, except that the change of strain, stress and the local mine stiffness took place ahead of each other for about one mining step. When the face is in the line with the pillars, the strain jumps and stress curve takes a dive into the residual stress range, which indicates total yielding of the pillars. The local mine stiffness decreases (absolute value) with the face advance for all pillar locations. The initial and final local mine stiffness for the three pillars are the same, i.e. from -91295 psi to -76795 psi (-629.5 MPa to -529.5 MPa).

Based on figure 5.5 and similar figures in Appendix C, it can be concluded that the locations along the entry direction really do not affect the behavior of the pillars, because all rows of the three pillars show the same strain, stress and local mine stiffness change pattern. Take the left pillar column for example, the only difference for pillar lm and ld is that the reaction of the pillar lm is ahead of pillar ld by one mining step, because the face approaches pillar lm one mining step ahead of pillar ld. This is significant because it eliminates the need to check every pillar within the same pillar column in the panel to evaluate the stability of the pillars. It is also because of this, that the following discussion only deals with the one row of three pillars in the middle of the panel.

(2) Cross pillar rows

The locations across the chain pillars might have some effect on the local mine stiffness because the tailgate pillar, the headgate pillar and the pillar in between have different loading patterns. The stress on the headgate pillar is mainly affected by the first longwall face passing. The tailgate pillar is affected by both the first and the second longwall face passing. Therefore, the stress and displacement on the tailgate pillar and headgate pillar are usually not uniform across the pillar. However, because of the support of the tailgate and headgate pillars, the middle pillar experiences relatively more uniform loading and displacement. The significance of the effect of the passing of the first longwall face and the second longwall face on these pillars is investigated.

Figure 5.6 shows the change of stress, strain and local mine stiffness for pillar lc, mc and rc with 750 ft (225 m) overburden. The local mine stiffness remains almost constant until the first face is very close. Then, it decreases (absolute value) abruptly as the face passes by. After the face moves away from the pillars, the local mine stiffness becomes relatively stable again.

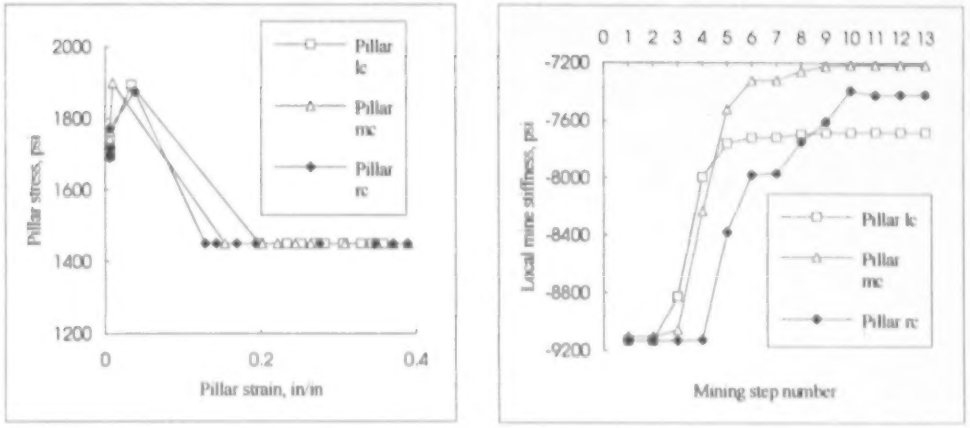

(A) Averaged stress-strain relation

(B) Local mine stiffness vs mining step number

Figure 5.6

Changes of stress, strain and local mine stiffness with the face advance cross pillar rows.

It is shown that headgate pillar (pillar lc) is only affected by the first panel mining, because the arrival of the second face in the line with the pillar does not cause a jump of the strain and the change of the local mine stiffness. But apparently, the tailgate pillar (pillar rc) is affected by both the first panel mining and second panel mining because of the two jumps in the strain curves and the continuous decrease in the local mine stiffness which coincides with the positions when the first and second faces are in the line with or have just passed away from the pillar. The reaction of pillar mc is something between that of pillars lc and rc. However, the final local mine stiffness for the center pillar position is the lowest (absolute value) with value of -72112 psi (497.2 MPa), compared with that of the tailgate and headgate pillar positions (-74164 psi (511.4 MPa) and -76793 psi (529.5 MPa) respectively). Head gate pillar (lc) has the least reduction of the local mine stiffness after the second panel is excavated. This indicates that the headgate pillar will have least bump potential and the center pillar will have biggest bump potential, if all pillars have the same shape and size.

(3) Effect of overburden

The thickness of the overburden will determine the final stress level of pillars in longwall mining. Because the local mine stiffness is found to decrease with the mining

advance which is closely associated with the stress change in the pillars, the significance of the overburden on the local mine stiffness is examined in the studies.

Figure 5.7 (B) shows the local mine stiffness change at pillar rc position with the three different overburdens conditions: 500 ft (150 m), 750 ft (225 m) and 1000 ft (300 m). The mining step numbers 4 and 10 correspond to the positions when first face and the second face are in the line with the pillar rc, respectively. The similar figures for other specified pillar locations are included in figures C.1 to C.3 of appendix C.

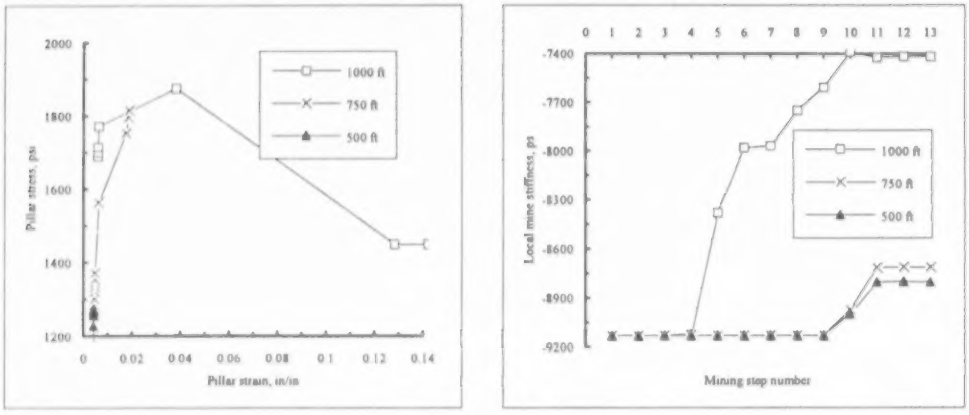

(A) Averaged stress-strain relation

(B) Local mine stiffness vs mining step number

Figure 5.7

Change of local mine stiffness with overburden (pillar rc position).

Figure 5.7 (B) shows that the drop (absolute value) of the local mine stiffness for 1000 ft overburden is significantly greater than that of 500 ft and 750 overburdens. The stress-strain relation in figure 5.7 (A) indicates that for 1000 ft overburden case, pillar went into the post-failure region after mining step 3. The drop of the local mine stiffness also started after mining step 3; for 500 ft and 750 ft cases, the drop of the local mine stiffness only started after the second face passed the pillar. This clearly shows that the overburden has significant effect on the magnitude of the final local mine stiffness, because the overburden is the main factor influencing when the pillar will go into post-failure region and the change of the local mine stiffness is closely associated with the post-failure behavior of pillars. It is also clear that because the passage of the longwall face creates a substantial change in the support system around the pillar, the coincidence

of the passage of the face and the change of the pillar behavior should not be a surprise. For the same reason, the coincidence of the passage of the face and the drop of the local mine stiffness is also understandable.

5.3.2 Effect of the modulus ratio of strata to coal

Zipf's results showed that modulus of the surrounding strata dominates the magnitude of the local mine stiffness for an element (size of 3 m). The ratio of the local mine stiffness to rock modulus always remains about 0.7, no matter what the modulus ratio of strata to seam.

To investigate the effect of the strata stiffness on the magnitude of the local mine stiffness for pillars, the local mine stiffness at locations lc, mc and rc in the non-elastic model is calculated through 13 mining steps. The modulus of the in seam material is kept constant as 290000 psi (2000 MPa). The modulus of the strata is varied as 145000 psi (1000 MPa) , 290000 psi (2000 MPa) and 725000 psi (5000 MPa) respectively. The corresponding modulus ratio of strata and coal will be 0.5, 1 and 2.5 respectively.

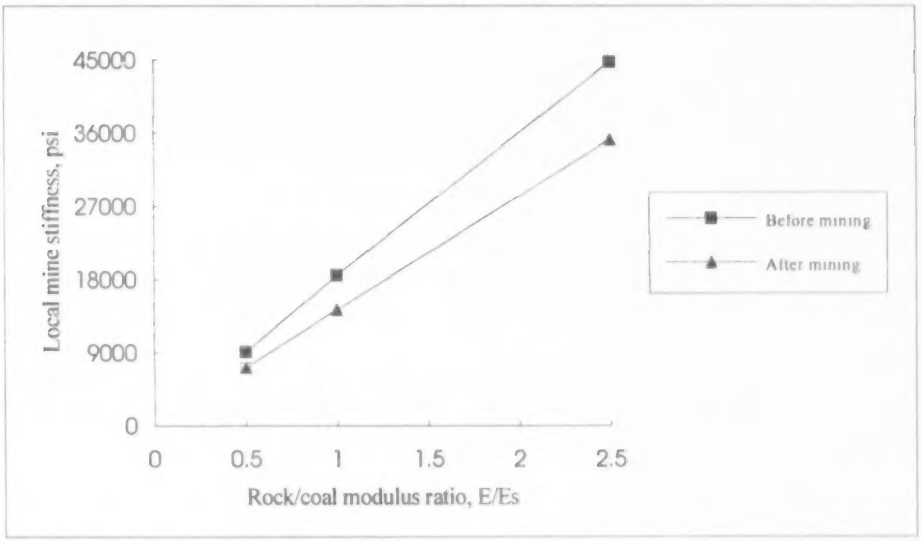

Figure 5.8

Relation between local mine stiffness and rock/coal mudulus ratio.

Figure 5.8 shows the averaged local mine stiffness of the pillar locations with an overburden 750 ft (225 m). It is seen from figure 5.8 that the calculated values of the local

mine stiffness for a pillar is almost linearly proportional to the rock/coal elastic modulus ratio, which indicates that the rock elastic modulus is still the dominant factor for the local mine stiffness even for a pillar of size of 80 ft (24 m). However, the value of the local mine stiffness is significantly less than the value of the rock elastic modulus. The ratio of the local mine stiffness to the rock modulus is about 0.05 which is one order less than Zipf's result for elements. Figure 5.8 also shows that after the two panels were extracted, the local mine stiffness dropped 20 percent with respect to the three different rock/coal elastic modulus ratios. This indicates that the longwall face advance does have the significant effect on the local mine stiffness.

5.3.3 Effect of the strain softening of coal

The effect of the strain-softening of coal on the local mine stiffness is also examined by varying the residual stress so as to vary the post-failure slope of the strain-stress curve of the coal model . The three different strain softening models are shown in figure 5.9.

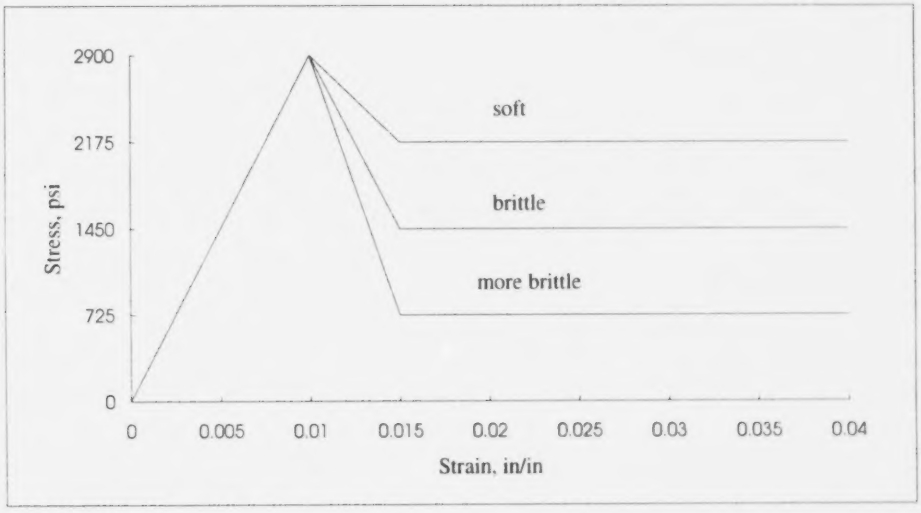

Figure 5.9

Three different strain softening models.

The strain softening model (will be referred to as the "brittle" model in following discussion) used in previous analysis, i.e. the model used in the analysis of effects of pillar location, overburden and strata stiffness, is modified by changing the residual stress from 1450 psi (10 MPa) to a higher residual stress 2538 psi (17.5 MPa) and to a lower residual stress 725 psi (5 MPa) respectively, while maintaining the residual strain as

0.015 in/in. As shown in figure 5.9, this process leads to a "soft" seam model, a "brittle" seam model and a "more brittle" model, which represent the material with different post-failure behaviors.

Figure 5.10 (B) shows that when coal gets more brittle (with lower residual stress), the changes of the local mine stiffness become more abrupt or steeper. Because the abrupt change of the local mine stiffness always occurs when the face is close to the pillar, the steeper local mine stiffness change implies that the possible bump area is closer to the face for this coal.

The relation of the strain softening with the local mine stiffness is closely associated with the different pillar strengths due to the different strain softening behaviors. The "soft" model corresponds the higher residual stress, which will lead a delayed pillar failure than the "more brittle" model as shown in figure 5.10 (A). As a result, the local mine stiffness of the three models at the same mining step is different.

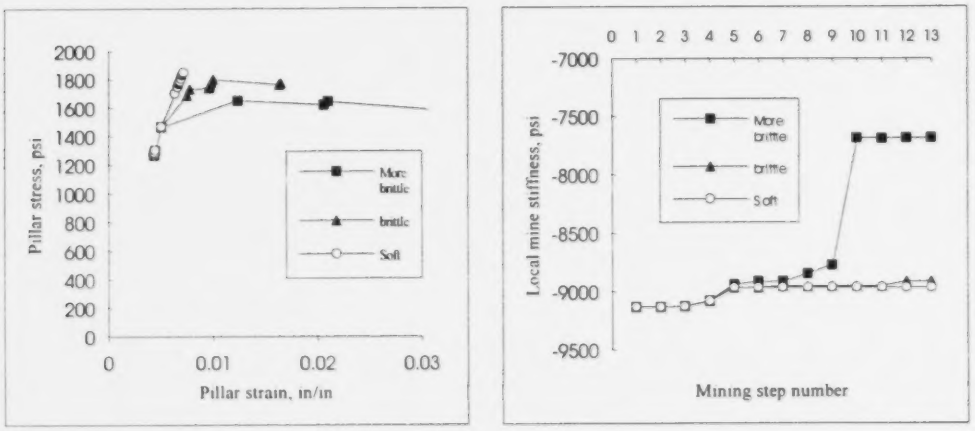

(A) Averaged stress-strain relation

(B) Local mine stiffness vs mining step number

Figure 5.10

Effect of the softening behavior of coal on the local mine stiffness.

5.3.4 Summary

All the results show that for a pillar in the panel, a sudden drop of the local mine stiffness always occurs when face is very close to the pillar site. The drop of the local

mine stiffness also corresponds to the abrupt change of the stress and strain of the pillar. Therefore, the change of the local mine stiffness might be used as an index which indicates the critical state of the pillar behavior under the specific roof and floor conditions.

For chain pillars in a longwall mine the pillar location in a chain pillar column has no effect on the local mine stiffness. However, the pillar location in a chain pillar row has some effect on the local mine stiffness. In a pillar row, the headgate pillar location has the least local mine stiffness reduction, and the middle pillar has the biggest reduction in local mine stiffness reduction, after the second panel is mined out. This may help to decide the location of the abutment pillar in the pillar row.

The effect of the overburden on the magnitude of the local mine stiffness change is obvious. The thicker the overburden, the greater the change of the local mine stiffness. This is consistent with the field observation that frequency of pillar pumps increases with the thickness of the overburden.

The modulus of the surrounding strata dominates the magnitude of the local mine stiffness, but the panel mining may significantly reduce the local mine stiffness. Therefore, the effect of the mining on the local mine stiffness cannot be neglected.

The strain-softening behavior of a seam has a significant effect on the local mine stiffness. The more brittle, the more abrupt change in the local mine stiffness is expected. The determination of strain-softening behavior of pillars before the start of mining would help to estimate the pillar bump potential.

5.3.5 Comparison of different chain pillar configurations

It was reported that a specific chain pillar configuration may improve or worsen the pillar bumps in longwall panels (Campoli, 1987, Carr, 1982, and Peng, 1984). A typical four entry longwall mining system consists of three columns of chain pillars, one of which is the abutment pillar and the other two are yield pillars.

Based on the structural analysis and field instrumentation results, Peng indicated that a design with the abutment pillars close to the tailgate side is better than that with the abutment pillar close to the headgate side for three entry (two chain pillar columns) system. He stated that because the headgate side abutment pillar will lead to a cleaner

caving line along the tail entry which will reduce the pressure imposed on the head entry of the next panel. For four entry longwall system he pointed out that there are no guidelines for the abutment pillar position except the local preference based on operational experiences. Experience in the Pocahontas No. 3 Coalbed showed that leaving abutment pillar row in the middle of the pillar system provided a better solution for the pillar bump problem (Campoli, 1989). However, the result of the equal size of pillars in the previous section indicated that the middle pillar position is the worst, compared to the tail entry and head entry abutment pillar positions.

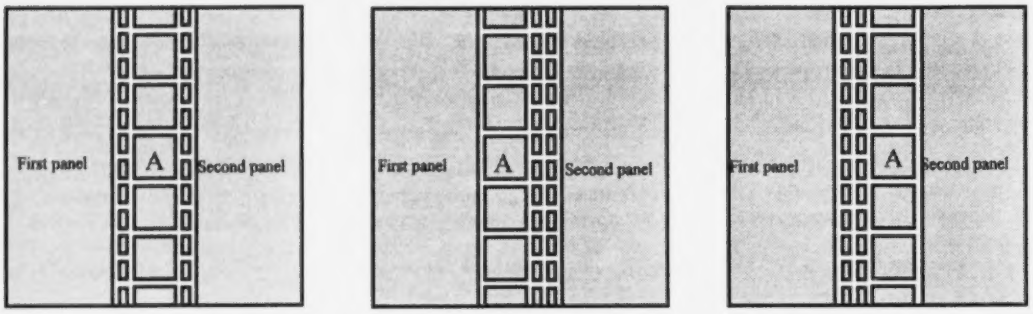

Center abutment (YAY) Head gate abutment (AYY) Tail gate abutment (YYA)

Figure 5.11

Fine meshes of the three chain pillar configurations.

To examine the effectiveness of the local mine stiffness as a guide to pillar design, three different chain pillar configurations, as shown in figure 5.11, are studied. The three chain pillar configurations have everything exactly the same, except the location of the abutment pillars. In the three pillar configurations the abutment pillar is placed at the headgate position, middle position and tailgate position of a pillar row respectively. The abutment pillars have a size of 120×120 ft (36×36 m). The yield pillars have a size of 30× 50 ft (12×15 m). The entries have a width of 20 ft (6 m). It is expected that the local mine stiffness difference for the different pillar configurations may provide insights for the location of the abutment pillar in pillar design. The typical mesh configuration, input parameters and output are included in appendix B.3 (AYY configuration).

The central abutment pillar (location A in figure 5.11) of the three configurations have been monitored throughout the mining of the two adjacent panels. The average stresses, strains and local mine stiffness are shown in figure 5.12. The typical normal

stress and closure distribution for the fine mesh zones are included in figures D.9 to D.12. of Appendix D.

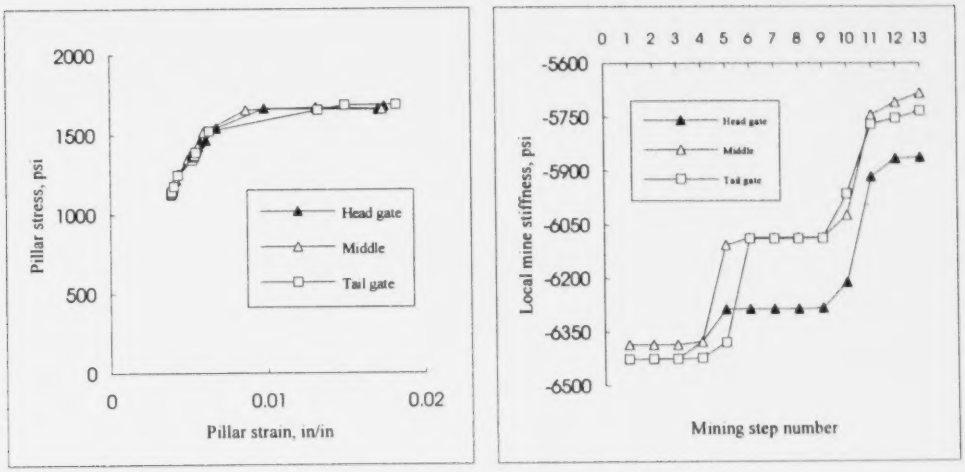

(A) Averaged stress-strain relation

(B) Local mine stiffness vs mining step number

Figure 5.12

Local mine stiffness change for three pillar configurations.

It is seen from figure 5.12 that the stress increases almost uniformly with the face advance. The strain first increases uniformly until the second face arrives (mining step 10), then the strain jumps, indicating yielding of the pillars. However, the local mine stiffness remains stable through all the other mining steps but takes two dives after the mining steps 4 and 10 which are the steps when the face is in line with the pillar. This suggests that the passing of the longwall face has a significant affect on the local mine stiffness.

Similar to the observations from the equal size chain pillars studies given in previous sections, figure 5.12 shows that after mining, the center abutment pillar has the greatest local mine stiffness reduction and the headgate abutment pillar has the least local mine stiffness reduction. However, the similarity in deformation and loading behavior for the three pillar configurations indicated that the yield pillars have almost no affect on the behavior of the abutment pillars. The difference in the local mine stiffness is mainly because of the location of the abutment pillars. Therefore, the headgate abutment pillar

has the least bump danger and the center abutment pillar has the biggest bump danger among the three pillar configurations.

5.4 Pillar post-failure stiffness determination

In longwall mining, there is a trend to increase the dimension of the abutment pillars to avoid pillar bumps because the wider pillars have lower post-failure stiffness. The literature review in chapter 3 indicated that most data of the post-failure stiffness came from the pillars with a width/height less than 5. For the pillars with width/height ratios beyond 9, there are no reliable post-failure stiffness data available. Hence the determination of post-failure stiffness of wide pillars needs to be addressed.

In chapter 3, the available field and laboratory data for coal were normalized with the initial Young's modulus and were presented in figure 3.5 against the pillar width/height ratio. Although the data are very scattered, the trend of stiffness decreasing with the increasing width/height ratio is still clear.

Attempts were made to fit this type of the data into a linear relation (Brady, 1980 and Ozbay, 1989). Based on the linear relation, Ozbay concluded that a pillar with width-height ratio greater than 5 could not bump because from the relation, the post-failure stiffness would be zero. However, it has been reported that even the pillars with a width-height ratio greater than 8 have experienced bump failures (Babcock, 1984 and Campoli, 1990).

Laboratory data from Das (1989) and Crouch (1972) indicated that the post-failure stiffness cannot be considered to be zero even after the width/height ratio passed 8. The post-failure stiffness data estimated by the field measurements (Wang, 1976 and Iannacchione, 1990) also showed that even for the pillars with a 13.4 width/height ratio, the post-failure stiffness is still close to the original elastic modulus of the pillar. The whole compilation of the collected post-failure stiffness data is attached in the back of the thesis as appendix E.

Therefore, it appears that any kind of interpolation of the data may be misleading. Instead of trying to fit all data with a specific relation, a curved upper boundary of the scattered data can be identified as shown in figure 5.13. Only the upper boundary data are used in curve fitting in figure 5.13. The numbers above the circles points in figure 5.13 represent the values of the upper boundary data points. The power function, log

function, exponential function and polynomial relations were considered to fit the boundary.

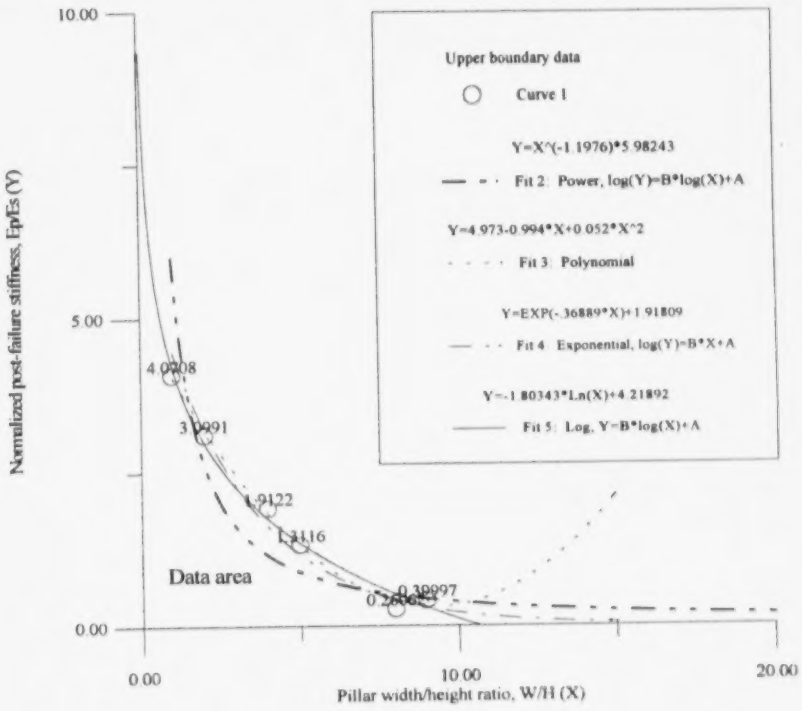

Figure 5.13

Upper boundary fitting of the field and laboratory data of the pillar post-failure stiffness.

Figure 5.13 shows that the log, exponential and quadratic polynomial relations fit the boundary data very well in the range of the available data. If the width/height (W/H) ratio is beyond the range (W/H = 0.5 to 9), the power function apparently fails; the log function has a cut off at the W/H = 11; the exponential function also has a cutoff at about W/H = 15. Compared to the log, exponential and quadratic polynomial functions, the power function has the poorest fit to the available data range. However, the power function is the only curve which can give reasonable post-failure pillar stiffness estimation until W/H = 20, considering the fact that the wider pillars with W/H = 13.7 and 20 also bumped (Campoli, 1990), which means these pillars may have non-zero post-failure stiffness, unless other mechanisms were involved in the bumps. Therefore, it is recommended that within the range of W/H = 9, all relations discussed can be used to

give the upper boundary of the post-failure stiffness, although the post-failure stiffness estimation by power function will be the worst. Beyond W/H = 9, only the power function is recommended for the upper boundary estimation of the post-failure stiffness. The power function derived from the data along the upper boundary of the data area follows as:

$$\frac{E_p}{E_s} = 5.98243\left(\frac{W}{H}\right)^{-1.1976} \tag{5.1}$$

where E_s and E_p are the Young's modulus and the post-failure stiffness of a pillar respectively; W and H are the width and the height of the pillar. Although the derivation of the equation (4.7) is crude, because the post-failure stiffness data of wide pillars are few and are hard to obtain, it still provides a tool to estimate the post-failure stiffness for these pillars. Obviously, these relations will provide the maximum possible post failure stiffness, which can only lead to a conservative pillar design. Based on the above considerations, it seems that power equation (5.1) might be used to give an upper bound of the pillar post-failure stiffness estimation over the range of the data. Any extrapolation beyond the data range should be carried out cautiously.

5.5 Conclusions

MULSIM/NL program has been successfully modified to include the local mine stiffness calculation for pillars within the regular numerical simulation of the longwall mining. The local mine stiffness is defined as the ratio of the unit perturbation displacement over the average load difference cross the pillars. A parametric study of the local mine stiffness has been performed. The parameters studied include longwall face advance, elastic modulus of the strata and the seam, softening behavior of coal, location in the panel, overburden and pillar configuration. Based on the results obtained in the previous sections, the following tentative conclusions are drawn:

(1) Local mine stiffness decreases with the advance of longwall face for both elastic model and non-elastic models;

(2) The greatest drop of the local mine stiffness occurs when face is close to the pillar location or when the pillar starts yielding;

(3) The overburden has significant effect on the final magnitude of the local mine stiffness; the thicker the overburden, the greater drop of the local mine stiffness will be expected;

(4) Brittle coal has greater local mine stiffness drop than the soft coal after panel excavation;

(5) The modulus of the surrounding strata dominates the magnitude of the local mine stiffness but the longwall face advance also has a significant effect;

(6) The pillars along the panel entry behave similarly, as far as strain, stress and local mine stiffness are concerned;

(7) The pillar across panel entries may behave differently. The headgate pillars have the least bump potential and the center pillars have the biggest bump potential, if they have the same size; in combination system of yield pillars and abutment pillars, the headgate abutment pillar design is the best for it has the least local mine stiffness reduction after the excavation of the second panel.

5.6 Pillar design methodology

Based on the results presented above, a chain pillar design approach similar to that proposed by Gill (1993) for the hard rock underground mine can be constructed. This should be especially suitable for the deep and bump-prone coal mines.

The core of the design approach is to include the stability evaluation in the longwall mining design. Therefore, the numerical model is first built according to the initial design and the results of site investigation and testing. The model is fine-tuned by fitting the calculated stress and deformation to the measured stress and deformation. The calculated stress and deformation should agree with the measured stress and deformation throughout the panel extraction, or agree with the estimated results from the experience if the measured results are not available.

Then, the local mine stiffness at the sites of interest are calculated through all the mining steps. Because the study showed that the critical stages occur when the longwall face is close or in the line with the pillars, therefore, the interested sites should be the pillar positions near the face. It is also seen that each pillar in a column parallel to the face advance direction behaves in a similar manner, whereas each pillar in the row

perpendicular to the face advance direction behaves differently. Therefore, only one row of pillars across the section of the entries needs to be considered.

Finally, the calculated local mine stiffness of a specific pillar is compared to the estimated post-failure stiffness of the pillar. To avoid pillar bumps, the local stiffness should be higher than the estimated post-failure stiffness through the panel excavation. Dimensions of the pillars and configurations of the pillars in the panel can be varied to control the time when the local mine stiffness approaches the post-failure stiffness, thus the time and place of the pillar bumps can be controlled in case the bumps cannot be avoided. It is also clear that, with the longwall face advancing, a design in which the changes of the local mine stiffness are slow and smooth is better than a design in which the changes are fast and abrupt, from the point of view of pillar bump potential.

Chapter 6

FIELD STUDY

6.1 Introduction

The U.S. Bureau of Mines initiated coal mine bump research in 1987 because of a series of coal bump-related fatalities and injuries in the Southern Appalachian Basin. As a part of the research, a comprehensive site monitoring program was carried out in the VP No. 3 mine, Virginia. Two different longwall gates were instrumented by hydraulic pressure cells, extensometers and convergence station arrays. Differential roof-sag indicators were used to monitor bedding separation in the immediate roof. The vertical pressure change in the pillars, the dilation of the pillar periphery and the closure of the entries were monitored throughout the recovery of the panels at both sides of the gates. The results of the monitoring program were reported by Campoli (1990). An up-date of the program was also published recently (Campoli, 1993). These results not only provided insights into the design of the longwall chain pillar design, but also provided a base for the back analysis by numerical modeling. In this chapter, the geological features of the mine are described, and the US Bureau of Mines' monitoring program and its results will be presented, followed by a geotechnical interpretation of the field results. These results will be used as case history for the application of the displacement discontinuity model. Chapter 7 will describe the model application to these field results.

6.2 Geology of the VP No. 3 mine

The VP No. 3 mine is located in the center of Virginia, USA. The mine extracts the Pocahontas No. 3 Coalbed, which has average thickness of 5.5 ft (1.65 m) and is in the Pocahontas Formation. The roof and floor consist of the very competent siltstone strata and are also in the Pocahontas Formation. The seam is under 1200 to 2200 ft (360 to 660 m) overburden and dips very gently (less than 3 degrees) from east to west. The average density of the overburden is 158 lbs/ft^3 which could be translated into the original vertical stress of 1.1 psi/ft (24.9 kPa/m). A total of 13 longwall panels have been mined in the mine prior to this study, among which 8 panels were mined on the north side of the barrier pillars, and 5 panel at the south side of the barrier pillars, as shown in figure 6.1. The instrumented sites are in the development entries between the south panel S-6, S-7

and S-8 as shown by the shaded areas in the figure. The two areas (labeled as study area 1 and study area 2 in figure 6.1) were monitored throughout the mining of panel S-6, panel S-7 and panel S-8, and are referred as development 7 and development 8 in the following sections.

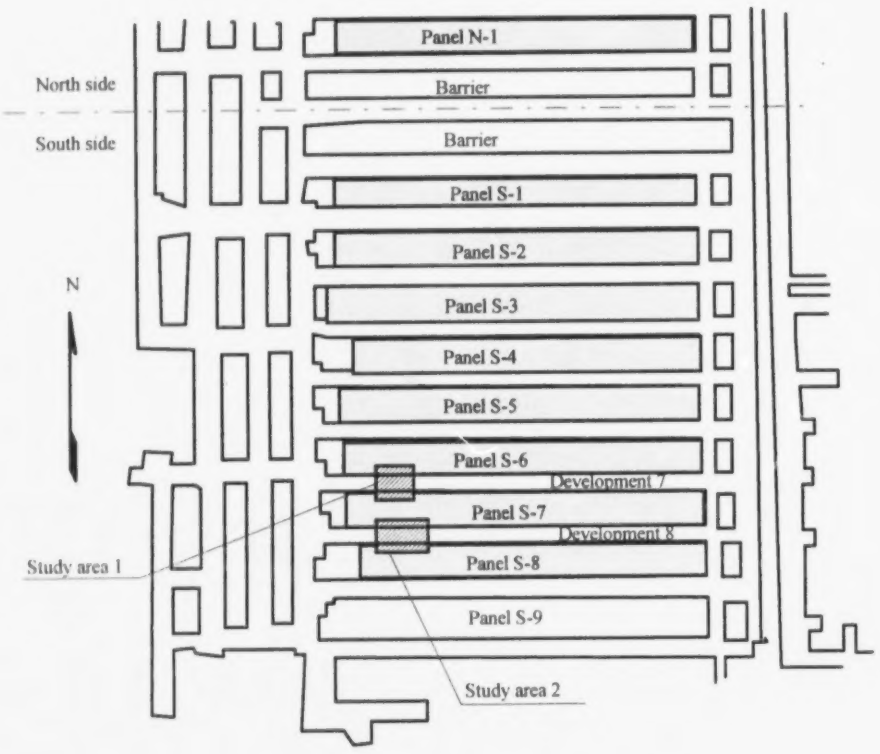

Figure 6.1

Mine map of No. 3 mine (after Campoli, 1990).

The immediate roof in the south side of the mine consists of a widely jointed siltstone overlain by a massive quartz arenite sandstone as the main roof. The floor consists of a combination of very competent siltstone and sandstone. Underground observation in the study area 1 and study area 2 (Iannacchione, 1988) revealed that there is a persistent absence of prominent roof and floor fractures or joints and the main roof is exceedingly difficult to break. A generalized stratigraphic column for the study area is shown in figure 6.2.

Table 6.1 Physical properties of the roof, coal and floor of study areas (specimen testing).

Rock type	Uniaxial compressive strength, psi	Young's modulus 10^6 psi	Poisson's ratio
Roof	12460-24230	3.8-7.7	0.24-0.34
Coal	1813	0.25-0.73	0.16-0.91
Floor	10620-25250	6.9	0.35

The physical properties of the strata are presented in table 6.1. Clearly, the roof and floor are very similar. The uniaxial compressive strength and Young's modulus for coal are about one tenth of that of the roof and floor.

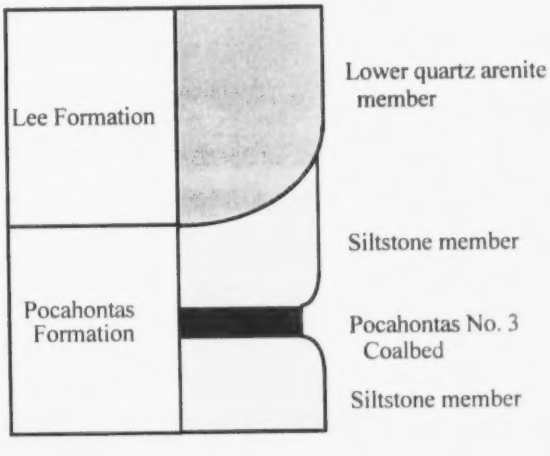

Figure 6.2

Generalized stratigraphic column for study area (after Iannacchione, 1988).

6.3 Site monitoring program

The mine used to have a 218 ft (65.4 m) wide yield-yield-abutment (YYA) pillar configuration with the yield pillars on 50 ft (15 m) centers on the tailgate side, the abutment pillars on 100 ft (30 m) centers, and all crosscuts on 100 ft (30 m) centers. The large 80 by 80 ft (24 by 24 m) abutment pillars in the tailgate side often bumped when

face was approaching. To improve the situation, the mine management decided to switch to yield-abutment-yield (YAY) pillar configuration as shown in figure 6.3. The modified design did not eliminate the abutment pillar bumps, but the side yield pillars successfully shielded the tail entry from the bumps of the middle abutment; this improved the safety of the personnel and equipment. However, when the mining progressed into panels S-6 and S-7, the tailgate abutment pillars began progressively bumping 500 ft (150 m) in advance of the longwall face. The continuous pillar bumps also led to a series of face bumps occurring at the tailgate side face corner.

In an attempt to better control ventilation between previous and active gobs, and to improve tailgate entry stability, the mine modified the yield-abutment-yield pillar design for the development 8 between panel S-7 and panel S-8. The modified design increased the abutment pillar dimension to 120 by 180 ft (36 by 54 m), but decreased yield pillar width to 20 ft (6 m). Between yield pillars, the crosscuts were driven at 60°, whereas between abutment pillars, the crosscuts were still driven at 90°, as shown in figure 6.4.

Because the geological conditions in development 7 and development 8 are very similar, the shift from the old pillar configuration (figure 6.3) to the new configuration (figure 6.4) provided an excellent opportunity to evaluate the different pillar designs. In cooperation with the mine, the US bureau of Mines started a comprehensive monitoring program which included the instrumentation in the two different pillar configurations at development 7 and development 8 respectively.

The instrument configurations of the two study areas are also shown in figure 6.3 and figure 6.4 respectively. There were 116 stainless steel borehole platened flatjacks (BPF) installed for measurement of the vertical stress change in the pillars ; there were 133 convergence stations setup throughout the two study areas for closure measurement of the roof and floor; there were 8 coal extensometers for measuring pillar dilation and some instruments for the indication of possible roof separation and floor heave.

In development 7, the vertical stress changes and closure across the section A-A (figure 6.3), which included three entries, two yield pillars and one abutment pillar, were monitored through the BPF instrument line and convergence station lines along A-A. The lateral dilation of the abutment pillar was measured by the three extensometers respectively installed in three sides of the pillar. The horizontal stress change of the

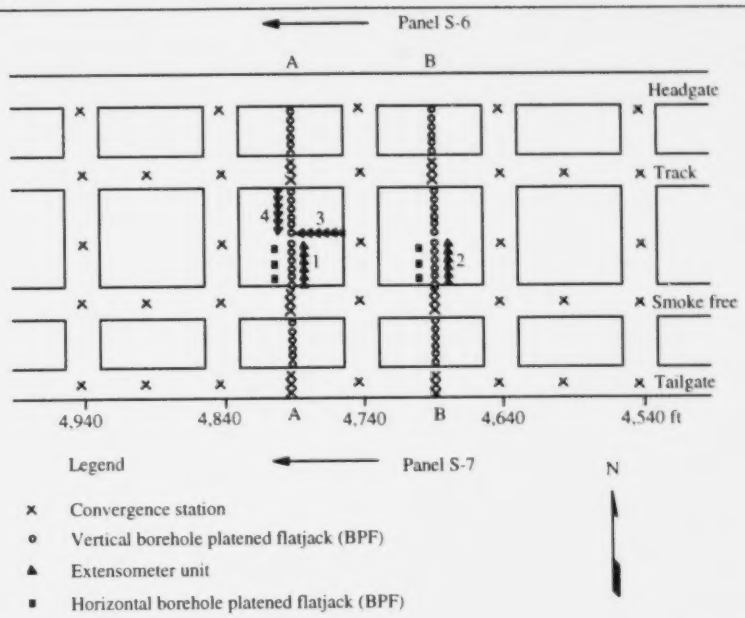

Figure 6.3

Plan of development 7 and instrument array.

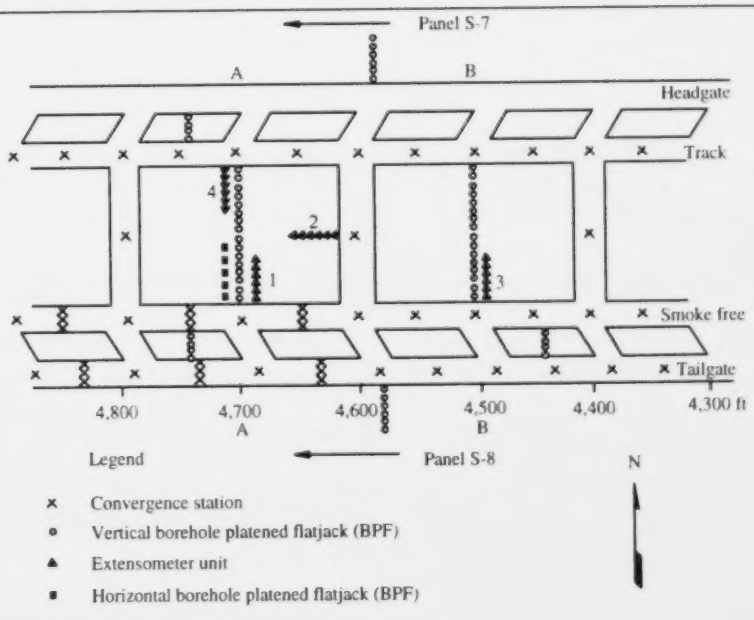

Figure 6.4

Plan of development 8 and instrument array.

abutment pillar was monitored through the three BPFs. The cross section B-B was also instrumented in a similar manner.

The instrumentation in development 8 (figure 6.4) is very similar to that in development 7. However, the edges of panel 7 and panel 8 close to the development 8 were also instrumented to examine the transfer of the stress from the failed pillars to the panel edges.

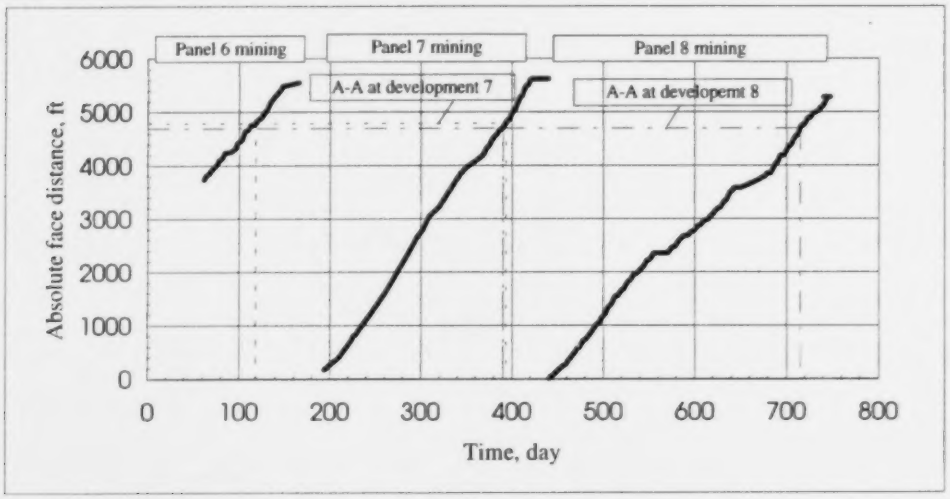

Figure 6.5

Correlation of the absolute longwall face position to time.

The mining of panel S-6, panel S-7 and panel S-8 (note the label "S" will be omitted when panels are referred in the following sections) took about 2 years. The readings of the instrument arrays were taken as long as conditions allowed. A graph of the absolute face position (the distance to the start-up room at the east end of panels) versus the time is given in figure 6.6. The absolute distance of the monitoring line A-A at development 7 and development 8 to the start-up room is 4800 ft (1440 m) and 4700 ft (1410 m) respectively. The relative distance of the face to the line A-A can be decided from figure 6.6. Because the face advanced almost uniformly at 20 ft/day (6 m/day) throughout the mining of the three panels, the relation of the face position and time was linearized for convenience. To be concise, the following terms "the first face" and " the second face" were used in the following sections. "The first face" means the longwall face at the headgate side panel (or the first panel) and "the second face" means the longwall face at the tailgate side panel (or the second panel). The terms "inby" (or minus sign in distance)

and "outby" (or positive distance) were also used to describe whether the longwall face is approaching the pillar or passing away from the pillar, respectively.

6.4 Interpretation of the field data

The vertical stress and the horizontal stress change in the pillars with face advance was measured. The entry convergence and pillar dilation were also recorded. The following is an analysis and geotechnical interpretation of the field data.

6.4.1 Vertical stress change

(1) Development 7

Figure 6.6 (A) and (B) present the change of the vertical stress in the abutment pillar at line A-A of development 7 with the face advance. The vertical stress changes at 5 ft (1.5 m), 15 ft (4.5 m), 24 ft (7.2 m) and 35 ft (10.5 m) into the headgate side, and at 8 ft (2.4 m, 13 ft (3.9 m), 18 ft (5.4 m) and 33 ft (9.9 m) into the tailgate side of the abutment pillar are included in the figures. The term "2nd face zero" in the figures means that the second face just comes in the line with the monitoring line A-A.

The sharp rise and fall of the stress change were observed throughout the panel mining, which suggested a violent failure process was occurring in the pillars. Generally, the vertical stress change was minimal before the first face was 800 ft (240 m) inby. The change accelerated during the face advancing from inby 400 ft (120 m) to outby 600 ft (180 m). The peak of the vertical stress change first occurred at the periphery (5 ft at headgate side and 8 ft at tailgate side), and then migrated into the pillar core (35 ft at head gate side and 33 ft at tailgate side) with the face advance. The maximum stress change is 12000 psi (82.7 MPa) occurring at the 15 ft (4.5 m) into the abutment pillar at the headgate side, and 13000 psi (89.6 MPa) occurring at 13 ft (3.9 m) into the pillar at the tailgate side. The stress change in the periphery decreased after the first face passed, but the stress change in the core (35 ft and 33 ft) remained high until the second face was 3000 ft (900 m) inby, then it fell gradually. This indicated the earlier yielding of the periphery than the pillar core. The abutment pillar bumped when the second face was 500 ft (150 m) inby the pillar.

Figure 6.7 (A) provides the cross section view of the vertical stress change at the A-A monitoring line of development 7, with respect to different face locations.

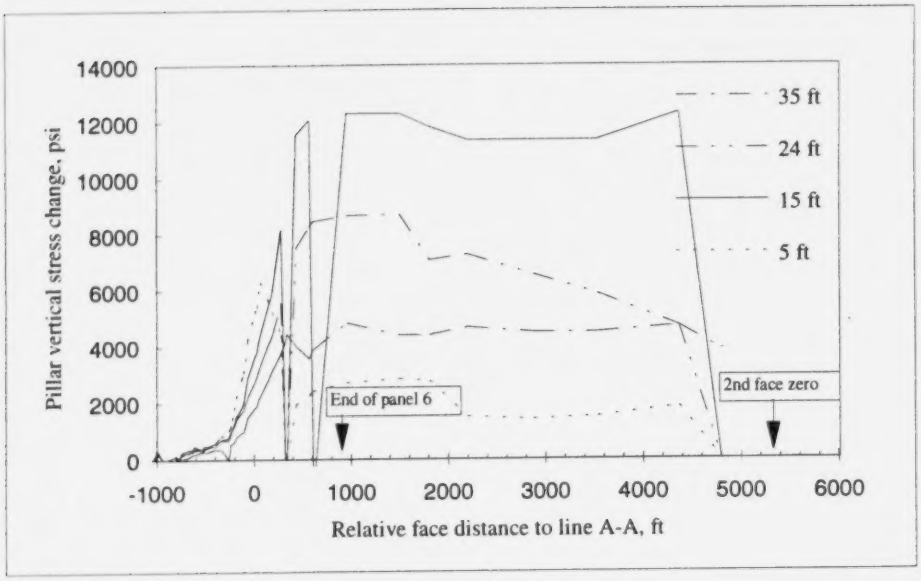

(A) Headgate side of abutment pillar

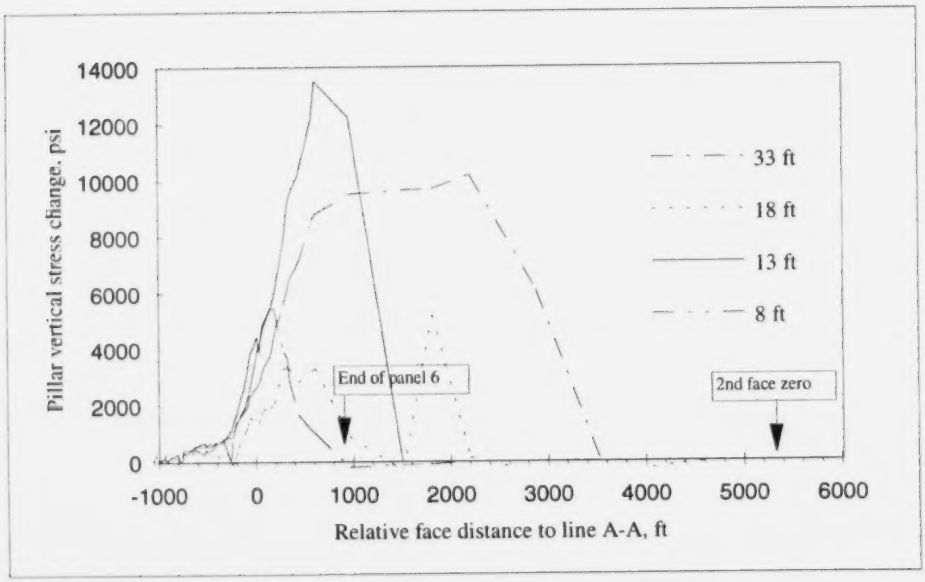

(B) Tailgate side of abutment pillar

Figure 6.6

Vertical stress change of the abutment pillar (development 7, A-A line).

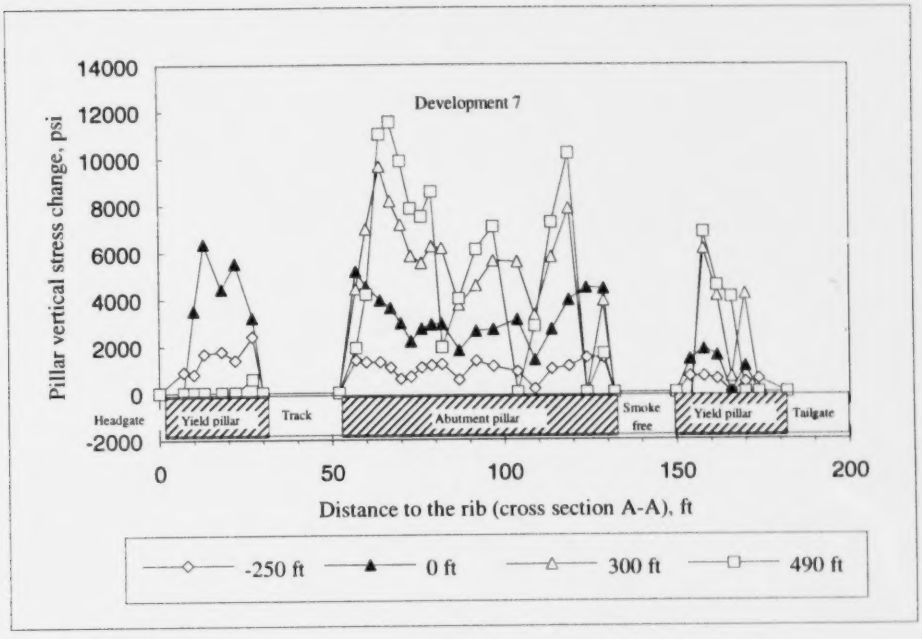

(A) Cross section view of vertical stress change at line A-A

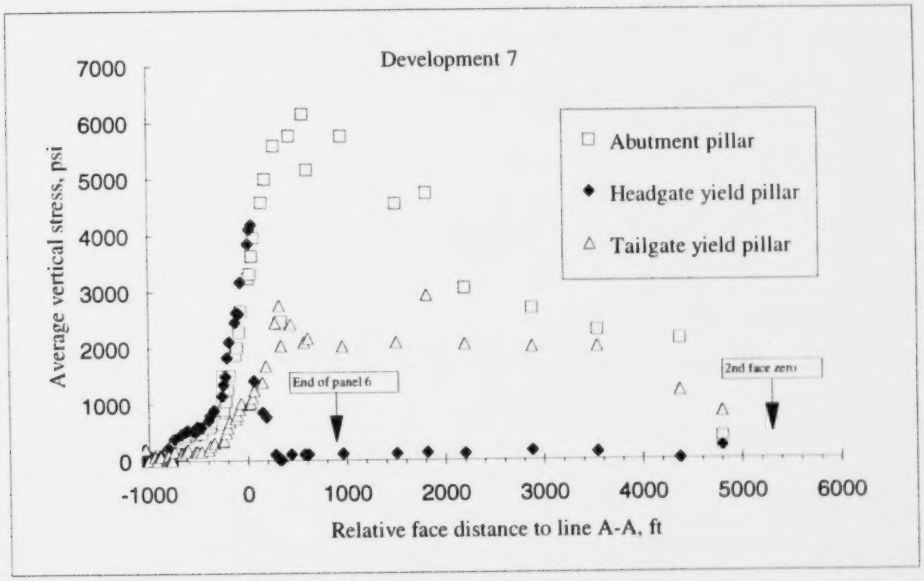

(B) Averaged vertical stress change

Figure 6.7

Vertical stress change of the cross section A-A of development 7.

Figure 6.7 (A) shows that the stress change in headgate yield pillar fell just after the first face passed, also showing yielding of the pillar. The stress change in tail gate yield pillar fell after the first face was outby 490 ft (147 m).

The vertical stress across line A-A was averaged and presented in figure 6.7 (B). The maximum average stress change is about 6200 psi (42.8 MPa) for the abutment pillar, 4200 psi (29 MPa) for the head gate yield pillar, and 2900 psi (20 MPa) for tailgate yield pillar. The average stress change also indicated that the headgate yield pillar failed first and apparently only retained its residual strength after the first face passed the pillar; the tailgate pillar failed after the first face was 490 ft (147 m) outby. The exact time of the abutment pillar failure can hardly be estimated from the average stress change because of the very non-uniform stress distribution for the wide pillar. However, the continuous decrease of the average vertical stress change after the first panel was 500 ft (150 m) outby did suggest that the failure process of the abutment pillar started at least after the first face was 500 ft (150 m) away from the pillar, although the final disintegration of the abutment pillar took place apparently during the mining of the second panel.

(2) Development 8

The vertical stress change at development 8 was more consistent and smooth than that at development 7, though the general trend was similar. Figure 6.8 (A) and (B) provided the typical change pattern of the vertical stress occurring for the abutment pillar at line A-A of development 8.

The vertical stress change accelerated when the first face traveled from 700 ft (210 m) inby to 500 ft (150 m) outby position. The migration of the peak of the vertical stress change from the pillar periphery into the pillar core was also clear at the headgate side. The vertical stress change in the 0-30 ft (0-9 m) headgate periphery zone of the abutment pillar started declining after the first face passed. This is the evidence that the 0-30 ft zone of the abutment pillar at the headgate side failed after the first face passed the pillar; the range of the vertical stress change in the zone was 3000-4000 psi (20.7-27.6 MPa).

However, the vertical stress change at the core and the tailgate side of the abutment pillar (except the 4-10 ft or 1.2-3 m periphery) remained high (5000-9000 psi or 34.5-62.1 MPa) after the first face passed, and even accelerated again when the second face was 500 ft (150 m) inby. This illustrated that, although the headgate periphery of the abutment pillar failed when the first face arrived, the core and the tailgate side of the abutment

pillar retained its integrity even after the second face passed. This is further clarified by the acceleration of the vertical stress change of the part of the pillar with the passage of the second face. The field observation indicated that 120×180 ft (36×54 m) abutment pillars did not bump until the second face was at least 500 ft outby (Campoli, 1990).

Figure 6.9 (A) is the cross section view of the vertical stress change at line A-A of development 8. The failure of the headgate side of the abutment pillar is also clear in the figure. The vertical stress change in the edge of the panel S-8 showed that the vertical stress change first accelerated with the arrival of the first face (shown in the figure) and accelerated again with the approaching of the second face (not shown in the figure), which revealed that load transfer started when the edge of the panel 7 was mined and that the edge of panel 8 remained stable until the second face was close.

Figure 6.9 (B) illustrates the average vertical stress change cross line A-A at development 8. Apparently, the average vertical stress change for yield pillars at development 8 was almost reverse of that at development 7 (figure 6.7 (B)). The maximum average vertical stress change was 3900 psi (26.9 MPa) for the abutment pillar, 900 psi (6.2 MPa) for headgate yield pillar, and 4500 psi (31 MPa) for the tailgate yield pillar.

The insignificant vertical stress change in the headgate yield pillars suggested that the headgate yield pillars may yield long before the first face arrived. The tailgate side yield pillars showed that the tailgate yield pillar failed immediately after the passage of the first face and only retained its residual strength thereafter. The average vertical stress change of the abutment pillar also confirmed that vertical stress of the abutment pillar remained high during the mining of the second panel (panel 8), and even increased when the second face arrived.

(3) Analysis

The vertical stress change at development 8 is much more uniform and smooth, compared with that at development 7, implying a more smooth failure process for abutment pillars in development 8 . The stress decreasing zone formed earlier around the abutment pillar indicated yielding of the pillar periphery when face was approaching. The yielding zone was about 10 ft (3 m) for both the development 7 and development 8 pillars.

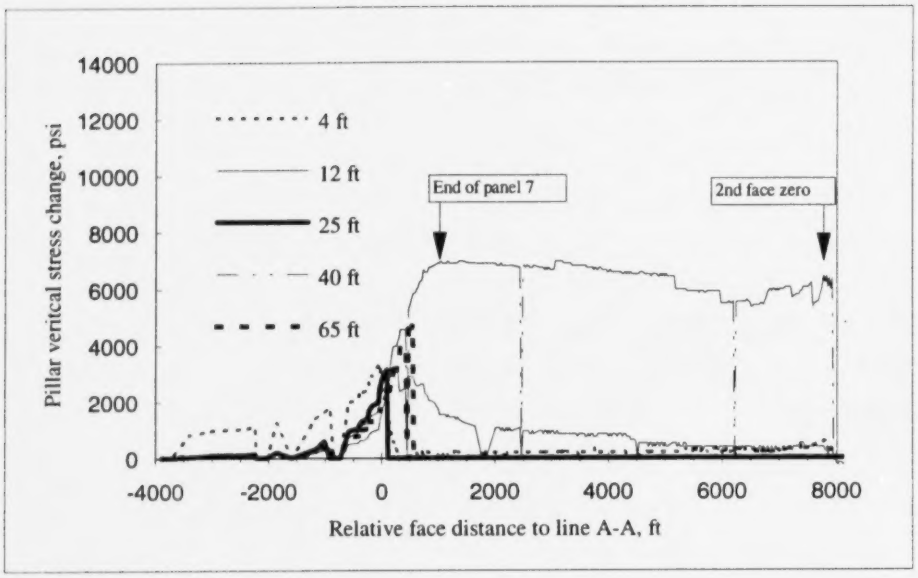

(A) Headgate side of abutment pillar

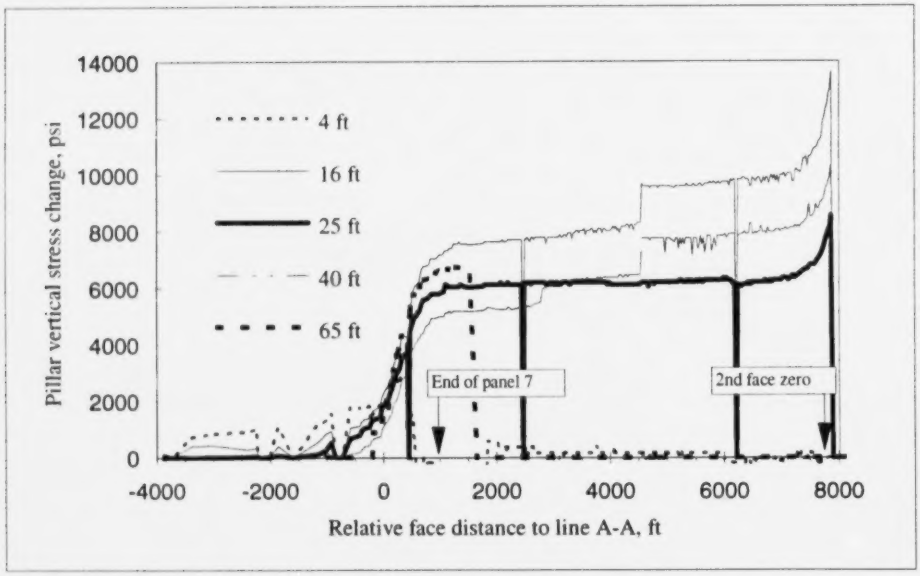

(B) Tailgate side of abutment pillar

Figure 6.8

Vertical stress change of the abutment pillar (development 8, A-A line).

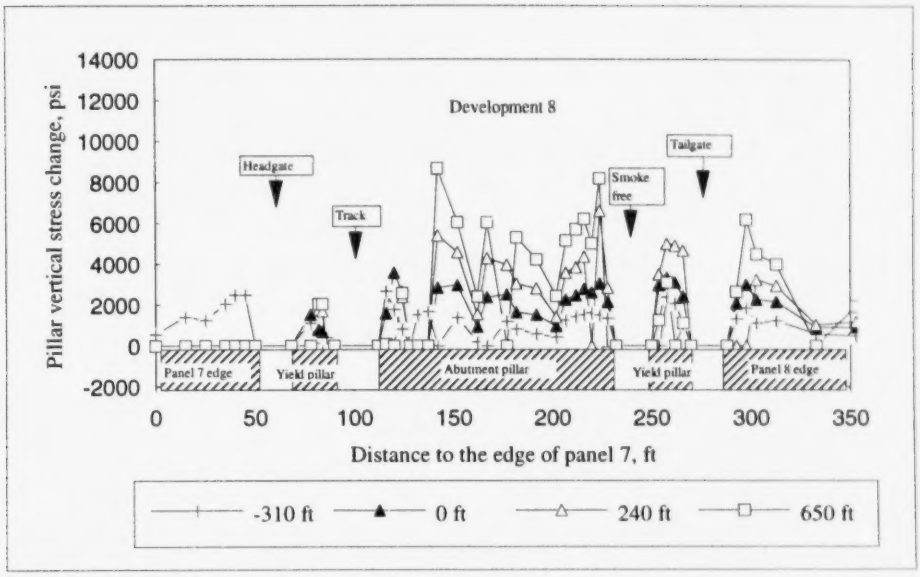

(A) Cross section view of vertical stress change at line A-A

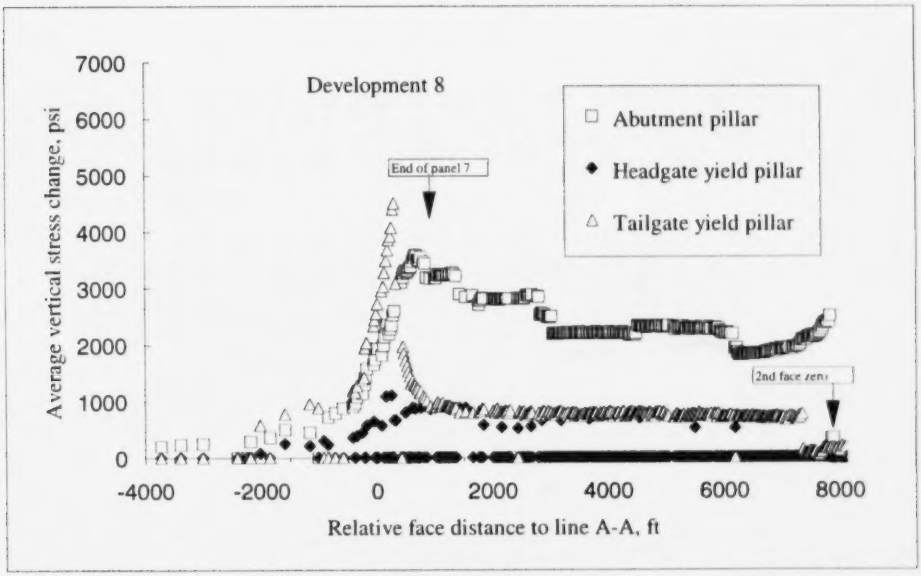

(B) Averaged vertical stress change

Figure 6.9

Vertical stress change of the cross section A-A of development 8.

For abutment pillars in development 7, the drop of the vertical stress change at the core occurred when the second face was 3000 ft (900 m) inby, indicating the beginning of the whole pillar failure. The pillar bump which occurred ahead of the second face 500 ft (150 m) further verified that the abutment pillar failed before the second face arrived.

The headgate side (about 30 ft or 9 m) of development 8 abutment pillar failed when the first face was in line with the pillar. However, the development 8 abutment pillars did not fully fail until the second face passed the pillars. The second increase of the average vertical stress of the abutment pillar with the arrival of the second face also indicated that the abutment pillar was not fully failed at that time. The pillar bump, observed when the second face was 500 ft (150 m) outby, provided further evidence that the abutment pillar did not fail until after the passage of the second face..

The 30 ft (12 m) headgate yield pillars of development 7 failed quickly just after the first face passed the pillars. The 30 ft (12 m) tailgate yield pillars yield at least after the first face was 490 ft (147 m) outby. The 20 ft (6 m) yield pillars in development 8 possibly yielded very early to the development load, but the 20 ft (6 m) tailgate yield pillar yield shortly after the first face passed.

During the panel excavation, the recorded maximum average vertical stress change at development 7 and development 8 was 3900 to 6200 psi (26.9 to 42.7 MPa) for abutment pillars, and 4200 psi to 4500 psi (29 to 31 MPa) for yield pillars. If we assume the average original stress of 2000 psi (13.8 MPa) with an overburden of 1800 ft (540 m) which has the unit weight of 1.1 psi/ft (24.88 KPa/m), the absolute average stress would be 5900 to 8200 psi (40.7 to 56.5 MPa) for abutment pillars and 6200 to 6500 psi (42.7 to 44.8 MPa) for yield pillars.

6.4.2 Vertical closure

(1) Development 7

Very consistent closure was recorded throughout the study area. The closure across section A-A is shown in figure 6.10 (A). The closure started when the first face was about 200 ft (60 m) inby. The closure accelerated during the passage of the first face, and remained stable after the face was 500 ft (150 m) outby. The closure accelerated again when the second face was 500 ft (150 m) inby.

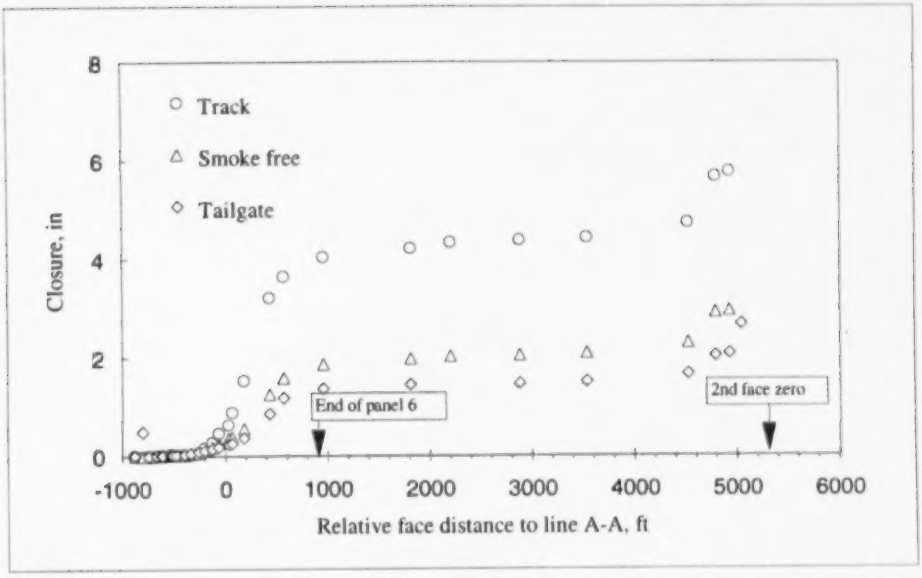

(A) Closure in entries (development 7, A-A line)

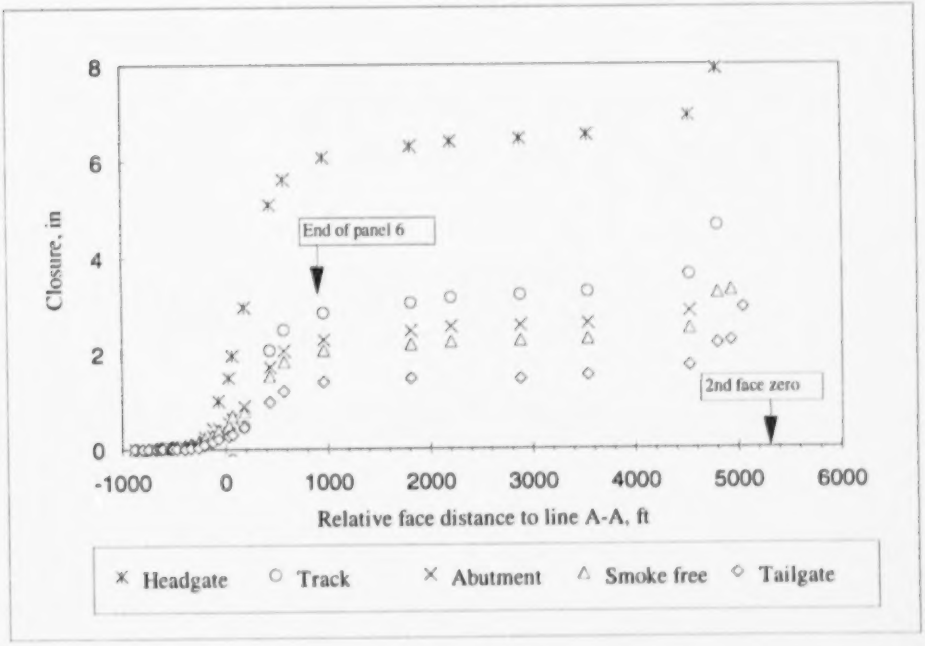

(B) Closure along the crosscut parallel to A-A line

Figure 6.10

Closure in entries at development 7.

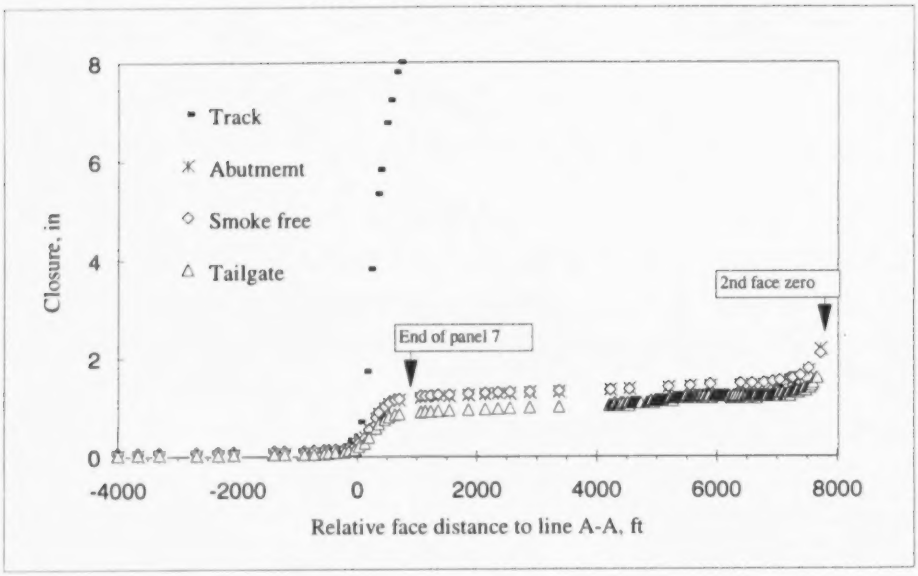

(A) Closure in the crosscut parallel to A-A line

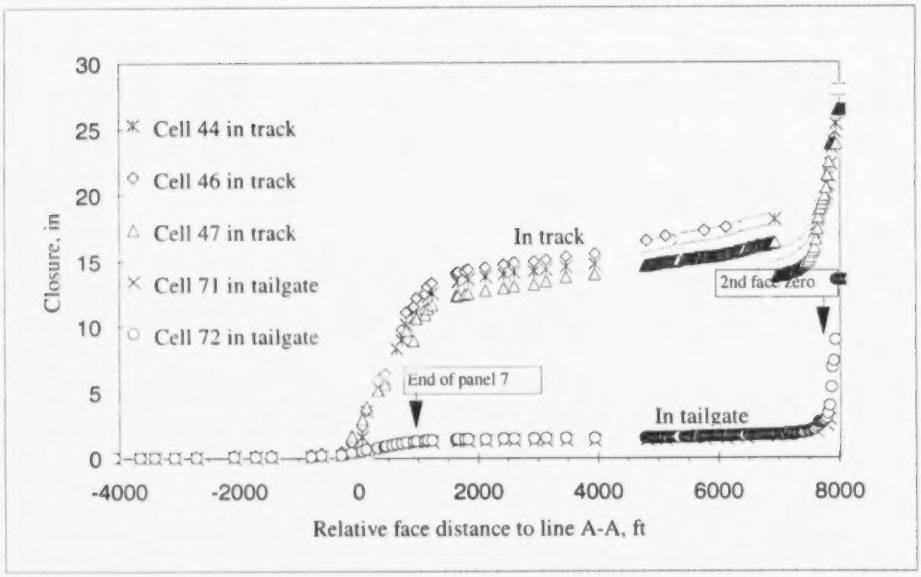

(B) Comparison of the closure in track and tailgate

Figure 6.11

Closure in entries at development 8.

Figure 6.10 (B) shows that after the passage of the first face the tailgate entry, the smoke free entry, the abutment pillar, and the track entry experienced 1, 2, 2.5, and 4 in (2.5, 5.1, 6.4 and 10.2 cm) closure respectively; the headgate entry experienced 6 to 8 in (15.2 to 20.3 cm) closure. This suggested that the entry roof inclined toward the gob. It appeared that the all closures accelerated again when the second face was in the line with the monitoring line. This second acceleration of the closures coincided with the observed abutment pillar bump, indicating the final disintegration of the abutment pillar.

(2) Development 8

The closure pattern at development 8 is similar to that at development 7 except the different magnitude of the closure. Figure 6.11 (A) presents the closure across A-A line of development 8. Figure 6.11 (B) compared the different magnitudes of the closure occurring in the track entry and the tailgate entry of development 8. The two figures showed that the first closure acceleration occurred when the first face was in the line with the convergence station array; the tailgate, smoke free entry and the tailgate side of the abutment pillar experienced 1 in (2.5 cm) uniform closure during the first face passage and virtually remained unchanged until the second face arrived. During the same period the track entry experienced 10 in (25.4 cm) closure; the closure gradually increased to 16 in (40.6 cm) when the second face was close. The closure at all entries started accelerating again when the second face was in the line with the convergence array. The data indicates that the closure went beyond the 25 in (63.5 cm) range after the second face passed. This is strong evidence that the abutment pillar might be totally failed after the second face passed the pillar.

(3) Analysis

The start of the closure acceleration lagged behind the start of the vertical stress change acceleration, which was probably because that the stress meters are more sensitive than the convergence meters. Actually, because the complexity of the calibration process of the stress meters (BPF), the measured magnitude of the vertical stress change is relatively less reliable than that of the closure change. Therefore, the obtained change pattern of the vertical stress is believed to be more meaningful than its absolute value. Both developments experienced closure of 1 in (2.5 cm) at the tailgate entries. However, track entries at development 7 and development 8 experienced significant closure of 4 in (10.2 cm) and 10 in (25.4 cm) during the first face passage, respectively. The closure data indicated that the roof at development 7 tilted towards the gob when the first face arrived

and collapsed when the second face was 500 ft (150 m) inby. The tailgate side of the roof at development 8 showed the uniform closure of 1 in (2.54 cm) and remained relatively stable until the second face approached very close; then it sank with the gob when the second face passed. This provided the indirect confirmation that development 7 abutment pillars failed before the second face arrived, but the abutment pillars at development 8 failed after the second face passed. The significant closure in track entry of development 8 also confirmed the earlier yielding of the headgate yield pillars at development 8.

6.4.3 Pillar dilation

(1) Development 7

The lateral expansion or dilation of the abutment pillars is also uniform and very smooth. As shown in figure 6.12, the abutment pillar periphery expanded laterally when the first face was 200 ft (60 m) inby. The lateral strain increased rapidly during the passage of the longwall face. The magnitude of the lateral strain increase decreased from the edge to the center of the abutment pillar, illustrating that the pillar edge experienced more lateral expansion than the pillar core.

The expansion zone (which has lateral strain over 0.05) was defined by the significant dilation at 17 ft (5.1 m) of the headgate side, 6 ft (1.8 m) of the crosscut side and 6 ft (1.8 m) of the tailgate side of the abutment pillar, which also indicated that the abutment pillar expanded to all directions, with the headgate side expanding most. The abutment pillar experienced average lateral strain of 0.15 in/in at 2 ft into the pillar and 0.7 in/in at 6 ft into the pillar. Because the lateral strain at 15 ft into the tailgate side and crosscut side of the abutment pillar have no significant change, the expansion zone or yield zone can be identified as about 10 ft (3 m) at the both sides of the pillar for the first face passage. For the similar reason, a 20 ft (6 m) yield zone at the headgate side of the abutment can also be identified.

If the previous vertical stress analysis first indicated the existence of the expansion zone around the abutment pillar by the vertical stress decrease zone, then the results of the lateral strain analysis directly identified its existence and thickness. The rapid increase of the pillar lateral deformation stopped when the face was 800 ft (180 m) outby. Then, the lateral deformation remained almost stable at least until the second face was 1000 ft (300 m) inby (not presented in the figure 6.12) and after that it was unavailable because of the deteriorated condition at the instrument line. The lateral strain at a depth of 15 ft

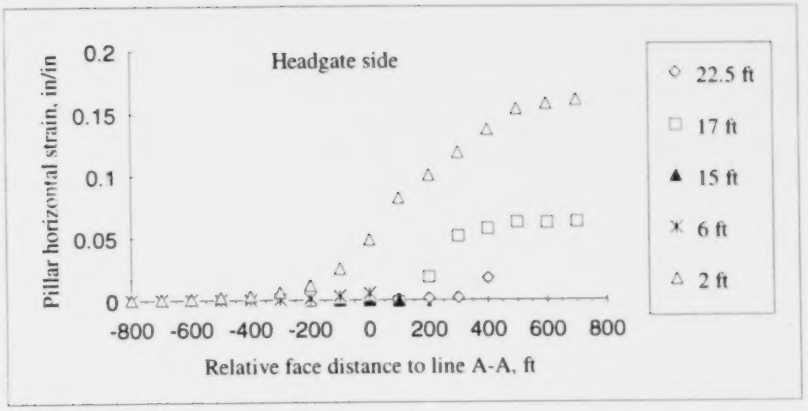

(A)

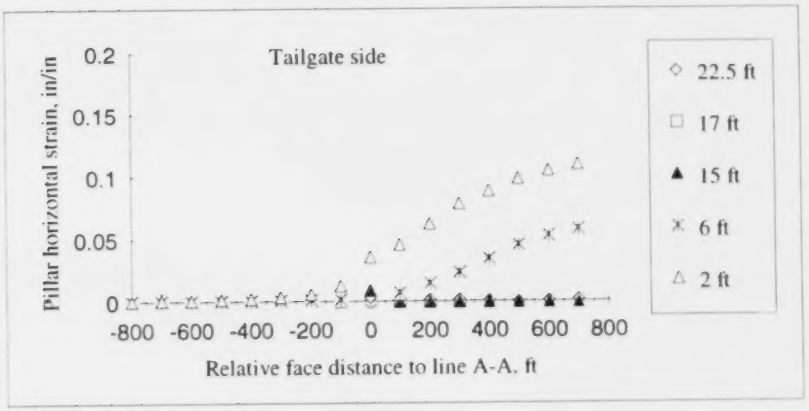

(B)

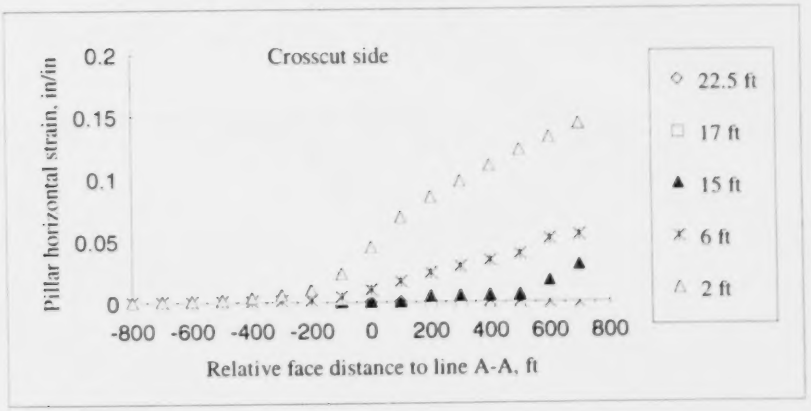

(C)

Figure 6.12

Lateral deformation of the abutment pillar (development 7, A-A line).

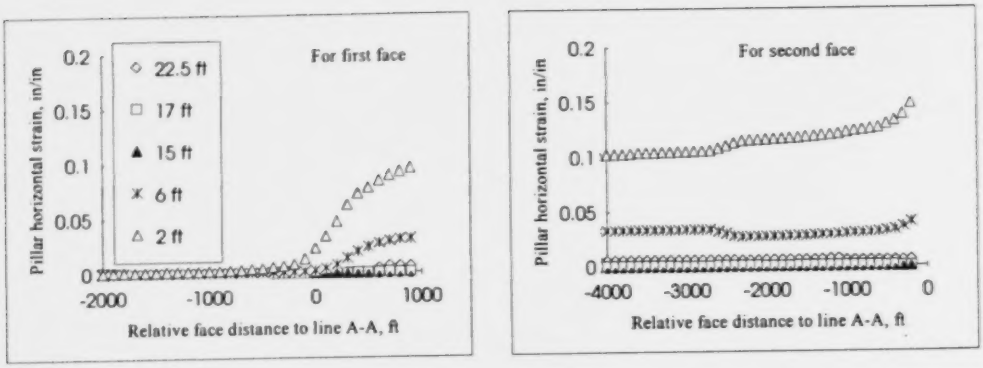

(A) Tailgate side of abutment pillar

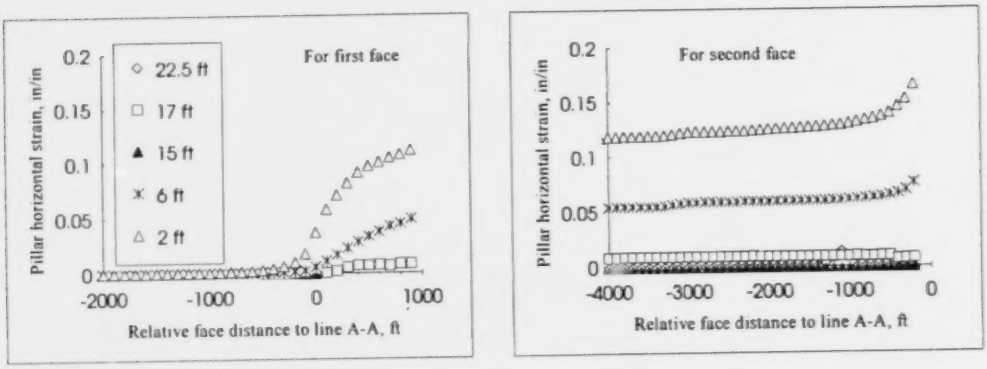

(B) Crosscut side of abutment pillar

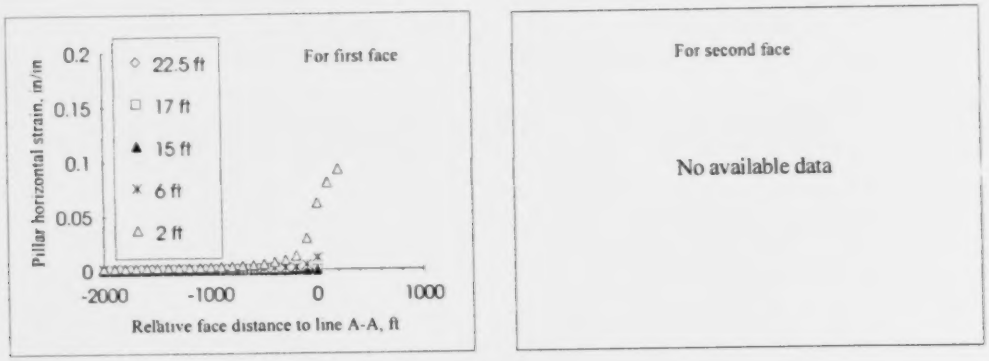

(C) Headgate side of abutment pillar

Figure 6.13

Lateral deformation of the abutment pillar (Development 8, A-A line).

into the crosscut side of the abutment pillar (figure 6.12. (C)) did show an increase after the first face was 500 ft (150 m) outby, signifying the initiation of the edge failure extending into the pillar core.

Less dilation was found at the tailgate side than the other sides of the abutment pillar, which is consistent with the intuition that the abutment pillar would expand more to the gob (headgate side) than to the intact panel (tailgate side).

(2) Development 8

The lateral deformation pattern of the abutment pillar at the development 8 is also very similar to that at development 7. As shown in figure 6.13 (A) and (B), the lateral deformation at the tailgate side and crosscut side of the abutment pillar increased rapidly after the first face was about 200 ft (60 m) inby, then remained stable until the second face was 200 ft (60 m) inby. After that, the lateral deformation accelerated again. The lateral strain at the headgate side (figure 6.13 (C)) accelerated to infinity during the passage of the first face, this also confirmed the earlier failure of the headgate side of the abutment pillar at development 8. A 10 ft (3 m) expansion zone can also be identified around the abutment pillar at development 8.

The abutment pillar experienced lateral strain 0.1 in/in at 2 ft (0.3 m) into the pillar and 0.05 in/in at 6 ft (1.8 m) into the pillar at both the crosscut side and tailgate side. However, the lateral strain at 15 ft (4.5 m) into the crosscut side and tailgate side of the abutment pillar remained minimal until the second face was 200 ft (60 m) inby. This indicated that the tailgate side of the development remained in relatively good condition at least until the second face was very close.

The extensometer at the headgate side of the abutment pillar only recorded the first dilation acceleration which appeared to be going to infinity. The extensometers at the tailgate side and crosscut side both picked up the first and the second acceleration of the lateral deformation. The pick up of the second acceleration occurring when the second face was 200 ft (60 m) inby was apparently because of the improved situation at the tailgate side of the development 8.

(3) Analysis

The results showed that longwall face did not affect the pillar dilation until the face was very close. The abutment pillars expanded in all directions with the headgate side

experiencing the biggest dilation when the faces were approaching. A 10 ft yield zone was identified for the abutment pillars at both developments. The abutment pillar at development 8 dilated less than that at development 7. The tailgate side expansion zone of the abutment pillar in development 8 remained below 15 ft even when the second face was very close. Therefore, compared with the development 7, the tailgate of development 8 was in better condition.

6.4.4 Horizontal stress change

The horizontal stress change was only measured at the tailgate side of the abutment pillars for both developments.

(1) Development 7

Figure 6.14 (A) shows that the horizontal stress change started accelerating when the first face was 300 ft (90 m) inby. The horizontal stress at 8 ft into the abutment pillar reached peak 5500 psi (37.9 MPa) when the first face was 500 ft outby and then decreased and remained at 4000 psi (27.6 MPa) until the second face was 1000 ft inby. The horizontal stress change at 28 ft into the abutment pillar reached peak when the first face was 1000 ft (300 m) outby and then declined when the second face was 1000 ft inby.

(2) Development 8

Figure 6.14 (B) is the horizontal stress change of the tailgate side of the abutment pillar at development 8. The horizontal stress change first accelerated when the first face was 700 ft (210 m) inby. The horizontal stress change at 7.5 ft into the abutment pillar peaked at 4500 psi (31 MPa) when the first face was 700 ft (210 m) outby and remained at 4000 psi (27.6 MPa) until the second face was 1000 ft inby. After that it decreased. However, the horizontal stress change at 30 ft into the abutment pillar accelerated to 3000 psi (20.7 MPa) and remained constant until the second face was 1000 ft inby. It accelerated again until the second face passed.

(3) Analysis

The acceleration of the horizontal stress is the indication that the vertical stress was still not beyond the ultimate strength of the material. Therefore, the decrease of the horizontal stress which occurred at the abutment pillar core of development 7, when the

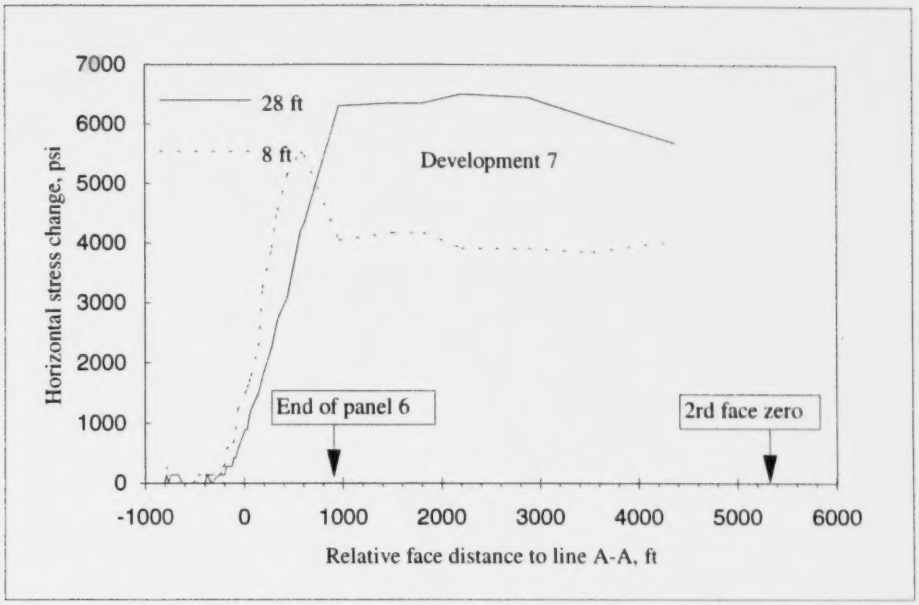

(A) Abutment pillar tailgate side at development 7

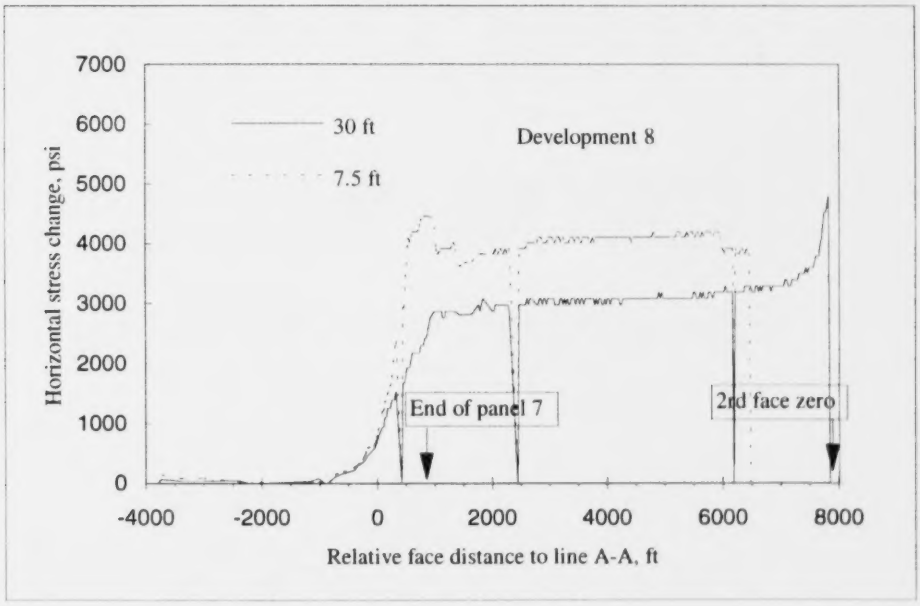

(B) Abutment pillar tailgate side at development 8

Figure 6.14

Horizontal stress change into the tailgate side of the abutment pillars.

second face was 3000 ft inby, suggested that the failure of the abutment pillar started before the arrival of the second face. Whereas, the second acceleration of the horizontal stress change at the abutment pillar core of development 8 revealed that the abutment pillar was still not totally failed when the second face was passing. This is consistent with the closure data and vertical stress change data discussed in previous sections.

6.5 Summary of the analysis

The advance of the longwall face only affects the behavior of the specific sections of the entries and pillars when the face is within a very close range of the sections. Out of this range, the change of the stress and deformation of the section was minimal. For VP No. 3 Mine discussed above, the range is about 800 ft (240 m) inby and outby the specific monitoring section. The stress was felt earlier than the deformation which suggested a delayed plastic deformation of the pillars. The averaged vertical stress change is in the range of 3900 to 6200 psi (26.9 to 42.7 MPa) for abutment pillars, and 4200 to 4500 psi (29 to 31 MPa) for yield pillars.

For development 7, when the first face came into the range, the vertical stress of the abutment pillar increased rapidly. The tailgate entry, smoke free entry, abutment and track entry experienced closure of 1 to 4 in (2.5 to 10.2 cm), and headgate entry experienced 8 in (20.3 cm) closure, showing that the roof tilted to the coming gob. The headgate yield pillar and the 10 ft (3 m) periphery zone of the abutment pillar yielded when the first face was in the line with the pillars, indicated by the earlier decline of the vertical stress and horizontal stress, and the significant dilation. The stress increase in the core of the abutment pillar continued until the first face was 500 ft (150 m) outby, but the closure increase continued until the first face was 1000 ft (300 m) outby. After that, the vertical stress in the abutment pillar fluctuated with the sharp change in magnitude, showing the fracture failure in the pillar. However, the entry convergence and pillar dilation did not change until the second face was 500 ft (150 m) inby, suggesting the abutment pillar still maintained its integrity until the second face was close. The final collapse of the abutment pillar was further confirmed by the pillar bump when the second face was 500 ft (150 m) inby.

For development 8, the behavior of the entries and pillars was similar to that at development 7 when the first face came within range. The 10 ft (3 m) yield zone was also observed with the arrival of the first face. However, the failure of the headgate side of the

abutment pillar when the face was in the line with the pillar was clearly shown by the different change patterns between the headgate side and tailgate side of the abutment pillar. The vertical stress at the headgate side of the abutment pillar dropped after the first face passed, accompanied by the acceleration of the dilation and the significant closure at the track entry (10 in or 25.4 cm). However, the tailgate entry, smoke free entry and abutment pillar only showed 1 in (2.5 cm) uniform closure. High vertical stress and low convergence at the tailgate side of the abutment pillar continued until the second face was very close, showing that the abutment pillar was still in good condition until that time. The vertical stress change and horizontal stress change even accelerated during the second face passage. This is a clear evidence that the final failure of the abutment pillar did not occur until the second face passed, which improved the stability of the tailgate entry significantly. Actually, the abutment pillar did not bump until the second face was 500 ft outby, which directly confirmed that the final collapse of the abutment occurred after the second face passage. The vertical stress change in the headgate yield pillar remained small suggesting that the yielding of the yield headgate pillar may occur long before the arrival of the first face.

Clearly, the chain pillar design at development 8 is much better than that at development 7. The obtained data showed that the shift of the development 7 design to the development 8 design improved the conditions in the tailgate side of the development 8. The stress change and deformation change were also more uniform and more consistent in the development 8. The abutment pillars did not bump until the second face was 500 ft (150 m) outby the pillars. The face bump problem was also eliminated.

Chapter 7

FIELD SIMULATION

The field data and analysis indicated that the design of the chain pillars in development 8 improved the entry and pillar stability. In this section, the mechanism of the chain pillar behavior in both the developments was investigated by the numerical back analysis in conjunction with the local mine stiffness concept. The numerical model was built on the results of the geotechnical interpretation and analysis in chapter 6. The field simulation also serves as a demonstration of evaluation of the chain pillar design by the application of the local mine stiffness approach suggested in chapters 4 and 5.

7.1 Fitting criteria

The field conditions for the study areas are summarized as: the longwall mining configurations as shown as study area 1 in figure 5.2, under 1900 ft (570 m) overburden, and as shown as study area 2 in figure 5.3, under 2000 ft (600 m) overburden, with an overburden stress of 1.1 psi/ft (24.9 kPa/m) for both areas; the Young's modulus for coal is about one tenth that of the surrounding strata. The numerical model built for the mine should perform as close as possible to the real material and generate the results which are close to the field measured results. To set up the numerical model, the results of the field monitoring program were summarized and simplified as follows:

(1) For both developments 7 and 8:

a. A 10 ft yield zone existed around the peripheries of the pillars and the panels, in which no significant stress change occurs;

b. The maximum vertical stress in the pillars and the panels is in the range of 6000 psi (41.4 MPa).

(2) For development 7:

a. The convergence was 6 to 8 in (12.7 to 20.3 cm) at the headgate entry, 4 in (10.2 cm) at the track entry and 2 in (5.1 cm) at the tailgate entry;

b. The abutment pillars fully failed after the second face was 1000 to 500 ft (300 to 150 m) in by;

c. The yield pillars in the headgate side yielded when the first face was in the line with the pillars, and the yield pillars in the tailgate side yield when the face was 300 ft (90 m) outby.

(3) For development 8:

a. The convergence was 10 to 16 in (25.4 to 40.6 cm) at the track entry and 1 in (2.5 cm) at the tailgate entry;

b. The abutment pillars failed after the second face was 500 ft outby;

c. The headgate yield pillars yielded to the development load.

7.2 Model setup

The building of the numerical model includes setting up the mine model mesh and modifying the material parameters to fit the above criteria derived from the analysis results of the field data.

7.2.1 Mine model mesh

The mining of panel 6, panel 7 and panel 8 are simulated in two cases. The first simulation case is intended to fit the results from the study area 1 at development 7, during mining of panel 6 and panel 7, with the overburden 1900 ft (570 m). The fine mesh (10×10 ft element or 3×3 m) includes the study area of development 7 as shown in figure 7.1, which covers the rectangular area of the length of 1000 ft (300 m) and the width of 850 ft (255 m). The coarse mesh (50×50 ft element or 15×15 m) covers the rectangular area of 2500×2000 ft (750×600 m) which includes panel 6, panel 7 and the parts of panel 5 and panel 8 as shown in figure 7.1, with the panel width of 600 ft (180 m) and the simulated panel length of 2000 ft (600 m). Panel 5 was assumed to be a mined-out area and filled with gob material. The panel 8 remained unmined throughout the mining of panel 6 and 7. The field analysis indicated that the range of the affected zone is about ±800 ft (240 m) to the specific pillar. Therefore, the boundary of the coarse mesh, which is ±1000 ft (300 m)to the pillar A in the middle of the mesh, assured that the whole of the affected zone was included in the model.

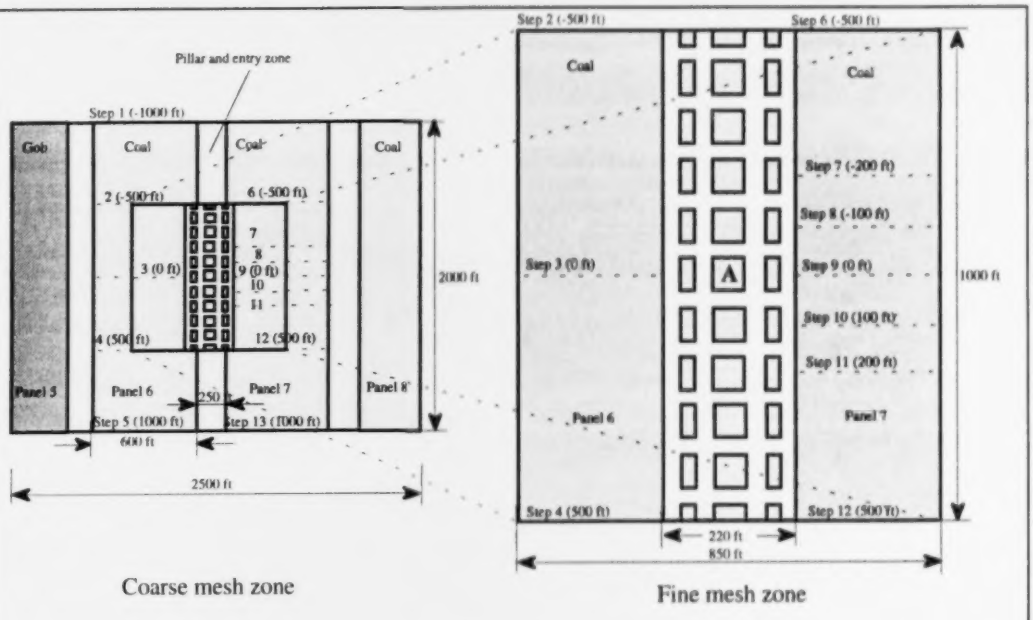

Figure 7.1

Coarse and fine mesh of the model for development 7.

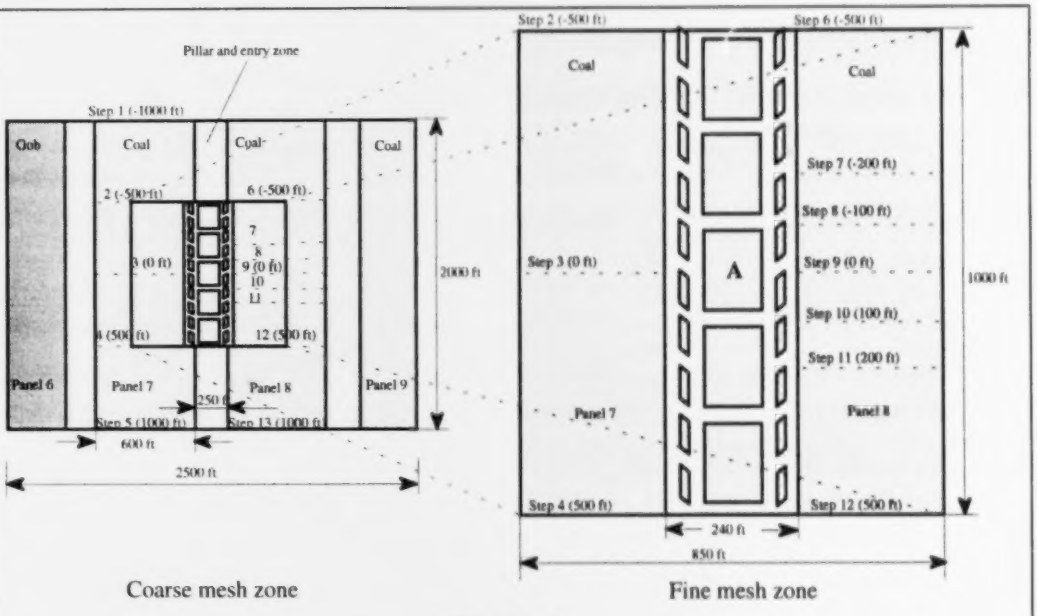

Figure 7.2

Coarse and fine mesh of the model for development 8.

The mining was simulated in 13 mining steps as indicated in figure 7.1. The pillar-entry system consists of the abutment pillars 80×80 ft (24×24 m) and the yield pillars 30 ×80 ft (9×24 m) with the entry width fixed at 20 ft (6 m), which gives the total width of 220 ft (66 m) for the pillar-entry system. The configuration of the model is very close to the pillar and entry configuration of development 7. The number of the coarse mesh elements totaled 2000, from which 20×17 were further divided into 8500 fine mesh elements.

The second case simulates the reaction of the study area 2 located in development 8 , during mining of panel 7 and panel 8. The overburden was assumed to be 2000 ft (600 m). The coarse mesh has a pattern similar to that in case 1, figure 7.1, except that the mesh was shifted to the south to include panel 6, panel 7, panel 8 and panel 9, as shown in figure 7.2. The pillar-entry system in the fine mesh consists of 120×180 ft (36×54 m) size abutment pillars, sided with the 20×80 ft (6×24 m) parallelogram shaped yield pillars, which is close to the configuration of the study area in development 8.

The detailed mesh configurations for both developments can be found in B.4 and B.5 of appendix B, respectively.

7.2.2 Model fitting and modification

Initially, the coal material model, which was originally derived by Heasley (1991) from the Olga Mine, USA, was examined to find out if it was suitable to the No. 3 Mine. The Olga Mine is extracting Pocahontas No. 4 seam which was about 60 ft (18 m) above the Poachontas No. 3 seam of VP No. 3 Mine. The geological conditions of the two mines are almost identical except the overburden depth and seam thickness. Both mines had experienced coal bumps.

Heasley's material model consists of four strengths of coal which are correlated with the location of the element in respect to a free surface, as shown in figure 7.3. The surrounding strata was assumed to be elastic with a Young's modulus 750000 psi (5171.3 MPa) and Poisson's ratio 0.25. The coal has the initial elastic modulus of 60000 psi (413.7 MPa) and the coal strength gradually falls to a residual strength after a specific peak strength is reached. The "external" coal material is located on the edge of the pillar and the peak and residual strength increases progressively toward the "core" material in the center of the pillar as shown in figure 7.4 (A).

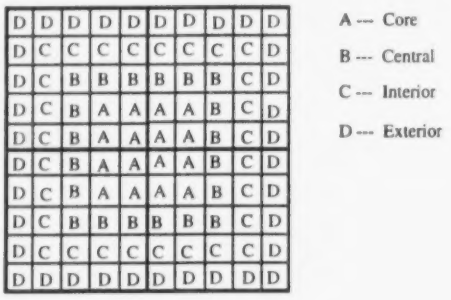
D D D D D D D D D D
D C C C C C C C C D
D C B B B B B B C D
D C B A A A A B C D
D C B A A A A B C D
D C B A A A A B C D
D C B A A A A B C D
D C B B B B B B C D
D C C C C C C C C D
D D D D D D D D D D
A --- Core
B --- Central
C --- Interior
D --- Exterior

Figure 7.3

Plane view of the fine mesh for a square pillar with different strength properties based on the location of the element to a free surface.

The "external" coal has the lowest strength and behaves more like a brittle material under the uniaxial compression, which drops its loading capacity immediately and only maintained a limited residual strength after the ultimate strength of the "external" coal is reached. This layer of coal is intended to simulate the periphery of the pillar which showed considerable fracture and yielding after the pillar was formed. To simulate the coal in the core of the pillar, the "core" coal is assigned the highest strength. The core coal behaves more like a ductile material because of the obvious triaxial compressive stress conditions. The "core" coal retains the most of its initial strength even after the ultimate load, with considerable plastic deformation. The "interior" and "central" coals have the strength in between the two extremes (exterior and core), as shown in figure 7.4 (A).

Assuming the surrounding siltstone strata has Young's modulus 690000 psi (4757.6 MPa), which is still about 10 times of the elastic modulus for coal, and Poisson's ratio 0.25, the results obtained from the application of Heasley's model properties to VP No. 3 mine immediately showed that Heasley's model led to an excessive convergence in the entries, and very weak abutment pillars which failed even before the first panel mining started. It was thought that the strengths of Heasley's model were too low for the pillars in VP No. 3 Mine.

Heasley's model properties were then modified extensively, and the results compared with the field data from the VP No. 3 Mine. The parameters in Heasley's model were adjusted until the model results corresponded as closely as possible to the observed convergence and pillar behavior which were summarized in the simplified criteria given

in the previous section. This process resulted in the modified model properties presented in figure 7.4 (B) and table 7.1.

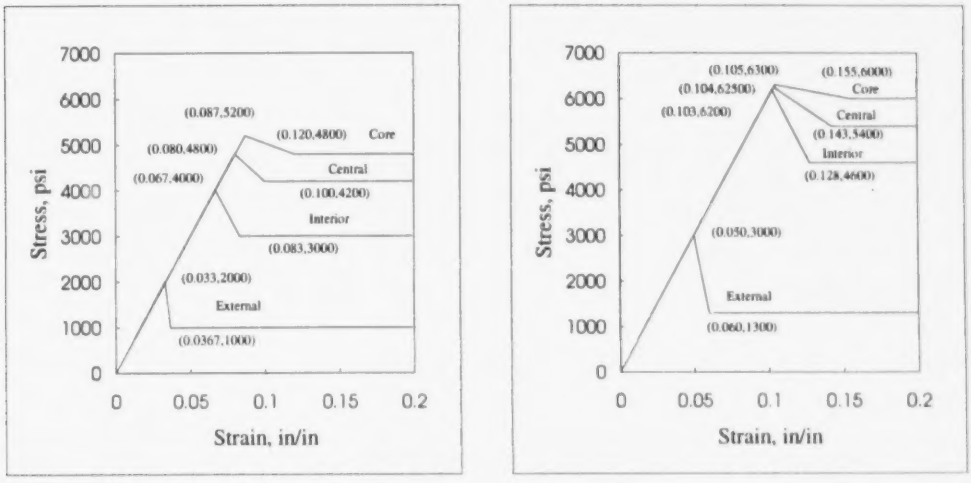

(A) Heasley's model (after Heasley, 1991) (B) Modified model after calibration

Figure 7.4

The comparison of the modified model with Heasley's model.

The estimation of the strength of the gob material needs some consideration because there are fewer studies on the mechanical and physical behavior during gob consolidation. Most researchers assume a linear elastic property for gob material in their numerical modeling, with the Young's modulus of about one-hundredth to one-fifty-seventh of that of the intact rock. (Maleki, 1990, Peng, 1984, Heasley, 1991 and Park, 1989). The behavior of gob material will affect the magnitude of the load distribution to the pillars and the deformation of the entry roof. Because of its loose and time-related consolidation nature, the assumption of the linear elastic behavior for the gob material is clearly a simplification due to the lack of the reliable studies. This may lead to either an underestimate of closure in the initial stage of gob material consolidation, or an overestimate of closure in the final stage of the consolidation.

Table 7.1 The material parameters array EPROP of the modified model.

Mode l	1	2	3	4	5	6	10	Comment
2	Strain softening coal	6300 (psi)	0.105	6000 (psi)	0.155	0.3	0	Core coal(A)
2	Strain softening coal	6250 (psi)	0.104	5400 (psi)	0.143	0.3	0	Central coal(B)
2	Strain softening coal	6200 (psi)	0.103	4600 (psi)	0.128	0.3	0	Interior coal (C)
2	Strain softening coal	3000 (psi)	0.05	1300 (psi)	0.06	0.3	0	Exterior coal (D)
5	Strain hardening gob	294 (psi)	27000 (psi)	2090 (psi)	1	0.4	0	Gob material (E)
2	Strain softening coal	2400 (psi)	0.74	2000 (psi)	0.165	0.3	0	Pillar and entry zone (F)
2	Strain softening coal	6300 (psi)	0.105	6000 (psi)	0.155	0.3	0	Coarse mesh for coal (G)

Zipf (1992) developed an impressive strain hardening gob material model when he was revising the MULSIM/NL program. The model was specified as type 5 strain hardening model in table 4.1, chapter 4. However, he did not specify a typical value for the initial and final moduli, or a method to derive them. A recent laboratory and field study (Mark, 1993) on the strain hardening behavior of shale, weak sandstone and strong sandstone gob materials suggested a simple formula for determination of the tangent modulus of gob materials. In the study approximate particle size gradations of gob material was obtained by digitizing photographs of actual mine gob. The gradations were scaled down to a laboratory scale. Uniaxial compression tests were performed on the laboratory scale gob material. The obtained formula is an approximation of the laboratory tests on the man-made gob materials and can be presented as:

$$E_t = 0.00181\sigma^2 + 9.33\sigma + 294 \qquad (7.1)$$

where E_t is the tangent modulus and σ is the the mean uniaxial applied stress on the material, with the units of psi for both E_t and σ.

Equation (7.1) indicates that the modulus of the gob material increases with the stress increase, due to the compacting and consolidation of the gob material with the roof deforming and caving. It is generally accepted that the maximum load the gob material can take is the overburden weight. Therefore, the modulus at $\sigma = 0$ and at $\sigma =$ overburden stress, will correspond to the initial or final value of the gob material modulus. For the above reason, the formula (equation 7.1) was used to estimate the required initial and final moduli for the Zipf's strain hardening model 5, which are presented in table 7.1 as the gob material model labeled by E.

The model given in table 7.1 was applied to simulate the longwall mining in VP No. 3 mine and the local mine stiffness of the pillar A (refer to figure 7.1 and 7.2) was calculated throughout the mining of the adjacent panels. The detailed input and output data for the simulation are included in appendix B.4 and B5. The material parameters for the local mine stiffness elements (labeled by H, I, J and K in the fine mesh of the model outputs in appendix B.4 and B.5) in the model are not listed in the table 7.1 because they are similar to those of the other pillars, except the 10th column of the material parameter array for the elements has the assigned value 1, instead of the value 0. The strength of the panel entry zone (labeled by F) in the model was reduced about 50% from the average strength of the solid coal because of 50% extraction ratio of the zone.

The detailed input parameters and program outputs for both developments 7 and 8 can be found in B.4 and B.5 of appendix B. The vertical stress and closure for selected mining steps of both developments are included in figures D.13 to D.16 of appendix D.

7.3 Comparison of the model with the observed results

The vertical stress in the abutment pillars and the closure of entries for both development models are analyzed and compared with the fitting criteria given in section 7.1. Emphasis is on the timing of the yielding of the yield pillars and the failure of the abutment pillars.

7.3.1 Development 7

A typical vertical stress distributions of the vertical stress and closure for development 7 model are presented in figure 7.5 (mining step 3). Similar figures for other mining steps are included in appendix F (figure F.1 through F.6). Figure 7.5 shows there is about 2000 psi (13.8 MPa) overburden pressure on the intact seam (figure 7.5 (A)) and the maximum closure of more that 20 in (5.1 cm) occurred at the center of the gob area (figure 7.5 (B)).

(1) Vertical stress

The vertical stress, at the cross section of pillar A in figure 7.5, with the face distance to the pillars is plotted in figure 7.7. It is interesting to compare figure 7.6 with the corresponding field result figure 6.9 (A). Because the field stress value was measured at specific points, but the simulated stress value was the average of the 10×10 ft (3×3 m) block, the fluctuation in figure 6.9 (A) is understandable. Note also that the measured data are supposed to be the change of the vertical stress. It is clear that the absolute magnitude of the measured vertical stress change is considerably higher than that of the simulation. However, the fitting of the absolute magnitude of the vertical stress is not a major concern because of doubts on BPF calibration of the field absolute stress data (Campoli, 1993). The values of the measured vertical stress at some points are considered too high for coal material. Therefore, the emphasis is placed on the simulation of the trend of the vertical stress change and the pillar behavior. Only the vertical stress change pattern was dealt with in the following discussion.

Figure 7.6 shows that the advance of the first longwall face from 1000 ft (300 m) in by to 500 ft (150 m) in by the pillars did not affect the vertical stress of the pillars at cross section A-A because the vertical stress distribution at 1000 ft (not in the figure) exactly duplicated that at 500 ft; the abutment pillar is still in good shape when the first face was in the line with the pillar (see also figure 7.5); the vertical stress built up around the abutment pillar edge when the first face was passing the pillars, and the core part of the pillar gradually failed as the face passed away from the outby 500 ft position. This behavior is very comparable to the field result (refer to figure 5.7 (A) and (B)).

(2) Closure

The entry closures of the simulated results at cross section of pillar A are presented in figure 7.7. Note that mining steps 3 and 9 correspond to the first face and the second

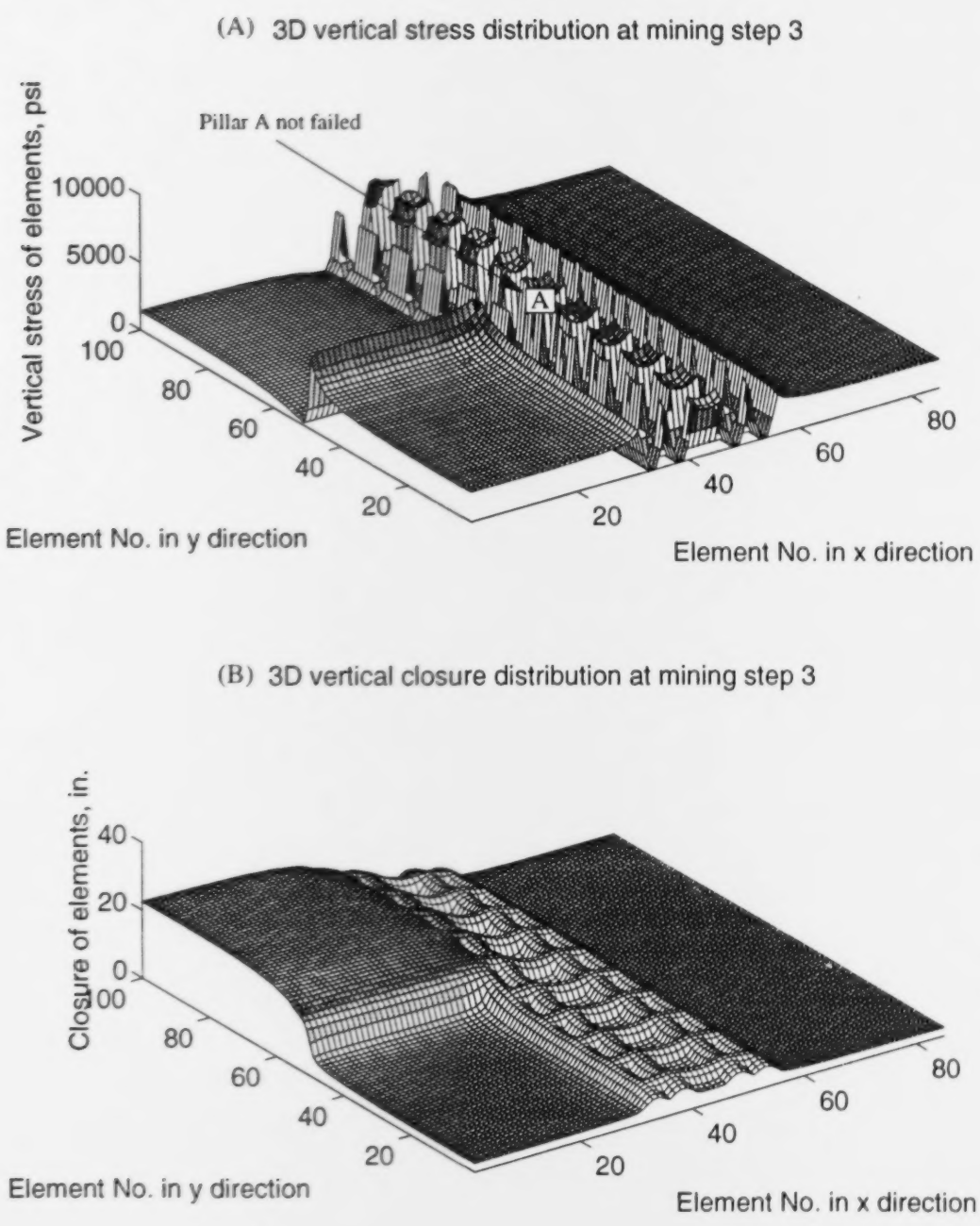

Figure 7.5

3D vertical stress and closure for development 7 model at mining step 3.

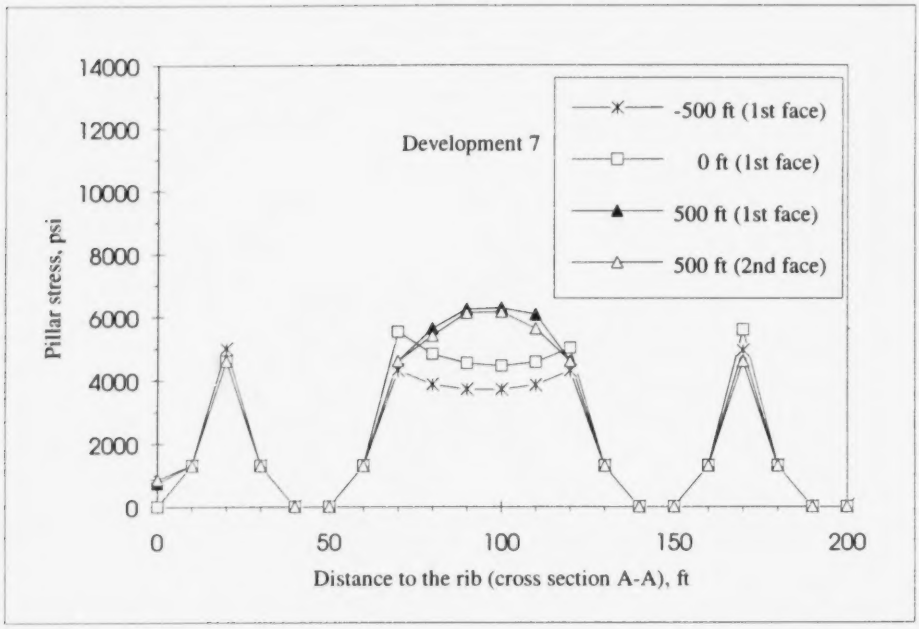

Figure 7.6

Cross section view of vertical stress at line A-A of the development 7 model.

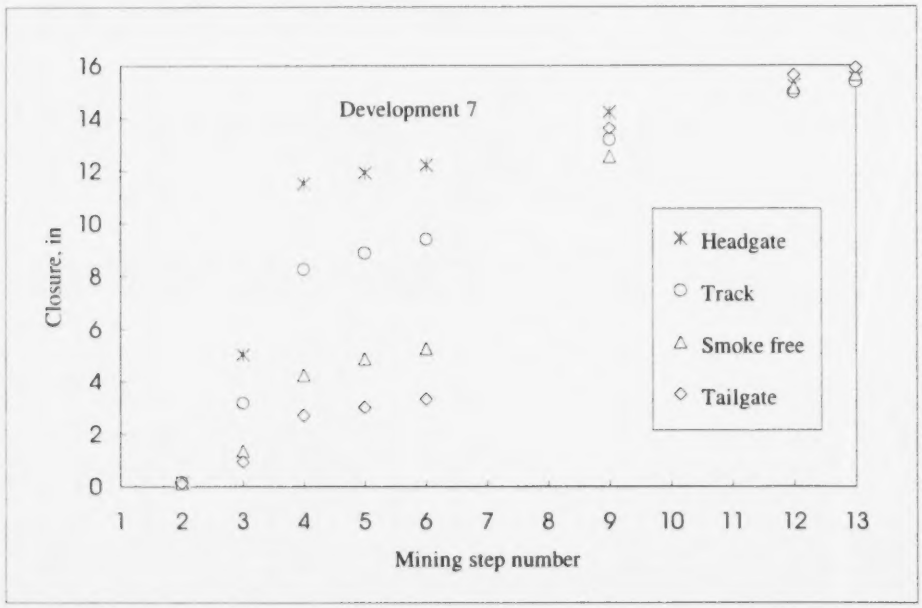

Figure 7.7

Closure of entries at cross section A-A of the development 7 model.

face being in the line with the monitoring pillar line, respectively. Again, similar to figure 6.10 (A) and (B), the effect of the first face advance on the abutment pillar occurred when the face was in the 500 ft (150 m, mining step 2) range from the abutment pillar; the tilt of the entry roof strata to the gob is also obvious. The magnitude (2 to 12 in or 5.1 to 30.5 cm from tailgate to headgate) of the closure in the panel entries is also in the range of the measured data range (2 to 8 in or 5.1 to 20.3 cm from tailgate to headgate).

(3) Failure of pillars

The failure of the yield pillars and abutment pillar are also consistent with the field results. Figures 7.6 and 7.7 show that the edges of pillars apparently yield to the development load in the simulation. The result in figure 6.6 indicates that the headgate yield pillar fell to its residual strength when the first face was in the line with the pillar (also compare figures F.1 and F.2 in appendix F); the tailgate yield pillar yielded when the first face was 500 ft (150 m) outby the pillar; the failure of the abutment pillar started when the first face was 500 ft outby (refer to figures F.2 and F.3 in appendix F); the abutment pillar only retained its residual strength after the second face was 500 ft in by (mining step 6, also compare figures F.4 and F.5 in appendix F).

7.3.2 Development 8

A typical three dimensional presentation of the vertical stress and the closure in development 8 is shown in figure 7.8 (mining step 9). Figure F.8 through F.15 in appendix F show the similar figures for selected mining steps.

(1) Vertical stress

Figure 7.9 shows the cross section view of the simulated vertical stress at line A-A of development 8. This figure also compares well with the field data in figure 6.9 (A). The stress first peaked around the boundary of the abutment pillar. With the failure of the highly stressed part of the pillar, the peak migrated into the pillar core. The abutment pillar and the edge of the second panel sustained the substantial loads even after the second face came very close, which protected the tailgate and smoke free entries from excessive closure.

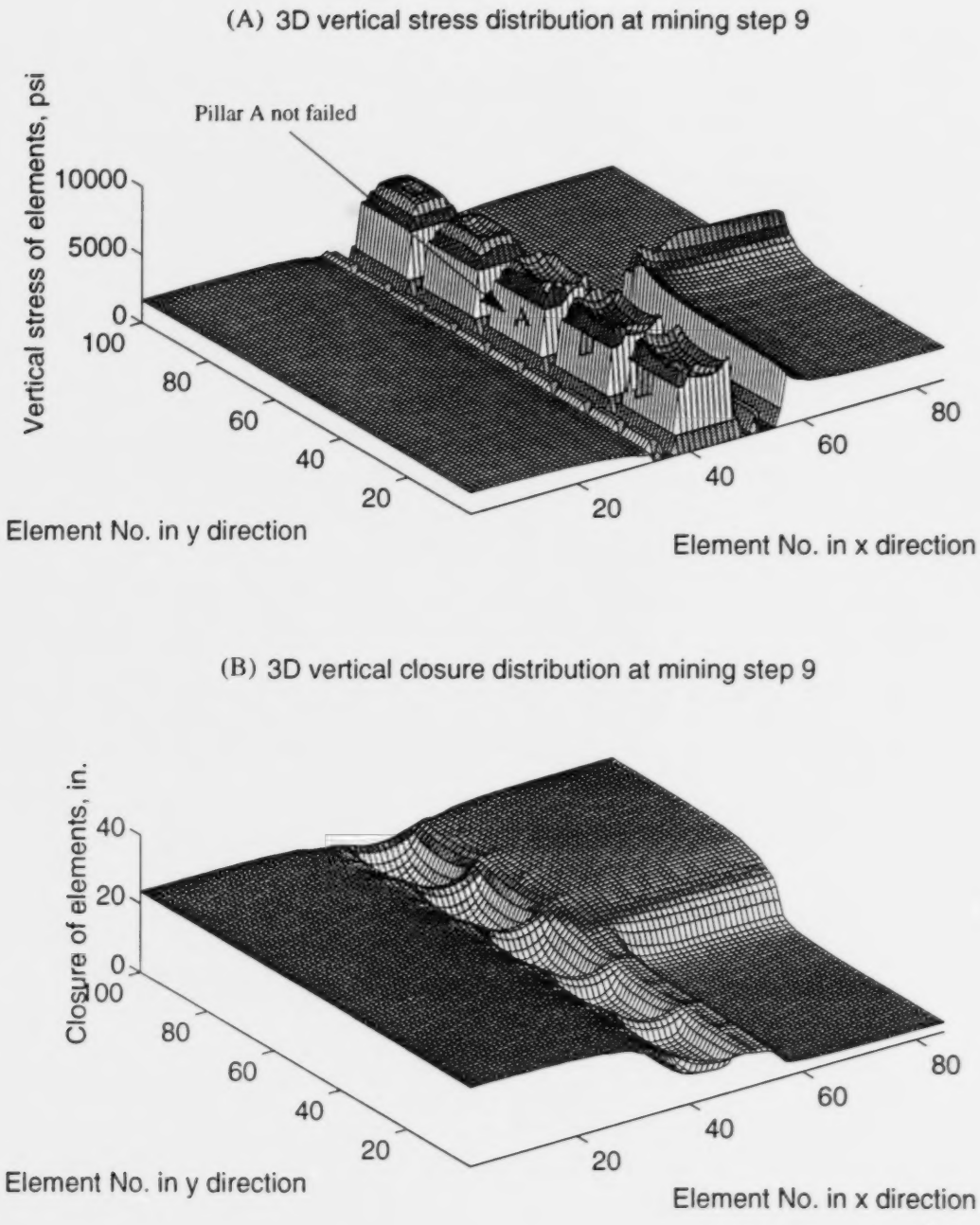

Figure 7.8

3D vertical stress and closure for development 8 model at mining step 9.

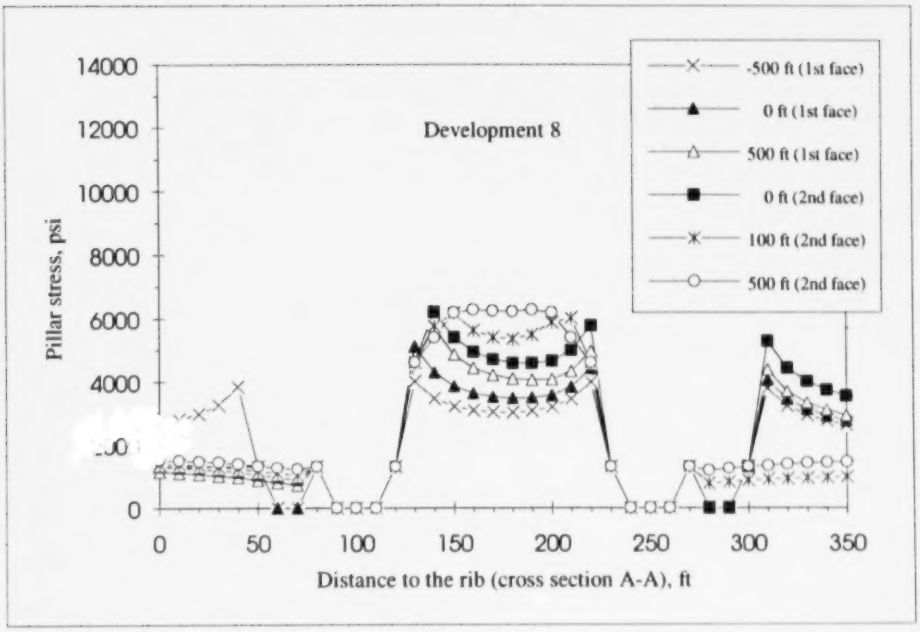

Figure 7.9

Cross section view of vertical stress at line A-A of the development 8 model.

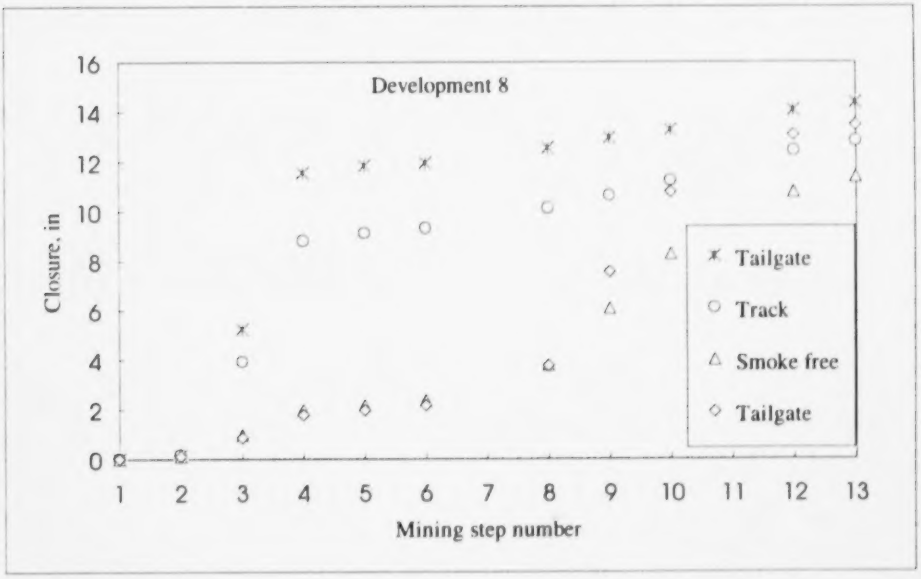

Figure 7.10

Closure of entries at cross section A-A of the development 8 model.

(2) Closure

As shown in figure 7.10, the closure of 9 in (22.9 cm) and 12 in (30.5 cm) in the track and headgate of development 8 is very similar to that of development 7, which is also very comparable to the field measured result of 10 in (25.4 cm) in track entry. The closure in the smoke free and tailgate entries remained at 2 in (5.1 cm) level through the passage of the first face and until the second face was very close (100 ft or 30 m in by, mining step 8). The closure accelerations and their timing are also consistent with the field measured data.

(3) Failure of pillars

As shown by figure 7.9, the headgate and tailgate yield pillars both yield very early to the development load. Figure 7.8 also shows that the abutment pillar was still in good shape when the second face was in the line with the pillar (also refer to figure 7.10), and did not fail until the second face was 500 ft (150 m) outby (compare figure F.9 through F.13 in appendix F). These are also consistent with the geotechnical interpretation of the field result in the previous chapter.

7.3.3 Summary

The patterns of the change in the measured vertical stress were demonstrated by the simulated model. The simulated closures in the headgate, track, smoke free and tailgate entries are comparable with the field data for both developments. The timing of the simulated yield and abutment pillars in both developments are also consistent with the geotechnical interpretation of the field measured results.

7.4 Local mine stiffness analysis

The comparison of the simulated results with the simplified field results suggested that the field reaction of the panel entries and pillars in development 7 and development 8 can be simulated reasonably well by the model developed in the previous sections. Therefore, this model can be used for the further stability study based on the stress-strain analysis and the local mine stiffness concept.

7.4.1 Development 7

The relation between the average stress, average strain and local mine stiffness of the abutment pillar in development 7 to the advance of the longwall face (represented by the mining step number) is presented in figure 7.11.

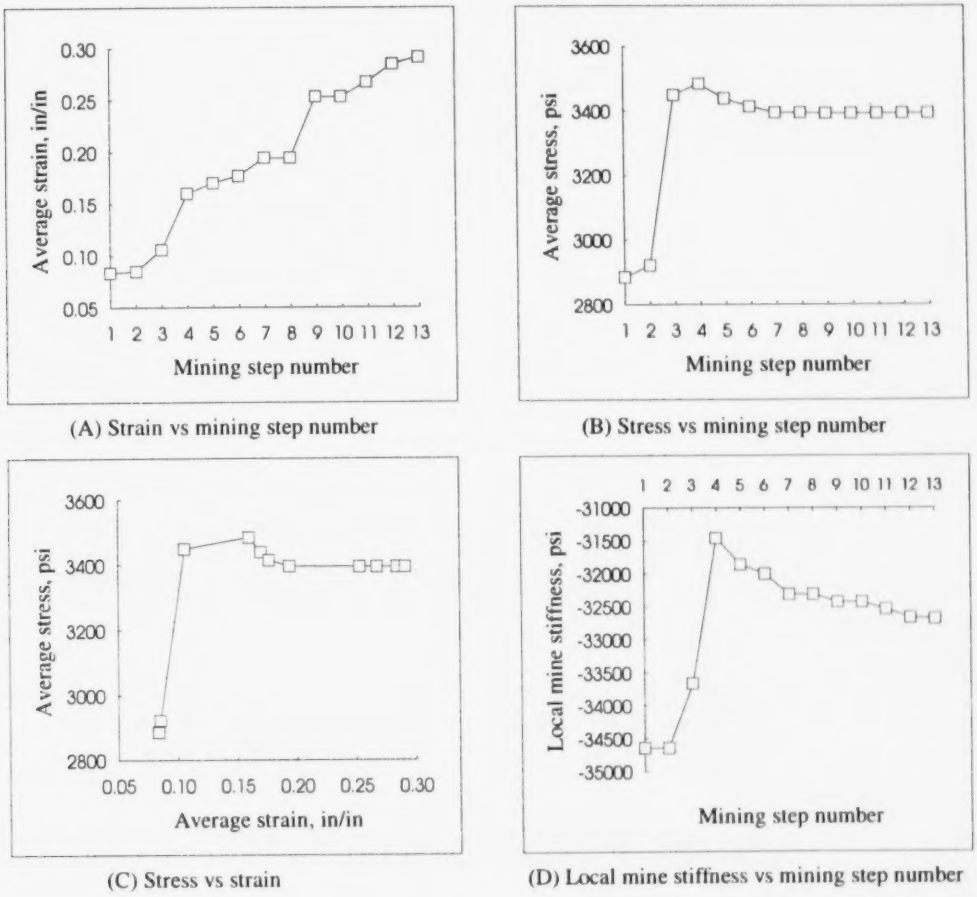

(A) Strain vs mining step number

(B) Stress vs mining step number

(C) Stress vs strain

(D) Local mine stiffness vs mining step number

Figure 7.11

Simulation result for development 7 model.

Although the three dimensional presentation of the vertical stress and closure of the development 7 clearly showed that the vertical stress and vertical deformation of the abutment pillars are non-uniform across the pillars, it is still surprising to find from figure 7.7 that how well the averaged vertical stress and strain across the pillars can represent the whole picture of the loading and deformation process of the abutment pillars.

It is seen from figure 7.11 that the deformation and loading of the abutment pillar is smooth except at mining steps 3, 4 and 9. Mining steps 3 and 9 correspond to the first face and the second face being in the line with the pillar, respectively. Mining step 4 is the position where the first face was 500 ft (150 m) outby the pillar. Clearly, the face being in the line with the pillar affected the behavior of the pillar significantly. The effect was represented by the jump of the deformation and vertical stress. The abutment pillar remained elastic during the first three mining steps, then the signs of failure of the abutment pillar emerged. The pillar apparently failed (decrease of the vertical stress) after mining step 4 and the failure process continued until mining step 7. After that, the pillar only retained its residual strength and deformed without any further loss of its loading capacity.

It will be noticed that although the arrival of the first face (mining step 3) caused the most significant load change in the pillar, the biggest local mine stiffness drop (absolute value) occurred at mining step 4. Because the pillar was still in an elastic condition at mining step 3 and obviously reached its ultimate strength at mining step 4 when the pillar entered its post-failure region, the greatest change in the local mine stiffness at mining step 4 implies that the failure of the pillar affected the local mine stiffness significantly in this case. This phenomena was also observed in the local mine stiffness analysis in chapter 4. Note that although the determination of the local mine stiffness for a specific pillar only depends on the other pillars around the pillar, not on the pillar itself, the effect of the specific pillar on its local mine stiffness appeared because the pillars that were close to the specific pillar also had the same shape, the same material property and a very similar loading and deformation status as the specific pillar, i.e., the adjacent pillars may have failed at the same time as the specific pillar, which may lead to the coincidence of the pillar failure and its minimum local mine stiffness.

Figure 7.11 (D) shows that after reaching its minimum (absolute value) at mining step 4, the local mine stiffness gradually rebounded with further mining. The rebound of the local mine stiffness after the pillar totally yielded is believed to be related to the readjustment of the roof because of the failure of the pillar.

Because the least values (absolute value) of the local stiffness occurred at mining steps 4 (31463 psi), 5 (31861 psi) and 6 (32004 psi), a logical prediction for the pillar bumps would be also correspond to the three mining steps. The post-failure stiffness of the abutment pillar was estimated by the power function approximation presented by equation (4.7) in chapter 4. With an initial elastic Young's modulus 60000 psi (413.7

MPa) and the width/height ratio 13.7, the estimated post-failure pillar stiffness would be 15620 psi (107.7 MPa). Because the local mine stiffness was greater than the estimated post-failure pillar stiffness (absolute value), a pillar bump was excluded theoretically. However, the extreme value of the local mine stiffness does suggest that if there were any unusual conditions (such as the irregularity in geology or in composition of the pillar leading to underestimation of the post-failure stiffness of the pillar), the most likely time for the pillar to bump would be between mining step 4 and mining step 6. The pillar actually bumped when the second face was 500 ft in by the pillar, which corresponds to mining step 6 in the simulation. On the other hand, some field data (appendix E.6 and E.7) indicated that for very wide pillars (W/H > 9), the post-failure stiffness is still close to its initial elastic modulus. This will put the post-failure stiffness of the abutment pillar in development 7 in the range of the local mine stiffness. Therefore, the pillar bump in development 7 can not be excluded.

7.4.2 Development 8

As shown in figure 7.12, the stress and strain of the abutment pillars in development 8 are much smoother than that in development 7. The average stress and strain increased with mining step number. The pillar reached its ultimate strength after the mining step 12 when the second face was 500 ft (150 m) outby. The mining steps 3 and 4 had most significant stress increases.

The local mine stiffness change is shown in figure 7.12 (D). The accuracy of the obtained local mine stiffness was checked by increasing the perturbation displacement from previous 0.1 in (0.254 cm) to 1 in (2.54 cm), while maintaining the stress convergence level at 0.01 psi (69 Pa). The increased perturbation result shows a small improvement of the local mine stiffness, which confirmed that the convergence error is not significant. However, the discussion below is still based on the 1 in perturbation result.

The local mine stiffness showed that the first significant decrease (absolute value) corresponded to the passage of the first face (mining step 3). The second significant change of the local mine stiffness occurred after mining step 6, which is the position when the second face was 500 ft in by. The local mine stiffness continued to decrease and reached its minimum 19866 psi (137 MPa) at mining step 9 when the second face was in the line with the pillar. After that, the local mine stiffness value had a small rebound from the minimum and remained at the lower level (20200 psi or 139.3 MPa) there after. It is

evident that a possible pillar bump could occur at mining step 9 and its following mining steps, if only the role of the local mine stiffness is considered. However, because the pillar entered its post-failure region after mining step 12, the most likely timing for the abutment pillar to bump would be mining step 12, when the second face was 500 ft (150 m) outby the pillar, and its following mining steps. This conclusion coincides with the field observed result that the abutment pillars in development 8 continued to bump after the second face was 500 ft outby.

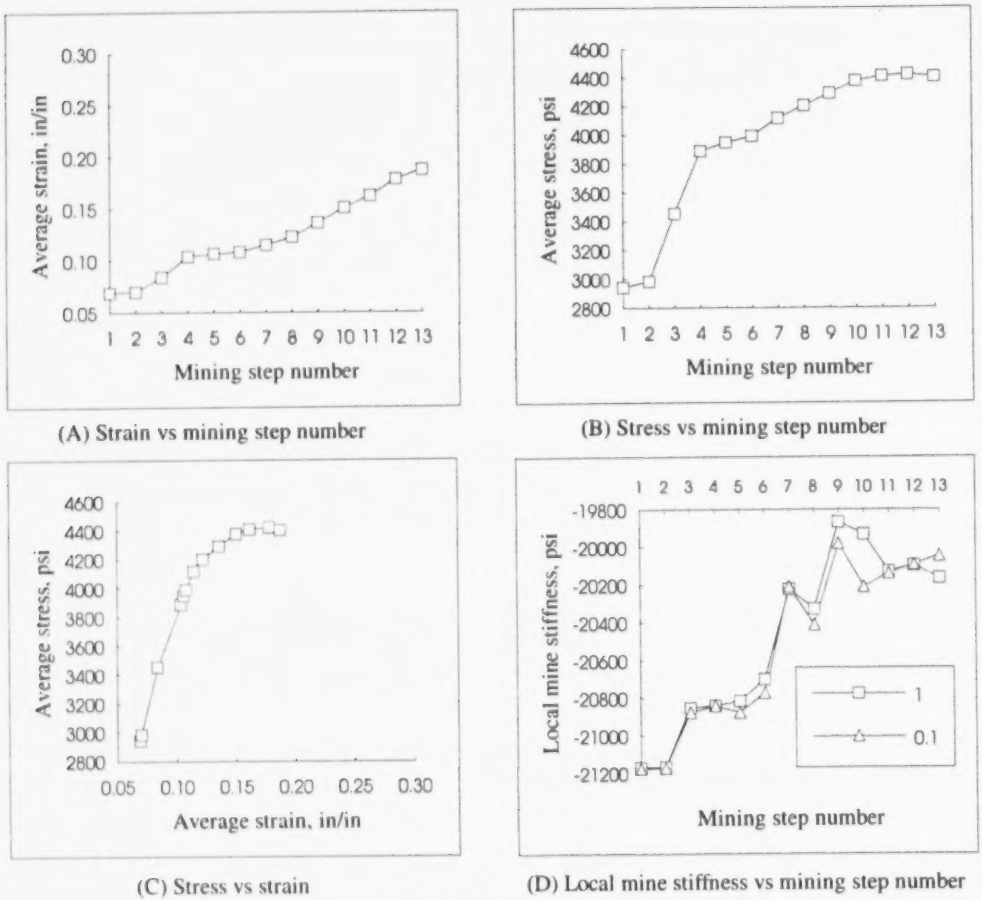

(A) Strain vs mining step number

(B) Stress vs mining step number

(C) Stress vs strain

(D) Local mine stiffness vs mining step number

Figure 7.12

Simulation result of development 8 model.

It is worthwhile noting that, unlike the abutment pillar in development 7, the timing when the local mine stiffness reached its minimum did not correspond to the time when the pillar entered its post-failure region in development 8. The reason for this is that the

local mine stiffness depends on the behavior of other pillars in the panel. Although the pillar may still be in its pre-failure region, the other pillars near by may have already entered their post-failure region, which may lead to the lowest value of the local mine stiffness for the non-failed pillar. This partially illustrates the fact that a pillar bump does not necessarily occur at the time when the local mine stiffness reaches its minimum, because the pillar may be still in its pre-failure region at that time.

7.4.3 Comparison of the two developments

The necessary condition for a pillar to bump is that the pillar must be in its post-failure region. This condition combined with the second condition that the post-failure stiffness must be equal or greater than the local mine stiffness, makes the necessary and sufficient conditions for a pillar to bump.

Surprisingly, the local mine stiffness of development 8 is smaller than that of development 7. This gave the first impression that the abutment pillars in development 8 are more prone to pillar bumps than that in development 7. However, because in development 8, the abutment pillars entered their post-failure region later and the post-failure pillar stiffness is also smaller compared to that in development 7, the difference of the magnitude of the local mine stiffness may not as significant as the difference in the post-failure pillar stiffness and of the time of entering the post-failure period.

The simulation results showed that the abutment pillars in development 7 are prone to bump during mining steps 4, 5 and 6. However, the abutment pillars in development 8 are not going to bump until mining step 12 when the second face was 500 ft (150 m) outby the pillars. Although the change of the pillar configuration in development 8 reduced the absolute magnitude of the local mine stiffness, it also reduced the post-failure pillar stiffness according to figure 5.13 and equation (5.1). The improvement of the condition of the abutment pillars in development 8 is obvious because of the strength improvement due to the increased pillar dimension.

7.5 Conclusions

The simulation results showed that the numerical model developed in this chapter simulated the field result reasonably well. Based on the model, the mechanism of the

pillar bumps which occurred in developments 7 and 8 is demonstrated by the stress-strain analysis and the local mine stiffness evaluation.

Clearly, the timing for abutment pillars in development 7 to bump is between mining steps 4 and 6, during which the pillar is in its post-failure region and its local mine stiffness is at its lowest level; the timing for the abutment pillar in development 8 to bump is at or after mining step 12 for the same reason.

The most efficient way to eliminate pillar bumps during face passage is to increase the pillar dimension. Although the local mine stiffness evaluation will give the most likely pillar bump timing, the exact bump prediction is still not possible because of the difficulty in determination of the post-failure stiffness of pillars in the field.

Chapter 8

SUMMARY, CONCLUSIONS AND RECOMMENDATIONS FOR FURTHER RESEARCH

8.1 Summary and conclusions

The local mine stiffness for chain pillars is defined by the given uniform displacement perturbation across the mid-pillar section and its associated average load difference. The defined local mine stiffness concept was implemented into the MULSIM/NL displacement discontinuity boundary element program to evaluate the stability of the chain pillars in longwall panels under the bump-prone conditions. The computer program was verified by comparing an available analytical solution and modeling results based on an elastic model. A series of parametric numerical studies were performed to examine the significance of the geological and geometric change of the seam, strata and longwall panel on the local mine stiffness defined above.

In particular, the following contributions are made to stability evaluation in longwall chain pillar design:

(1) This is the first implementation of the whole pillar perturbation concept into a three dimensional displacement discontinuity boundary program for the determination of the local mine stiffness.

(2) This is the first comprehensive examination of the effect of the pillar configuration, strata stiffness, pillar strain softening behavior and longwall face advance on the local mine stiffness defined in the thesis.

(3) This is also the first case study and three dimensional model simulation incorporated with the local mine stiffness estimation to evaluate the stability of a longwall mine with different pillar configurations which experienced serious pillar bumps problems, and to demonstrate the application of the local mine stiffness evaluation process developed in the thesis.

The following conclusions were drawn from the examination on the local mine stiffness:

For a pillar location in the elastic model:

(1) The local mine stiffness decreases with the face advance and the biggest decrease of the local mine stiffness occurs when the face is close to or in the line with the pillar.

(2) The magnitude of the local mine stiffness drops because of the passage of the longwall face is significantly lower than that of the strain-softening model.

For a pillar location in a strain-softening coal model:

(1) The magnitude of the local mine stiffness drop increases with the increase of the overburden.

(2) The local mine stiffness decreases with the face advance and the significant decrease of the local mine stiffness occurs when the face is close to or in line with the pillar; the biggest local stiffness drop occurs when the pillar has failed or is close to failure.

(3) The modulus of the surrounding strata dominates the magnitude of the local mine stiffness but the longwall face advance also has a significant effect; the brittle coal has greater local mine stiffness drop than the soft coal because of the earlier failure and lower residual strength of the brittle coal.

(4) The pillars along the panel entry behave similarly, but the pillars across panel entries may behave differently, as far as strain, stress and local mine stiffness are concerned. This suggests that only the stability of one row of pillars (i.e. a headgate pillar, a tailgate pillar and the pillar in between) needs to be evaluated instead of all the pillars in the longwall panels.

(5) The headgate pillars have the least bump potential and the center pillars have the biggest bump potential, if they have the same size; in a combination system of yield pillars and abutment pillars, the headgate abutment pillar design is the best because it experiences the least local mine stiffness reduction after the excavation of the second panel.

The available post-failure pillar stiffness data from field and laboratory tests were collected and analyzed, from which an approximate power function relationship for the post-failure pillar stiffness and the pillar width/height ratio was derived. This power

function defines the upper boundary of the post-failure pillar stiffness in the range of the available data. Beyond this range of the data, the post-failure pillar stiffness can also be estimated crudely by the function. However, the estimation beyond the data range may not necessarily be the upper boundary of the post-failure pillar stiffness.

Based on the results of the parametric studies on the local mine stiffness and analysis of the post-failure pillar stiffness, a methodology of the chain pillar design in the bump prone coal beds was proposed as follows:

(1) The numerical model is first built according to the initial design and the results of site investigation and testing. The model is fine-tuned by fitting the calculated stress and deformation to the measured stress and deformation. The calculated stress and deformation should agree with the measured stress and deformation throughout the panel extraction, or agree with the estimated results from the experience if the measured results are not available.

(2) Then, the local mine stiffness at the sites of interest (which should be the sites close to the face) are calculated through all the mining steps. Only one row of pillars across the section of the entries needs to be considered.

(3) Finally, the calculated local mine stiffness of a specific pillar is compared to the estimated post-failure stiffness of the pillar. To avoid pillar bumps, the local stiffness should be higher than the estimated post-failure stiffness through the panel excavation. Dimensions of the pillars and configurations of the pillars in the panel can be varied to control the time when the local mine stiffness approaches the post-failure stiffness, thus the time and place of the pillar bumps can be controlled in case the bumps cannot be avoided.

The application of the local mines stiffness evaluation and pillar design methodology were demonstrated by a numerical back analysis. To set up the numerical model for the back analysis, the field data of VP No. 3 mine collected by the US Bureau of Mines were subjected to a geomechanical interpretation and analysis, which resulted in a guideline for the setting up of the numerical displacement discontinuity boundary element model.

The behavior of the two different longwall developments during the excavation of the adjacent panels, were simulated by the numerical model. The pillar behavior and the pillar bump mechanism in the two developments was well demonstrated by the stress-strain analysis and the local mine stiffness evaluation based on the derived numerical

model. The following conclusions were drawn from the model simulation and the local mine stiffness evaluation:

(1) The behavior of chain pillars in longwall panels can be simulated reasonably well by the numerical model which is based on the field measurement or estimate;

(2) The timing and location of the potential pillar bumps can be predicted by the numerical stress-strain analysis and the local mine stiffness evaluation.

(3) The pillar bumps in longwall mining may be unavoidable because of the close gap between the local mine stiffness and the post-failure pillar stiffness; However, the timing of the potential pillar bumps can be delayed and the bump location can be isolated by increasing the pillar dimension.

8.2 Recommendations for further research

The simulation of the field mining and the calculation of the local mine stiffness for a longwall panel often involves great numbers of fine mesh elements (in the 100×100 order) and coarse mesh elements (in the 50×50 order). With the Gauss-Seidel iteration, there is no problem with the solution convergence speed when there are only the elastic elements or when the nonlinear elements are still in the elastic range in the model. When the nonlinear behavior occurs (strain-softening for coal or strain-hardening for gob), the solution convergence slows down considerably. The solution for one mining step at yielding stage may take more than 30 hours CPU time for a IBM RS/6000-220 workstation or a Sun Sparc workstation (IPX), or 10 hours for a IBM RS/6000-550. It is especially painful when the model is still in the modification stage, because the frequent adjustments of the input parameters and frequent checks of the results are essential at this stage. The time constraints of the computer CPU is also the main reason that prevented author from a more detailed study of the post-failure pillar stiffness and from "best fitting" the field results. Therefore, it is recommended here that a faster workstaion will be more practical for future numerical simulations of the longwall mining and calculations of the local mine stiffness.

It is also clear that more studies are needed to derive or to measure the post-failure pillar stiffness, especially for the wide or squat pillars with width/height ratio beyond 9. It is felt that there are some available field data which need close examination for the

possibility of deriving the post-failure stiffness for wide pillars. On the other hand, it is possible for the numerical model to give an estimate of the average post-failure pillar stiffness at a specific mining step by specifying another small mining step (advancing the longwall face a very short distance). However, this process will complicate the input file and will double the computing time and input work. The examination of the significance of the small mining step on the post-failure pillar stiffness is also needed before the implementation can be made.

To compensate for the effect of lack of lateral confinement between elements in the displacement discontinuity model, the input strength parameters for the elements of a pillar are changed according to the distance of the elements from the free surface. This not only makes the input more complex but leads to a greater difficulty in model fitting; it also delays the solution convergence significantly. The results from fitting the model to the field data indicated that specifing a strength increase with the distance to the free surface may not be necessary because, if this is not done, the final results showed little difference. Therefore, it is thought that the material model might be further simplified by using fewer material types without changing the overall conclusions.

Although the MULSIM/NL and its modified local mine stiffness version can handle the seams with different inclinations, all studies and the conclusions drawn in this thesis concern only the horizontal or very flat strata. The shear behavior of the inclined seams on the local mine stiffness is not examined in the thesis. The effect of the original horizontal stress and the angle of the inclination of the strata on the local mine stiffness have to be studied before the local mine stiffness concept defined in the thesis, and the proposed pillar design methodology, can be applied to the inclined seams.

REFERENCES

Babcock, C. O. (1990). True uniaxial compressive strengths of rock or coal specimens are independent of diameter-to-length ratio. RI 9316, U.S.B.M.

Babcock, C. O., & Bickel, D. L. (1984). Constraint - the missing variable in the coal burst problem. Proceedings of the 25th U.S. Symposium on Rock Mechanics, 639-647.

Barron, K. (1983). The analytical approach to the design of coal pillars. Part 1: the analytical model. Part 2: application of the model to case histories (ISQ 80-00161). Dept. Supply and Services, Ottawa.

Barron, K. (1984). An analytical approach to the design of coal pillars. CIM Bulletin, (August), 37-44.

Barron, K. (1988). A study of pillar behavior in bursting conditions in a longwall mine (PO 382044). U.S. Bureau of Mines.

Barron, K., & Pen, Y. (1992). A revised model for coal pillars, IC 9315, U.S.B.M., 144-157

Bieniawski, Z. T. (1967). The mechanism of brittle fracture of rock . International Journal of Rock Mechanics and Mining Sciences, 4, 396-435.

Bieniawski, Z. T. (1968). The effect of specimen size on compressive strength of coal. Int. J. Rock Mech. Min. Sci., 5, 325-335.

Bieniawski, Z. T. (1992). Ground control. SME Mining Engineering Handbook (Vol. 1, second edition), 923-937.

Brady, B. H. G., & Brown, E. T. (1980). Energy changes and stability in underground mining: design applications of boundary element methods. Trans. Inst. Min. Metall., 90(Section A), A61-68.

Campoli, A. A., Kertis, C. A., & Goode, C. A. (1987). Coal mine bumps: five case studies in the Eastern United States, IC 9149, U.S. Bureau of Mines.

Campoli, A. A., & Heasley, K. (1989). Coal mine bump research: providing tools for rational longwall design. Proceedings of the 23rd International Conference of Safety in Mines Research Institutes, Washington, D.C., 666-676.

Campoli, A. A., Barton, T. M., Dyke, F. C. V., & Gauna, M. (1990). Mitigating destructive longwall bumps through conventional gate entry design, RI 9325, U.S. Bureau of Mines.

Campoli, A. A., Barton, T. M., Dyke, F. C. V., & Gauna, M. (1993). Mitigating destructive longwall bumps through conventional gate entry design, RI 9445, U.S. Bureau of Mines.

Carr, P., & Wilson, A. H. (1982). A new approach to the design of multi-entry developments for retreat longwall mining. Proceedings of the 2nd Conference on Ground Control in Mining, Morgantown, 1-21.

Carr, F., Martin, E., & Gardner, B. H. (1984). How to eliminate roof and floor failures with yield pillars (Part I and Part II). Coal Mining, Vol. 21(Dec.), 62-72.

Choi, D. S., & McCain, D. L. (1980). Design of Longwall systems. Transactions of SME of AIME, 268, 1761-1764.

Coates, D. F. (1965). Rock Mechanics Principles. Ottawa: CANMET.

Cook, N. G. W. (1965). A note on rockbursts considered as a problem of stability. Journal of the South African Institute of Mining and Metallurgy, 65(March), 437-446.

Cook, N. G. W. (1967). Contribution to discussion (Salamon, M.D.G. and Munro, A.H. A study of the strength of coal pillars). J. S. Afr. Inst. Min. Metall., 68(November), 192-195.

Cook, N. G. W., Hodgson, K., & Hojem, J. P. M. (1971). A 100-MN jacking system for testing coal pillars underground. Journal of the South African Institute of Mining and Metallurgy, (June), 215-224.

Crouch, S. L., & Fairhurst, C. (1973). The mechanics of coal mine bumps and the interaction between coal pillars mine roof and floor (H0101778). U.S.B.M.

Das, M. D. (1986). Influence of width/height ratio on post-failure behavior . International Journal of Mining and Geological Engineering, (4), 79-89.

Gaddy, F. L. (1956). A study of the ultimate strength of coal as related to absolute size of the cubical specimens tested. Bulletin of the Virginia Polytechnic Institute (Engineering Experiment Station Series No. 112, August). 1-27

Gill, D. E., Aubertin, M., & Simon, R. (1993). A practical engineering approach to the evaluation of rockburst potential. Draft paper for proceedings, private communication. 1-6

Haramy, K. Y., & McDonnell, J. P. (1988). Causes and control of coal mine bumps. RI 9255, U.S. Bureau of Mines.

Heasley, K. (1991). An examination of energy calculations applied to coal bump prediction. J. C. Roegiers (Ed.), Proceedings of the 32nd U.S. Symposium on Rock Mechanics. University of Oklahoma, Norman: A. A. Balkema, 481-490

Heasley, K. A., & Zelanko, J. C. (1992). Pillar design in bump-prone ground using numerical models with energy calculations. IC 9315, U.S. Bureau of Mines. 50-60.

Heerden, W. L. V. (1975). In situ complete stress-strain characteristics of large coal specimens. Journal of the South African Institute of Mining and Metallurgy, (March), 207-217.

Hoek, E., & Brown, E.T. (1980). Underground Excavations in Rock. London: Instn. Min. Metall.

Holland, C. T. (1955). Rock burst or bumps in coal mines. Colliery Engineering, (April), 145-153.

Holland, C. T. (1964). The strength of coal in mine pillars. Proceedings of the 6th Symposium on Rock Mechanics. University of MO, Rollars, MO, 450-466

Holland, C. T. (1973). Mine pillar design. SME Mining Engineering Handbook (Vol. 1, first edition) 97-118.

Hsiung, S. M., & Peng, S. S. (1984). Chain pillar design for U.S. longwall panels. SME-AIME Fall meeting. Denver, Colorado, 1-17.

Hustrulid, W. A. (1976). A review of coal pillar strength formulas. Rock Mechanics, (8), 115-145.

Iannacchione, A. T. (1990). Behavior of a coal pillar prone to burst in the southern Appalachian basin of the United States. Proceedings of Rockbursts and Seismicity in Mines. A.A. Balkema. 295-300

Iannacchione, A. T. (1990). The effects of roof and floor interface slip on coal pillar behavior. Proceedings of the 31st U.S. Symposium on Rock Mechanics, Colorado School of Mines, Golden, 153-160.

Iannacchione, A. T., & DeMarco, M. J. (1991). Optimum mine designs to minimize coal bumps: A review of past and present U.S. practices. Proceedings of the Conference on Deposit Exploitation in Natural Hazard Conditions, Cracow, Poland. 1-14.

King, H. J., & Whittaker, B. N. (1971). A review of current knowledge on roadway behavior. Proc. Symp. on Roadway Strata Control. IMM, London, 73-87

Madden, B. J. (1991). A re-assessment of coal-pillar design. J. S. Afr. Inst. Min. Metall., 91(1), 27-37.

Maleki, H. N. (1990). Development of modeling procedures for coal mine stability evaluation. W. G. Hustrulid, & G. A. Johnson (Ed.), Proceedings of the 31th U.S. Symposium on Rock Mechanics. Denver, CO: A.A. Balkema. 85-92

Mark, C. (1987). Analysis of longwall pillar stability. Ph. D. Thesis, Department of Mineral Engineering of The Pennsylvania State University.

Mark, C. (1989). Longwall pillar design - some recent developments. SME Annual Meeting. Las Vegas, Nevada, 20

Obert, L., & Duvall, W. I. (1967). Rock Mechanics and the Design of Structures in Rock. New York: Wiley.

Ozbay, M. U. (1989). The stability and design of yield pillars located at shallow and moderate depths. J. S. Afr. Int. Min. Metall., 89(3), 73-79.

Pappas, D. M., & Mark, C. (1993). Behavior of simulated longwall gob material. RI 9458, U.S.B.M. 39.

Pariseau, W. G. (1975). Limit design of mine pillars under uncertainty. Paper in Proceedings of the 16th U.S. Symposium on Rock Mechanics . University of Minnesota, Minneapolis, 287-301.

Park, D. W., & Gall, V. (1989). Supercomputer assisted three-dimensional finite element analysis of a longwall panel. Rock Mechanics as a Guide for Efficient Utilization of Natural Resources, Proceedings of the 30th U.S. Symposium on Rock Mechanics, 133-140.

Peng, S. S. (1986). Coal Mine Ground Control (Second Edition). New York: John Wiley & Sons.

Peng, S. S., & Chiang, H. S. (1984). Longwall Mining. New York: John Wiley & Sons.

Rongved, L., & Hill, M. (1957). Dislocation over a bounded plane area in an infinite solid. Journal of Applied Mechanics, (24), 252-254.

Salamon, M. D. G., & Munro, A. H. (1967). A study of the strength of coal pillars. Journal of the South African Institute of Mining and Metallurgy, (September), 55-67.

Salamon, M. D. G. (1963). Elastic analysis of displacements and stresses induced by the mining of seam or reef deposits, Part I. Journal of the South African Institute of Mining and Metallurgy, (Oct.), 130-149.

Salamon, M. D. G. (1964a). Elastic analysis of dicplacements and stresses induced by the mining of seam or reef deposits, Part II. Journal of the South African Institute of Mining and Metallurgy , (January), 197-218.

Salamon, M. D. G. (1964b). Elastic analysis of displacements and stresses induced by the mining of seam or reef deposits, Part III. Journal of the South African Institute of Mining and Metallurgy , (May), 469-501.

Salamon, M. D. G. (1968). Two-dimensional treatment of problems arising from mining tabular deposits in isotropic or transversely isotropic ground. Int. J. Rock Mech. Min. Sci., (5), 159-185.

Salamon, M. D. G. (1970). Stability, instability and design of pillar workings. Int. J. Rock Mech. Min. Sci., 7, 613-631.

Salamon, M. D. G., & Wagner, H. (1985). Practical experiences in the design of coal pillars. Safety in Mine Research. Proceedings of the 21st International Conference, Sydney.

Salamon, M. D. G. (1992). Strength and stability of coal pillars. IC 9315, U.S. Bureau of Mines. 94-121.

Seedsman, R. W., & Hornby, P. (1991). Controlled and uncontrolled pillar collapse, NERDDC End of Grant Report, Australia, 71

Sinha, K. P. (1979). Displacement discontinuity technique for analyzing stresses and displacements due to mining in seam deposits. Ph. D., University of Minnesota.

Starfield, A. M., & Wawersik, W. R. (1968). Pillars as structural components in room-and-pillar mine design. 10th U.S. Symposium on Rock Mechanics, 793-809.

Starfield, A. M., & Crouch, S. L. (1972). Elastic analysis of single seam extraction. Rock Mechanics-1972, Proceedings of the 13th U.S. Symposium on Rock Mechanics, 421-439.

Tsang, P., Peng, S. S., & Hsiung, S. M. (1989). Yield pillar application under strong roof and strong floor condition-a case study. Rock Mechanics as a Guide for Efficient Utilization of Natural Resources, Proceedings of the 30th U.S. Symposium on Rock Mechanics, 411-418

Wagner, H. (1974). Determination of the complete load-deformation characteristics of coal pillars. Proceedings of the 3rd ISRM Congress. Denver, 1076-1081

Wagner, H., & Madden, J. J. (1984). Fifteen years of experience with the design of coal pillars in shallow South African collieries: an evaluation of the performance of the design procedures and recent improvements. In Design and Performance of Underground Excavations. USRM/BGS Cambridge, 391-399

Wang, F. D., Skelly, W. A., & Wolgamott, J. (1976). In-situ coal pillar strength study (H0242022). U.S.B.M.

Wilson, A. H., & Ashwin, D. P. (1972). Research into the determination of pillar size, Part 1 An hypothesis concerning pillar stability. The Mining Engineer, 131(141), 409-417.

Wilson, A. H. (1977). The effect of yield zones on the control of ground. The 6th International Strata Control Conference. Banff, Canada, 21

Wilson, A. H. (1982). Pillar stability in longwall mining. State of the Art in Ground Control in Longwall Mining and Mining Subsidence, AIME, 85-95.

Wilson, A. H. (1983). The stability of underground workings in the soft rocks of the coal measures. International Journal of Mining Engineering , (1), 91-187.

Zipf, R. K., Jr. (1992a). Analysis of stable and unstable pillar failure using local mine stiffness method. IC, 9315, U.S.B.M., 128-143.

Zipf, R. K., Jr. (1992b). MULSIM/NL Application and practitioner's manual. IC 9322, U.S.B.M.

Zipf, R. K., Jr. (1992c). MULSIM/NL Theoretical and programmer's manual. IC 9321, U.S.B.M.

Appendix A

CONCEPT OF DISPLACEMENT DISCONTINUITY THEORY

A.1 Assumptions

(1) For relatively deep mining, the inelastic behavior is confined to the immediate vicinity of the excavation and the mass rock beyond the vicinity behaves elastically;

(2) Workings are sufficiently deep, that the influence of irregular surface can be neglected;

(3) Compared to the transverse dimensions, the seam has negligible thickness t, so that it can be treated as a plane.

A.2 Definitions

The origin of local coordinate system is located in the seam as shown by figure A.1. The bottom of the plane is defined by $z = 0_-$ and the top of the plane is defined by $z = 0_+$.

Let u, v and w be the displacements along x, y and z axes. The displacements will be continuous elsewhere, except across the plane $z = 0$. The relative displacements between $z = 0_-$ and $z = 0_+$ are defined as:

$$\begin{aligned} S_x &= u_- - u_+ \\ S_y &= v_- - v_+ \\ S_z &= w_- - w_+ \end{aligned} \qquad \text{(A.1)}$$

Horizontal relative movements S_x and S_y are called rides. The vertical relative movement S_z is called closure.

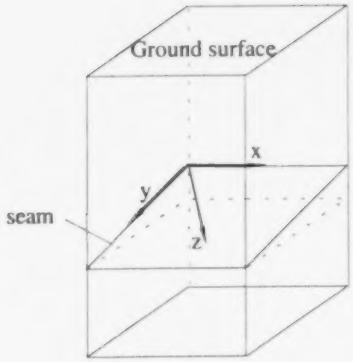

Figure A.1

Coordinate axes of the seam.

A.3 Boundary conditions

The mining area is defined by domain A, which can be further specified as:

(1) Unmined area

$$\sigma_{zz} = E_s \frac{S_z}{t} \qquad \sigma_{xz} = G_s \frac{S_x}{t} \qquad \sigma_{yz} = G_s \frac{S_z}{t} \tag{A.2}$$

where E_s - compression modulus of the seam;

G_s - shear modulus of the seam;

t - thickness of the seam.

(2) Mined-out area

If there is no contact between the roof and the floor, the induced forces on the roof and the floor will balance the primitive forces. Therefore, the resultant forces are zero on the planes, i.e.

$$\sigma_{zz} = -P_{zz} \qquad \sigma_{xz} = -P_{xz} \qquad \sigma_{yz} = -P_{yz} \tag{A.3}$$

where P_{zz}, P_{xz} and P_{yz} are primitive stresses relative to the seam plane.

A.4 Mathematical solution

The solution of this problem can be expressed in the terms of three harmonic functions ϕ_1, ϕ_2 and ϕ_3 (Salamon, 1963, 1964), i.e.

$$
\begin{aligned}
u &= 2(1-\mu)\frac{\partial \phi_1}{\partial z} - (1-2\mu)\frac{\partial \phi_3}{\partial x} - z\frac{\partial \phi}{\partial z} \\
v &= 2(1-\mu)\frac{\partial \phi_2}{\partial z} - (1-2\mu)\frac{\partial \phi_3}{\partial y} - z\frac{\partial \phi}{\partial y} \\
w &= 2(1-\mu)\frac{\partial \phi_3}{\partial z} + (1-2\mu)\left(\frac{\partial \phi_1}{\partial x} + \frac{\partial \phi_2}{\partial y}\right) - z\frac{\partial \phi}{\partial z}
\end{aligned}
\qquad \text{(A.4)}
$$

where

$$
\phi = \frac{\partial \phi_1}{\partial x} + \frac{\partial \phi_2}{\partial y} + \frac{\partial \phi_3}{\partial z} \qquad \text{(A.5)}
$$

and μ is Poisson's ratio for the rock mass.

If G is the shear modulus for rock mass, then according to Hook's law the stresses corresponding to these displacements are

$$
\begin{aligned}
\sigma_{xx} &= 2G\left[\frac{\partial^2 \phi_3}{\partial z^2} + 2\frac{\partial^2 \phi_3}{\partial x \partial z} + 2\mu\frac{\partial^2 \phi_2}{\partial y \partial z} + (1-2\mu)\frac{\partial^2 \phi_3}{\partial y^2} - z\frac{\partial^2 \phi}{\partial x^2}\right] \\
\sigma_{yy} &= 2G\left[\frac{\partial^2 \phi_3}{\partial z^2} + 2\frac{\partial^2 \phi_3}{\partial y \partial z} + 2\mu\frac{\partial^2 \phi_2}{\partial x \partial z} + (1-2\mu)\frac{\partial^2 \phi_3}{\partial x^2} - z\frac{\partial^2 \phi}{\partial y^2}\right] \\
\sigma_{zz} &= 2G\left(\frac{\partial^2 \phi_3}{\partial z^2} - \frac{\partial^2 \phi}{\partial z^2}\right) \\
\sigma_{xz} &= 2G\left[\frac{\partial^2 \phi_1}{\partial z^2} + \mu\frac{\partial}{\partial y}\left(\frac{\partial \phi_1}{\partial y} - \frac{\partial \phi_2}{\partial x}\right) - z\frac{\partial^2 \phi}{\partial x \partial z}\right] \\
\sigma_{yz} &= 2G\left[\frac{\partial^2 \phi_1}{\partial z^2} - \mu\frac{\partial}{\partial x}\left(\frac{\partial \phi_1}{\partial y} - \frac{\partial \phi_2}{\partial x}\right) - z\frac{\partial^2 \phi}{\partial y \partial z}\right] \\
\sigma_{xy} &= 2G\left[(1-\mu)\frac{\partial}{\partial z}\left(\frac{\partial \phi_1}{\partial y} + \frac{\partial \phi_2}{\partial x}\right) - (1-2\mu)\frac{\partial^2 \phi_3}{\partial x \partial y} - z\frac{\partial^2 \phi}{\partial x \partial y}\right]
\end{aligned}
\qquad \text{(A.6)}
$$

The problem is to find the three harmonic functions ϕ_1, ϕ_2 and ϕ_3 which satisfy the boundary conditions (A.2) and (A.3). Salamon (1963, 1964) has provided the three harmonic functions as

$$\phi_1 = -\frac{U}{r} \quad \phi_2 = -\frac{V}{r} \quad \phi_3 = -\frac{W}{r} \tag{A.7}$$

where, U, V and W are constants which are defined later and r is the distance from point (ξ , η, 0) in the seam where displacement discontinuities S_x, S_y and S_z occur to any other point (x ,y ,z) in the seam or in the surrounding rock mass where displacements and stresses are sought.

$$r = \sqrt{(x-\xi)^2 + (y-\eta)^2 + z^2}$$

Solutions ϕ_1, ϕ_2 and ϕ_3 satisfy the following conditions:

$$\iint_A S_x dxdy = \iint_A S_y dxdy = \iint_A S_z dxdy = 0 \tag{A.8}$$

When point (x, y, z) in domain A does not include point (ξ , η, 0), i.e. $x \neq \xi$, $y \neq \eta$ or $z \neq 0$ in A;

and

$$\begin{aligned} \iint_A S_x dxdy &= -8\pi U(1-\mu) \\ \iint_A S_y dxdy &= -8\pi V(1-\mu) \\ \iint_A S_z dxdy &= -8\pi W(1-\mu) \end{aligned} \tag{A.9}$$

when point (x, y, z) in domain A does include point (ξ , η, 0), i.e. $x = \xi$, $y = \eta$ and $z = 0$ in A.

A.5 Discretizing the seam

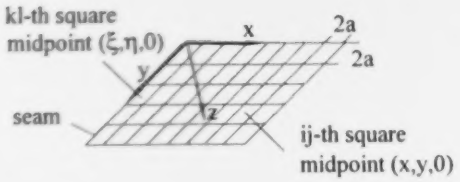

Figure A.2

Discretizing the seam plane.

Divide the seam plane z=0 into a large numbers of squares in such way that the ij-th square is the ith along y-axis and the jth along the x-axis, as shown in figure A.2. Let $(S_x)_{ij}$, $(S_y)_{ij}$, and $(S_z)_{ij}$ be the average rides and closure components over the ij-th square which has width of 2a; let $(\sigma_{zz})_{ij}$, $(\sigma_{zx})_{ij}$ and $(\sigma_{zy})_{ij}$ are average stress components over the ij-th square. For kl-th square on the seam plane z=0, the three harmonic functions are:

$$\phi_1 = \frac{a^2(S_x)_{kl}}{2\pi(1-\mu)r} \quad \phi_2 = \frac{a^2(S_y)_{kl}}{2\pi(1-\mu)r} \quad \phi_3 = \frac{a^2(S_z)_{kl}}{2\pi(1-\mu)r} \tag{A.10}$$

where, U, V and W have been substituted by equations from (A.9) as

$$\begin{aligned} U &= -\frac{\iint_A S_x dA}{8\pi(1-\mu)} = -\frac{S_x(2a)^2}{8\pi(1-\mu)} = -\frac{S_x a^2}{2\pi(1-\mu)} \\ V &= -\frac{S_y a^2}{2\pi(1-\mu)} \\ W &= -\frac{S_z a^2}{2\pi(1-\mu)} \end{aligned} \tag{A.11}$$

where $(\xi, \eta, 0)$ is the midpoint of the kl-th square and (x, y, 0) is the midpoint of ij-th square. Substitute (A.10) into equations (A.5) and (A.6), the average stresses over the ij-th square are (from equation (A.6)):

$$
\begin{aligned}
(\sigma_{zz})_{ij} &= a_{ijkl}(S_z)_{kl} \\
(\sigma_{xz})_{ij} &= (a_{ijkl} - \mu b_{ijkl})(S_x)_{kl} - \mu d_{ijkl}(S_y)_{kl} \\
(\sigma_{yz})_{ij} &= (a_{ijkl} - \mu c_{ijkl})(S_y)_{kl} - \mu d_{ijkl}(S_x)_{kl}
\end{aligned}
\tag{A.12}
$$

where a_{ijkl}, b_{ijkl}, c_{ijkl}, and d_{ijkl} are derivatives of the harmonic functions according to equation (A.6). Therefore, they also are the functions of midpoint coordinates of ij-th square and kl-th square and elastic properties of surround rock mass.

If rides and closure take place at all the squares (such as k from 1 to n, and l from 1 to m) in seam, then the stresses at ij-th square will be the summation of the contribution from all the squares, i.e.

$$
\begin{aligned}
(\sigma_{zz})_{ij} &= \sum_{k=1}^{n}\sum_{l=1}^{m} a_{ijkl}(S_z)_{kl} \\
(\sigma_{xz})_{ij} &= \sum_{k=1}^{n}\sum_{l=1}^{m} (a_{ijkl} - \mu b_{ijkl})(S_x)_{kl} - \mu \sum_{k=1}^{n}\sum_{l=1}^{m} d_{ijkl}(S_y)_{kl} \\
(\sigma_{yz})_{ij} &= \sum_{k=1}^{n}\sum_{l=1}^{m} (a_{ijkl} - \mu c_{ijkl})(S_y)_{kl} - \mu \sum_{k=1}^{n}\sum_{l=1}^{m} d_{ijkl}(S_x)_{kl}
\end{aligned}
\tag{A.13}
$$

Equations (13) can be written in a matrix form as

$$
\sigma_{ij} = \sum_{k=1}^{n}\sum_{l=1}^{m} k_{ijkl} S_{kl} \tag{A.14}
$$

where

$$
\sigma_{ij} = \begin{bmatrix} (\sigma_{xz})_{ij} \\ (\sigma_{yz})_{ij} \\ (\sigma_{zz})_{ij} \end{bmatrix} \qquad k_{ijkl} = \begin{bmatrix} a_{ijkl} - \mu c_{ijkl} & -\mu d_{ijkl} & 0 \\ -\mu d_{ijkl} & a_{ijkl} - \mu b_{ijkl} & 0 \\ 0 & 0 & a_{ijkl} \end{bmatrix} \qquad S_{ij} = \begin{bmatrix} (S_x)_{ij} \\ (S_y)_{ij} \\ (S_z)_{ij} \end{bmatrix} \tag{A.15}
$$

It is obvious that there are 3×m×n equations in (A.14), in which there are 6×m×n unknowns. Another 3×m×n equations are needed to solve the whole problem. These equations come from boundary conditions (A.2) and (A.3).

A.6 Application of boundary conditions

Substitute equations (A.2) and (A.3) into equation (A.14), there will be only 3×m×n equations and 3×m×n unknowns, which is as follows:

(1) ij-th square is mined:

$$P_{ij} = \sum_{k=1}^{n} \sum_{l=1}^{m} k_{ijkl} S_{kl} \tag{A.16}$$

where

$$P_{ij} = \begin{bmatrix} -(P_{xz})_{ij} \\ -(P_{yz})_{ij} \\ -(P_{zz})_{ij} \end{bmatrix} \tag{A.17}$$

are the primitive stresses. The equation (A.16) is the application of equation (A.3).

(2) ij-th square is unmined:

$$D_{ij} S_{ij} = \sum_{k=1}^{n} \sum_{l=1}^{m} k_{ijkl} S_{kl} \tag{A.18}$$

where

$$D_{ij} = \begin{bmatrix} \frac{E_s}{t} & \frac{G_s}{t} & \frac{G_s}{t} \end{bmatrix} \tag{A.19}$$

The equation (A.18) is simply the application of equation (A.2).

The method of Gauss-Seidel successive over-relaxation is applied to equations (A.16) and (A.18) to solve for the displacement discontinuities over squares.

Appendix B

PROGRAM INPUT PARAMETERS AND OUTPUT FOR THE MODELS

The format of the input file for the modified MULSIM/NL program for local mine stiffness calculation is same as the original input format for MULSIM/NL (refer to Zipf (1992b and 1992c) for detailed input format), except the magnitude of the perturbation displacement should be given immediately following the first input record (Young's modulus and Poisson's ratio for strata and the number of seams). The letter "A" through "K" in the fine and coarse output meshes of the following sections represent one of the six types of materials provided by MULSIM/NL program. The number "1" in the fine meshes represents the excavated elements and "0" in coarse meshes represents the fine mesh zone.

B.1 Test elastic model

Two entries with one row of pillars (80x80 ft)

```
IN THE FOLLOWING X,Y,Z REFER TO GLOBAL AXES OR COORDINATES
AND X1,X2,X3  OR  1,2,3 REFER TO LOCAL AXES OR COORDINATES.


ROCK MASS PROPERTIES
POISSONS RATIO          --            0.25
MODULUS OF ELASTICITY --        900000.00
NO. OF SEAMS            --      1
NO. OF MATERIALS        --      5
PERTURBATION DSPL       --      0.0100


IN-SEAM MATERIAL PROPERTIES
VALID MATERIAL PROPERTY CODES ARE:
0 1 2 A B C D E F G H I J K L M N O P Q R S T U V W X Y Z


MATERIAL NUMBER         1 (A)
LINEAR ELASTIC COAL           1.0
YOUNGS MODULUS          0.50000E+06
SHEAR MODULUS           0.21700E+06


MATERIAL NUMBER         2 (B)
LINEAR ELASTIC GOB            6.0
YOUNGS MODULUS          0.50000E+04
SHEAR MODULUS           0.17900E+04
GOB HEIGHT FACTOR       0.10000E+01


MATERIAL NUMBER         3 (C)
LINEAR ELASTIC COAL           1.0
YOUNGS MODULUS          0.27500E+06
SHEAR MODULUS           0.11900E+06


MATERIAL NUMBER         4 (D)
ELASTIC PLASTIC COAL        3.00000
PEAK STRESS             0.50000E+03
PEAK STRAIN             0.25000E-02
```

```
PLASTIC MODULUS          0.00000E+00
POISSONS RATIO           0.30000E+00


MATERIAL NUMBER          5 (E)
LINEAR ELASTIC COAL                1.0
YOUNGS MODULUS           0.50000E+06
SHEAR MODULUS            0.21700E+06


PRIMITIVE STRESS PARAMETERS

PRIMITIVE STRESSES ARE GIVEN AS
PXX =    0.0000     0.0458    * Z
PXY =    0.0000     0.0000    * Z
PXZ =    0.0000     0.0000    * Z
PYY =    0.0000     0.0458    * z
PYZ =    0.0000     0.0000    * z
PZZ =    0.0000     0.0917    * z


MODEL CONTROL AND MODEL DATA

NO. OF PARALLEL SEAMS                    --         1
WIDTH OF BLOCKS                          --    600.00
NO. OF BLOCKS ALONG X  AXIS              --        50
NO. OF BLOCKS ALONG Y  AXIS              --        32
NUMBER OF OFF-SEAM PLANES SELECTED       --         0
FINE MESH STARTING BLOCK X-AXIS          --        16
FINE MESH ENDING   BLOCK X-AXIS          --        31
FINE MESH STARTING BLOCK Y-AXIS          --         9
FINE MESH ENDING   BLOCK Y-AXIS          --        24


GLOBAL COORDINATES OF LOCAL ORIGINS AND SEAM THICKNESSES
SEAM NO.          X           Y           Z     THICKNESS
     1         0.00        0.00    -6000.00       72.00

DIRECTION COSINES OF LOCAL SEAM AXES WITH RESPECT TO THE GLOBAL AXES


EN(1,X) =    1.00000  EN(2,X) =    0.00000  EN(3,X) =    0.00000
EN(1,Y) =    0.00000  EN(2,Y) =    1.00000  EN(3,Y) =    0.00000
EN(1,Z) =    0.00000  EN(2,Z) =    0.00000  EN(3,Z) =    1.00000


PROGRAM FLOW CONTROL PARAMETERS

OVER RELAXATION FACTOR     1.35
MAXIMUM NO. OF ITERATIONS SPECIFIED      200
STRESS CONVERGENCE CRITERION  0.10000E-02
STARTING MINING STEP NUMBER          1
NUMBER OF NEW STEPS                  7


PRIMITIVE STRESSES AT LOCAL SEAM ORIGINS
SEAM #     PSX          PSY          PSZ

   1  0.0000E+00  0.0000E+00  0.5502E+03

STRESS GRADIENTS
PXDX =   0.0000E+00
PYDX =   0.0000E+00
PZDX =   0.0000E+00
PXDY =   0.0000E+00
PYDY =   0.0000E+00
PZDY =   0.0000E+00


TIME TO READ, CALCULATE AND PRINT BASIC PARAMETERS =      0 SECONDS


TIME TO CALCULATE INFLUENCE COEFFICIENTS =      0 SECONDS


MINING STEP NUMBER =   1   FINE MESH SEAM NUMBER = 1
```

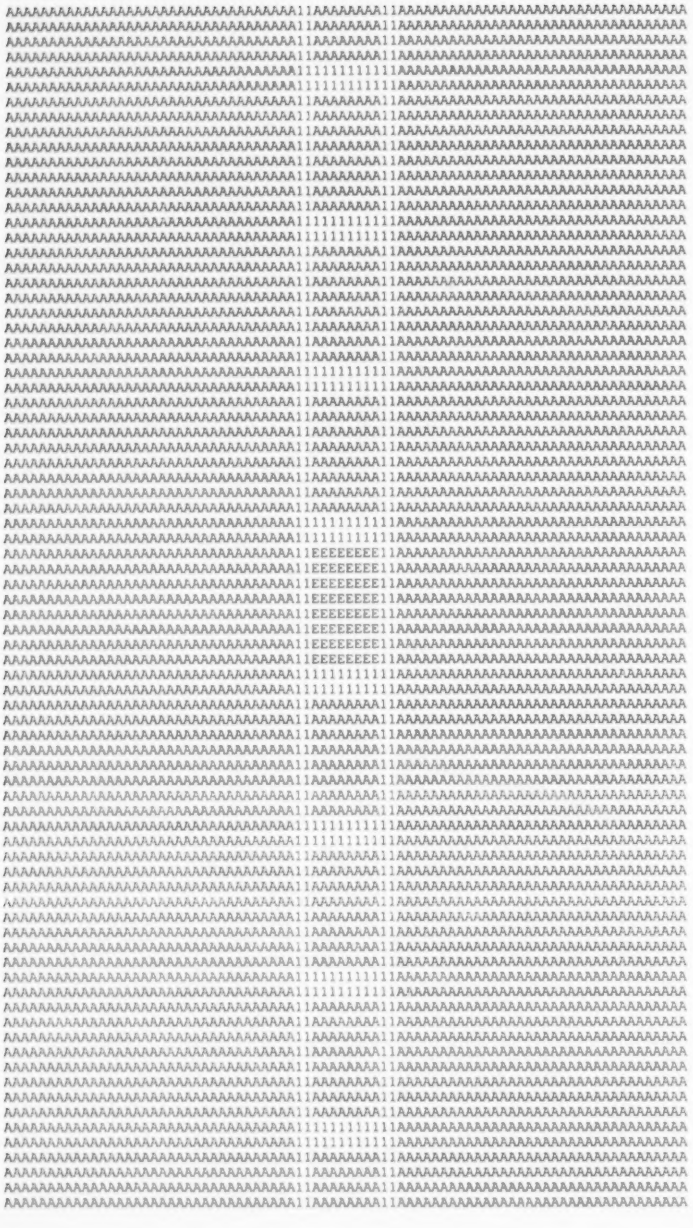

MINING STEP NUMBER = 1 COARSE MESH SEAM NUMBER = 1

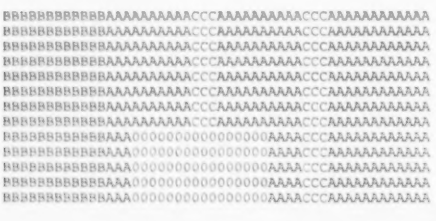

```
TIME TO READ, PRINT AND CONVERT MATERIAL PROPERTIES
FOR THIS MINING STEP =      0 SECONDS


SOLUTION PROGRESS FOR MINING STEP NUMBER =      1

iteration number =    1     ermaxb =    0.1676E+01       ermaxe =    0.3446E+00
iteration number =    2     ermaxb =    0.8452E+00       ermaxe =    0.1659E+00
iteration number =    3     ermaxb =    0.4203E+00       ermaxe =    0.4966E-01
iteration number =    4     ermaxb =    0.1995E+00       ermaxe =    0.1335E-01
iteration number =    5     ermaxb =    0.8934E-01       ermaxe =    0.7398E-02
iteration number =    6     ermaxb =    0.3713E-01       ermaxe =    0.2065E-02
iteration number =    7     ermaxb =    0.1383E-01       ermaxe =    0.8891E-03
iteration number =    8     ermaxb =    0.4723E-02       ermaxe =    0.3349E-03
iteration number =    9     ermaxb =    0.1350E-02       ermaxe =    0.1292E-03
iteration number =   10     ermaxb =    0.3894E-03       ermaxe =    0.5531E-04
iteration number =   11     ermaxb =    0.1416E-03       ermaxe =    0.2184E-04
iteration number =   12     ermaxb =    0.4940E-04       ermaxe =    0.9082E-05
iteration number =   13     ermaxb =    0.2179E-04       ermaxe =    0.3545E-05
iteration number =   14     ermaxb =    0.9596E-05       ermaxe =    0.1315E-05
iteration number =   15     ermaxb =    0.4148E-05       ermaxe =    0.5905E-06
iteration number =   16     ermaxb =    0.1814E-05       ermaxe =    0.2719E-06

TIME TO SOLVE FOR STRESSES AND DISPLACEMENTS IN THIS MINING STEP =      0 SECONDS


MINING STEP NUMBER =    1
NUMBER OF ITERATIONS TO SOLVE =     16


MAXIMUM ERROR IN THE BLOCK DISPLACEMENTS =  0.181E-05

MAXIMUM ERROR IN THE ELEMENTS DISPLACEMENTS =  0.272E-06

TIME TO PRINT OUT STRESSES AND DISPLACEMENTS IN THIS MINING STEP =      0 SECONDS


TIME TO COMPUTE AND PRINT STRESSES AND DISPLACEMENTS
ON OFF-SEAM PLANES DURING THIS MINING STEP =      0 SECONDS

iteration number =    1     ermaxb =    0.9850E-06       ermaxe =    0.4273E-02
iteration number =    2     ermaxb =    0.3738E-05       ermaxe =    0.1566E-02
iteration number =    3     ermaxb =    0.1613E-05       ermaxe =    0.3766E-03
iteration number =    4     ermaxb =    0.6761E-06       ermaxe =    0.1138E-03
iteration number =    5     ermaxb =    0.2994E-06       ermaxe =    0.6152E-04
iteration number =    6     ermaxb =    0.1335E-06       ermaxe =    0.1687E-04
iteration number =    7     ermaxb =    0.5746E-07       ermaxe =    0.9229E-05
iteration number =    8     ermaxb =    0.2291E-07       ermaxe =    0.3081E-05
iteration number =    9     ermaxb =    0.8114E-08       ermaxe =    0.1386E-05
iteration number =   10     ermaxb =    0.2473E-08       ermaxe =    0.5123E-06
iteration number =   11     ermaxb =    0.6952E-09       ermaxe =    0.2120E-06

TIME TO SOLVE FOR STRESSES AND DISPLACEMENTS IN THIS MINING STEP =      0 SECONDS


MINING STEP NUMBER =    1
NUMBER OF ITERATIONS TO SOLVE =     11


MAXIMUM ERROR IN THE BLOCK DISPLACEMENTS =  0.695E-09
```

MAXIMUM ERROR IN THE ELEMENTS DISPLACEMENTS = 0.212E-06

TIME TO PRINT OUT STRESSES AND DISPLACEMENTS IN THIS MINING STEP = 0 SECONDS

TIME TO COMPUTE AND PRINT STRESSES AND DISPLACEMENTS
ON OFF-SEAM PLANES DURING THIS MINING STEP = 0 SECONDS

MINING STEP NUMBER = 2 FINE MESH SEAM NUMBER = 1

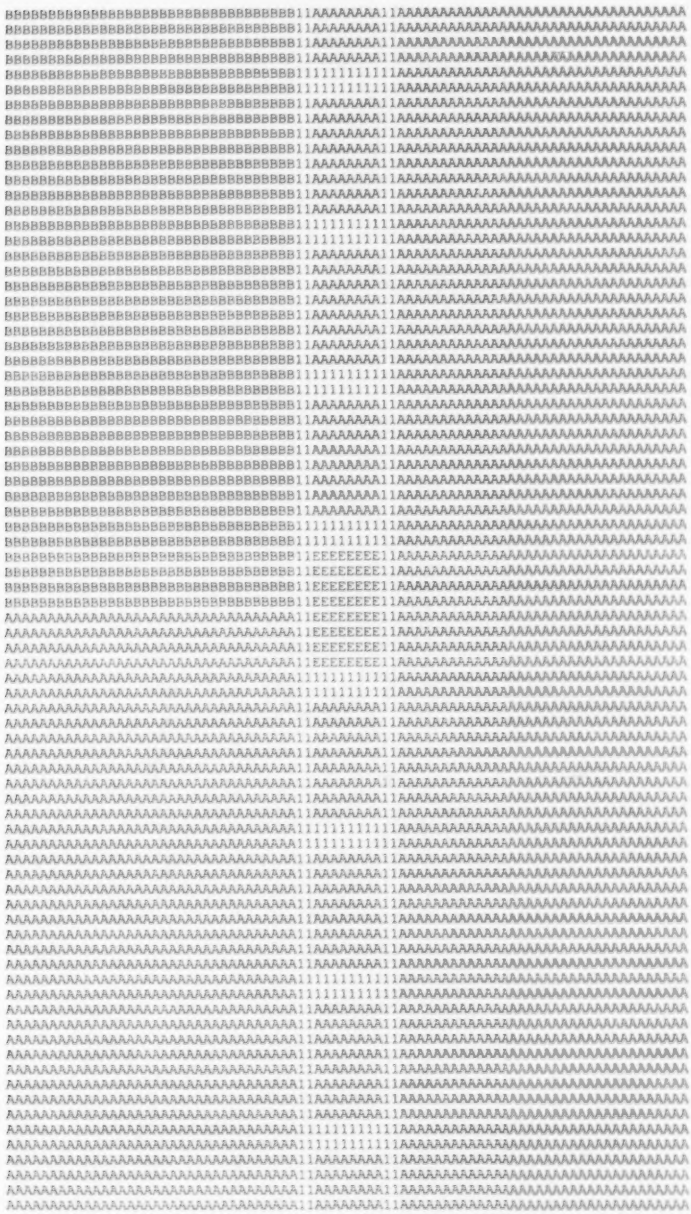

MINING STEP NUMBER = 2 COARSE MESH SEAM NUMBER = 1

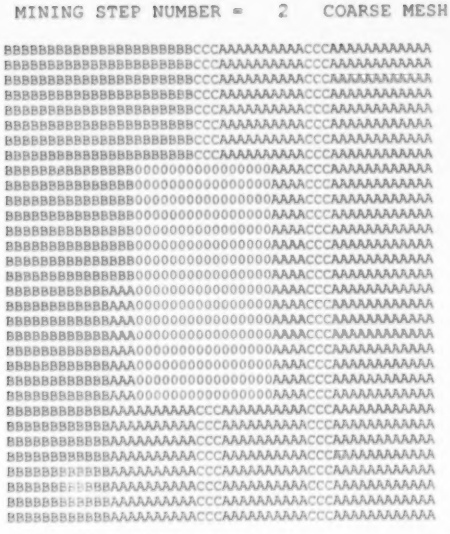

TIME TO READ, PRINT AND CONVERT MATERIAL PROPERTIES
FOR THIS MINING STEP = 0 SECONDS

SOLUTION PROGRESS FOR MINING STEP NUMBER = 2

iteration number =	1	ermaxb =	0.1773E+01	ermaxe =	0.1287E+01
iteration number =	2	ermaxb =	0.9345E+00	ermaxe =	0.1144E+01
iteration number =	3	ermaxb =	0.4612E+00	ermaxe =	0.6345E+00
iteration number =	4	ermaxb =	0.2238E+00	ermaxe =	0.4051E+00
iteration number =	5	ermaxb =	0.1526E+00	ermaxe =	0.3018E+00
iteration number =	6	ermaxb =	0.1113E+00	ermaxe =	0.2256E+00
iteration number =	7	ermaxb =	0.8325E-01	ermaxe =	0.1759E+00
iteration number =	8	ermaxb =	0.6236E-01	ermaxe =	0.1353E+00
iteration number =	9	ermaxb =	0.4753E-01	ermaxe =	0.1053E+00
iteration number =	10	ermaxb =	0.3640E-01	ermaxe =	0.8147E-01
iteration number =	11	ermaxb =	0.2787E-01	ermaxe =	0.6255E-01
iteration number =	12	ermaxb =	0.2133E-01	ermaxe =	0.4781E-01
iteration number =	13	ermaxb =	0.1631E-01	ermaxe =	0.3642E-01
iteration number =	14	ermaxb =	0.1246E-01	ermaxe =	0.2779E-01
iteration number =	15	ermaxb =	0.9508E-02	ermaxe =	0.2128E-01
iteration number =	16	ermaxb =	0.7245E-02	ermaxe =	0.1624E-01
iteration number =	17	ermaxb =	0.5514E-02	ermaxe =	0.1237E-01
iteration number =	18	ermaxb =	0.4191E-02	ermaxe =	0.9403E-02
iteration number =	19	ermaxb =	0.3183E-02	ermaxe =	0.7137E-02
iteration number =	20	ermaxb =	0.2414E-02	ermaxe =	0.5411E-02
iteration number =	21	ermaxb =	0.1830E-02	ermaxe =	0.4099E-02
iteration number =	22	ermaxb =	0.1386E-02	ermaxe =	0.3102E-02
iteration number =	23	ermaxb =	0.1049E-02	ermaxe =	0.2347E-02
iteration number =	24	ermaxb =	0.7937E-03	ermaxe =	0.1775E-02
iteration number =	25	ermaxb =	0.6003E-03	ermaxe =	0.1341E-02
iteration number =	26	ermaxb =	0.4538E-03	ermaxe =	0.1014E-02
iteration number =	27	ermaxb =	0.3430E-03	ermaxe =	0.7660E-03
iteration number =	28	ermaxb =	0.2594E-03	ermaxe =	0.5787E-03
iteration number =	29	ermaxb =	0.1961E-03	ermaxe =	0.4371E-03
iteration number =	30	ermaxb =	0.1482E-03	ermaxe =	0.3301E-03
iteration number =	31	ermaxb =	0.1120E-03	ermaxe =	0.2493E-03
iteration number =	32	ermaxb =	0.8459E-04	ermaxe =	0.1883E-03
iteration number =	33	ermaxb =	0.6390E-04	ermaxe =	0.1422E-03
iteration number =	34	ermaxb =	0.4827E-04	ermaxe =	0.1074E-03
iteration number =	35	ermaxb =	0.3645E-04	ermaxe =	0.8108E-04
iteration number =	36	ermaxb =	0.2753E-04	ermaxe =	0.6122E-04
iteration number =	37	ermaxb =	0.2079E-04	ermaxe =	0.4623E-04
iteration number =	38	ermaxb =	0.1570E-04	ermaxe =	0.3490E-04
iteration number =	39	ermaxb =	0.1186E-04	ermaxe =	0.2635E-04
iteration number =	40	ermaxb =	0.8952E-05	ermaxe =	0.1990E-04
iteration number =	41	ermaxb =	0.6760E-05	ermaxe =	0.1502E-04
iteration number =	42	ermaxb =	0.5104E-05	ermaxe =	0.1134E-04

```
iteration number =  43    ermaxb =   0.3854E-05      ermaxe =   0.8565E-05
iteration number =  44    ermaxb =   0.2910E-05      ermaxe =   0.6467E-05
iteration number =  45    ermaxb =   0.2197E-05      ermaxe =   0.4883E-05
iteration number =  46    ermaxb =   0.1659E-05      ermaxe =   0.3687E-05
iteration number =  47    ermaxb =   0.1253E-05      ermaxe =   0.2784E-05
iteration number =  48    ermaxb =   0.9458E-06      ermaxe =   0.2102E-05
iteration number =  49    ermaxb =   0.7141E-06      ermaxe =   0.1587E-05
iteration number =  50    ermaxb =   0.5391E-06      ermaxe =   0.1198E-05

TIME TO SOLVE FOR STRESSES AND DISPLACEMENTS IN THIS MINING STEP =      0 SECONDS


MINING STEP NUMBER =   2
NUMBER OF ITERATIONS TO SOLVE =    50


MAXIMUM ERROR IN THE BLOCK DISPLACEMENTS =  0.539E-06

MAXIMUM ERROR IN THE ELEMENTS DISPLACEMENTS =  0.120E-05

TIME TO PRINT OUT STRESSES AND DISPLACEMENTS IN THIS MINING STEP =      0 SECONDS


TIME TO COMPUTE AND PRINT STRESSES AND DISPLACEMENTS
ON OFF-SEAM PLANES DURING THIS MINING STEP =      0 SECONDS

iteration number =   1    ermaxb =   0.1010E-05      ermaxe =   0.4275E-02
iteration number =   2    ermaxb =   0.9605E-05      ermaxe =   0.1734E-02
iteration number =   3    ermaxb =   0.4536E-05      ermaxe =   0.5983E-03
iteration number =   4    ermaxb =   0.3194E-05      ermaxe =   0.2044E-03
iteration number =   5    ermaxb =   0.2532E-05      ermaxe =   0.8428E-04
iteration number =   6    ermaxb =   0.2187E-05      ermaxe =   0.4180E-04
iteration number =   7    ermaxb =   0.1877E-05      ermaxe =   0.2271E-04
iteration number =   8    ermaxb =   0.1600E-05      ermaxe =   0.1337E-04
iteration number =   9    ermaxb =   0.1352E-05      ermaxe =   0.8750E-05
iteration number =  10    ermaxb =   0.1132E-05      ermaxe =   0.5866E-05
iteration number =  11    ermaxb =   0.9378E-06      ermaxe =   0.4103E-05
iteration number =  12    ermaxb =   0.7695E-06      ermaxe =   0.2918E-05
iteration number =  13    ermaxb =   0.6253E-06      ermaxe =   0.2090E-05
iteration number =  14    ermaxb =   0.5034E-06      ermaxe =   0.1525E-05
iteration number =  15    ermaxb =   0.4016E-06      ermaxe =   0.1148E-05

TIME TO SOLVE FOR STRESSES AND DISPLACEMENTS IN THIS MINING STEP =      0 SECONDS


MINING STEP NUMBER =   2
NUMBER OF ITERATIONS TO SOLVE =    15


MAXIMUM ERROR IN THE BLOCK DISPLACEMENTS =  0.402E-06

MAXIMUM ERROR IN THE ELEMENTS DISPLACEMENTS =  0.115E-05

TIME TO PRINT OUT STRESSES AND DISPLACEMENTS IN THIS MINING STEP =      0 SECONDS


TIME TO COMPUTE AND PRINT STRESSES AND DISPLACEMENTS
ON OFF-SEAM PLANES DURING THIS MINING STEP =      0 SECONDS


.
.
.

Mining step 3 through 7 were omitted

.
.
.

Local mine stiffness result:

Step No.  Ptd dspl  Rsd stress  Plr modulus  LMS    Plr dspl  No. of elmts
   1      0.01000     810.827  500000.000       0.000  0.11676    64
   1      0.01000     803.422  500000.000  -53316.156  0.12676    64
   2      0.01000    1034.401  500000.000       0.000  0.14895    64
   2      0.01000    1027.119  500000.000  -52434.176  0.15895    64
```

3	0.01000	1476.833	500000.000	0.000	0.21266	64
3	0.01000	1469.747	500000.000	-51018.642	0.22266	64
4	0.01000	1509.063	500000.000	0.000	0.21731	64
4	0.01000	1501.978	500000.000	-51015.920	0.22731	64
5	0.01000	1750.286	500000.000	0.000	0.25204	64
5	0.01000	1743.331	500000.000	-50075.718	0.26204	64
6	0.01000	2153.807	500000.000	0.000	0.31015	64
6	0.01000	2147.061	500000.000	-48572.175	0.32015	64
7	0.01000	2262.542	500000.000	0.000	0.32581	64
7	0.01000	2255.798	500000.000	-48555.276	0.33581	64

Summary of the result:

No.	Strain	Stress	LMS
1	0.16217E-02	0.81083E+03	-0.53316E+05
2	0.20688E-02	0.10344E+04	-0.52434E+05
3	0.29537E-02	0.14768E+04	-0.51019E+05
4	0.30181E-02	0.15091E+04	-0.51016E+05
5	0.35006E-02	0.17503E+04	-0.50076E+05
6	0.43076E-02	0.21538E+04	-0.48572E+05
7	0.45251E-02	0.22625E+04	-0.48555E+05

End of output for elastic model

****

B.2 Model with four entries and three rows of equal size of pillars

Overburden 750 ft (9000 in)

```
IN THE FOLLOWING X,Y,Z REFER TO GLOBAL AXES OR COORDINATES
AND X1,X2,X3  OR  1,2,3 REFER TO LOCAL AXES OR COORDINATES.


ROCK MASS PROPERTIES
POISSONS RATIO          --              .25
MODULUS OF ELASTICITY   --       145000.00
NO. OF SEAMS            --      1
NO. OF MATERIALS        --      5
PERTURBATION DSPL       --       .0010


IN-SEAM MATERIAL PROPERTIES
VALID MATERIAL PROPERTY CODES ARE:
0 1 2 A B C D E F G H I J K L M N O P Q R S T U V W X Y Z


MATERIAL NUMBER       1 (A)
STRAIN SOFTENING COAL      2.00000
PEAK STRESS              .29000E+04
PEAK STRAIN              .10000E-01
RESIDUAL STRESS          .14500E+04
RESIDUAL STRAIN          .15000E-01
POISSONS RATIO           .30000E+00


MATERIAL NUMBER       2 (B)
LINEAR ELASTIC GOB            6.0
YOUNGS MODULUS           .29000E+04
SHEAR MODULUS            .11600E+04
GOB HEIGHT FACTOR        .10000E+01


MATERIAL NUMBER       3 (C)
STRAIN SOFTENING COAL      2.00000
PEAK STRESS              .18000E+04
PEAK STRAIN              .10000E-01
RESIDUAL STRESS          .89900E+03
RESIDUAL STRAIN          .15000E-01
POISSONS RATIO           .32000E+00


MATERIAL NUMBER       4 (D)
LINEAR ELASTIC COAL           1.0
YOUNGS MODULUS           .29000E+06
SHEAR MODULUS            .11600E+06


MATERIAL NUMBER       5 (E)
STRAIN SOFTENING COAL      2.00000
PEAK STRESS              .29000E+04
PEAK STRAIN              .10000E-01
RESIDUAL STRESS          .14500E+04
RESIDUAL STRAIN          .15000E-01
POISSONS RATIO           .30000E+00


PRIMITIVE STRESS PARAMETERS

PRIMITIVE STRESSES ARE GIVEN AS
PXX =     .0000     .0458   * Z
PXY =     .0000     .0000   * Z
PXZ =     .0000     .0000   * Z
PYY =     .0000     .0458   * z
PYZ =     .0000     .0000   * z
PZZ =     .0000     .0917   * z


MODEL CONTROL AND MODEL DATA

NO. OF PARALLEL SEAMS                --        1
```

```
WIDTH OF BLOCKS                          --   600.00
NO. OF BLOCKS ALONG X  AXIS              --       49
NO. OF BLOCKS ALONG Y  AXIS              --       40
NUMBER OF OFF-SEAM PLANES SELECTED       --        0
FINE MESH STARTING BLOCK X-AXIS          --       17
FINE MESH ENDING   BLOCK X-AXIS          --       32
FINE MESH STARTING BLOCK Y-AXIS          --       13
FINE MESH ENDING   BLOCK Y-AXIS          --       28


GLOBAL COORDINATES OF LOCAL ORIGINS AND SEAM THICKNESSES
SEAM NO.         X           Y           Z      THICKNESS
     1         .00         .00    -9000.00        72.00

DIRECTION COSINES OF LOCAL SEAM AXES WITH RESPECT TO THE GLOBAL AXES


EN(1,X) =    1.00000  EN(2,X) =     .00000  EN(3,X) =     .00000
EN(1,Y) =     .00000  EN(2,Y) =    1.00000  EN(3,Y) =     .00000
EN(1,Z) =     .00000  EN(2,Z) =     .00000  EN(3,Z) =    1.00000


PROGRAM FLOW CONTROL PARAMETERS

OVER RELAXATION FACTOR     1.35
MAXIMUM NO. OF ITERATIONS SPECIFIED      400
STRESS CONVERGENCE CRITERION   .10000E-03
STARTING MINING STEP NUMBER          1
NUMBER OF NEW STEPS                 13


PRIMITIVE STRESSES AT LOCAL SEAM ORIGINS
SEAM #     PSX          PSY          PSZ

   1   .0000E+00    .0000E+00    .8253E+03

STRESS GRADIENTS
PXDX =     .0000E+00
PYDX =     .0000E+00
PZDX =     .0000E+00
PXDY =     .0000E+00
PYDY =     .0000E+00
PZDY =     .0000E+00

TIME TO READ, CALCULATE AND PRINT BASIC PARAMETERS =      0 SECONDS

TIME TO CALCULATE INFLUENCE COEFFICIENTS =      0 SECONDS

MINING STEP NUMBER =   1   FINE MESH SEAM NUMBER = 1
```

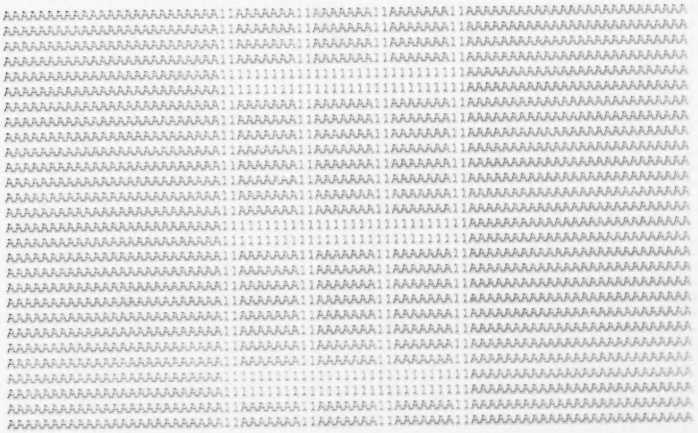

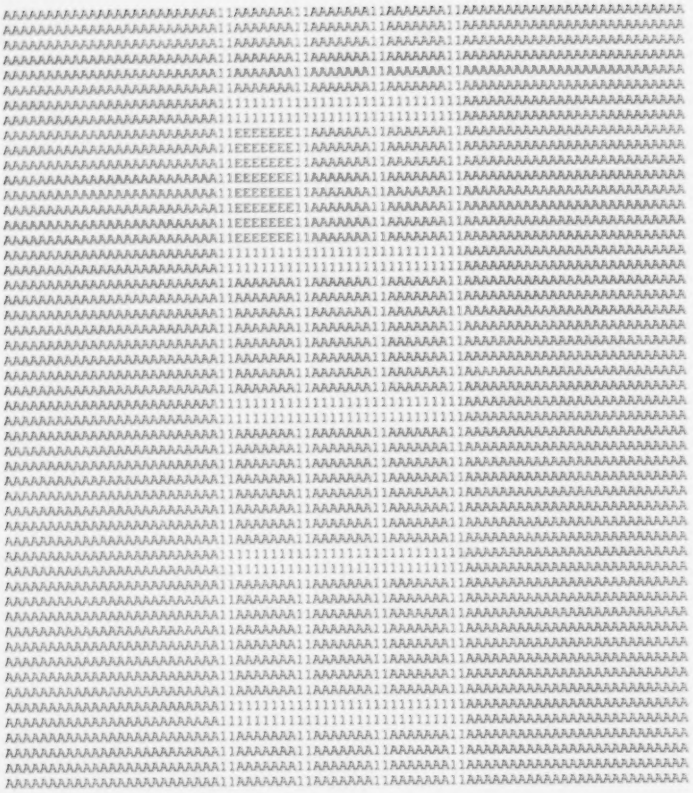

MINING STEP NUMBER = 1 COARSE MESH SEAM NUMBER = 1

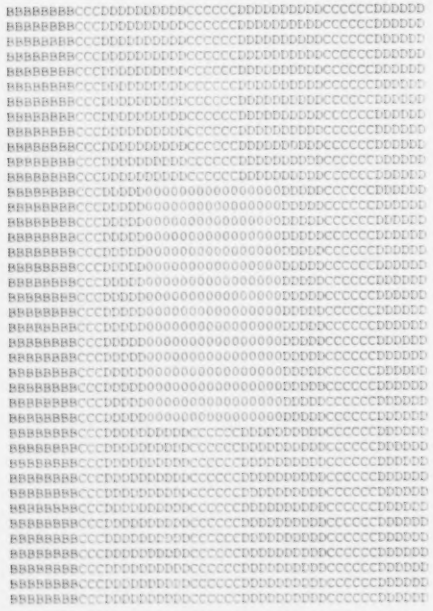

TIME TO READ, PRINT AND CONVERT MATERIAL PROPERTIES
FOR THIS MINING STEP = 0 SECONDS

```
SOLUTION PROGRESS FOR MINING STEP NUMBER =     1

iteration number =   1    ermaxb =     .9912E+01      ermaxe =     .3173E+01
iteration number =   2    ermaxb =     .3415E+01      ermaxe =     .1427E+01
iteration number =   3    ermaxb =     .1081E+01      ermaxe =     .3129E+00
iteration number =   4    ermaxb =     .4020E+00      ermaxe =     .1158E+00
iteration number =   5    ermaxb =     .1332E+00      ermaxe =     .4325E-01
iteration number =   6    ermaxb =     .5205E-01      ermaxe =     .2148E-01
iteration number =   7    ermaxb =     .1932E-01      ermaxe =     .7576E-02
iteration number =   8    ermaxb =     .7474E-02      ermaxe =     .3015E-02
iteration number =   9    ermaxb =     .3363E-02      ermaxe =     .1037E-02
iteration number =  10    ermaxb =     .1347E-02      ermaxe =     .4992E-03
iteration number =  11    ermaxb =     .5345E-03      ermaxe =     .1839E-03
iteration number =  12    ermaxb =     .2275E-03      ermaxe =     .7920E-04
iteration number =  13    ermaxb =     .8837E-04      ermaxe =     .2531E-04
iteration number =  14    ermaxb =     .4168E-04      ermaxe =     .9896E-05
iteration number =  15    ermaxb =     .1687E-04      ermaxe =     .4950E-05
iteration number =  16    ermaxb =     .7739E-05      ermaxe =     .1854E-05
iteration number =  17    ermaxb =     .3239E-05      ermaxe =     .1021E-05
iteration number =  18    ermaxb =     .1411E-05      ermaxe =     .3790E-06
iteration number =  19    ermaxb =     .5836E-06      ermaxe =     .1756E-06
iteration number =  20    ermaxb =     .2718E-06      ermaxe =     .6786E-07

TIME TO SOLVE FOR STRESSES AND DISPLACEMENTS IN THIS MINING STEP =  4283 SECONDS


MINING STEP NUMBER =   1
NUMBER OF ITERATIONS TO SOLVE =    20


MAXIMUM ERROR IN THE BLOCK DISPLACEMENTS =   .272E-06

MAXIMUM ERROR IN THE ELEMENTS DISPLACEMENTS =   .679E-07

TIME TO PRINT OUT STRESSES AND DISPLACEMENTS IN THIS MINING STEP =     0 SECONDS


TIME TO COMPUTE AND PRINT STRESSES AND DISPLACEMENTS
ON OFF-SEAM PLANES DURING THIS MINING STEP =     0 SECONDS

iteration number =   1    ermaxb =     .1096E-06      ermaxe =     .4206E-03
iteration number =   2    ermaxb =     .1154E-06      ermaxe =     .1480E-03
iteration number =   3    ermaxb =     .2936E-07      ermaxe =     .3675E-04
iteration number =   4    ermaxb =     .9819E-08      ermaxe =     .1206E-04
iteration number =   5    ermaxb =     .3896E-08      ermaxe =     .5952E-05
iteration number =   6    ermaxb =     .1937E-08      ermaxe =     .1364E-05
iteration number =   7    ermaxb =     .8433E-09      ermaxe =     .9236E-06
iteration number =   8    ermaxb =     .3784E-09      ermaxe =     .2547E-06
iteration number =   9    ermaxb =     .1639E-09      ermaxe =     .1358E-06
iteration number =  10    ermaxb =     .8001E-10      ermaxe =     .4335E-07

TIME TO SOLVE FOR STRESSES AND DISPLACEMENTS IN THIS MINING STEP =  2138 SECONDS


MINING STEP NUMBER =   1
NUMBER OF ITERATIONS TO SOLVE =    10


MAXIMUM ERROR IN THE BLOCK DISPLACEMENTS =   .800E-10

MAXIMUM ERROR IN THE ELEMENTS DISPLACEMENTS =   .434E-07

TIME TO PRINT OUT STRESSES AND DISPLACEMENTS IN THIS MINING STEP =     0 SECONDS


TIME TO COMPUTE AND PRINT STRESSES AND DISPLACEMENTS
ON OFF-SEAM PLANES DURING THIS MINING STEP =     0 SECONDS


MINING STEP NUMBER =   2   FINE MESH SEAM NUMBER = 1

AAAAAAAAAAAAAAAAAAAAAAAAAAAA11AAAAAAAA11AAAAAAAA11AAAAAAAA11AAAAAAAAAAAAAAAAAAAAAAAAAAAA
AAAAAAAAAAAAAAAAAAAAAAAAAAAA11AAAAAAAA11AAAAAAAA11AAAAAAAA11AAAAAAAAAAAAAAAAAAAAAAAAAAAA
AAAAAAAAAAAAAAAAAAAAAAAAAAAA11AAAAAAAA11AAAAAAAA11AAAAAAAA11AAAAAAAAAAAAAAAAAAAAAAAAAAAA
AAAAAAAAAAAAAAAAAAAAAAAAAAAA11AAAAAAAA11AAAAAAAA11AAAAAAAA11AAAAAAAAAAAAAAAAAAAAAAAAAAAA
```

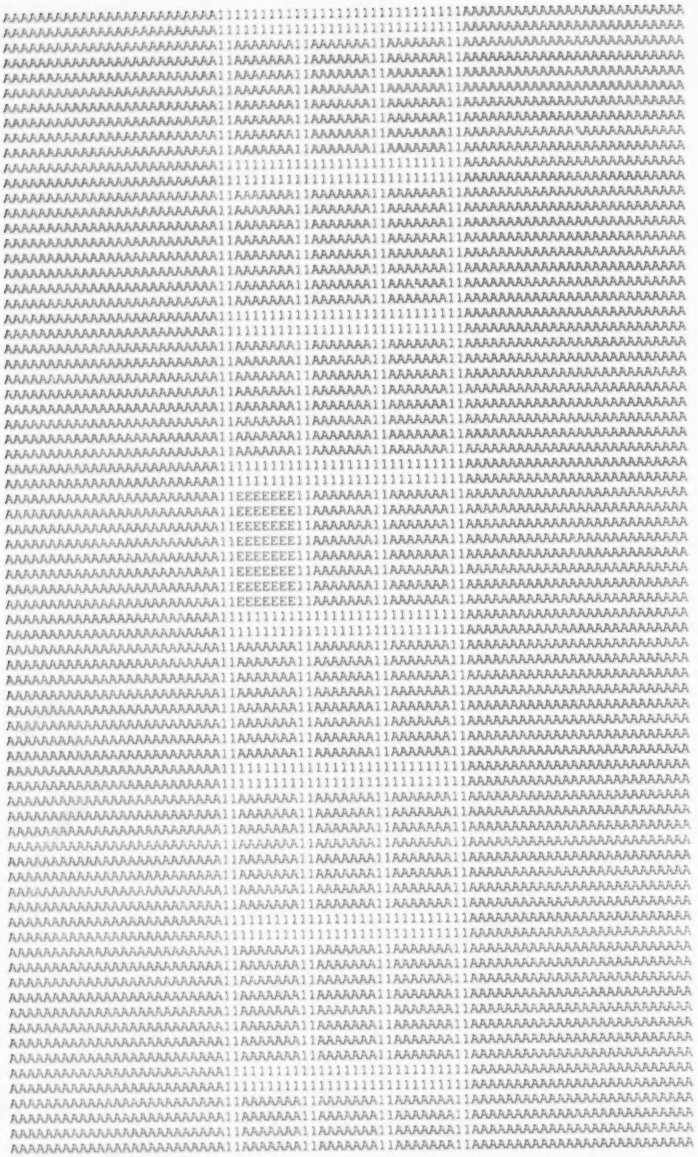

MINING STEP NUMBER = 2 COARSE MESH SEAM NUMBER = 1

```
BBBBBBBBCCCDDDDDOOO
```

TIME TO SOLVE FOR STRESSES AND DISPLACEMENTS IN THIS MINING STEP = 2146 SECONDS

MINING STEP NUMBER = 2
NUMBER OF ITERATIONS TO SOLVE = 10

MAXIMUM ERROR IN THE BLOCK DISPLACEMENTS = .432E-10

MAXIMUM ERROR IN THE ELEMENTS DISPLACEMENTS = .433E-07

TIME TO PRINT OUT STRESSES AND DISPLACEMENTS IN THIS MINING STEP = 0 SECONDS

TIME TO COMPUTE AND PRINT STRESSES AND DISPLACEMENTS
ON OFF-SEAM PLANES DURING THIS MINING STEP = 0 SECONDS

.
.
.
.
.
.

Mining step 3 through 13 were omitted

.
.
.
.
.
.

Local mine stiffness result:

Step No.	Ptd dspl	Rsd stress	Plr modulus	LMS	Plr dspl	No. of elmts
1	.00100	1270.632	290000.000	.000	.31547	56
1	.00100	1270.505	290000.000	-9129.399	.31647	56
2	.00100	1281.784	290000.000	.000	.31824	56
2	.00100	1281.658	290000.000	-9129.377	.31924	56
3	.00100	1301.632	290000.000	.000	.32316	56
3	.00100	1301.506	290000.000	-9128.849	.32416	56
4	.00100	1464.944	290000.000	.000	.36371	56
4	.00100	1464.818	228478.571	-9082.175	.36471	56
5	.00100	1686.627	280628.240	.000	.54107	56
5	.00100	1686.503	166957.143	-8966.986	.54207	56
6	.00100	1730.542	280576.156	.000	.55948	56
6	.00100	1730.418	166957.143	-8965.954	.56048	56
7	.00100	1738.579	271188.943	.000	.69197	56
7	.00100	1738.454	166957.143	-8956.623	.69297	56
8	.00100	1746.142	271174.712	.000	.69596	56
8	.00100	1746.017	166957.143	-8957.250	.69696	56
9	.00100	1755.603	271158.754	.000	.70073	56
9	.00100	1755.478	166957.143	-8956.353	.70173	56
10	.00100	1776.338	271128.909	.000	.71051	56
10	.00100	1776.213	166957.143	-8956.902	.71151	56
11	.00100	1800.025	271096.946	.000	.72152	56
11	.00100	1799.901	166957.143	-8956.470	.72252	56
12	.00100	1761.604	242468.048	.000	1.17539	56
12	.00100	1761.481	166957.143	-8913.478	1.17639	56
13	.00100	1771.934	242421.240	.000	1.18672	56
13	.00100	1771.810	166957.143	-8913.350	1.18772	56

Summary of the result:

No.	Strain	Stress	LMS
1	.43815E-02	.12706E+04	-.91294E+04
2	.44199E-02	.12818E+04	-.91294E+04
3	.44884E-02	.13016E+04	-.91288E+04
4	.50515E-02	.14649E+04	-.90822E+04
5	.75149E-02	.16866E+04	-.89670E+04
6	.77705E-02	.17305E+04	-.89660E+04
7	.96106E-02	.17386E+04	-.89566E+04
8	.96662E-02	.17461E+04	-.89573E+04
9	.97324E-02	.17556E+04	-.89564E+04
10	.98682E-02	.17763E+04	-.89569E+04

```
11    .10021E-01   .18000E+04 -.89565E+04
12    .16325E-01   .17616E+04 -.89135E+04
13    .16482E-01   .17719E+04 -.89134E+04

  TIME TO COMPUTE AND PRINT ENERGIES, STRESSES AND
  DISPLACEMENTS FOR ALL MINING STEPS =      153639 SECONDS
```

End of output for three rows of equal size pillar model

****

B.3 Model with AYY pillar configuration

Headgate abutment pillars(120X120 ft); center and tailgate yield pillars(30X50 ft)
Overburden 750 ft (9000 in)

```
IN THE FOLLOWING X,Y,Z REFER TO GLOBAL AXES OR COORDINATES
AND X1,X2,X3  OR  1,2,3 REFER TO LOCAL AXES OR COORDINATES.


ROCK MASS PROPERTIES
POISSONS RATIO          --              .25
MODULUS OF ELASTICITY --          145000.00
NO. OF SEAMS            --      1
NO. OF MATERIALS        --      5
PERTURBATION DSPL       --       .0010


IN-SEAM MATERIAL PROPERTIES
VALID MATERIAL PROPERTY CODES ARE:
0 1 2 A B C D E F G H I J K L M N O P Q R S T U V W X Y Z


MATERIAL NUMBER       1 (A)
STRAIN SOFTENING COAL       2.00000
PEAK STRESS               .29000E+04
PEAK STRAIN               .10000E-01
RESIDUAL STRESS           .14500E+04
RESIDUAL STRAIN           .15000E-01
POISSONS RATIO            .30000E+00


MATERIAL NUMBER       2 (B)
LINEAR ELASTIC GOB             6.0
YOUNGS MODULUS            .29000E+04
SHEAR MODULUS             .11600E+04
GOB HEIGHT FACTOR         .10000E+01


MATERIAL NUMBER       3 (C)
STRAIN SOFTENING COAL       2.00000
PEAK STRESS               .18000E+04
PEAK STRAIN               .10000E-01
RESIDUAL STRESS           .89900E+03
RESIDUAL STRAIN           .15000E-01
POISSONS RATIO            .32000E+00


MATERIAL NUMBER       4 (D)
LINEAR ELASTIC COAL            1.0
YOUNGS MODULUS            .29000E+06
SHEAR MODULUS             .11600E+06


MATERIAL NUMBER       5 (E)
STRAIN SOFTENING COAL       2.00000
PEAK STRESS               .29000E+04
PEAK STRAIN               .10000E-01
RESIDUAL STRESS           .14500E+04
RESIDUAL STRAIN           .15000E-01
POISSONS RATIO            .30000E+00


PRIMITIVE STRESS PARAMETERS

PRIMITIVE STRESSES ARE GIVEN AS
PXX =     .0000      .0458    * Z
PXY =     .0000      .0000    * Z
PXZ =     .0000      .0000    * Z
PYY =     .0000      .0458    * z
PYZ =     .0000      .0000    * z
PZZ =     .0000      .0917    * z


MODEL CONTROL AND MODEL DATA
```

```
NO. OF PARALLEL SEAMS                    --        1
WIDTH OF BLOCKS                          --   600.00
NO. OF BLOCKS ALONG X  AXIS              --       49
NO. OF BLOCKS ALONG Y  AXIS              --       40
NUMBER OF OFF-SEAM PLANES SELECTED       --        0
FINE MESH STARTING BLOCK X-AXIS          --       17
FINE MESH ENDING   BLOCK X-AXIS          --       32
FINE MESH STARTING BLOCK Y-AXIS          --       13
FINE MESH ENDING   BLOCK Y-AXIS          --       28


GLOBAL COORDINATES OF LOCAL ORIGINS AND SEAM THICKNESSES
SEAM NO.          X           Y           Z      THICKNESS
     1          .00         .00    -9000.00        72.00

DIRECTION COSINES OF LOCAL SEAM AXES WITH RESPECT TO THE GLOBAL AXES


EN(1,X) =     1.00000  EN(2,X) =      .00000  EN(3,X) =      .00000
EN(1,Y) =      .00000  EN(2,Y) =     1.00000  EN(3,Y) =      .00000
EN(1,Z) =      .00000  EN(2,Z) =      .00000  EN(3,Z) =     1.00000


PROGRAM FLOW CONTROL PARAMETERS

OVER RELAXATION FACTOR     1.35
MAXIMUM NO. OF ITERATIONS SPECIFIED      400
STRESS CONVERGENCE CRITERION    .10000E-03
STARTING MINING STEP NUMBER          1
NUMBER OF NEW STEPS                 13


PRIMITIVE STRESSES AT LOCAL SEAM ORIGINS
SEAM #     PSX          PSY          PSZ

   1    .0000E+00    .0000E+00    .8253E+03

STRESS GRADIENTS
PXDX =     .0000E+00
PYDX =     .0000E+00
PZDX =     .0000E+00
PXDY =     .0000E+00
PYDY =     .0000E+00
PZDY =     .0000E+00


TIME TO READ, CALCULATE AND PRINT BASIC PARAMETERS =      0 SECONDS


TIME TO CALCULATE INFLUENCE COEFFICIENTS =      0 SECONDS


MINING STEP NUMBER =   1   FINE MESH SEAM NUMBER = 1
```

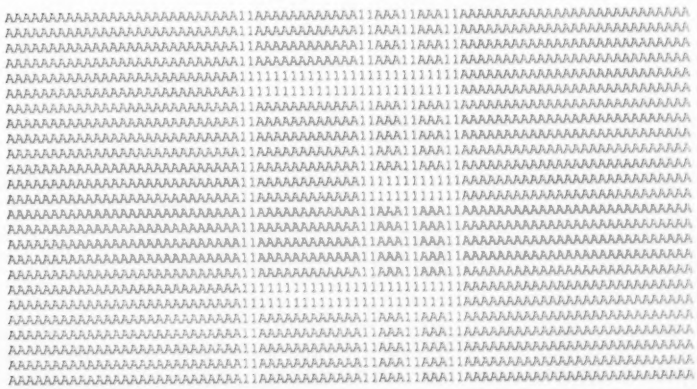

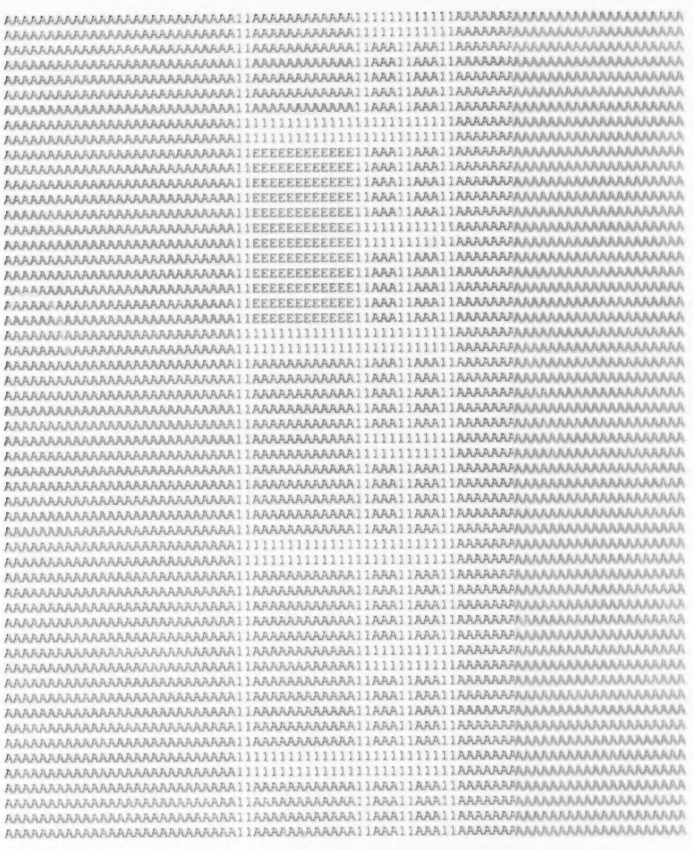

MINING STEP NUMBER = 1 COARSE MESH SEAM NUMBER = 1

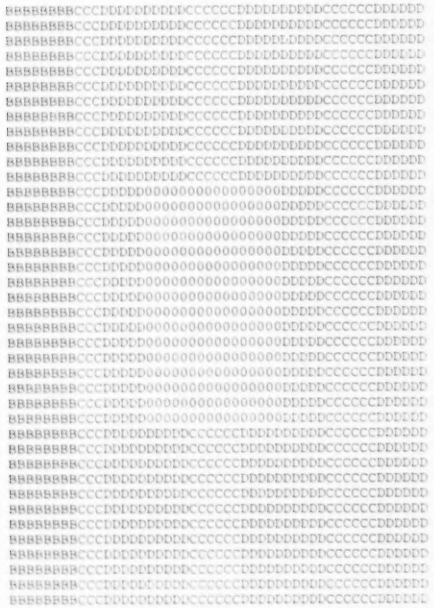

TIME TO READ, PRINT AND CONVERT MATERIAL PEOPERTIES

```
FOR THIS MINING STEP =      0 SECONDS

SOLUTION PROGRESS FOR MINING STEP NUMBER =      1

iteration number =   1     ermaxb =     .9912E+01       ermaxe =     .3185E+01
iteration number =   2     ermaxb =     .3415E+01       ermaxe =     .1394E+01
iteration number =   3     ermaxb =     .1081E+01       ermaxe =     .3190E+00
iteration number =   4     ermaxb =     .4021E+00       ermaxe =     .1150E+00
iteration number =   5     ermaxb =     .1332E+00       ermaxe =     .4007E-01
iteration number =   6     ermaxb =     .5205E-01       ermaxe =     .2138E-01
iteration number =   7     ermaxb =     .1932E-01       ermaxe =     .6211E-02
iteration number =   8     ermaxb =     .7474E-02       ermaxe =     .2790E-02
iteration number =   9     ermaxb =     .3363E-02       ermaxe =     .1038E-02
iteration number =  10     ermaxb =     .1347E-02       ermaxe =     .5125E-03
iteration number =  11     ermaxb =     .5345E-03       ermaxe =     .1871E-03
iteration number =  12     ermaxb =     .2275E-03       ermaxe =     .8162E-04
iteration number =  13     ermaxb =     .8837E-04       ermaxe =     .2637E-04
iteration number =  14     ermaxb =     .4168E-04       ermaxe =     .1073E-04
iteration number =  15     ermaxb =     .1687E-04       ermaxe =     .5193E-05
iteration number =  16     ermaxb =     .7739E-05       ermaxe =     .1974E-05
iteration number =  17     ermaxb =     .3239E-05       ermaxe =     .9474E-06
iteration number =  18     ermaxb =     .1411E-05       ermaxe =     .3776E-06
iteration number =  19     ermaxb =     .5836E-06       ermaxe =     .1598E-06

TIME TO SOLVE FOR STRESSES AND DISPLACEMENTS IN THIS MINING STEP =  1614 SECONDS


MINING STEP NUMBER =   1
NUMBER OF ITERATIONS TO SOLVE =    19


MAXIMUM ERROR IN THE BLOCK DISPLACEMENTS =   .584E-06

MAXIMUM ERROR IN THE ELEMENTS DISPLACEMENTS =   .160E-06

TIME TO PRINT OUT STRESSES AND DISPLACEMENTS IN THIS MINING STEP =     3 SECONDS


TIME TO COMPUTE AND PRINT STRESSES AND DISPLACEMENTS
ON OFF-SEAM PLANES DURING THIS MINING STEP =     0 SECONDS

iteration number =   1     ermaxb =     .2718E-06       ermaxe =     .4486E-03
iteration number =   2     ermaxb =     .2236E-06       ermaxe =     .1603E-03
iteration number =   3     ermaxb =     .6985E-07       ermaxe =     .4849E-04
iteration number =   4     ermaxb =     .2371E-07       ermaxe =     .1454E-04
iteration number =   5     ermaxb =     .9730E-08       ermaxe =     .5589E-05
iteration number =   6     ermaxb =     .4220E-08       ermaxe =     .1265E-05
iteration number =   7     ermaxb =     .1743E-08       ermaxe =     .8182E-06
iteration number =   8     ermaxb =     .8241E-09       ermaxe =     .2270E-06
iteration number =   9     ermaxb =     .3579E-09       ermaxe =     .1284E-06
iteration number =  10     ermaxb =     .1595E-09       ermaxe =     .4438E-07

TIME TO SOLVE FOR STRESSES AND DISPLACEMENTS IN THIS MINING STEP =   849 SECONDS


MINING STEP NUMBER =   1
NUMBER OF ITERATIONS TO SOLVE =    10


MAXIMUM ERROR IN THE BLOCK DISPLACEMENTS =   .160E-09

MAXIMUM ERROR IN THE ELEMENTS DISPLACEMENTS =   .444E-07

TIME TO PRINT OUT STRESSES AND DISPLACEMENTS IN THIS MINING STEP =     3 SECONDS


TIME TO COMPUTE AND PRINT STRESSES AND DISPLACEMENTS
ON OFF-SEAM PLANES DURING THIS MINING STEP =     0 SECONDS

.
.
.

Mining step 2 through 13 were omitted
.
```

.
.

Local mine stiffness result:

Step No.	Ptd dspl	Rsd stress	Plr modulus	LMS	Plr dspl	No. of elmts
1	.00100	1124.801	290000.000	.000	.27926	144
1	.00100	1124.712	290000.000	-6425.764	.28026	144
2	.00100	1133.844	290000.000	.000	.28151	144
2	.00100	1133.754	290000.000	-6425.727	.28251	144
3	.00100	1149.861	290000.000	.000	.28548	144
3	.00100	1149.772	290000.000	-6425.241	.28648	144
4	.00100	1256.301	290000.000	.000	.31191	144
4	.00100	1256.213	278037.500	-6377.740	.31291	144
5	.00100	1398.337	286366.153	.000	.39336	144
5	.00100	1398.250	266261.863	-6286.914	.39436	144
6	.00100	1430.709	286342.393	.000	.40462	144
6	.00100	1430.621	266241.521	-6285.602	.40562	144
7	.00100	1448.876	286332.722	.000	.41058	144
7	.00100	1448.789	266234.972	-6285.362	.41158	144
8	.00100	1455.986	286330.206	.000	.41274	144
8	.00100	1455.899	266233.984	-6286.140	.41374	144
9	.00100	1465.878	284507.600	.000	.44019	144
9	.00100	1465.791	266232.577	-6283.503	.44119	144
10	.00100	1541.190	282664.785	.000	.48692	144
10	.00100	1541.104	264377.541	-6211.967	.48792	144
11	.00100	1664.151	269791.422	.000	.70787	144
11	.00100	1664.069	243154.536	-5916.660	.70887	144
12	.00100	1656.958	238151.537	.000	1.22983	144
12	.00100	1656.877	146467.322	-5866.742	1.23083	144
13	.00100	1676.112	238033.295	.000	1.25852	144
13	.00100	1676.031	145858.440	-5863.404	1.25952	144

Summary of the result:

No.	Strain	Stress	LMS
1	.38786E-02	.11248E+04	-.64258E+04
2	.39098E-02	.11338E+04	-.64257E+04
3	.39650E-02	.11499E+04	-.64252E+04
4	.43321E-02	.12563E+04	-.63777E+04
5	.54633E-02	.13983E+04	-.62869E+04
6	.56197E-02	.14307E+04	-.62856E+04
7	.57026E-02	.14489E+04	-.62854E+04
8	.57325E-02	.14560E+04	-.62861E+04
9	.61138E-02	.14659E+04	-.62835E+04
10	.67628E-02	.15412E+04	-.62120E+04
11	.98315E-02	.16642E+04	-.59167E+04
12	.17081E-01	.16570E+04	-.58667E+04
13	.17479E-01	.16761E+04	-.58634E+04

TIME TO COMPUTE AND PRINT ENERGIES, STRESSES AND
DISPLACEMENTS FOR ALL MINING STEPS = 85800 SECONDS

End of output for headgate abutment pillar model (AYY)

****

B.4 Development 7 model

30X80 and 80X80 ft pillars & 20 ft entries, Pocahntas No.3 Coalbed Overburden 1900 ft (22800 in)

```
IN THE FOLLOWING X,Y,Z REFER TO GLOBAL AXES OR COORDINATES
AND X1,X2,X3  OR  1,2,3 REFER TO LOCAL AXES OR COORDINATES.


ROCK MASS PROPERTIES
POISSONS RATIO          --             .25
MODULUS OF ELASTICITY   --       690000.00
NO. OF SEAMS            --      1
NO. OF MATERIALS        --     11
PERTURBATION DSPL       --       .1000


IN-SEAM MATERIAL PROPERTIES
VALID MATERIAL PROPERTY CODES ARE:
0 1 2 A B C D E F G H I J K L M N O P Q R S T U V W X Y Z


MATERIAL NUMBER       1 (A)
STRAIN SOFTENING COAL      2.00000
PEAK STRESS              .63000E+04
PEAK STRAIN              .10500E+00
RESIDUAL STRESS          .60000E+04
RESIDUAL STRAIN          .15500E+00
POISSONS RATIO           .30000E+00


MATERIAL NUMBER       2 (B)
STRAIN SOFTENING COAL      2.00000
PEAK STRESS              .62500E+04
PEAK STRAIN              .10400E+00
RESIDUAL STRESS          .54000E+04
RESIDUAL STRAIN          .14300E+00
POISSONS RATIO           .30000E+00


MATERIAL NUMBER       3 (C)
STRAIN SOFTENING COAL      2.00000
PEAK STRESS              .62000E+04
PEAK STRAIN              .10300E+00
RESIDUAL STRESS          .46000E+04
RESIDUAL STRAIN          .12800E+00
POISSONS RATIO           .30000E+00


MATERIAL NUMBER       4 (D)
STRAIN SOFTENING COAL      2.00000
PEAK STRESS              .30000E+04
PEAK STRAIN              .50000E-01
RESIDUAL STRESS          .13000E+04
RESIDUAL STRAIN          .60000E-01
POISSONS RATIO           .30000E+00


MATERIAL NUMBER       5 (E)
STRAIN HARDENING GOB                5.00000
INITIAL MODULUS AT ZERO STRESS    .29400E+03
FINAL MODULUS AT PEAK STRESS      .27000E+05
PEAK STRESS                       .20900E+04
GOB HEIGHT FACTOR                 .10000E+01
POISSONS RATIO                    .40000E+00


MATERIAL NUMBER       6 (F)
STRAIN SOFTENING COAL      2.00000
PEAK STRESS              .24000E+04
PEAK STRAIN              .74000E-01
RESIDUAL STRESS          .20000E+04
RESIDUAL STRAIN          .16500E+00
POISSONS RATIO           .30000E+00
```

```
MATERIAL NUMBER       7 (G)
STRAIN SOFTENING COAL      2.00000
PEAK STRESS              .63000E+04
PEAK STRAIN              .10500E+00
RESIDUAL STRESS          .60000E+04
RESIDUAL STRAIN          .15500E+00
POISSONS RATIO           .30000E+00


MATERIAL NUMBER       8 (H)
STRAIN SOFTENING COAL      2.00000
PEAK STRESS              .63000E+04
PEAK STRAIN              .10500E+00
RESIDUAL STRESS          .60000E+04
RESIDUAL STRAIN          .15500E+00
POISSONS RATIO           .30000E+00


MATERIAL NUMBER       9 (I)
STRAIN SOFTENING COAL      2.00000
PEAK STRESS              .62500E+04
PEAK STRAIN              .10400E+00
RESIDUAL STRESS          .54000E+04
RESIDUAL STRAIN          .14300E+00
POISSONS RATIO           .30000E+00


MATERIAL NUMBER      10 (J)
STRAIN SOFTENING COAL      2.00000
PEAK STRESS              .62000E+04
PEAK STRAIN              .10300E+00
RESIDUAL STRESS          .46000E+04
RESIDUAL STRAIN          .12800E+00
POISSONS RATIO           .30000E+00


MATERIAL NUMBER      11 (K)
STRAIN SOFTENING COAL      2.00000
PEAK STRESS              .30000E+04
PEAK STRAIN              .50000E-01
RESIDUAL STRESS          .13000E+04
RESIDUAL STRAIN          .60000E-01
POISSONS RATIO           .30000E+00


PRIMITIVE STRESS PARAMETERS

PRIMITIVE STRESSES ARE GIVEN AS
PXX =    .0000     .1250   * Z
PXY =    .0000     .0000   * Z
PXZ =    .0000     .0000   * Z
PYY =    .0000     .1250   * z
PYZ =    .0000     .0000   * z
PZZ =    .0000     .0917   * z


MODEL CONTROL AND MODEL DATA

NO. OF PARALLEL SEAMS                --        1
WIDTH OF BLOCKS                      --   600.00
NO. OF BLOCKS ALONG X  AXIS          --       50
NO. OF BLOCKS ALONG Y  AXIS          --       40
NUMBER OF OFF-SEAM PLANES SELECTED   --        0
FINE MESH STARTING BLOCK X-AXIS      --       18
FINE MESH ENDING   BLOCK X-AXIS      --       34
FINE MESH STARTING BLOCK Y-AXIS      --       11
FINE MESH ENDING   BLOCK Y-AXIS      --       30


GLOBAL COORDINATES OF LOCAL ORIGINS AND SEAM THICKNESSES
SEAM NO.          X           Y           Z      THICKNESS
     1          .00         .00   -22800.00       70.00

DIRECTION COSINES OF LOCAL SEAM AXES WITH RESPECT TO T        HE GLOBAL AXES
```

```
EN(1,X) =    1.00000  EN(2,X) =     .00000  EN(3,X) =     .00000
EN(1,Y) =     .00000  EN(2,Y) =    1.00000  EN(3,Y) =     .00000
EN(1,Z) =     .00000  EN(2,Z) =     .00000  EN(3,Z) =    1.00000


PROGRAM FLOW CONTROL PARAMETERS

OVER RELAXATION FACTOR     1.35
MAXIMUM NO. OF ITERATIONS SPECIFIED      300
STRESS CONVERGENCE CRITERION   .10000E+00
STARTING MINING STEP NUMBER          1
NUMBER OF NEW STEPS                  1


PRIMITIVE STRESSES AT LOCAL SEAM ORIGINS
SEAM #    PSX          PSY          PSZ

   1   .0000E+00   .0000E+00   .2091E+04

STRESS GRADIENTS
PXDX =     .0000E+00
PYDX =     .0000E+00
PZDX =     .0000E+00
PXDY =     .0000E+00
PYDY =     .0000E+00
PZDY =     .0000E+00


TIME TO READ, CALCULATE AND PRINT BASIC PARAMETERS =     0 SECONDS


TIME TO CALCULATE INFLUENCE COEFFICIENTS =     0 SECONDS
.
.
.
Mining step 1 through 2 were omitted
.
.
.
MINING STEP NUMBER =   3   FINE MESH SEAM NUMBER = 1
```

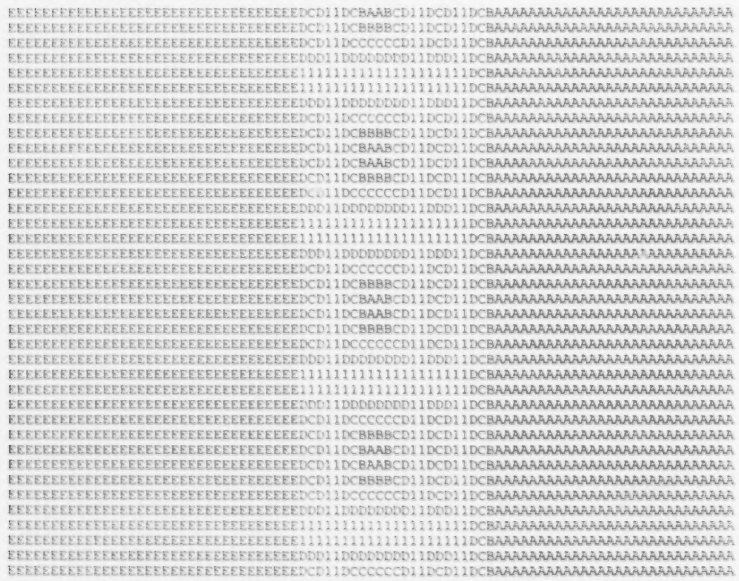

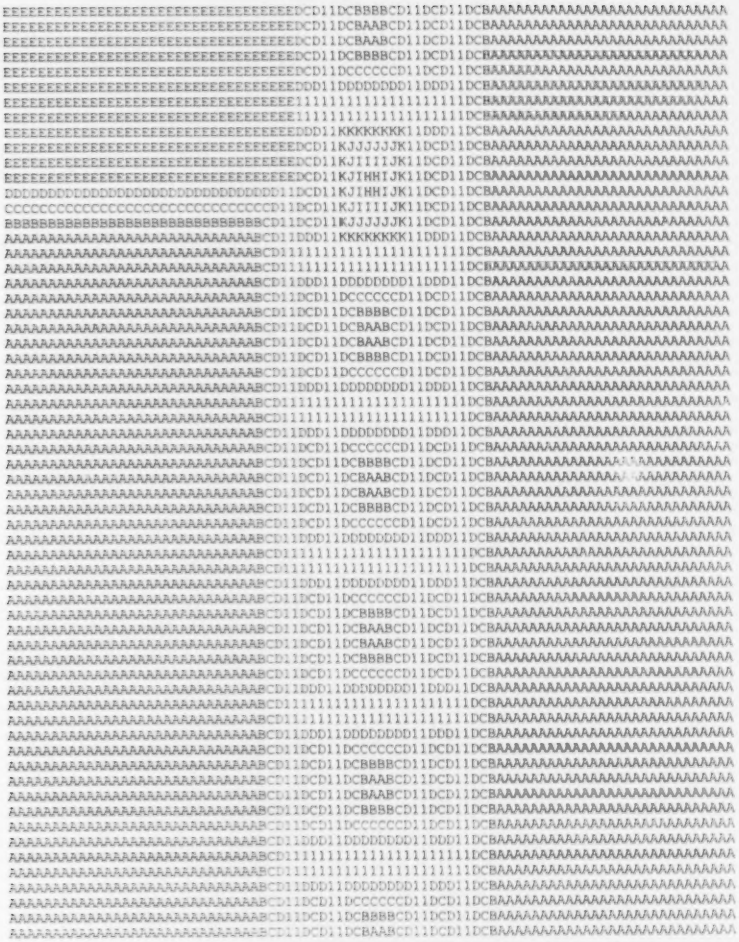

MINING STEP NUMBER = 3 COARSE MESH SEAM NUMBER = 1

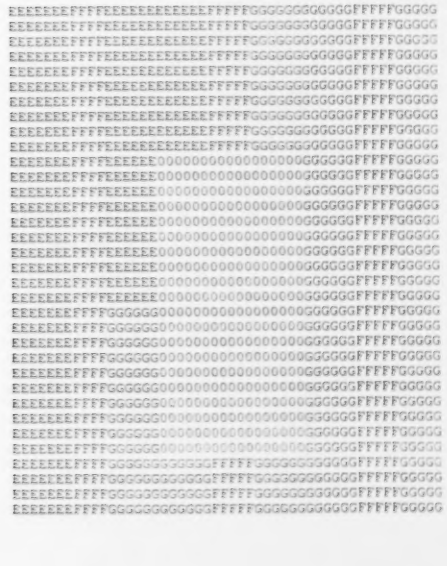

```
EEEEEEEFFFFGGGGGGGGGGGGFFFFFGGGGGGGGGGGGFFFFFGGGGG
EEEEEEEFFFFGGGGGGGGGGGGFFFFFGGGGGGGGGGGGFFFFFGGGGG
EEEEEEEFFFFGGGGGGGGGGGGFFFFFGGGGGGGGGGGGFFFFFGGGGG
EEEEEEEFFFFGGGGGGGGGGGGFFFFFGGGGGGGGGGGGFFFFFGGGGG
EEEEEEEFFFFGGGGGGGGGGGGFFFFFGGGGGGGGGGGGFFFFFGGGGG
EEEEEEEFFFFGGGGGGGGGGGGFFFFFGGGGGGGGGGGGFFFFFGGGGG
```

TIME TO READ, PRINT AND CONVERT MATERIAL PROPERTIES
FOR THIS MINING STEP = 0 SECONDS

SOLUTION PROGRESS FOR MINING STEP NUMBER = 3

iteration number =	1	ermaxb =	.6015E+01	ermaxe =	.4102E+01
iteration number =	2	ermaxb =	.2946E+01	ermaxe =	.3444E+01
iteration number =	3	ermaxb =	.1798E+01	ermaxe =	.1993E+01
iteration number =	4	ermaxb =	.1227E+01	ermaxe =	.1804E+01
iteration number =	5	ermaxb =	.1232E+01	ermaxe =	.1272E+01
iteration number =	6	ermaxb =	.1241E+01	ermaxe =	.9831E+00
iteration number =	7	ermaxb =	.1244E+01	ermaxe =	.8419E+00
iteration number =	8	ermaxb =	.1225E+01	ermaxe =	.7517E+00
iteration number =	9	ermaxb =	.9713E+00	ermaxe =	.7054E+00
iteration number =	10	ermaxb =	.7230E+00	ermaxe =	.6408E+00
iteration number =	11	ermaxb =	.5536E+00	ermaxe =	.6826E+00
iteration number =	12	ermaxb =	.4411E+00	ermaxe =	.6620E+00
iteration number =	13	ermaxb =	.3401E+00	ermaxe =	.5450E+00
iteration number =	14	ermaxb =	.2667E+00	ermaxe =	.5020E+00
iteration number =	15	ermaxb =	.2104E+00	ermaxe =	.3011E+00
iteration number =	16	ermaxb =	.1716E+00	ermaxe =	.2753E+00
iteration number =	17	ermaxb =	.1382E+00	ermaxe =	.2524E+00
iteration number =	18	ermaxb =	.1208E+00	ermaxe =	.2321E+00
iteration number =	19	ermaxb =	.1079E+00	ermaxe =	.2169E+00
iteration number =	20	ermaxb =	.9672E-01	ermaxe =	.1975E+00
iteration number =	21	ermaxb =	.8738E-01	ermaxe =	.1830E+00
iteration number =	22	ermaxb =	.7947E-01	ermaxe =	.1699E+00
iteration number =	23	ermaxb =	.7262E-01	ermaxe =	.1580E+00
iteration number =	24	ermaxb =	.6531E-01	ermaxe =	.1472E+00
iteration number =	25	ermaxb =	.5956E-01	ermaxe =	.1373E+00
iteration number =	26	ermaxb =	.5395E-01	ermaxe =	.1283E+00
iteration number =	27	ermaxb =	.4964E-01	ermaxe =	.1201E+00
iteration number =	28	ermaxb =	.4577E-01	ermaxe =	.1125E+00
iteration number =	29	ermaxb =	.4226E-01	ermaxe =	.1055E+00
iteration number =	30	ermaxb =	.3910E-01	ermaxe =	.9903E-01
iteration number =	31	ermaxb =	.3624E-01	ermaxe =	.9306E-01
iteration number =	32	ermaxb =	.3365E-01	ermaxe =	.8754E-01
iteration number =	33	ermaxb =	.3129E-01	ermaxe =	.8241E-01
iteration number =	34	ermaxb =	.2914E-01	ermaxe =	.7764E-01
iteration number =	35	ermaxb =	.2717E-01	ermaxe =	.7321E-01
iteration number =	36	ermaxb =	.2526E-01	ermaxe =	.6907E-01
iteration number =	37	ermaxb =	.2345E-01	ermaxe =	.6521E-01
iteration number =	38	ermaxb =	.2180E-01	ermaxe =	.6161E-01
iteration number =	39	ermaxb =	.2031E-01	ermaxe =	.5824E-01
iteration number =	40	ermaxb =	.1895E-01	ermaxe =	.5508E-01
iteration number =	41	ermaxb =	.1773E-01	ermaxe =	.5214E-01
iteration number =	42	ermaxb =	.1662E-01	ermaxe =	.4939E-01
iteration number =	43	ermaxb =	.1562E-01	ermaxe =	.4681E-01
iteration number =	44	ermaxb =	.1470E-01	ermaxe =	.4438E-01
iteration number =	45	ermaxb =	.1384E-01	ermaxe =	.4209E-01
iteration number =	46	ermaxb =	.1304E-01	ermaxe =	.3994E-01
iteration number =	47	ermaxb =	.1228E-01	ermaxe =	.3791E-01
iteration number =	48	ermaxb =	.1159E-01	ermaxe =	.3600E-01
iteration number =	49	ermaxb =	.1094E-01	ermaxe =	.3420E-01
iteration number =	50	ermaxb =	.1033E-01	ermaxe =	.3249E-01

.
.
.
.

iteration number =	231	ermaxb =	.2345E-05	ermaxe =	.9462E-05
iteration number =	232	ermaxb =	.2243E-05	ermaxe =	.9051E-05
iteration number =	233	ermaxb =	.2145E-05	ermaxe =	.8657E-05
iteration number =	234	ermaxb =	.2051E-05	ermaxe =	.8281E-05
iteration number =	235	ermaxb =	.1961E-05	ermaxe =	.7921E-05
iteration number =	236	ermaxb =	.1875E-05	ermaxe =	.7577E-05
iteration number =	237	ermaxb =	.1793E-05	ermaxe =	.7247E-05
iteration number =	238	ermaxb =	.1714E-05	ermaxe =	.6932E-05
iteration number =	239	ermaxb =	.1639E-05	ermaxe =	.6631E-05
iteration number =	240	ermaxb =	.1568E-05	ermaxe =	.6343E-05

```
iteration number = 241    ermaxb =    .1499E-05      ermaxe =    .6067E-05
iteration number = 242    ermaxb =    .1433E-05      ermaxe =    .5803E-05
iteration number = 243    ermaxb =    .1371E-05      ermaxe =    .5551E-05
iteration number = 244    ermaxb =    .1311E-05      ermaxe =    .5309E-05
iteration number = 245    ermaxb =    .1253E-05      ermaxe =    .5079E-05
iteration number = 246    ermaxb =    .1198E-05      ermaxe =    .4858E-05
iteration number = 247    ermaxb =    .1146E-05      ermaxe =    .4646E-05
iteration number = 248    ermaxb =    .1096E-05      ermaxe =    .4444E-05
iteration number = 249    ermaxb =    .1048E-05      ermaxe =    .4251E-05
iteration number = 250    ermaxb =    .1002E-05      ermaxe =    .4066E-05
iteration number = 251    ermaxb =    .9580E-06      ermaxe =    .3889E-05
iteration number = 252    ermaxb =    .9160E-06      ermaxe =    .3720E-05
iteration number = 253    ermaxb =    .8760E-06      ermaxe =    .3558E-05

TIME TO SOLVE FOR STRESSES AND DISPLACEMENTS IN THIS MINING STEP = 65972 SECONDS


MINING STEP NUMBER =   3
NUMBER OF ITERATIONS TO SOLVE =   253


MAXIMUM ERROR IN THE BLOCK DISPLACEMENTS =   .876E-06

MAXIMUM ERROR IN THE ELEMENTS DISPLACEMENTS =   .356E-05

TIME TO PRINT OUT STRESSES AND DISPLACEMENTS IN THIS MINING STEP =    10 SECONDS


TIME TO COMPUTE AND PRINT STRESSES AND DISPLACEMENTS
ON OFF-SEAM PLANES DURING THIS MINING STEP =     0 SECONDS

iteration number =   1    ermaxb =    .3389E-04      ermaxe =    .4346E-01
iteration number =   2    ermaxb =    .4577E-04      ermaxe =    .1861E-01
iteration number =   3    ermaxb =    .4141E-04      ermaxe =    .7709E-02
iteration number =   4    ermaxb =    .3917E-04      ermaxe =    .3845E-02
iteration number =   5    ermaxb =    .3658E-04      ermaxe =    .2766E-02
iteration number =   6    ermaxb =    .3390E-04      ermaxe =    .2091E-02
iteration number =   7    ermaxb =    .3131E-04      ermaxe =    .1571E-02
iteration number =   8    ermaxb =    .2886E-04      ermaxe =    .1230E-02
iteration number =   9    ermaxb =    .2660E-04      ermaxe =    .9658E-03
iteration number =  10    ermaxb =    .2452E-04      ermaxe =    .7645E-03
iteration number =  11    ermaxb =    .2262E-04      ermaxe =    .6097E-03
iteration number =  12    ermaxb =    .2089E-04      ermaxe =    .4909E-03
iteration number =  13    ermaxb =    .1930E-04      ermaxe =    .4022E-03
iteration number =  14    ermaxb =    .1786E-04      ermaxe =    .3539E-03
iteration number =  15    ermaxb =    .1654E-04      ermaxe =    .3148E-03
iteration number =  16    ermaxb =    .1534E-04      ermaxe =    .2805E-03
iteration number =  17    ermaxb =    .1424E-04      ermaxe =    .2504E-03
iteration number =  18    ermaxb =    .1324E-04      ermaxe =    .2243E-03
iteration number =  19    ermaxb =    .1232E-04      ermaxe =    .2022E-03
iteration number =  20    ermaxb =    .1147E-04      ermaxe =    .1838E-03
iteration number =  21    ermaxb =    .1070E-04      ermaxe =    .1677E-03
iteration number =  22    ermaxb =    .9992E-05      ermaxe =    .1531E-03
iteration number =  23    ermaxb =    .9340E-05      ermaxe =    .1398E-03
iteration number =  24    ermaxb =    .8740E-05      ermaxe =    .1278E-03
iteration number =  25    ermaxb =    .8188E-05      ermaxe =    .1169E-03
iteration number =  26    ermaxb =    .7679E-05      ermaxe =    .1070E-03
iteration number =  27    ermaxb =    .7209E-05      ermaxe =    .9809E-04
iteration number =  28    ermaxb =    .6774E-05      ermaxe =    .9024E-04
iteration number =  29    ermaxb =    .6372E-05      ermaxe =    .8354E-04
iteration number =  30    ermaxb =    .6000E-05      ermaxe =    .7737E-04
iteration number =  31    ermaxb =    .5654E-05      ermaxe =    .7186E-04
iteration number =  32    ermaxb =    .5333E-05      ermaxe =    .6678E-04
iteration number =  33    ermaxb =    .5035E-05      ermaxe =    .6207E-04
iteration number =  34    ermaxb =    .4756E-05      ermaxe =    .5772E-04
iteration number =  35    ermaxb =    .4497E-05      ermaxe =    .5370E-04
iteration number =  36    ermaxb =    .4255E-05      ermaxe =    .4998E-04
iteration number =  37    ermaxb =    .4029E-05      ermaxe =    .4667E-04
iteration number =  38    ermaxb =    .3817E-05      ermaxe =    .4360E-04
iteration number =  39    ermaxb =    .3619E-05      ermaxe =    .4075E-04
iteration number =  40    ermaxb =    .3433E-05      ermaxe =    .3813E-04
iteration number =  41    ermaxb =    .3258E-05      ermaxe =    .3572E-04
iteration number =  42    ermaxb =    .3094E-05      ermaxe =    .3347E-04
iteration number =  43    ermaxb =    .2940E-05      ermaxe =    .3137E-04
iteration number =  44    ermaxb =    .2794E-05      ermaxe =    .2941E-04
iteration number =  45    ermaxb =    .2657E-05      ermaxe =    .2758E-04
```

```
iteration number =  46    ermaxb =    .2528E-05      ermaxe =    .2587E-04
iteration number =  47    ermaxb =    .2406E-05      ermaxe =    .2427E-04
iteration number =  48    ermaxb =    .2290E-05      ermaxe =    .2280E-04
iteration number =  49    ermaxb =    .2181E-05      ermaxe =    .2144E-04
iteration number =  50    ermaxb =    .2078E-05      ermaxe =    .2017E-04
iteration number =  51    ermaxb =    .1980E-05      ermaxe =    .1900E-04
iteration number =  52    ermaxb =    .1887E-05      ermaxe =    .1791E-04
iteration number =  53    ermaxb =    .1799E-05      ermaxe =    .1687E-04
iteration number =  54    ermaxb =    .1716E-05      ermaxe =    .1591E-04
iteration number =  55    ermaxb =    .1637E-05      ermaxe =    .1499E-04
iteration number =  56    ermaxb =    .1561E-05      ermaxe =    .1414E-04
iteration number =  57    ermaxb =    .1490E-05      ermaxe =    .1333E-04
iteration number =  58    ermaxb =    .1422E-05      ermaxe =    .1258E-04
iteration number =  59    ermaxb =    .1358E-05      ermaxe =    .1188E-04
iteration number =  60    ermaxb =    .1296E-05      ermaxe =    .1122E-04
iteration number =  61    ermaxb =    .1238E-05      ermaxe =    .1060E-04
iteration number =  62    ermaxb =    .1182E-05      ermaxe =    .1002E-04
iteration number =  63    ermaxb =    .1129E-05      ermaxe =    .9468E-05
iteration number =  64    ermaxb =    .1078E-05      ermaxe =    .8949E-05
iteration number =  65    ermaxb =    .1030E-05      ermaxe =    .8466E-05
iteration number =  66    ermaxb =    .9843E-06      ermaxe =    .8012E-05
iteration number =  67    ermaxb =    .9406E-06      ermaxe =    .7583E-05
iteration number =  68    ermaxb =    .8988E-06      ermaxe =    .7179E-05
iteration number =  69    ermaxb =    .8590E-06      ermaxe =    .6796E-05
iteration number =  70    ermaxb =    .8211E-06      ermaxe =    .6435E-05
iteration number =  71    ermaxb =    .7848E-06      ermaxe =    .6094E-05
iteration number =  72    ermaxb =    .7503E-06      ermaxe =    .5772E-05
iteration number =  73    ermaxb =    .7172E-06      ermaxe =    .5468E-05
iteration number =  74    ermaxb =    .6857E-06      ermaxe =    .5180E-05
iteration number =  75    ermaxb =    .6556E-06      ermaxe =    .4908E-05
iteration number =  76    ermaxb =    .6269E-06      ermaxe =    .4651E-05
iteration number =  77    ermaxb =    .5994E-06      ermaxe =    .4408E-05
iteration number =  78    ermaxb =    .5732E-06      ermaxe =    .4179E-05
iteration number =  79    ermaxb =    .5482E-06      ermaxe =    .3961E-05
iteration number =  80    ermaxb =    .5242E-06      ermaxe =    .3756E-05
iteration number =  81    ermaxb =    .5014E-06      ermaxe =    .3564E-05
iteration number =  82    ermaxb =    .4795E-06      ermaxe =    .3382E-05
iteration number =  83    ermaxb =    .4586E-06      ermaxe =    .3210E-05
iteration number =  84    ermaxb =    .4387E-06      ermaxe =    .3048E-05

 TIME TO SOLVE FOR STRESSES AND DISPLACEMENTS IN THIS MINING STEP = 22076 SECONDS


 MINING STEP NUMBER =   3
 NUMBER OF ITERATIONS TO SOLVE =    84


 MAXIMUM ERROR IN THE BLOCK DISPLACEMENTS =   .439E-06

 MAXIMUM ERROR IN THE ELEMENTS DISPLACEMENTS =   .305E-05

 TIME TO PRINT OUT STRESSES AND DISPLACEMENTS IN THIS MINING STEP =    10 SECONDS


 TIME TO COMPUTE AND PRINT STRESSES AND DISPLACEMENTS
 ON OFF-SEAM PLANES DURING THIS MINING STEP =     0 SECONDS


Step No.  Ptd dspl  Rsd stress  Plr modulus  LMS   Plr dspl  No. of elmts
   3       .10000    3449.842   38015.240       .000   7.42163    64
   3       .10000    3401.745   10395.459 -33667.749   7.52163    64

 TIME TO COMPUTE AND PRINT ENERGIES, STRESSES AND
 DISPLACEMENTS FOR THIS MINING STEPS =      88072 SECONDS

.
.
.

Mining step 4 through 13 were omitted
.
.
.

Summary of the result:
```

No.	Strain	Stress	LMS
1	.83671E-01	.28850E+04	-.34640E+05
2	.85104E-01	.29229E+04	-.34639E+05
3	.10602E+00	.34498E+04	-.33668E+05
4	.15993E+00	.34844E+04	-.31463E+05
5	.16991E+00	.34388E+04	-.31861E+05
6	.17692E+00	.34147E+04	-.32004E+05
7	.19422E+00	.33959E+04	-.32315E+05
8	.19422E+00	.33959E+04	-.32315E+05
9	.25311E+00	.33938E+04	-.32433E+05
10	.25311E+00	.33938E+04	-.32433E+05
11	.26749E+00	.33938E+04	-.32543E+05
12	.28466E+00	.33938E+04	-.32670E+05
13	.29151E+00	.33938E+04	-.32687E+05

End of output for development 7 model

****

B.5 Development 8 model

20X80 and 120X180 ft pillars & 20 ft entries, Pocahntas No.3 Coalbed
Overburden 2000 ft (24000 in)

```
IN THE FOLLOWING X,Y,Z REFER TO GLOBAL AXES OR COORDINATES
AND X1,X2,X3  OR  1,2,3 REFER TO LOCAL AXES OR COORDINATES.


ROCK MASS PROPERTIES
POISSONS RATIO          --              .25
MODULUS OF ELASTICITY --          690000.00
NO. OF SEAMS            --      1
NO. OF MATERIALS        --     11
PERTURBATION DSPL       --      1.0000


IN-SEAM MATERIAL PROPERTIES
VALID MATERIAL PROPERTY CODES ARE:
0 1 2 A B C D E F G H I J K L M N O P Q R S T U V W X Y Z


MATERIAL NUMBER        1 (A)
STRAIN SOFTENING COAL       2.00000
PEAK STRESS               .63000E+04
PEAK STRAIN               .10500E+00
RESIDUAL STRESS           .60000E+04
RESIDUAL STRAIN           .15500E+00
POISSONS RATIO            .30000E+00


MATERIAL NUMBER        2 (B)
STRAIN SOFTENING COAL       2.00000
PEAK STRESS               .62500E+04
PEAK STRAIN               .10400E+00
RESIDUAL STRESS           .54000E+04
RESIDUAL STRAIN           .14300E+00
POISSONS RATIO            .30000E+00


MATERIAL NUMBER        3 (C)
STRAIN SOFTENING COAL       2.00000
PEAK STRESS               .62000E+04
PEAK STRAIN               .10300E+00
RESIDUAL STRESS           .46000E+04
RESIDUAL STRAIN           .12800E+00
POISSONS RATIO            .30000E+00


MATERIAL NUMBER        4 (D)
STRAIN SOFTENING COAL       2.00000
PEAK STRESS               .30000E+04
PEAK STRAIN               .50000E-01
RESIDUAL STRESS           .13000E+04
RESIDUAL STRAIN           .60000E-01
POISSONS RATIO            .30000E+00


MATERIAL NUMBER        5 (E)
STRAIN HARDENING GOB                  5.00000
INITIAL MODULUS AT ZERO STRESS      .29400E+03
FINAL MODULUS AT PEAK STRESS        .27000E+05
PEAK STRESS                         .20900E+04
GOB HEIGHT FACTOR                   .10000E+01
POISSONS RATIO                      .40000E+00


MATERIAL NUMBER        6 (F)
STRAIN SOFTENING COAL       2.00000
PEAK STRESS               .24000E+04
PEAK STRAIN               .74000E-01
RESIDUAL STRESS           .20000E+04
RESIDUAL STRAIN           .16500E+00
POISSONS RATIO            .30000E+00
```

```
MATERIAL NUMBER       7 (G)
STRAIN SOFTENING COAL      2.00000
PEAK STRESS              .63000E+04
PEAK STRAIN              .10500E+00
RESIDUAL STRESS          .60000E+04
RESIDUAL STRAIN          .15500E+00
POISSONS RATIO           .30000E+00


MATERIAL NUMBER       8 (H)
STRAIN SOFTENING COAL      2.00000
PEAK STRESS              .63000E+04
PEAK STRAIN              .10500E+00
RESIDUAL STRESS          .60000E+04
RESIDUAL STRAIN          .15500E+00
POISSONS RATIO           .30000E+00


MATERIAL NUMBER       9 (I)
STRAIN SOFTENING COAL      2.00000
PEAK STRESS              .62500E+04
PEAK STRAIN              .10400E+00
RESIDUAL STRESS          .54000E+04
RESIDUAL STRAIN          .14300E+00
POISSONS RATIO           .30000E+00


MATERIAL NUMBER      10 (J)
STRAIN SOFTENING COAL      2.00000
PEAK STRESS              .62000E+04
PEAK STRAIN              .10300E+00
RESIDUAL STRESS          .46000E+04
RESIDUAL STRAIN          .12800E+00
POISSONS RATIO           .30000E+00


MATERIAL NUMBER      11 (K)
STRAIN SOFTENING COAL      2.00000
PEAK STRESS              .30000E+04
PEAK STRAIN              .50000E-01
RESIDUAL STRESS          .13000E+04
RESIDUAL STRAIN          .60000E-01
POISSONS RATIO           .30000E+00


PRIMITIVE STRESS PARAMETERS

PRIMITIVE STRESSES ARE GIVEN AS
PXX =     .0000      .1250    * Z
PXY =     .0000      .0000    * Z
PXZ =     .0000      .0000    * Z
PYY =     .0000      .1250    * z
PYZ =     .0000      .0000    * z
PZZ =     .0000      .0917    * z


MODEL CONTROL AND MODEL DATA

NO. OF PARALLEL SEAMS                    --         1
WIDTH OF BLOCKS                          --    600.00
NO. OF BLOCKS ALONG X  AXIS              --        50
NO. OF BLOCKS ALONG Y  AXIS              --        40
NUMBER OF OFF-SEAM PLANES SELECTED       --         0
FINE MESH STARTING BLOCK X-AXIS          --        18
FINE MESH ENDING   BLOCK X-AXIS          --        34
FINE MESH STARTING BLOCK Y-AXIS          --        11
FINE MESH ENDING   BLOCK Y-AXIS          --        30


GLOBAL COORDINATES OF LOCAL ORIGINS AND SEAM THICKNESSES
SEAM NO.          X           Y           Z      THICKNESS
     1          .00         .00   -24000.00       70.00

DIRECTION COSINES OF LOCAL SEAM AXES WITH RESPECT TO T        HE GLOBAL AXES
```

```
EN(1,X) =    1.00000  EN(2,X) =     .00000  EN(3,X) =     .00000
EN(1,Y) =     .00000  EN(2,Y) =    1.00000  EN(3,Y) =     .00000
EN(1,Z) =     .00000  EN(2,Z) =     .00000  EN(3,Z) =    1.00000


PROGRAM FLOW CONTROL PARAMETERS

OVER RELAXATION FACTOR     1.35
MAXIMUM NO. OF ITERATIONS SPECIFIED      300
STRESS CONVERGENCE CRITERION    .10000E-01
STARTING MINING STEP NUMBER          1
NUMBER OF NEW STEPS                  1


PRIMITIVE STRESSES AT LOCAL SEAM ORIGINS
SEAM #     PSX          PSY          PSZ

   1    .0000E+00    .0000E+00    .2201E+04

STRESS GRADIENTS
PXDX =     .0000E+00
PYDX =     .0000E+00
PZDX =     .0000E+00
PXDY =     .0000E+00
PYDY =     .0000E+00
PZDY =     .0000E+00


TIME TO READ, CALCULATE AND PRINT BASIC PARAMETERS =     0 SECONDS


TIME TO CALCULATE INFLUENCE COEFFICIENTS =     0 SECONDS

.
.
.
Mining step 1 through 5 were omitted
.
.
.


MINING STEP NUMBER =   6   FINE MESH SEAM NUMBER = 1
```

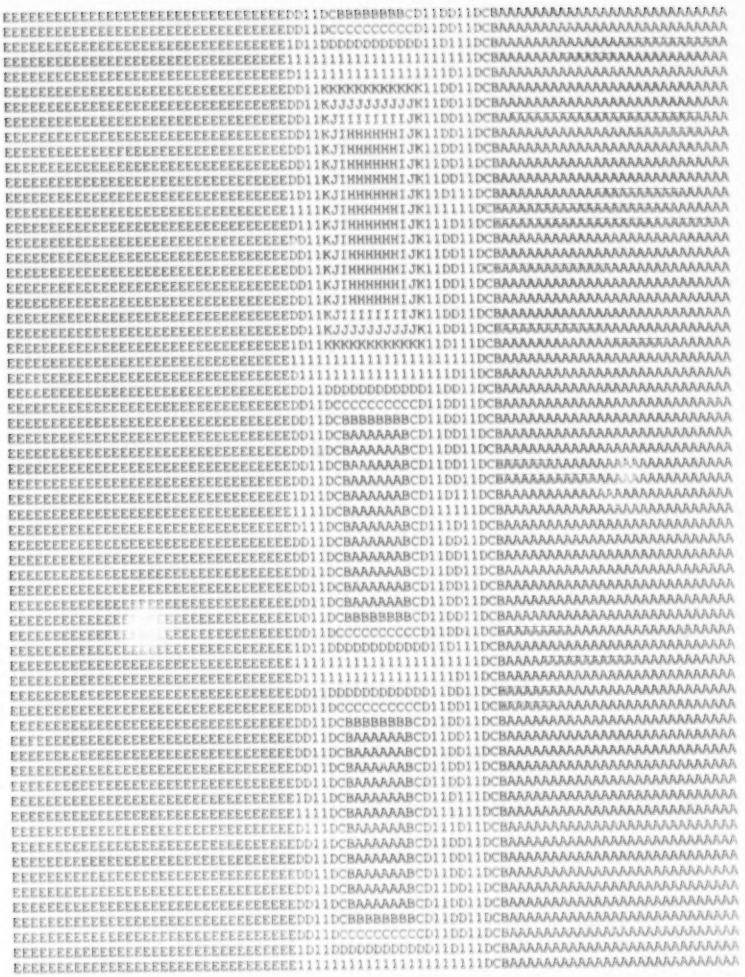

MINING STEP NUMBER = 6 COARSE MESH SEAM NUMBER = 1

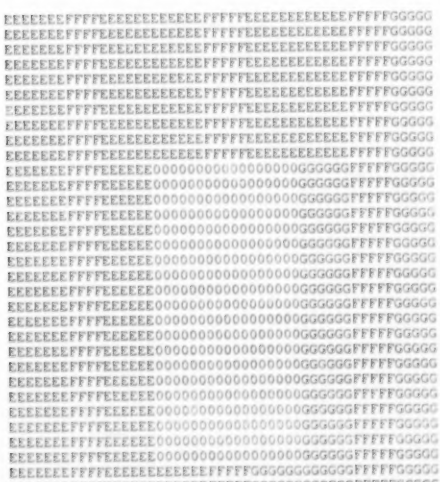

```
EEEEEEEFFFFEEEEEEEEEEEEFFFFFGGGGGGGGGGGGFFFFFGGGGG
EEEEEEEFFFFEEEEEEEEEEEEFFFFFGGGGGGGGGGGGFFFFFGGGGG
EEEEEEEFFFFEEEEEEEEEEEEFFFFFGGGGGGGGGGGGFFFFFGGGGG
EEEEEEEFFFFEEEEEEEEEEEEFFFFFGGGGGGGGGGGGFFFFFGGGGG
EEEEEEEFFFFEEEEEEEEEEEEFFFFFGGGGGGGGGGGGFFFFFGGGGG
EEEEEEEFFFFEEEEEEEEEEEEFFFFFGGGGGGGGGGGGFFFFFGGGGG
EEEEEEEFFFFEEEEEEEEEEEEFFFFFGGGGGGGGGGGGFFFFFGGGGG
EEEEEEEFFFFEEEEEEEEEEEEFFFFFGGGGGGGGGGGGFFFFFGGGGG
```

TIME TO READ, PRINT AND CONVERT MATERIAL PROPERTIES
FOR THIS MINING STEP = 0 SECONDS

SOLUTION PROGRESS FOR MINING STEP NUMBER = 6

iteration number =	1	ermaxb =	.6269E+01	ermaxe =	.4968E+01
iteration number =	2	ermaxb =	.3047E+01	ermaxe =	.3564E+01
iteration number =	3	ermaxb =	.1861E+01	ermaxe =	.2100E+01
iteration number =	4	ermaxb =	.1478E+01	ermaxe =	.2096E+01
iteration number =	5	ermaxb =	.1638E+01	ermaxe =	.1341E+01
iteration number =	6	ermaxb =	.1652E+01	ermaxe =	.9486E+00
iteration number =	7	ermaxb =	.1685E+01	ermaxe =	.8055E+00
iteration number =	8	ermaxb =	.1208E+01	ermaxe =	.6956E+00
iteration number =	9	ermaxb =	.8919E+00	ermaxe =	.6061E+00
iteration number =	10	ermaxb =	.8054E+00	ermaxe =	.5338E+00
iteration number =	11	ermaxb =	.6278E+00	ermaxe =	.4757E+00
iteration number =	12	ermaxb =	.4447E+00	ermaxe =	.4830E+00
iteration number =	13	ermaxb =	.3182E+00	ermaxe =	.4452E+00
iteration number =	14	ermaxb =	.2536E+00	ermaxe =	.3874E+00
iteration number =	15	ermaxb =	.2119E+00	ermaxe =	.3573E+00
iteration number =	16	ermaxb =	.1794E+00	ermaxe =	.3013E+00
iteration number =	17	ermaxb =	.1541E+00	ermaxe =	.2740E+00
iteration number =	18	ermaxb =	.1338E+00	ermaxe =	.2470E+00
iteration number =	19	ermaxb =	.1174E+00	ermaxe =	.2277E+00
iteration number =	20	ermaxb =	.1038E+00	ermaxe =	.2105E+00
iteration number =	21	ermaxb =	.9256E-01	ermaxe =	.1949E+00
iteration number =	22	ermaxb =	.8310E-01	ermaxe =	.1809E+00
iteration number =	23	ermaxb =	.7484E-01	ermaxe =	.1681E+00
iteration number =	24	ermaxb =	.6764E-01	ermaxe =	.1587E+00
iteration number =	25	ermaxb =	.6136E-01	ermaxe =	.1518E+00
iteration number =	26	ermaxb =	.5574E-01	ermaxe =	.1429E+00
iteration number =	27	ermaxb =	.5068E-01	ermaxe =	.1320E+00
iteration number =	28	ermaxb =	.4611E-01	ermaxe =	.1195E+00
iteration number =	29	ermaxb =	.4199E-01	ermaxe =	.1120E+00
iteration number =	30	ermaxb =	.3826E-01	ermaxe =	.1051E+00
iteration number =	50	ermaxb =	.9925E-02	ermaxe =	.3378E-01
iteration number =	51	ermaxb =	.9378E-02	ermaxe =	.3206E-01
iteration number =	52	ermaxb =	.8867E-02	ermaxe =	.3043E-01
iteration number =	53	ermaxb =	.8385E-02	ermaxe =	.2890E-01
iteration number =	54	ermaxb =	.7924E-02	ermaxe =	.2744E-01
iteration number =	55	ermaxb =	.7484E-02	ermaxe =	.2607E-01
iteration number =	56	ermaxb =	.7067E-02	ermaxe =	.2477E-01
iteration number =	57	ermaxb =	.6676E-02	ermaxe =	.2354E-01
iteration number =	58	ermaxb =	.6310E-02	ermaxe =	.2237E-01
iteration number =	59	ermaxb =	.5958E-02	ermaxe =	.2126E-01
iteration number =	60	ermaxb =	.5622E-02	ermaxe =	.2022E-01

.
.
.

iteration number =	260	ermaxb =	.2719E-06	ermaxe =	.1418E-05
iteration number =	261	ermaxb =	.2590E-06	ermaxe =	.1351E-05
iteration number =	262	ermaxb =	.2468E-06	ermaxe =	.1288E-05
iteration number =	263	ermaxb =	.2351E-06	ermaxe =	.1227E-05
iteration number =	264	ermaxb =	.2240E-06	ermaxe =	.1170E-05
iteration number =	265	ermaxb =	.2134E-06	ermaxe =	.1115E-05
iteration number =	266	ermaxb =	.2033E-06	ermaxe =	.1063E-05
iteration number =	267	ermaxb =	.1937E-06	ermaxe =	.1013E-05
iteration number =	268	ermaxb =	.1846E-06	ermaxe =	.9651E-06
iteration number =	269	ermaxb =	.1758E-06	ermaxe =	.9198E-06
iteration number =	270	ermaxb =	.1675E-06	ermaxe =	.8766E-06
iteration number =	271	ermaxb =	.1596E-06	ermaxe =	.8355E-06
iteration number =	272	ermaxb =	.1521E-06	ermaxe =	.7962E-06
iteration number =	273	ermaxb =	.1449E-06	ermaxe =	.7588E-06
iteration number =	274	ermaxb =	.1380E-06	ermaxe =	.7232E-06
iteration number =	275	ermaxb =	.1315E-06	ermaxe =	.6892E-06
iteration number =	276	ermaxb =	.1253E-06	ermaxe =	.6569E-06
iteration number =	277	ermaxb =	.1194E-06	ermaxe =	.6260E-06

```
iteration number = 278    ermaxb =    .1137E-06      ermaxe =    .5966E-06
iteration number = 279    ermaxb =    .1084E-06      ermaxe =    .5686E-06
iteration number = 280    ermaxb =    .1032E-06      ermaxe =    .5419E-06
iteration number = 281    ermaxb =    .9837E-07      ermaxe =    .5164E-06
iteration number = 282    ermaxb =    .9372E-07      ermaxe =    .4921E-06
iteration number = 283    ermaxb =    .8929E-07      ermaxe =    .4690E-06

TIME TO SOLVE FOR STRESSES AND DISPLACEMENTS IN THIS MINING STEP = 72898 SECONDS


MINING STEP NUMBER =   1
NUMBER OF ITERATIONS TO SOLVE =   283


MAXIMUM ERROR IN THE BLOCK DISPLACEMENTS =   .893E-07

MAXIMUM ERROR IN THE ELEMENTS DISPLACEMENTS =   .469E-06

TIME TO PRINT OUT STRESSES AND DISPLACEMENTS IN THIS MINING STEP =     0 SECONDS


TIME TO COMPUTE AND PRINT STRESSES AND DISPLACEMENTS
ON OFF-SEAM PLANES DURING THIS MINING STEP =     0 SECONDS

iteration number =   1    ermaxb =    .1175E-02      ermaxe =    .4820E+00
iteration number =   2    ermaxb =    .1287E-02      ermaxe =    .2131E+00
iteration number =   3    ermaxb =    .9863E-03      ermaxe =    .8582E-01
iteration number =   4    ermaxb =    .8188E-03      ermaxe =    .5853E-01
iteration number =   5    ermaxb =    .6845E-03      ermaxe =    .3674E-01
iteration number =   6    ermaxb =    .5732E-03      ermaxe =    .2435E-01
iteration number =   7    ermaxb =    .4808E-03      ermaxe =    .1555E-01
iteration number =   8    ermaxb =    .4044E-03      ermaxe =    .1120E-01
iteration number =   9    ermaxb =    .3402E-03      ermaxe =    .9536E-02
iteration number =  10    ermaxb =    .2869E-03      ermaxe =    .8199E-02
iteration number =  11    ermaxb =    .2430E-03      ermaxe =    .7108E-02
iteration number =  12    ermaxb =    .2070E-03      ermaxe =    .6251E-02
iteration number =  13    ermaxb =    .1776E-03      ermaxe =    .5627E-02
iteration number =  14    ermaxb =    .1535E-03      ermaxe =    .5071E-02
iteration number =  15    ermaxb =    .1339E-03      ermaxe =    .4576E-02
iteration number =  16    ermaxb =    .1181E-03      ermaxe =    .4136E-02
iteration number =  17    ermaxb =    .1056E-03      ermaxe =    .3745E-02
iteration number =  18    ermaxb =    .9738E-04      ermaxe =    .3396E-02
iteration number =  19    ermaxb =    .9021E-04      ermaxe =    .3085E-02
iteration number =  20    ermaxb =    .8390E-04      ermaxe =    .2807E-02
iteration number =  21    ermaxb =    .7832E-04      ermaxe =    .2558E-02
iteration number =  22    ermaxb =    .7332E-04      ermaxe =    .2348E-02
iteration number =  23    ermaxb =    .6883E-04      ermaxe =    .2164E-02
iteration number =  24    ermaxb =    .6477E-04      ermaxe =    .1996E-02
iteration number =  25    ermaxb =    .6106E-04      ermaxe =    .1841E-02
iteration number =  26    ermaxb =    .5766E-04      ermaxe =    .1700E-02
iteration number =  27    ermaxb =    .5454E-04      ermaxe =    .1571E-02
iteration number =  28    ermaxb =    .5164E-04      ermaxe =    .1452E-02
iteration number =  29    ermaxb =    .4895E-04      ermaxe =    .1344E-02
iteration number =  30    ermaxb =    .4645E-04      ermaxe =    .1244E-02
iteration number =  31    ermaxb =    .4411E-04      ermaxe =    .1158E-02
iteration number =  32    ermaxb =    .4191E-04      ermaxe =    .1078E-02
iteration number =  33    ermaxb =    .3985E-04      ermaxe =    .1005E-02
iteration number =  34    ermaxb =    .3791E-04      ermaxe =    .9362E-03
iteration number =  35    ermaxb =    .3608E-04      ermaxe =    .8727E-03
iteration number =  36    ermaxb =    .3435E-04      ermaxe =    .8137E-03
iteration number =  37    ermaxb =    .3272E-04      ermaxe =    .7590E-03
iteration number =  38    ermaxb =    .3118E-04      ermaxe =    .7082E-03
iteration number =  39    ermaxb =    .2971E-04      ermaxe =    .6610E-03
iteration number =  40    ermaxb =    .2832E-04      ermaxe =    .6172E-03
iteration number =  41    ermaxb =    .2701E-04      ermaxe =    .5765E-03
iteration number =  42    ermaxb =    .2576E-04      ermaxe =    .5386E-03
iteration number =  43    ermaxb =    .2457E-04      ermaxe =    .5034E-03
iteration number =  44    ermaxb =    .2344E-04      ermaxe =    .4714E-03
iteration number =  45    ermaxb =    .2236E-04      ermaxe =    .4419E-03
iteration number =  46    ermaxb =    .2134E-04      ermaxe =    .4144E-03
iteration number =  47    ermaxb =    .2037E-04      ermaxe =    .3887E-03
iteration number =  48    ermaxb =    .1944E-04      ermaxe =    .3646E-03
iteration number =  49    ermaxb =    .1856E-04      ermaxe =    .3421E-03
iteration number =  50    ermaxb =    .1772E-04      ermaxe =    .3210E-03
```

```
.
.
 iteration number = 140    ermaxb =    .2902E-06      ermaxe =    .2128E-05
 iteration number = 141    ermaxb =    .2767E-06      ermaxe =    .2020E-05
 iteration number = 142    ermaxb =    .2639E-06      ermaxe =    .1918E-05
 iteration number = 143    ermaxb =    .2516E-06      ermaxe =    .1821E-05
 iteration number = 144    ermaxb =    .2400E-06      ermaxe =    .1729E-05
 iteration number = 145    ermaxb =    .2288E-06      ermaxe =    .1642E-05
 iteration number = 146    ermaxb =    .2182E-06      ermaxe =    .1560E-05
 iteration number = 147    ermaxb =    .2080E-06      ermaxe =    .1481E-05
 iteration number = 148    ermaxb =    .1983E-06      ermaxe =    .1407E-05
 iteration number = 149    ermaxb =    .1891E-06      ermaxe =    .1336E-05
 iteration number = 150    ermaxb =    .1802E-06      ermaxe =    .1269E-05
 iteration number = 151    ermaxb =    .1718E-06      ermaxe =    .1205E-05
 iteration number = 152    ermaxb =    .1638E-06      ermaxe =    .1145E-05
 iteration number = 153    ermaxb =    .1562E-06      ermaxe =    .1088E-05
 iteration number = 154    ermaxb =    .1488E-06      ermaxe =    .1033E-05
 iteration number = 155    ermaxb =    .1419E-06      ermaxe =    .9815E-06
 iteration number = 156    ermaxb =    .1352E-06      ermaxe =    .9324E-06
 iteration number = 157    ermaxb =    .1289E-06      ermaxe =    .8858E-06
 iteration number = 158    ermaxb =    .1229E-06      ermaxe =    .8416E-06
 iteration number = 159    ermaxb =    .1171E-06      ermaxe =    .7995E-06
 iteration number = 160    ermaxb =    .1116E-06      ermaxe =    .7596E-06
 iteration number = 161    ermaxb =    .1064E-06      ermaxe =    .7217E-06
 iteration number = 162    ermaxb =    .1014E-06      ermaxe =    .6857E-06
 iteration number = 163    ermaxb =    .9662E-07      ermaxe =    .6516E-06
 iteration number = 164    ermaxb =    .9208E-07      ermaxe =    .6191E-06
 iteration number = 165    ermaxb =    .8775E-07      ermaxe =    .5883E-06
 iteration number = 166    ermaxb =    .8362E-07      ermaxe =    .5590E-06
 iteration number = 167    ermaxb =    .7969E-07      ermaxe =    .5312E-06
 iteration number = 168    ermaxb =    .7594E-07      ermaxe =    .5048E-06

 TIME TO SOLVE FOR STRESSES AND DISPLACEMENTS IN THIS MINING STEP = 43247 SECONDS


 MINING STEP NUMBER =   6
 NUMBER OF ITERATIONS TO SOLVE =   168

 MAXIMUM ERROR IN THE BLOCK DISPLACEMENTS =    .759E-07

 MAXIMUM ERROR IN THE ELEMENTS DISPLACEMENTS =    .505E-06

 TIME TO PRINT OUT STRESSES AND DISPLACEMENTS IN THIS MINING STEP =     0 SECONDS


 TIME TO COMPUTE AND PRINT STRESSES AND DISPLACEMENTS
 ON OFF-SEAM PLANES DURING THIS MINING STEP =     0 SECONDS


Step No.  Ptd dspl  Rsd stress  Plr modulus  LMS   Plr dspl  No. of elmts
   6      1.00000    3992.728   44105.130       .000   7.56273   216
   6      1.00000    3697.020    8506.104  -20699.523   8.56273   216

 TIME TO COMPUTE AND PRINT ENERGIES, STRESSES AND
 DISPLACEMENTS FOR THIS MINING STEPS =     116147 SECONDS
.
.
.
Mining step 7 through 13 were omitted
.
.
.
Summary of the result:

No.   Strain  Stress    LMS
1       0.07    2944   -21170
2       0.07    2985   -21168
3       0.08    3454   -20852
4       0.10    3890   -20842
5       0.11    3948   -20816
6       0.11    3993   -20700
7       0.11    4117   -20223
```

8	0.12	4203	-20326
9	0.14	4291	-19866
10	0.15	4376	-19930
11	0.16	4409	-20129
12	0.18	4421	-20096
13	0.19	4404	-20163

End of output for development 8 model

****

Appendix C

CHANGES OF AVERAGE VERTICAL PILLAR STRESS, STRAIN AND LOCAL MINE STIFFNESS WITH THE MINING STEPS

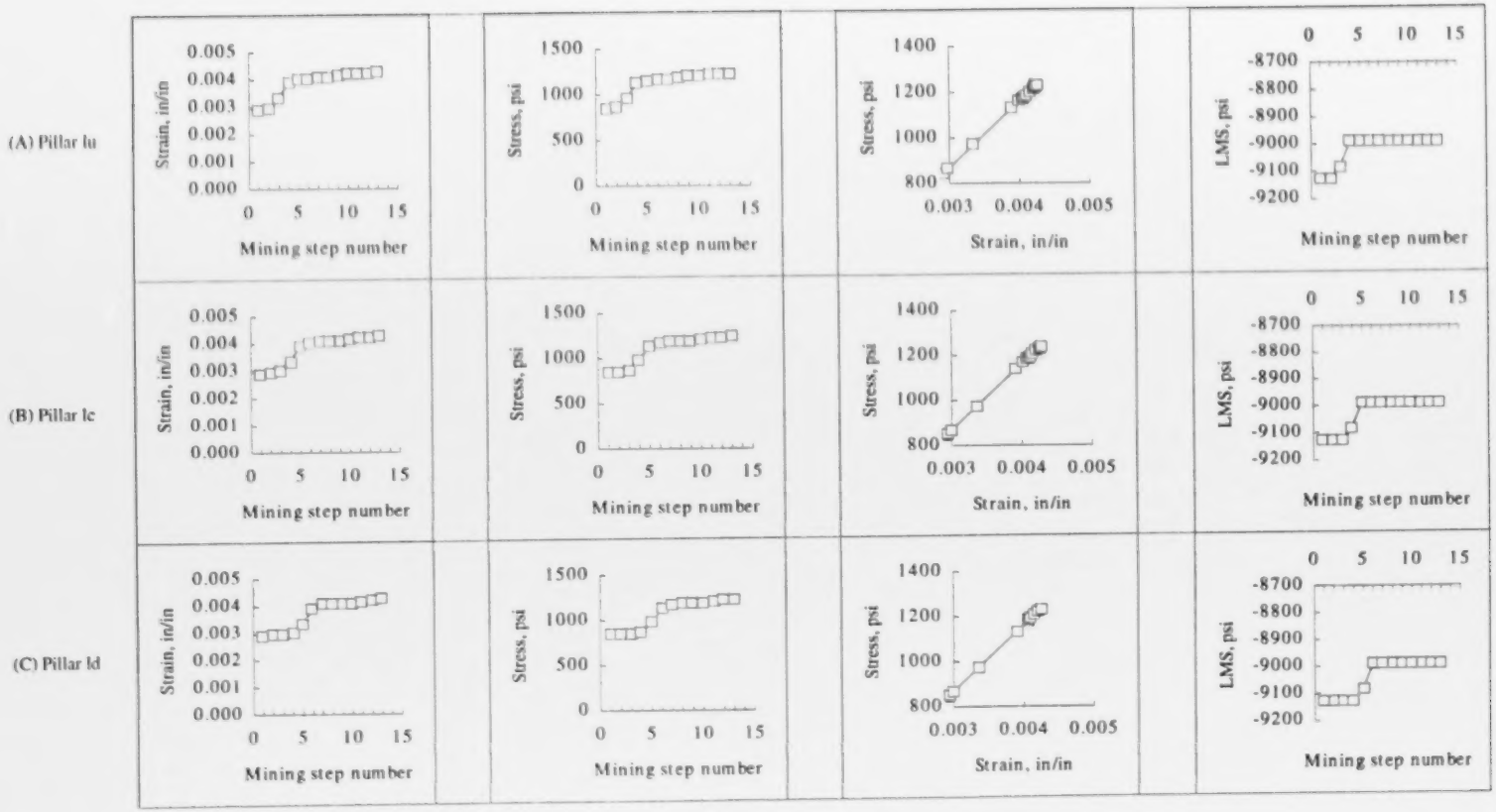

Figure C.1.1

Pillar stress, strain and local mine stiffness change with mining step number, model with three rows of equal size pillars, 500 ft overburden. Strata modulus E = 145000 psi, seam modulus Es = 290000 psi, E/Es = 0.5. (Brittle).

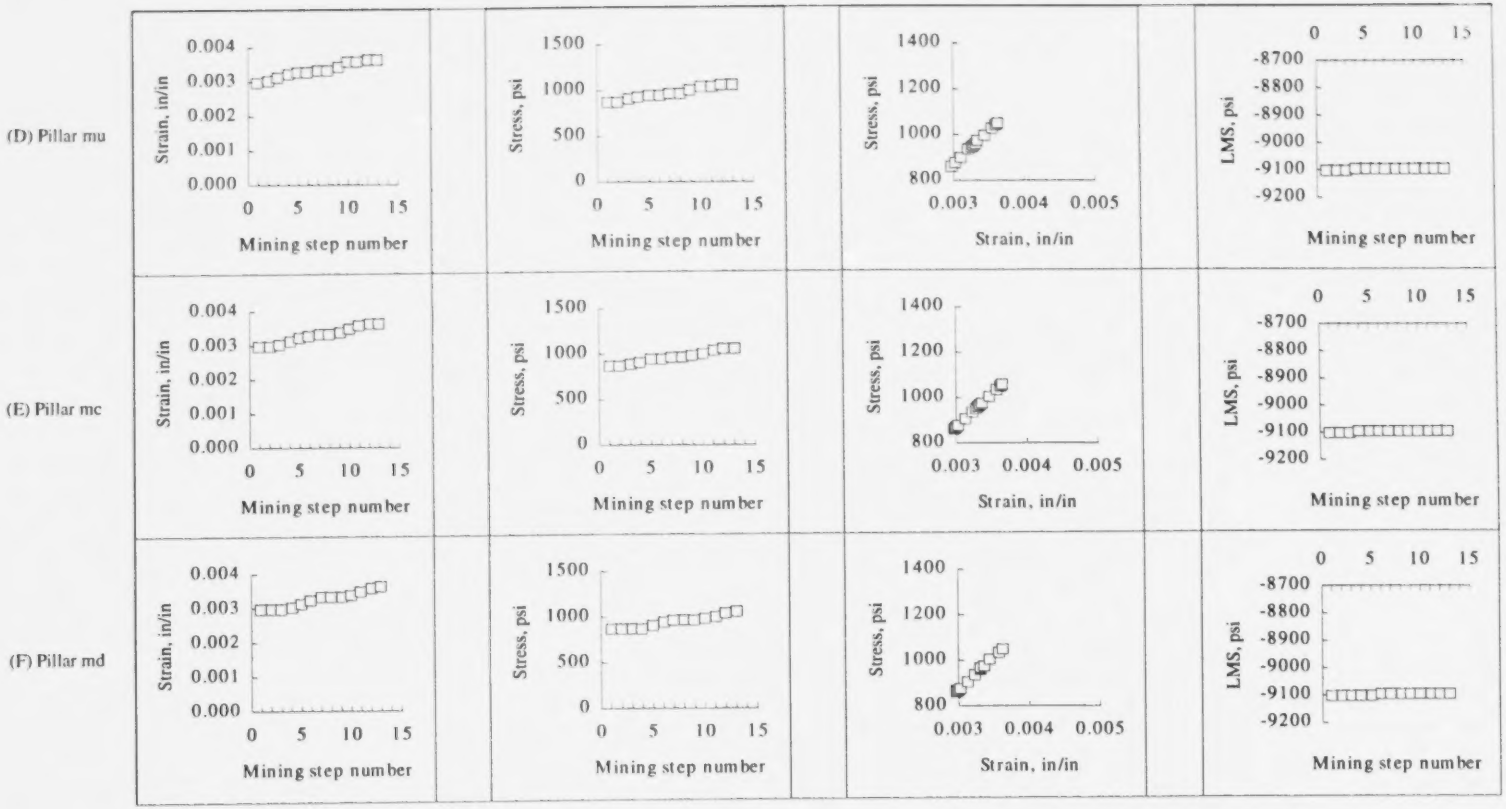

Figure C.1.2

Pillar stress, strain and local mine stiffness change with mining step number, model with three rows of equal size pillars, 500 ft overburden. Strata modulus E = 145000 psi, seam modulus Es = 290000 psi, E/Es = 0.5. (Brittle).

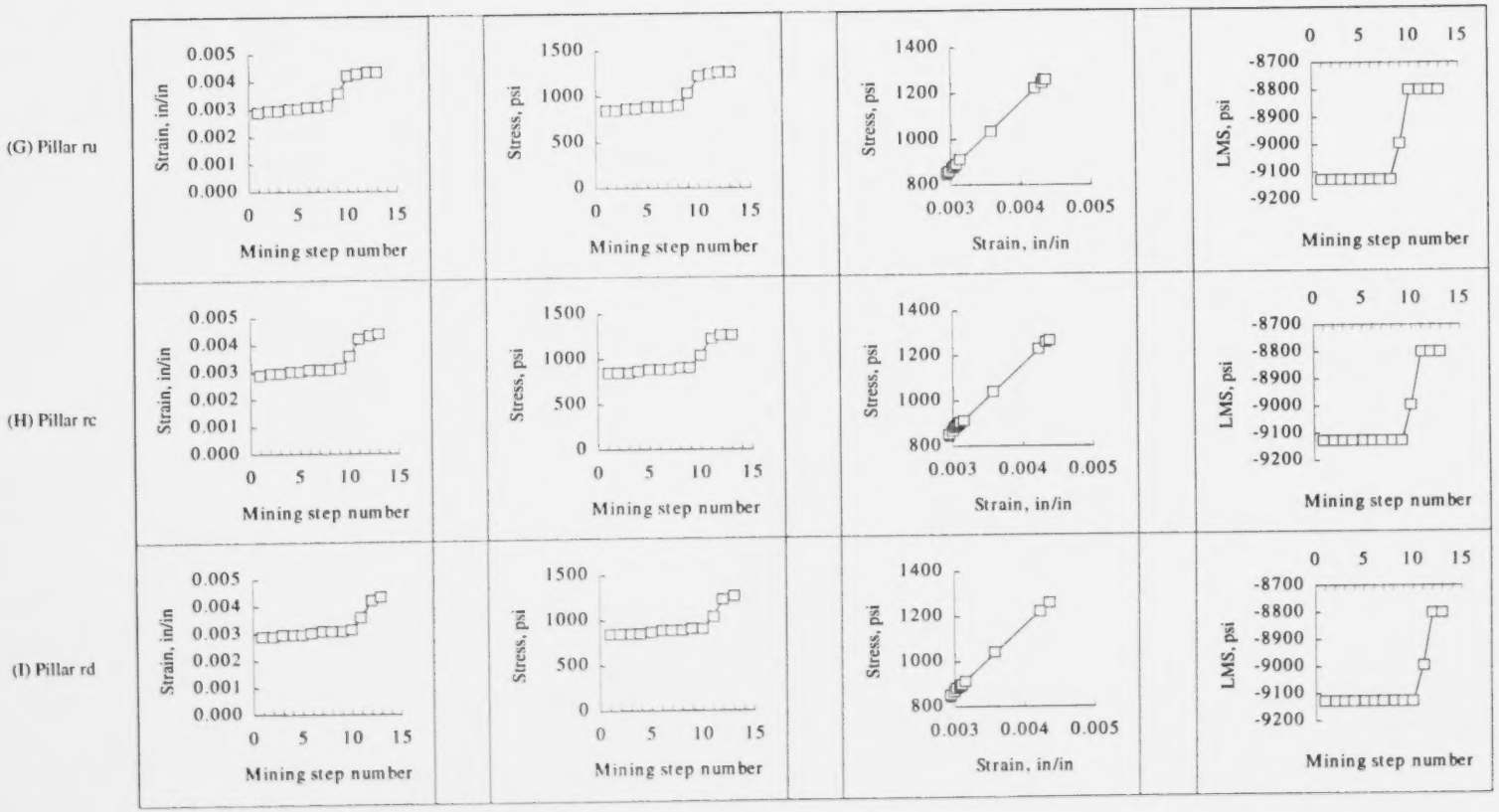

Figure C.1.3

Pillar stress, strain and local mine stiffness change with mining step number, model with three rows of equal size pillars, 500 ft overburden. Strata modulus E = 145000 psi, seam modulus Es = 290000 psi, E/Es = 0.5. (Brittle).

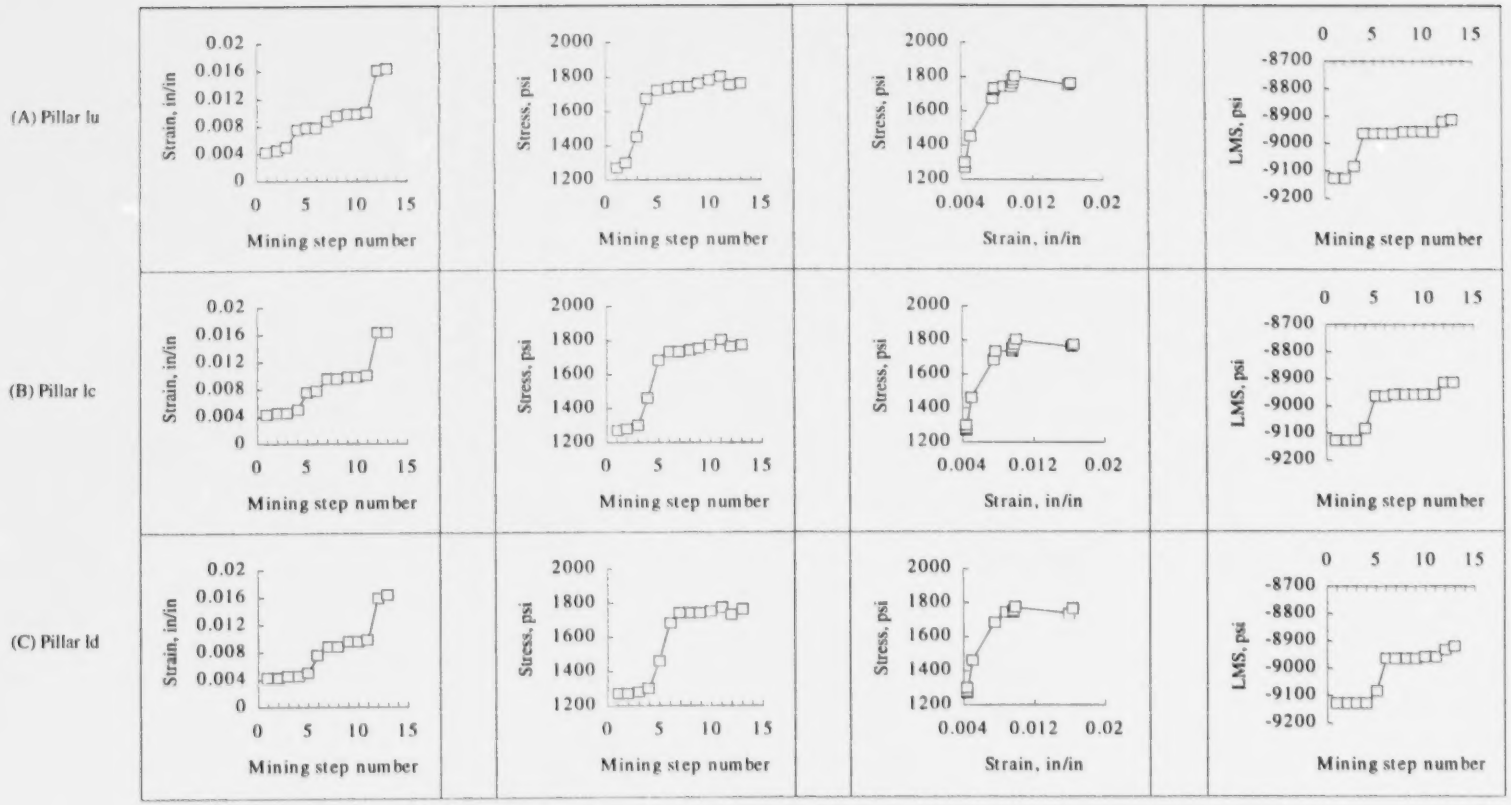

Figure C.2.1

Pillar stress, strain and local mine stiffness change with mining step number, model with three rows of equal size pillars, 750 ft overburden. Strata modulus E = 145000 psi, seam modulus Es = 290000 psi, E/Es = 0.5. (Brittle).

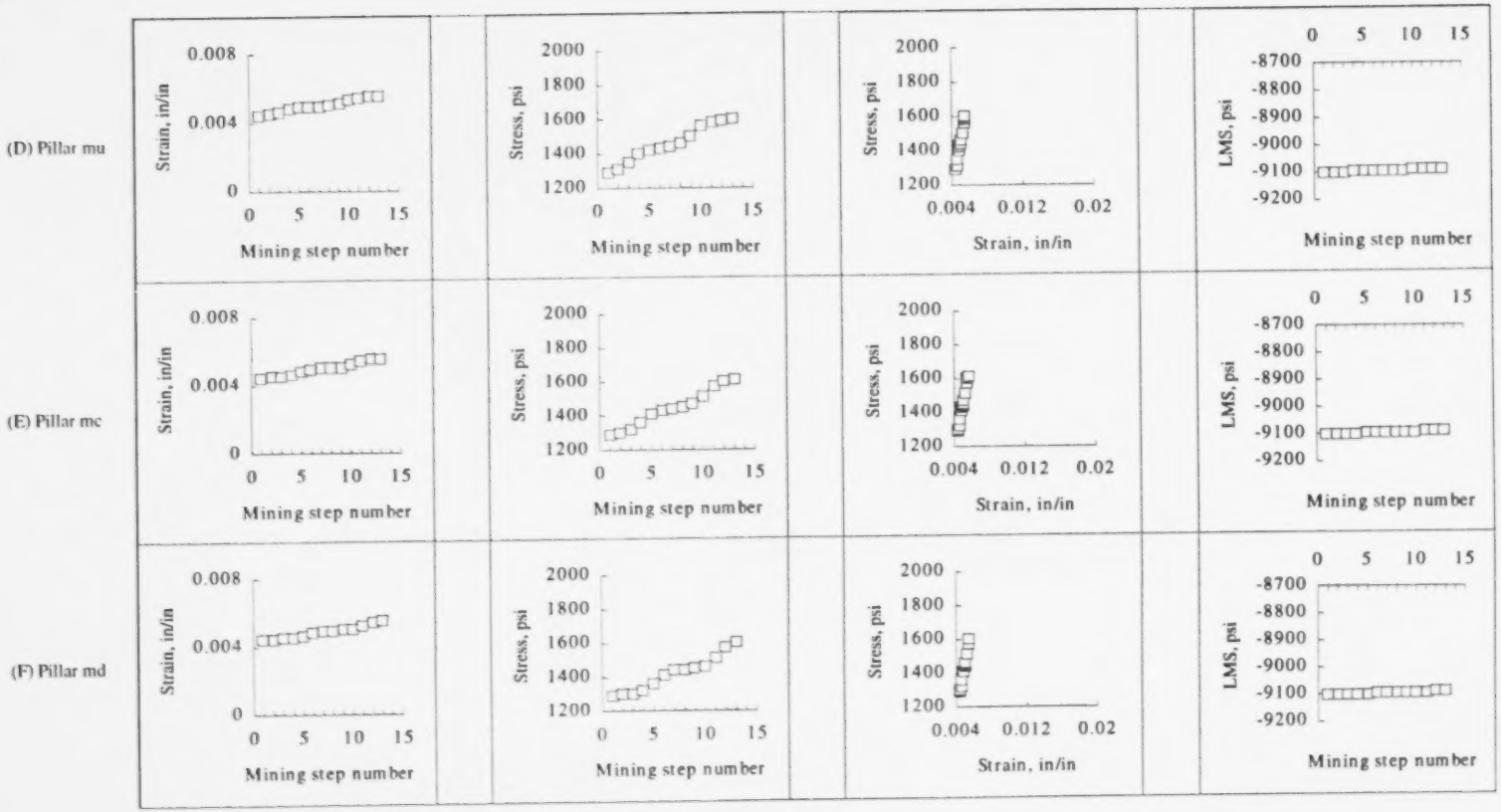

Figure C.2.2

Pillar stress, strain and local mine stiffness change with mining step number, model with three rows of equal size pillars, 750 ft overburden. Strata modulus E = 145000 psi, seam modulus Es = 290000 psi, E/Es = 0.5. (Brittle).

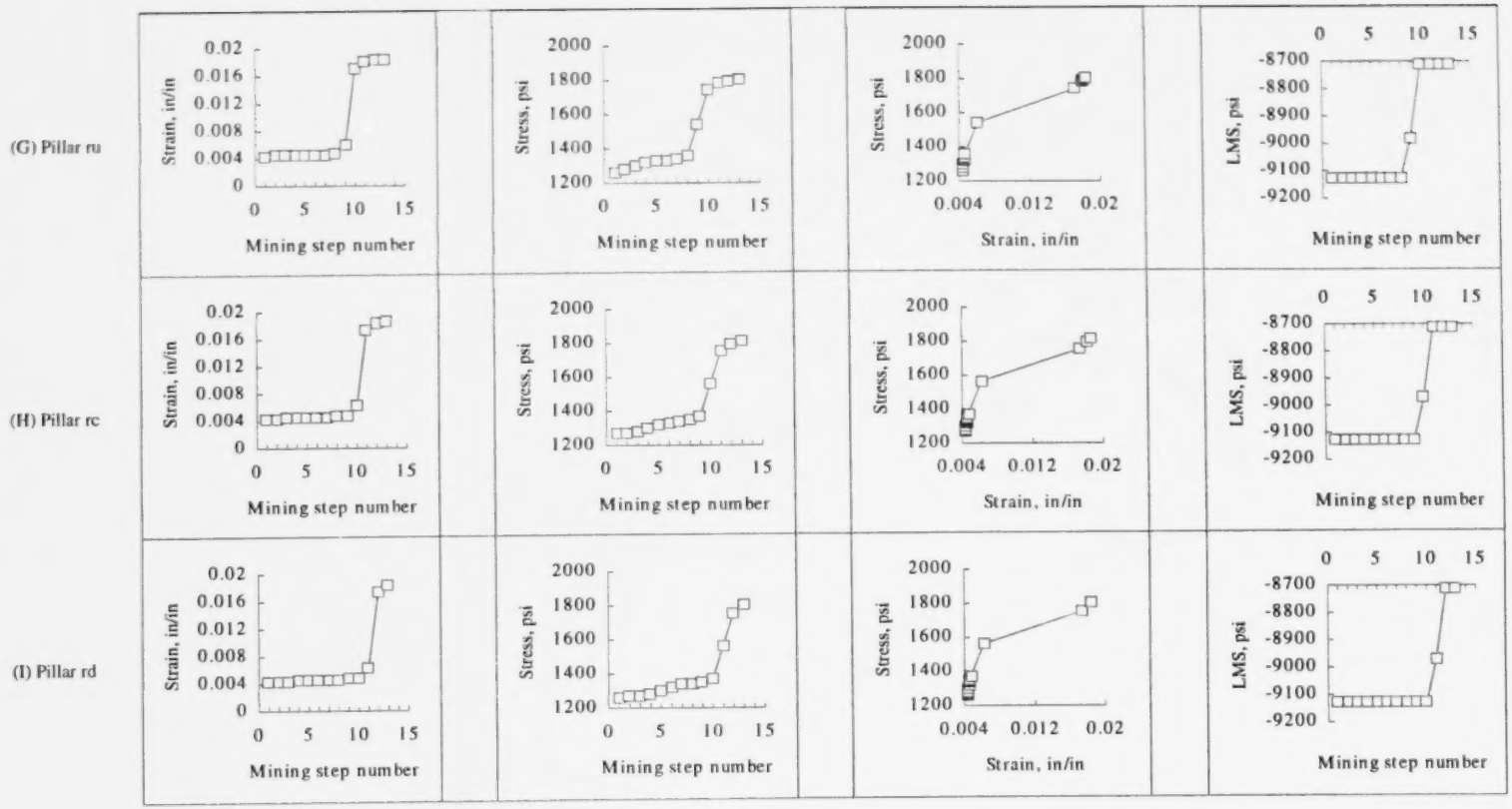

Figure C.2.3

Pillar stress, strain and local mine stiffness change with mining step number, model with three rows of equal size pillars, 750 ft overburden. Strata modulus E = 145000 psi, seam modulus Es = 290000 psi, E/Es = 0.5. (Brittle).

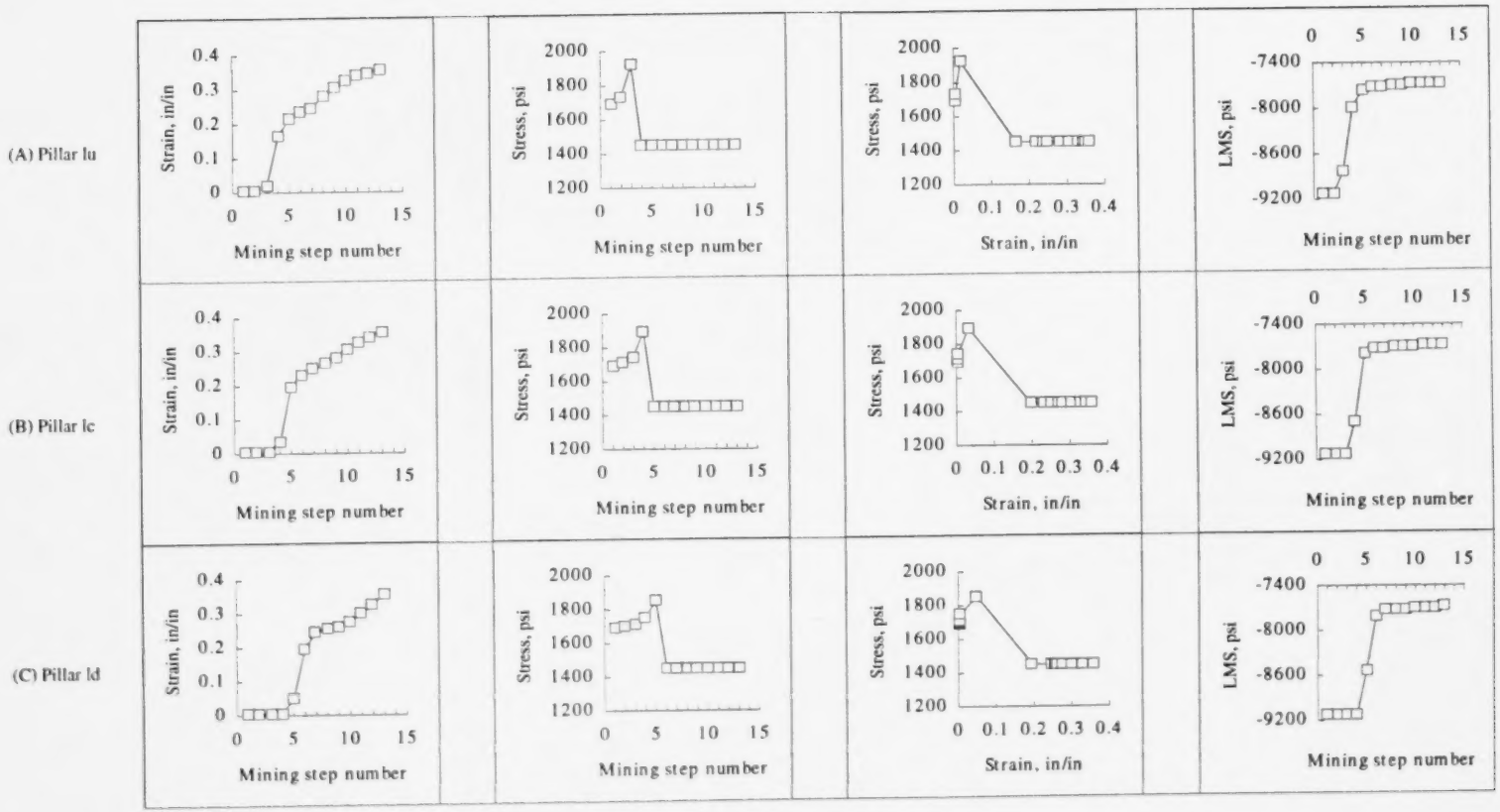

Figure C.3.1

Pillar stress, strain and local mine stiffness change with mining step number, model with three rows of equal size pillars, 1000 ft overburden. Strata modulus E = 145000 psi, seam modulus Es = 290000 psi, E/Es = 0.5. (Brittle).

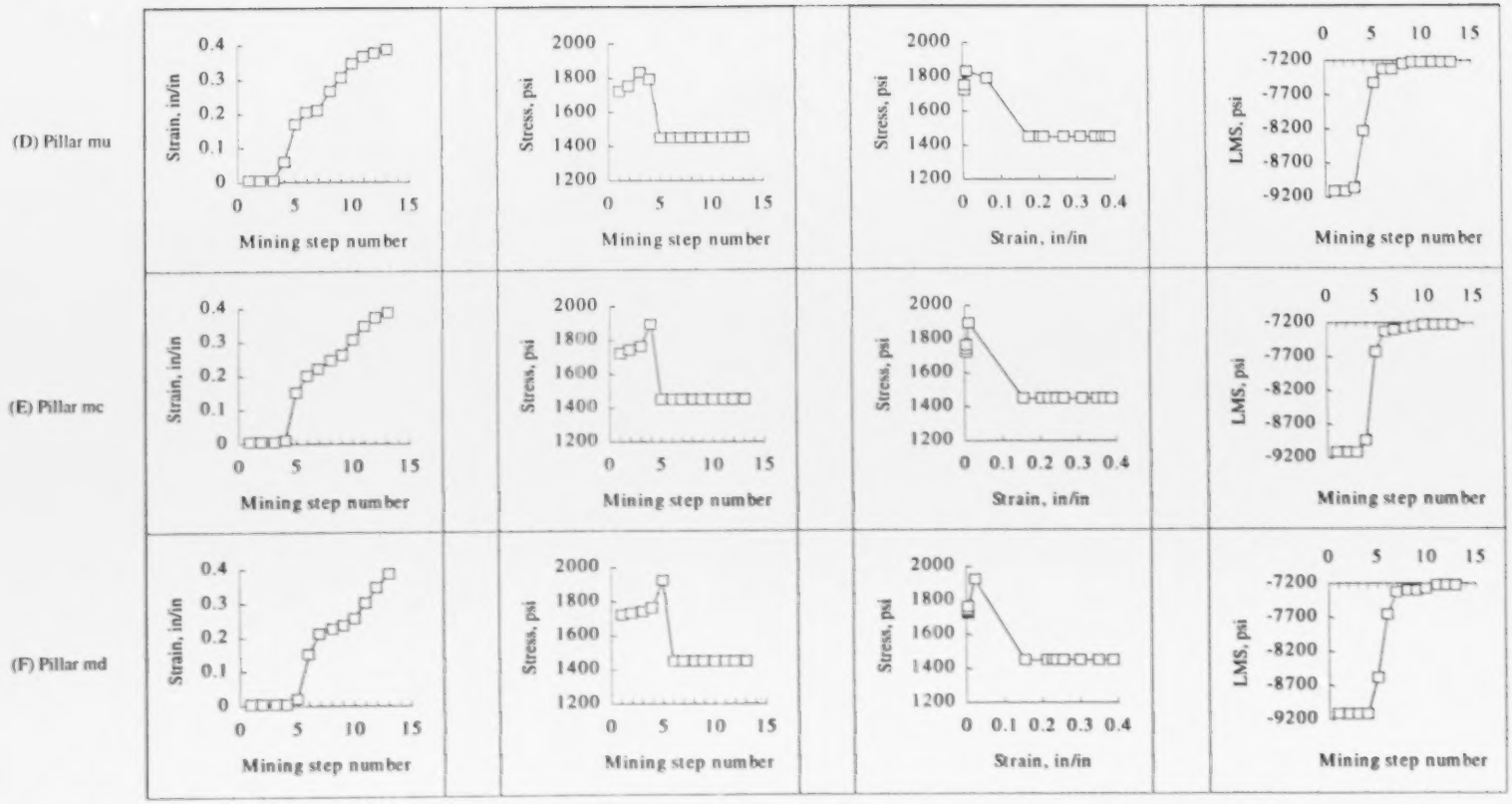

Figure C.3.2

Pillar stress, strain and local mine stiffness change with mining step number, model with three rows of equal size pillars, 1000 ft overburden. Strata modulus E = 145000 psi, seam modulus Es = 290000 psi, E/Es = 0.5. (Brittle).

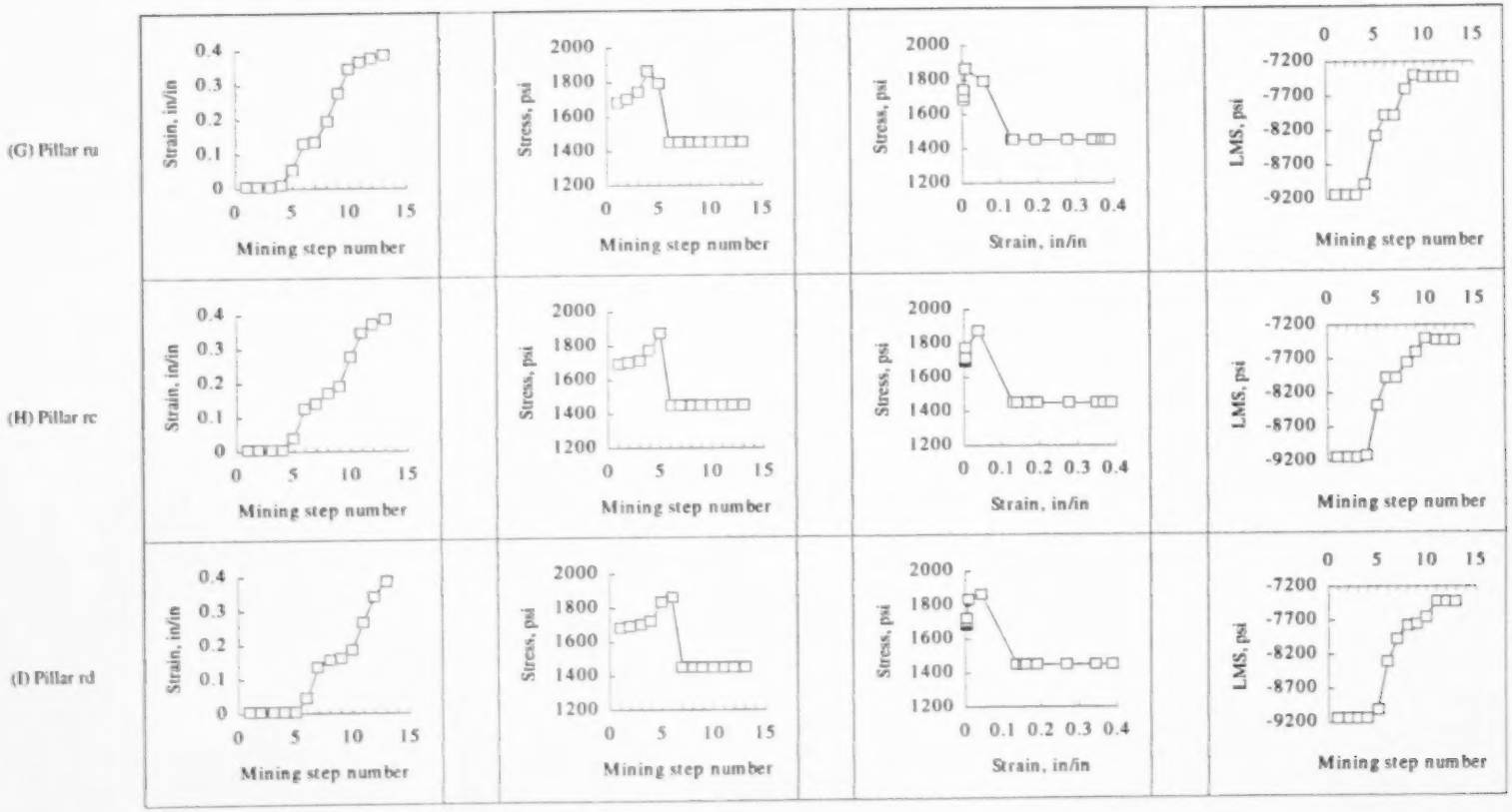

Figure C.3.3

Pillar stress, strain and local mine stiffness change with mining step number, model with three rows of equal size pillars, 1000 ft overburden. Strata modulus E = 145000 psi, seam modulus Es = 290000 psi, E/Es = 0.5. (Brittle).

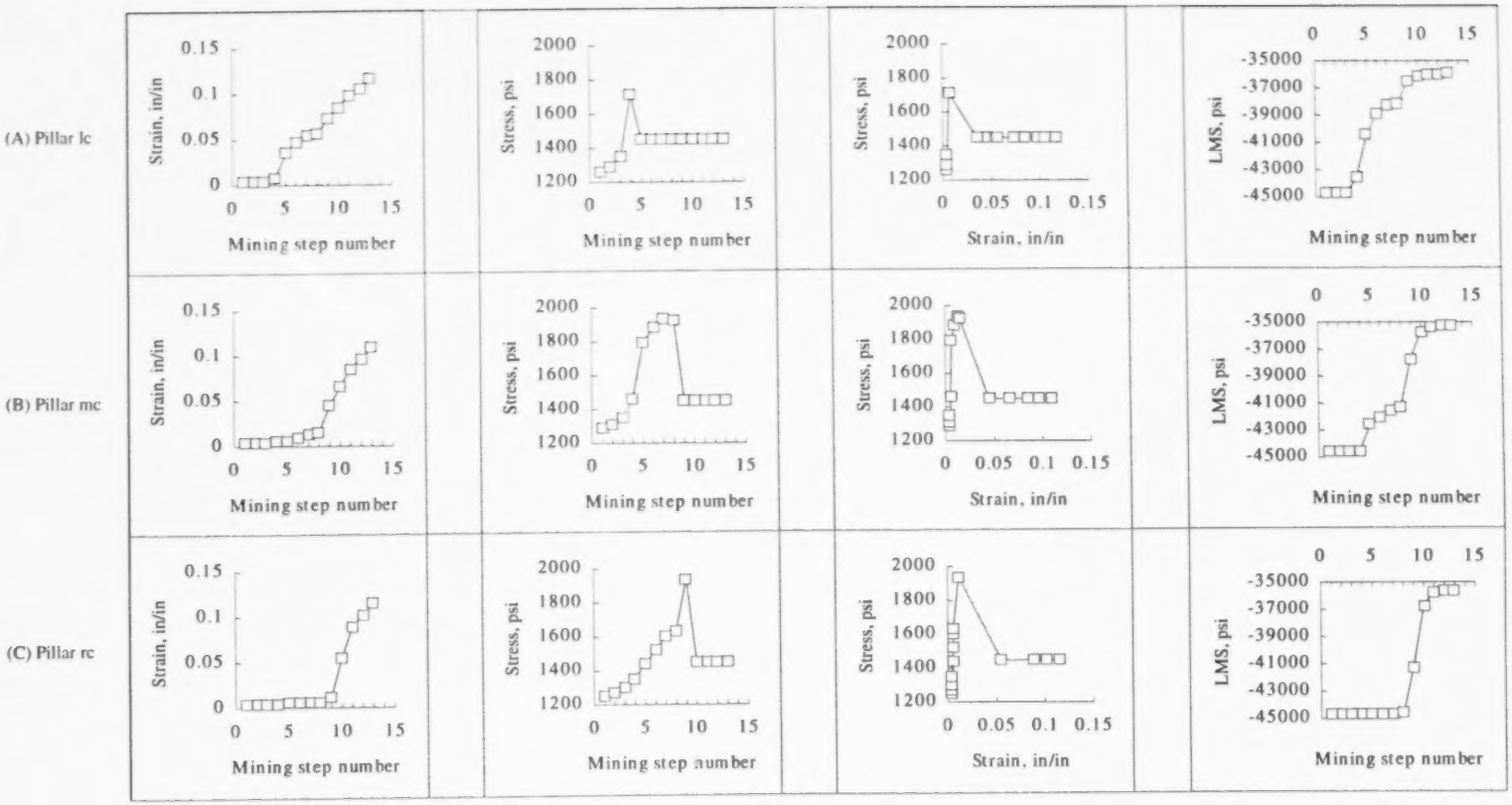

Figure C.4

Pillar stress, strain and local mine stiffness change with mining step number, model with three rows of equal size pillars, 750 ft overburden. Strata modulus E = 725000 psi, seam modulus Es = 290000, E/Es = 2.5 psi. (Brittle).

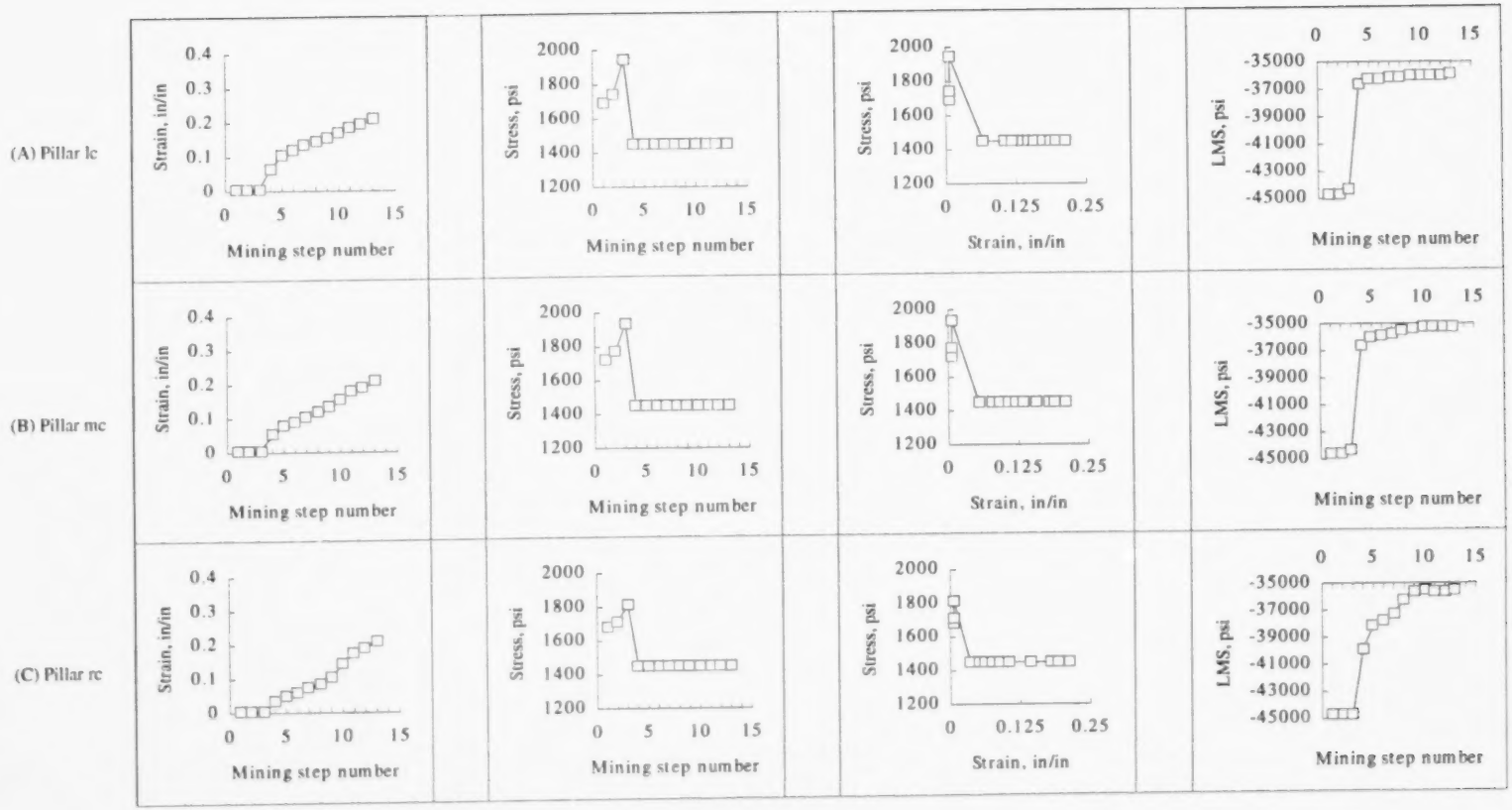

Figure C.5

Pillar stress, strain and local mine stiffness change with mining step number, model with three rows of equal size pillars, 1000 ft overburden. Strata modulus E = 725000 psi, seam modulus Es = 290000 psi, E/Es = 2.5. (Brittle)

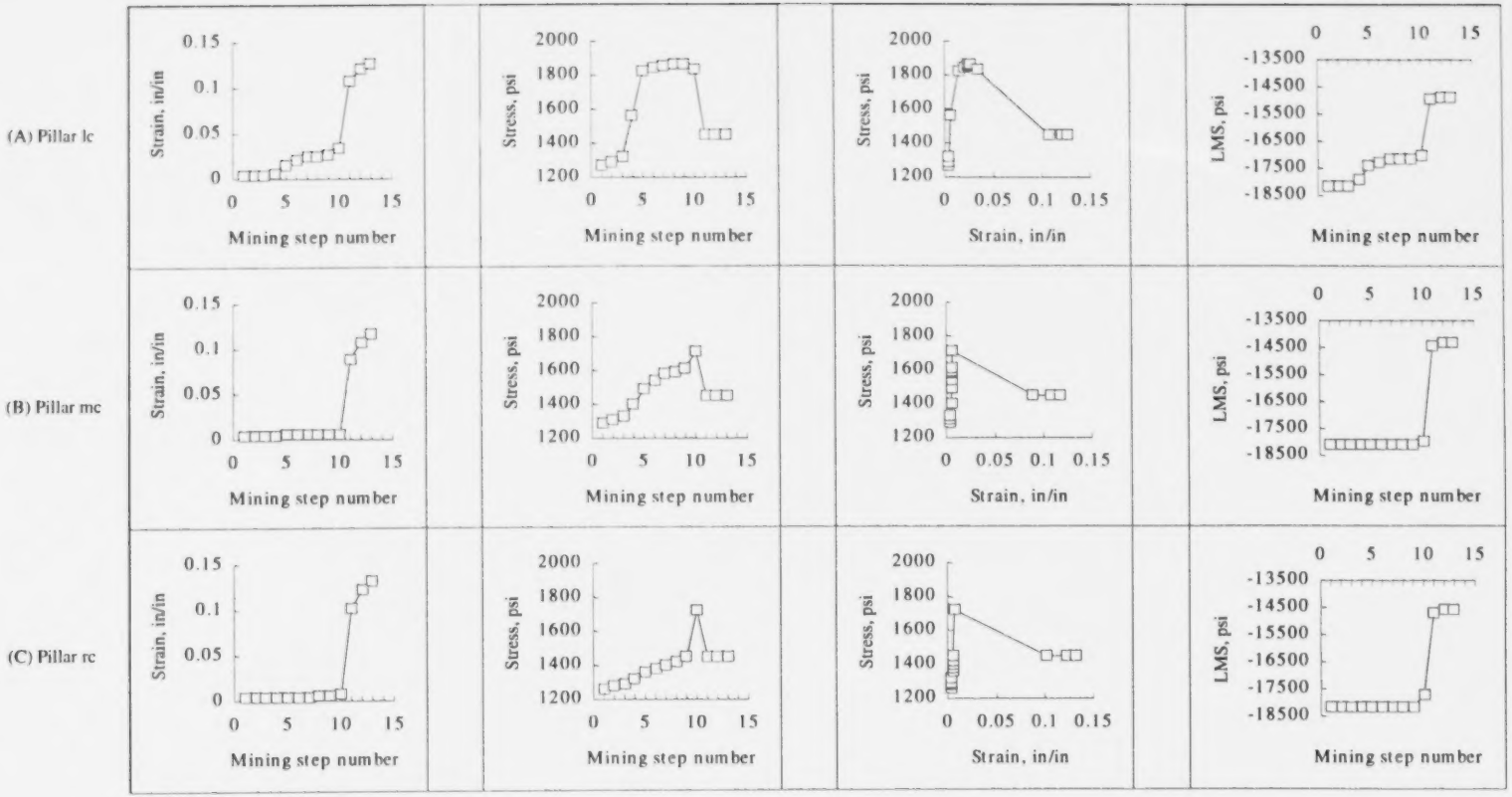

Figure C.6

Pillar stress, strain and local mine stiffness change with mining step number, model with three rows of equal size pillars, 750 ft overburden. Strata modulus E = 290000 psi, seam modulus Es = 290000 psi, E/Es = 1.(Brittle).

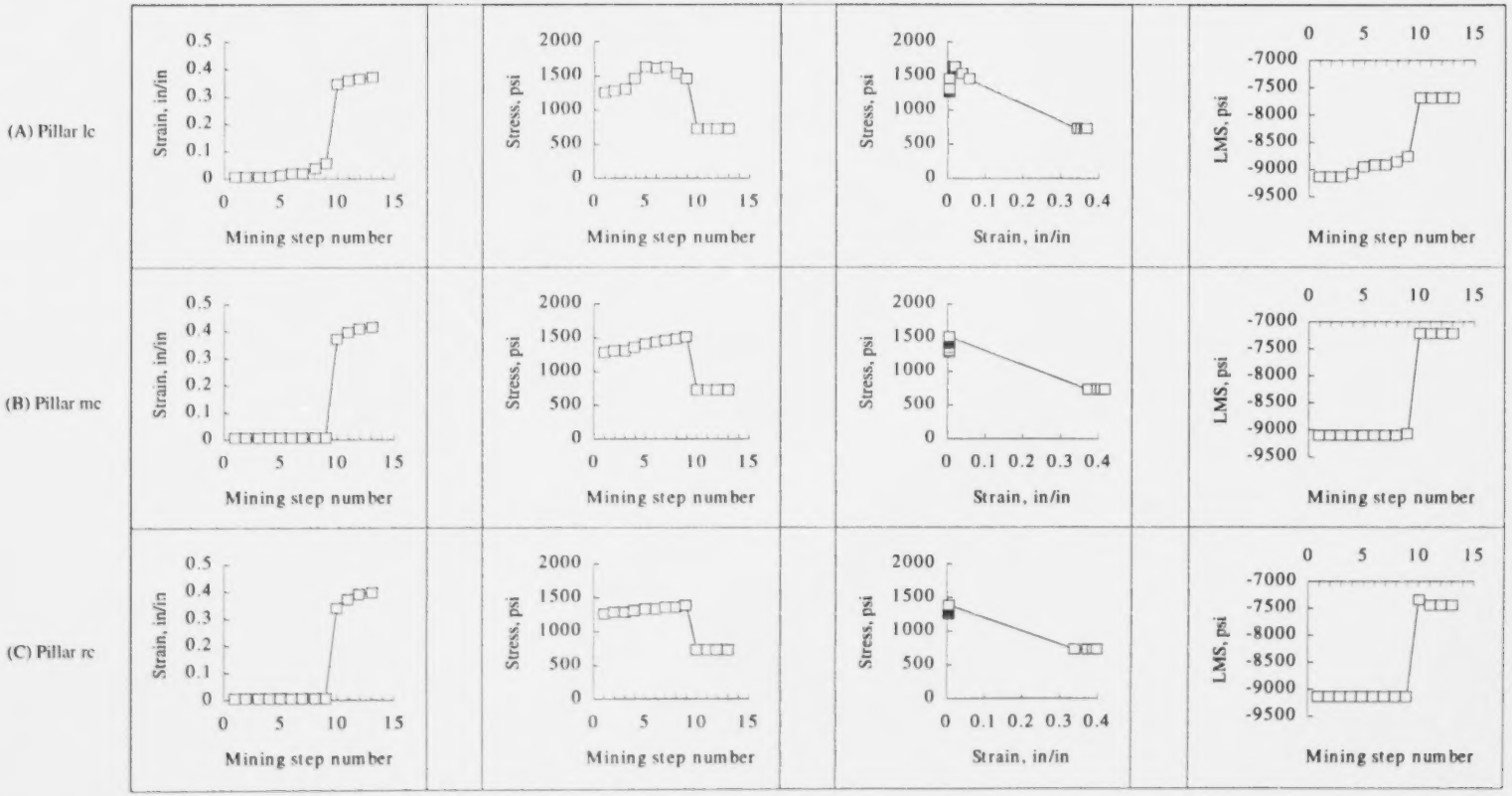

Figure C.7

Pillar stress, strain and local mine stiffness change with mining step number, model with three rows of equal size pillars, 750 ft overburden. Strata modulus E = 145000 psi, seam modulus Es = 290000 psi. (More brittle).

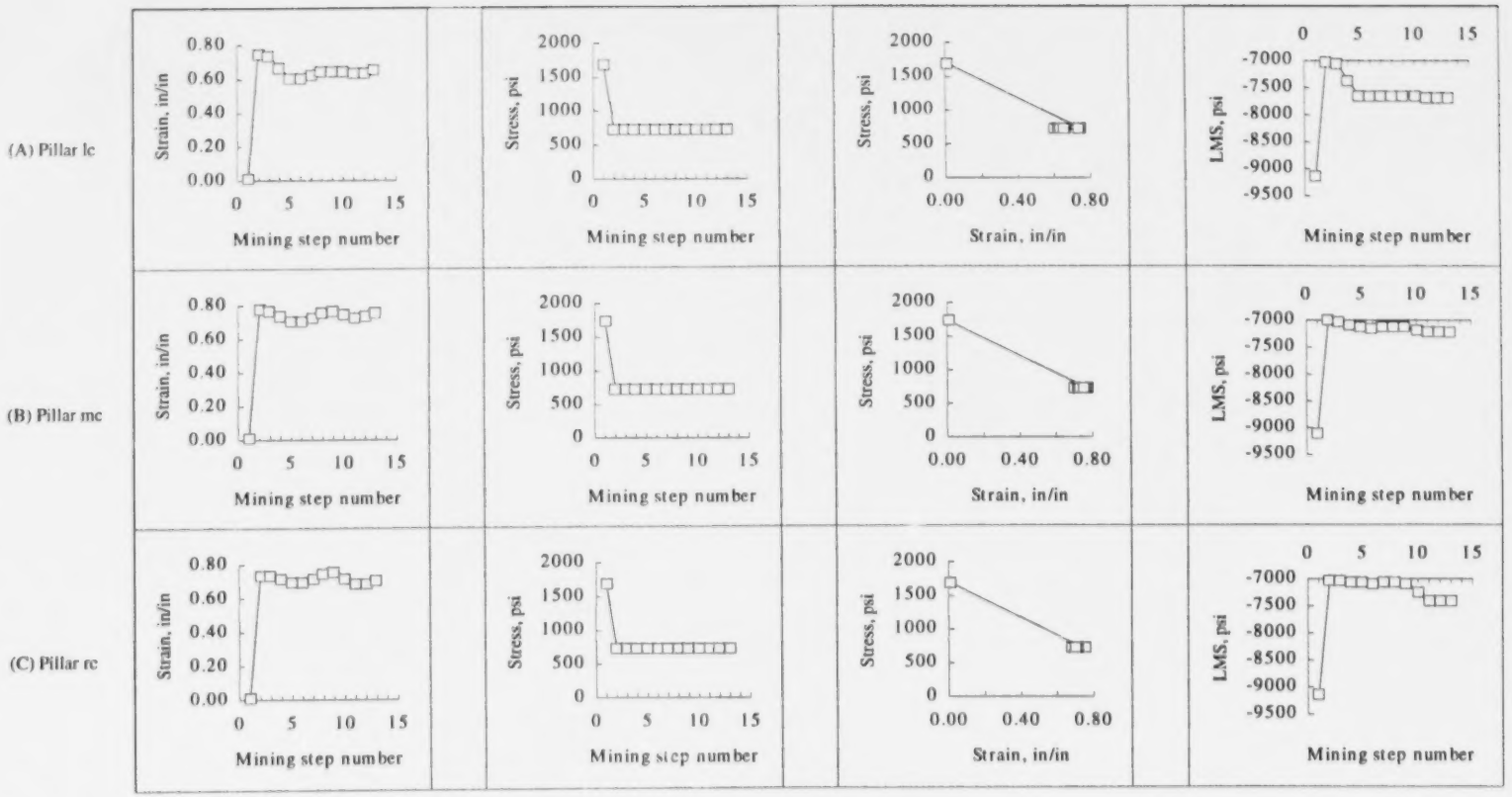

Figure C.8

Pillar stress, strain and local mine stiffness change with mining step number, model with three rows of equal size pillars, 1000 ft overburden. Strata modulus E = 145000 psi, seam modulus Es = 290000 psi. (More brittle).

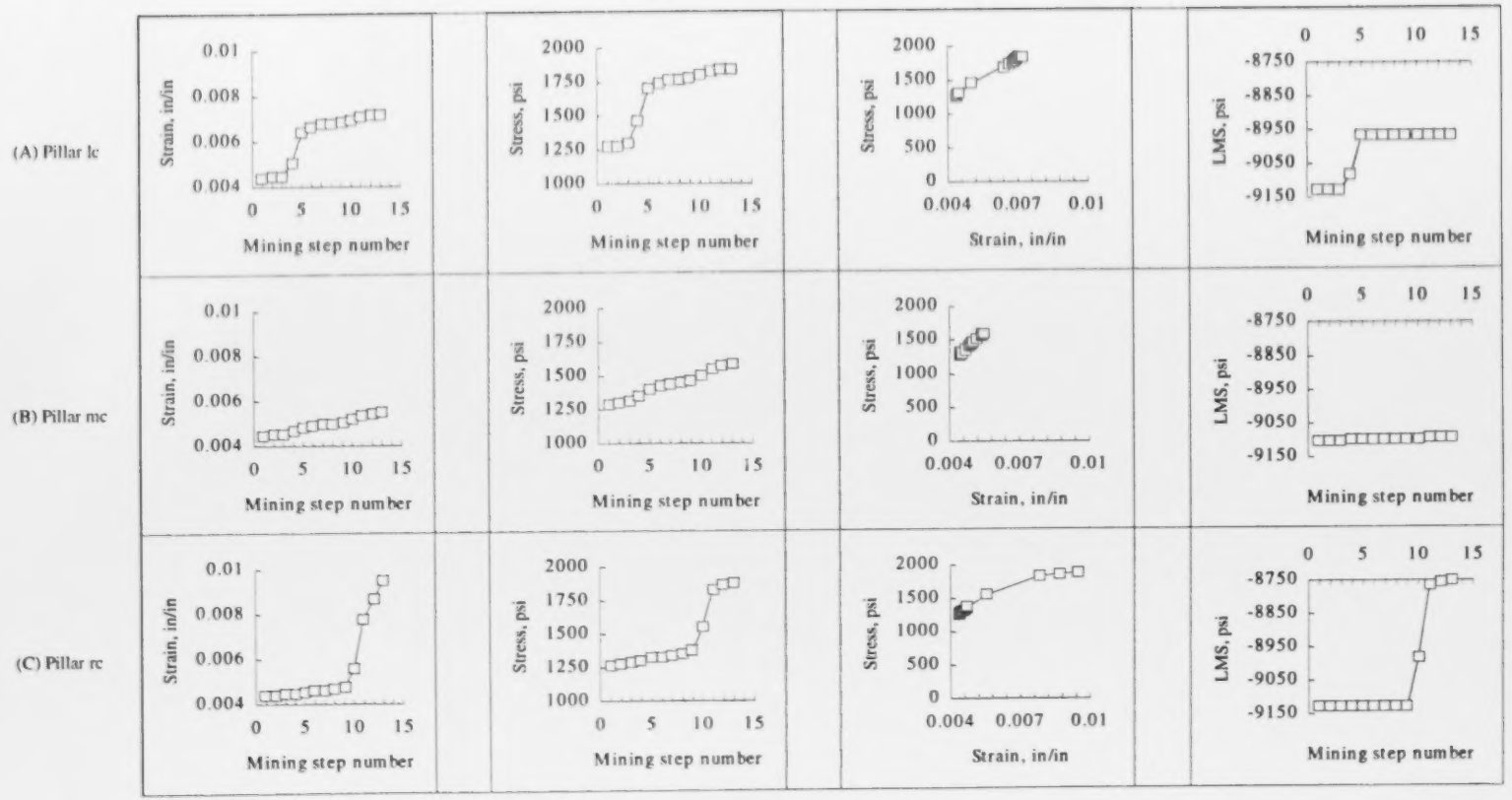

Figure C.9

Pillar stress, strain and local mine stiffness change with mining step number, model with three rows of equal size pillars, 750 ft overburden. Strata modulus E = 145000 psi, seam modulus Es = 290000 psi. (Soft).

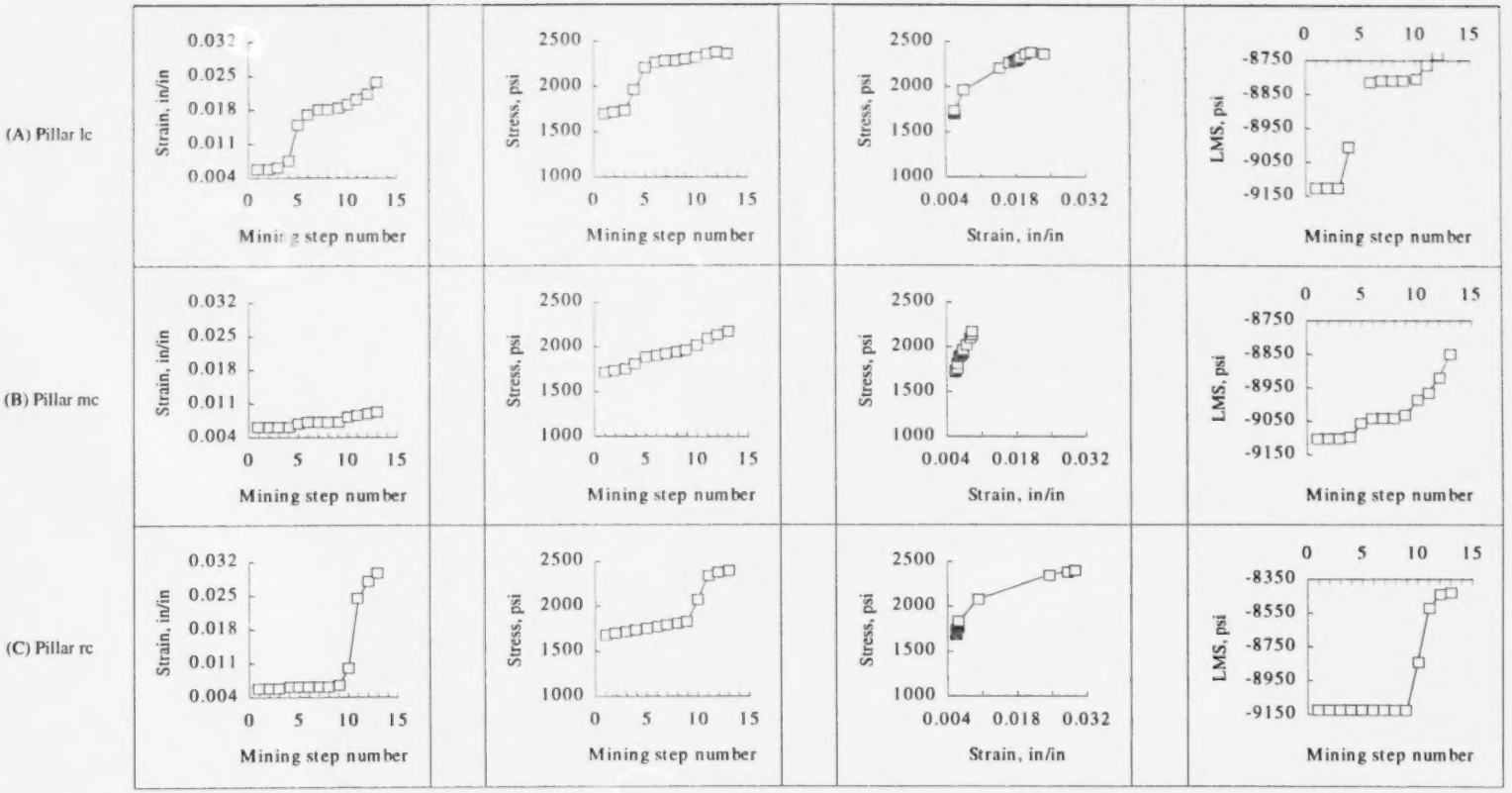

Figure C.10

Pillar stress, strain and local mine stiffness change with mining step number, model with three rows of equal size pillars, 1000 ft overburden. Strata modulus E = 145000 psi, seam modulus Es = 290000 psi. (Soft).

Appendix D

STRESS AND CLOSURE DISTRIBUTIONS FOR SELECTED MODELS

The following are the vertical stress and closure distributions in the fine mesh zones for the selected mining steps for the two entry model (elastic seam), four entries with three rows of equal size pillar model (strain softening seam), four entries with central abutment pillar model (strain softening seam), development 7 model and development 8 model. The unit for stress is psi. The unit for closure and is inch (in). The x (horizontal axis with units of inches) and y (vertical axis with units of inches) of the fine mesh zone figures represent the coordinates of the mesh zone area in the coarse mesh models with the origin at the lower left corner of the coarse mesh zone (not included). The xmin and ymin represent the coordinates of the lower left corner of the fine mesh zone, and the xmax and ymax represent the upper right corner of the fine mesh zone respectively.

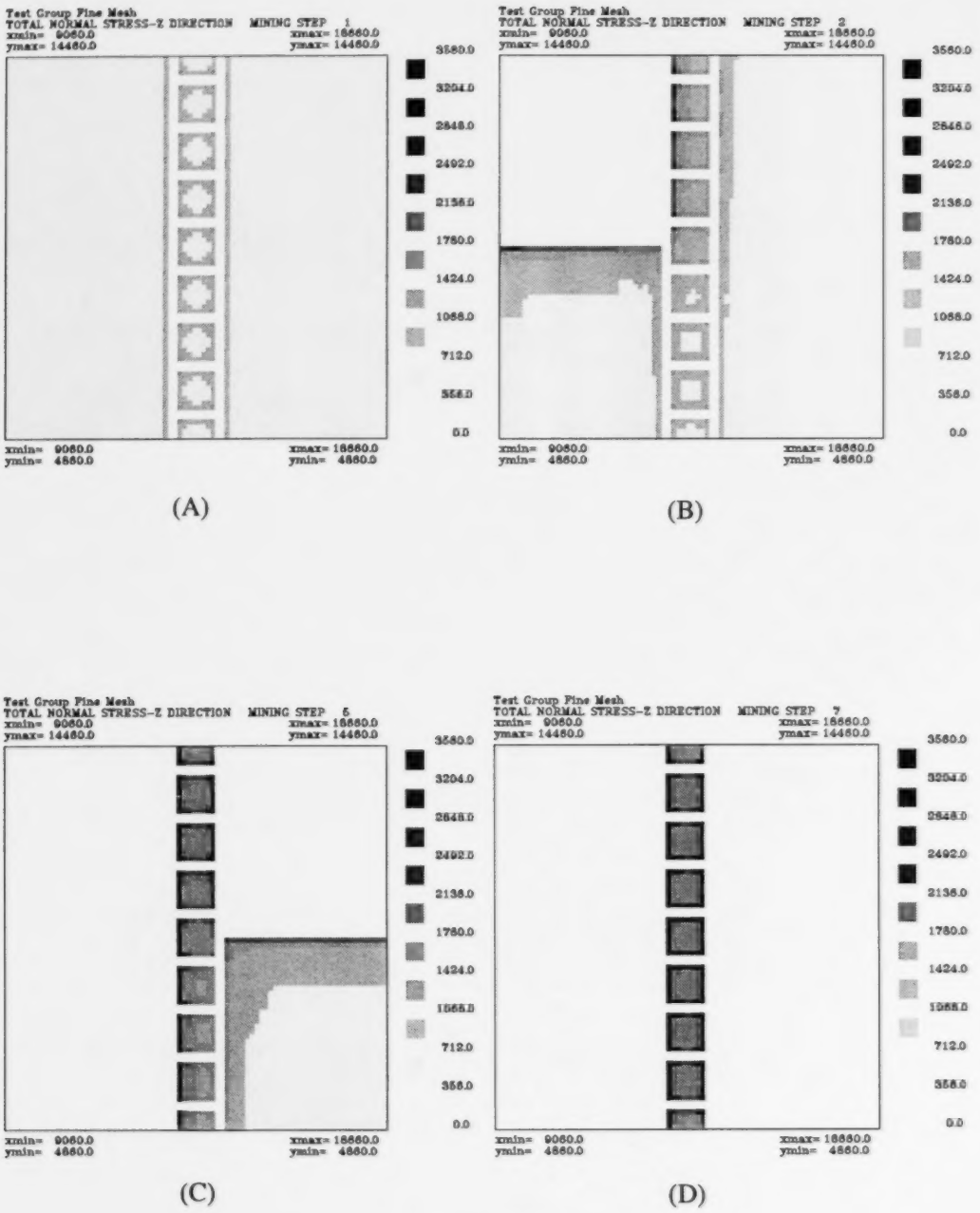

Figure D.1

Vertical stress in the fine mesh zone through the selected mining steps for the two entries elastic model (500 ft overburden).

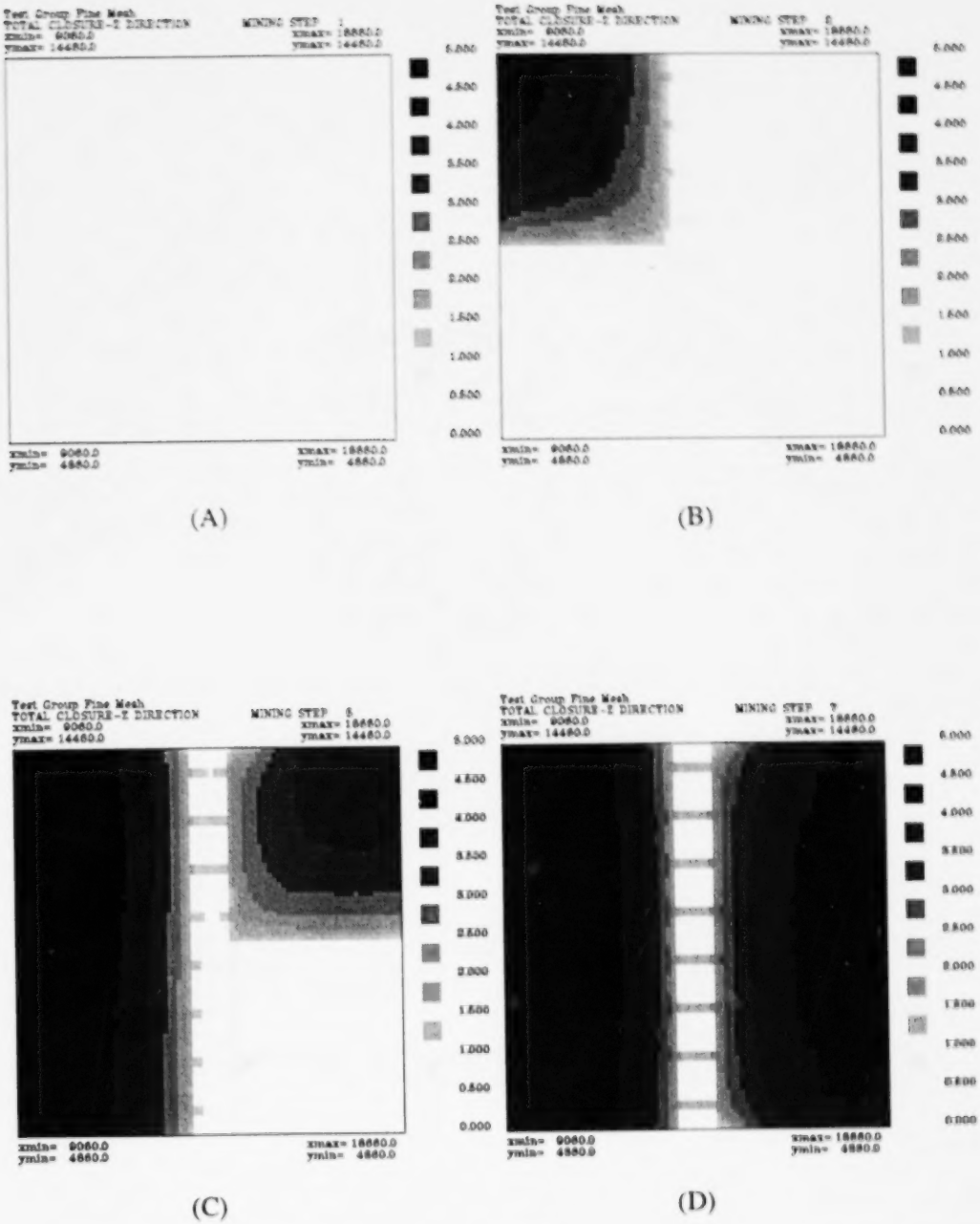

Figure D.2

Vertical closure in the fine mesh zone through the selected mining steps for the two entries elastic model (500 ft overburden).

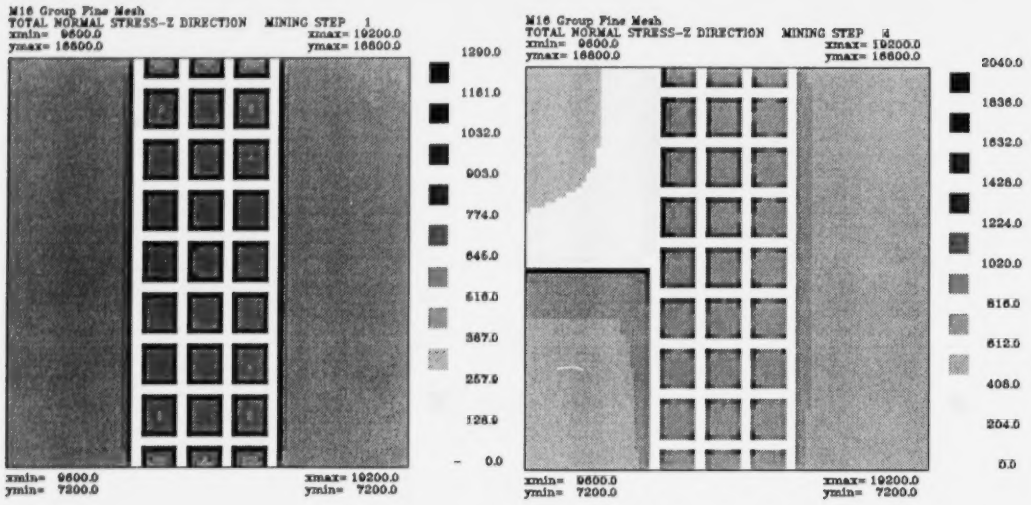

(A) (B)

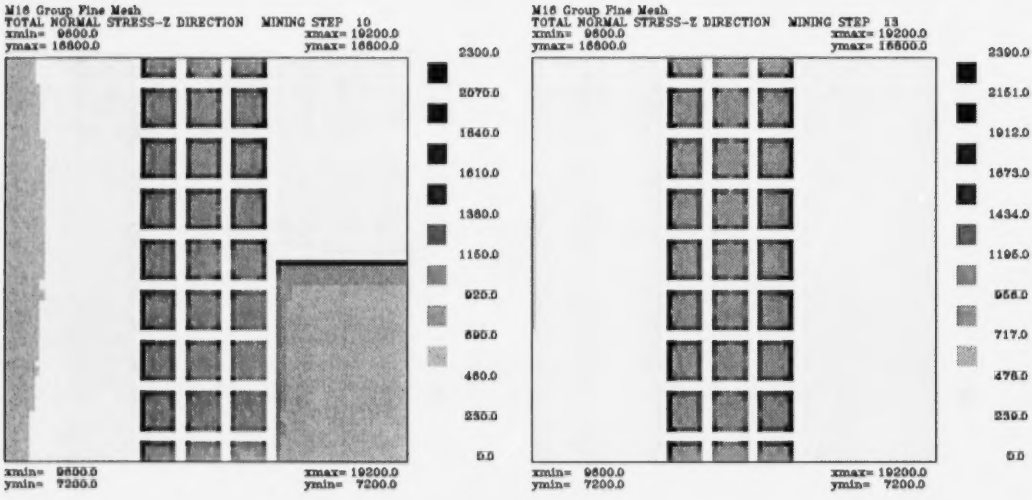

(C) Figure D.3 (D)

Vertical stress in the fine mesh zone through the selected mining steps for the four entries with three rows of equal size pillars model (500 ft overburden, strain softening seam, brittle).

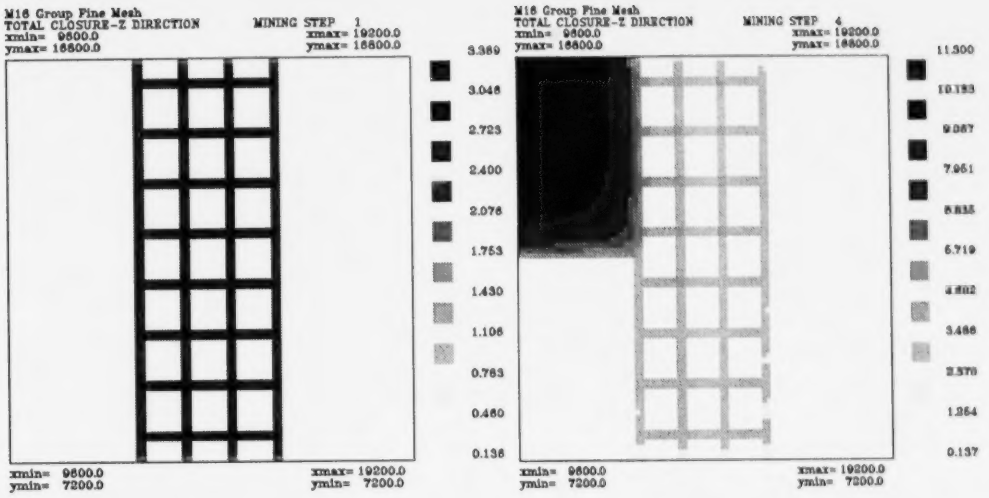

(A) (B)

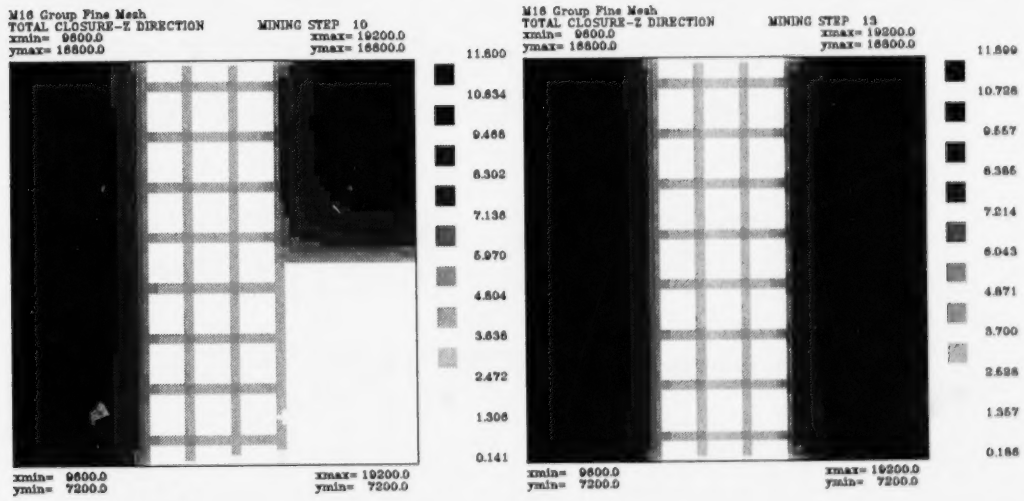

(C) (D)

Figure D.4

Vertical closure in the fine mesh zone through the selected mining steps for the four entries with three rows of equal size pillars model (500 ft overburden, strain softening seam, brittle).

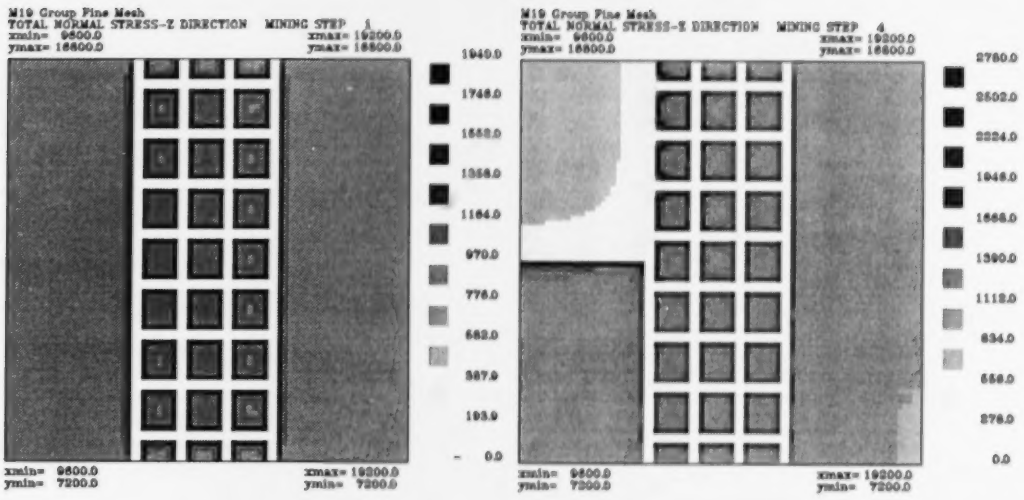

(A) (B)

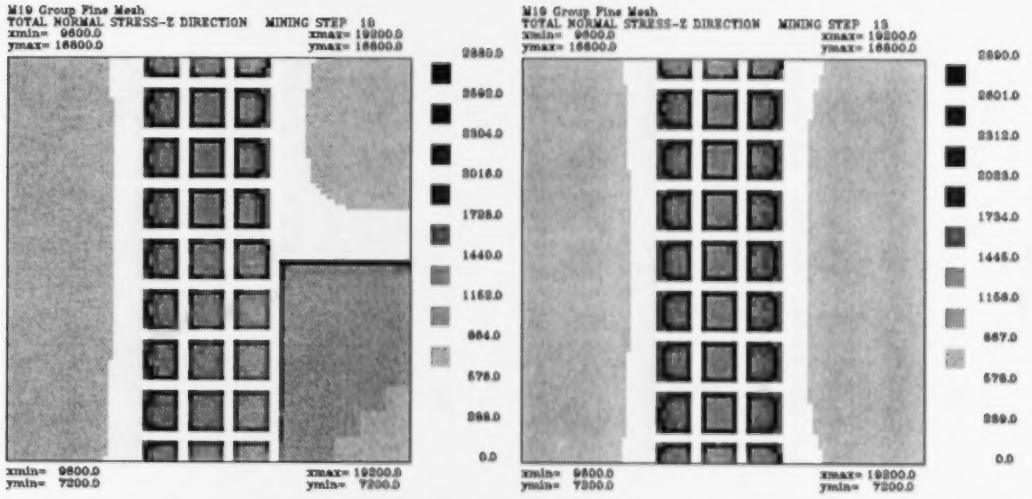

(C) (D)

Figure D.5

Vertical stress in the fine mesh zone through the selected mining steps for the four entries with three rows of equal size pillars model (750 ft overburden, strain softening seam, brittle).

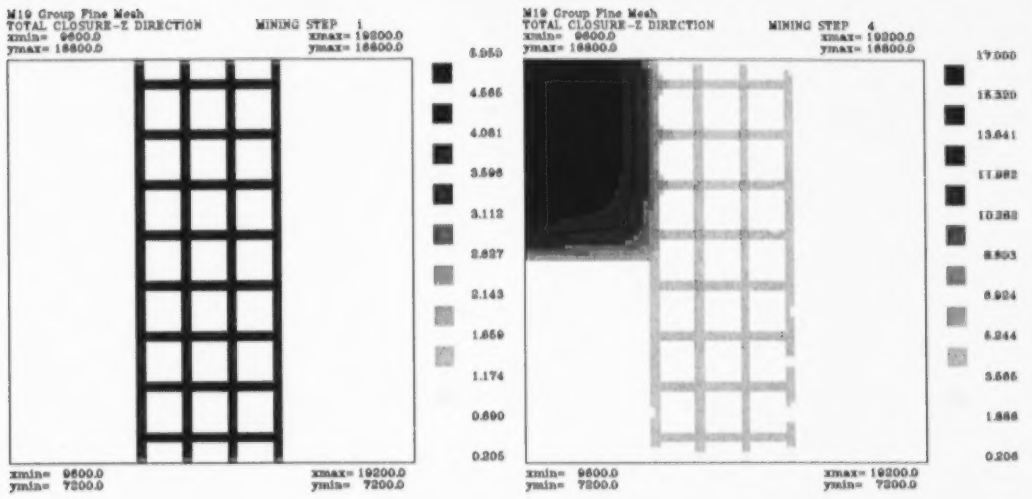

(A) (B)

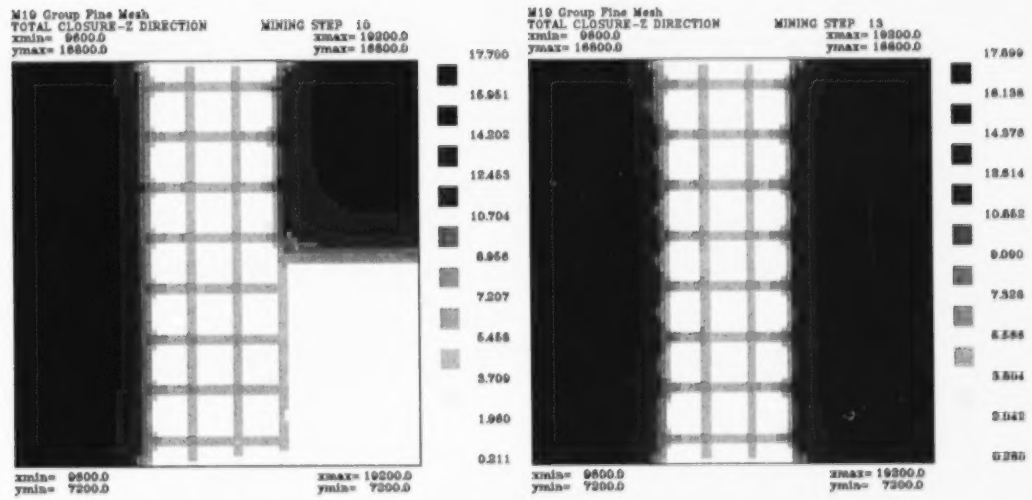

(C) (D)

Figure D.6

Vertical closure in the fine mesh zone through the selected mining steps for the four entries with three rows of equal size pillars model (750 ft overburden, strain softening seam, brittle).

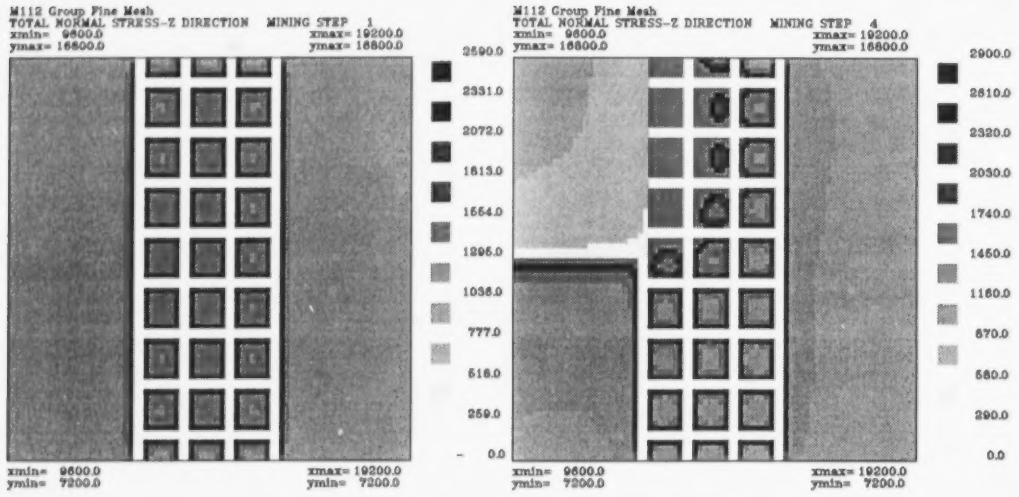

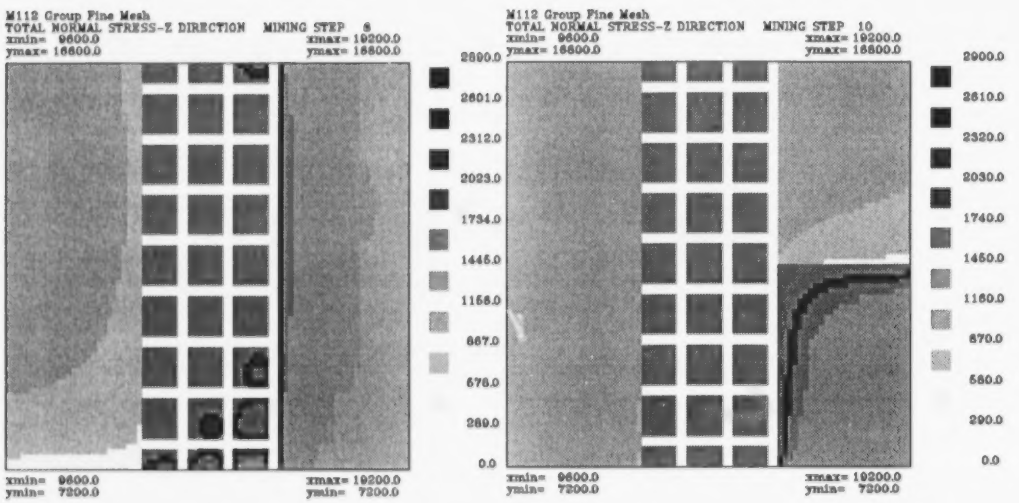

Figure D.7

Vertical stress in the fine mesh zone through the selected mining steps for the four entries with three rows of equal size pillars model (1000 ft overburden, strain softening seam, brittle).

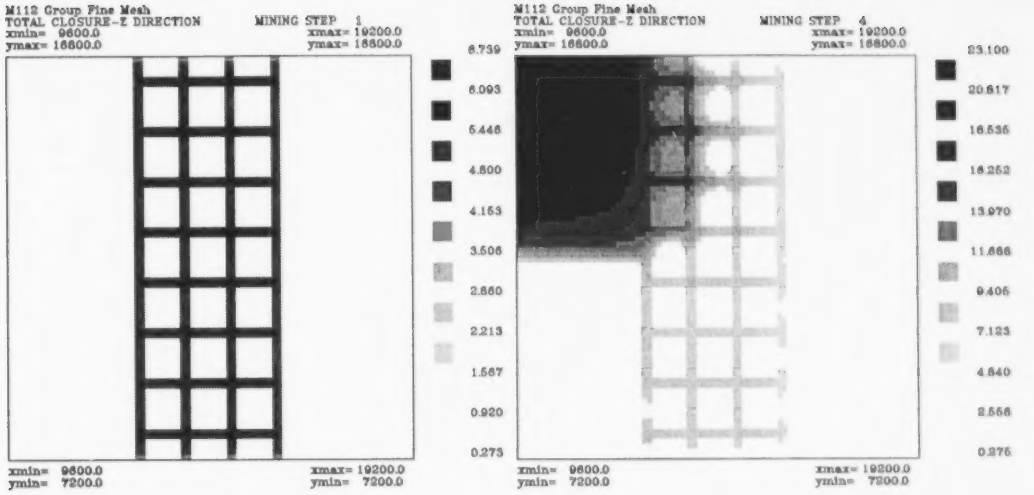

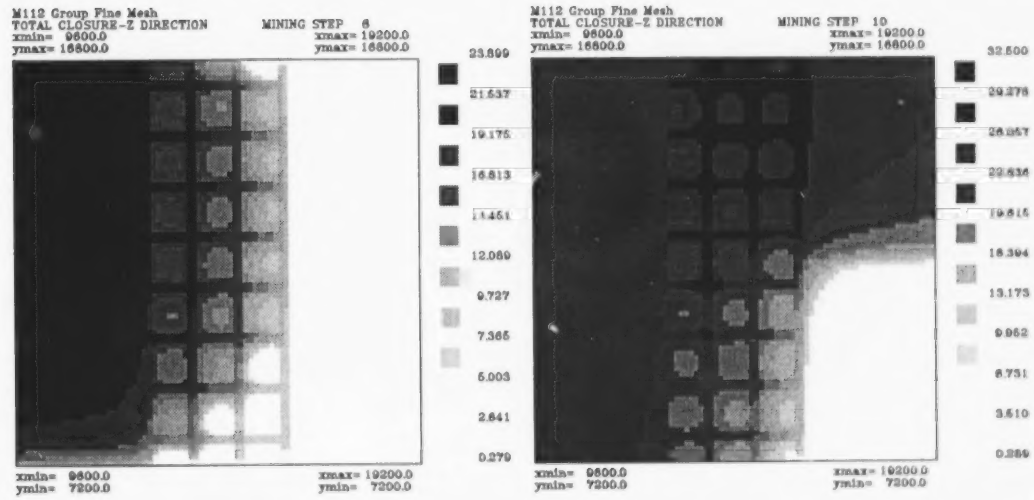

Figure D.8

Vertical closure in the fine mesh zone through the selected mining steps for the four entries with three rows of equal size pillars model (1000 ft overburden, strain softening seam, brittle).

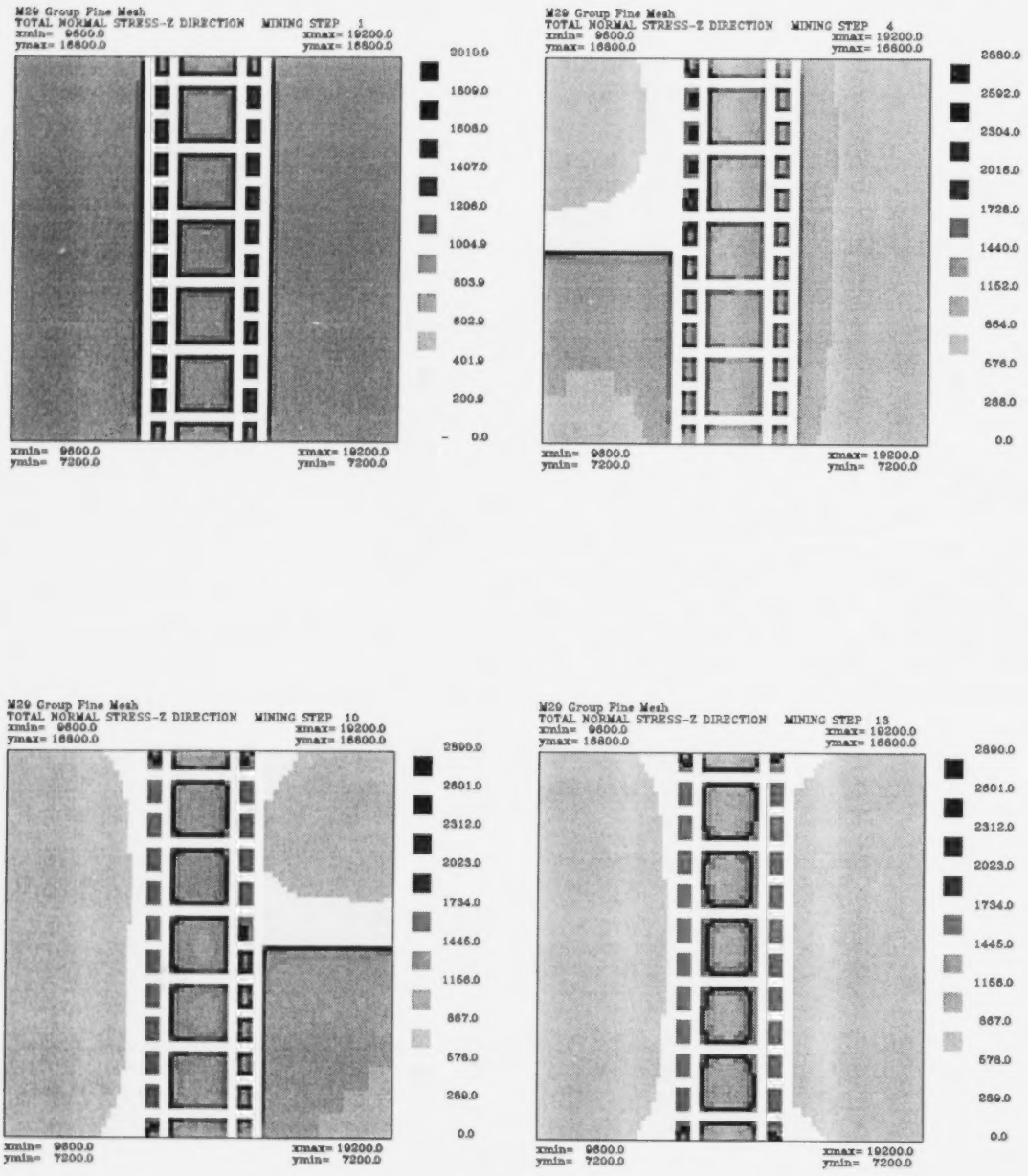

Figure D.9

Vertical stress in the fine mesh zone through the selected mining steps for the four entries with central abutment pillar (YAY) model (750 ft overburden, strain softening seam, brittle).

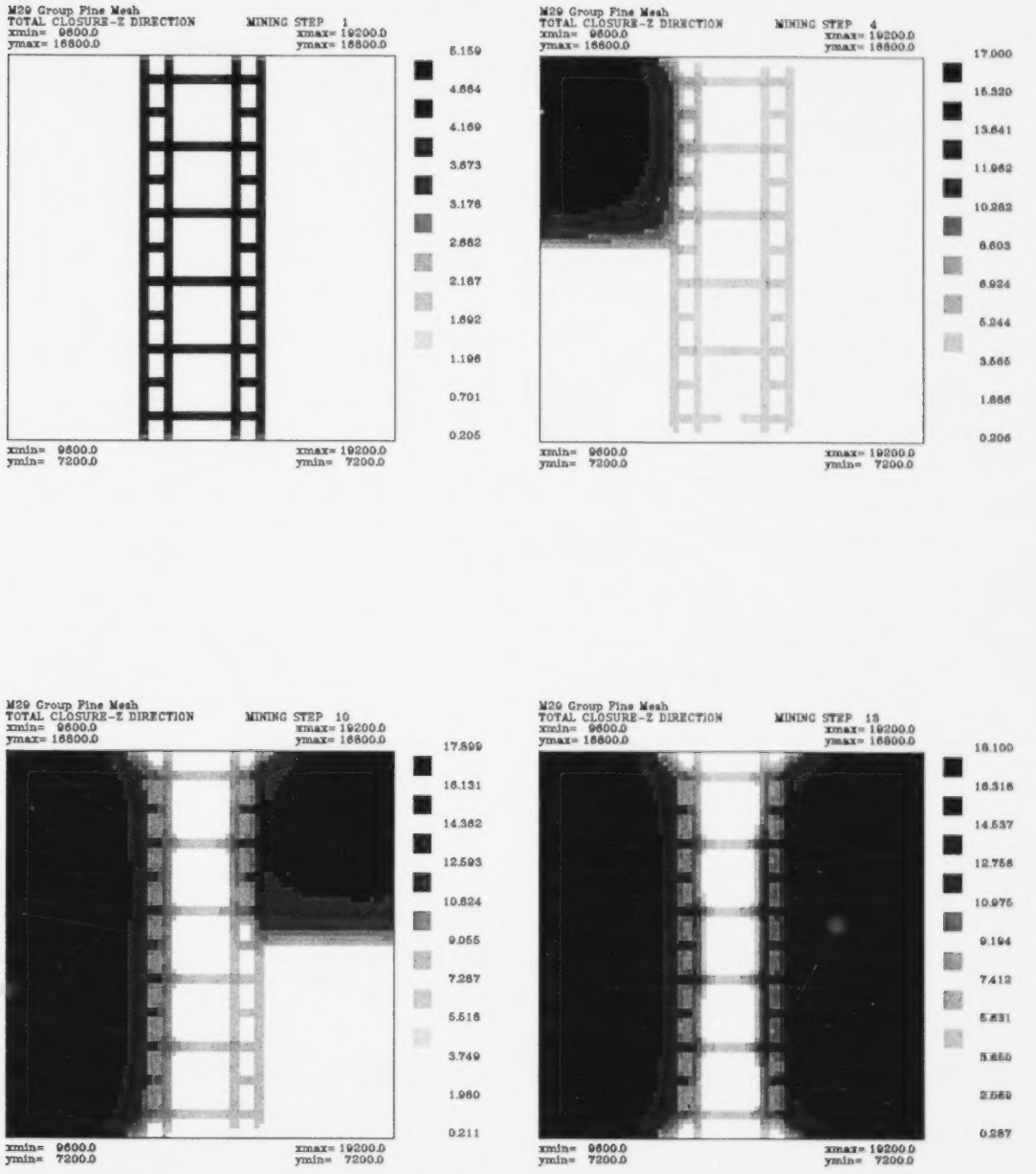

Figure D.10

Vertical closure in the fine mesh zone through the selected mining steps for the four entries with central abutment pillar (YAY) model (750 ft overburden, strain softening seam, brittle).

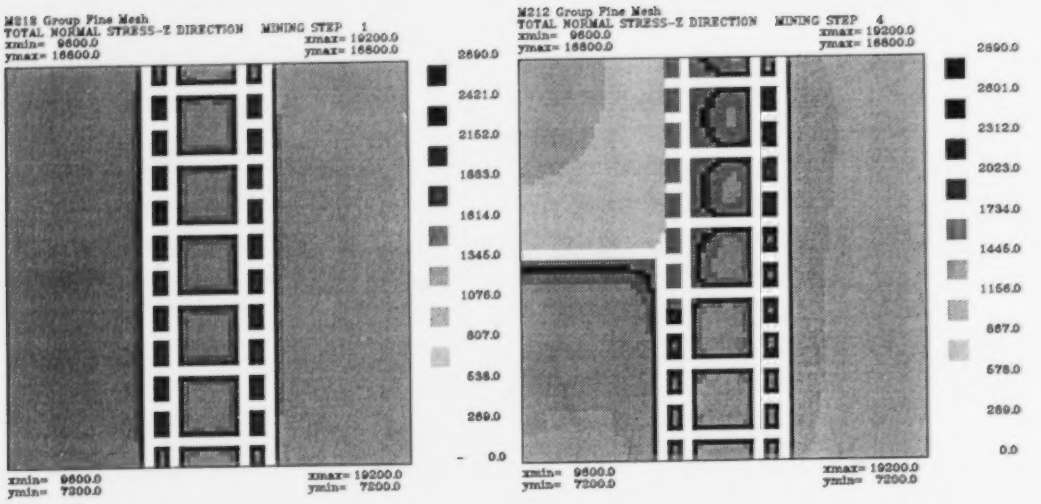

(A) (B)

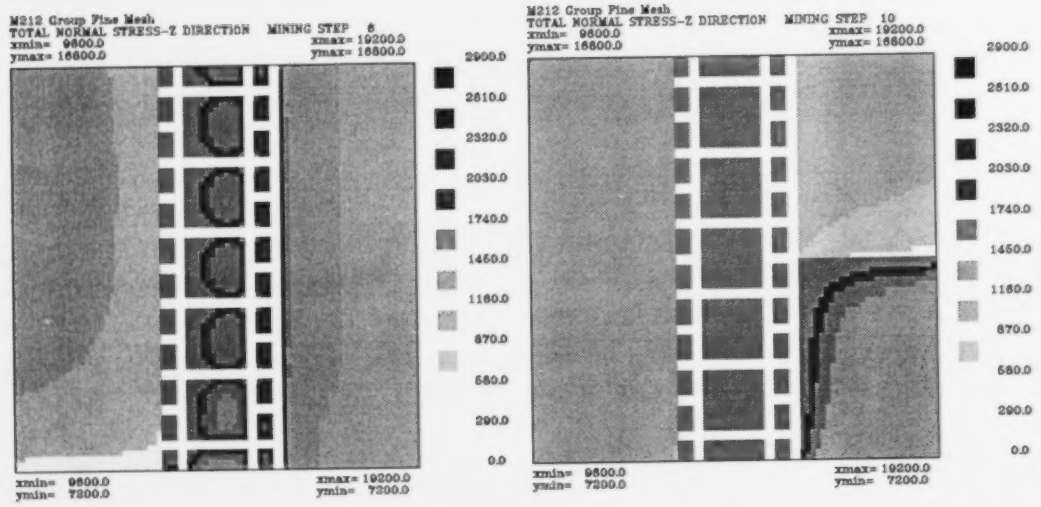

(C) (D)

Figure D.11

Vertical stress in the fine mesh zone through the selected mining steps for the four entries with central abutment pillar (YAY) model (1000 ft overburden, strain softening seam, brittle).

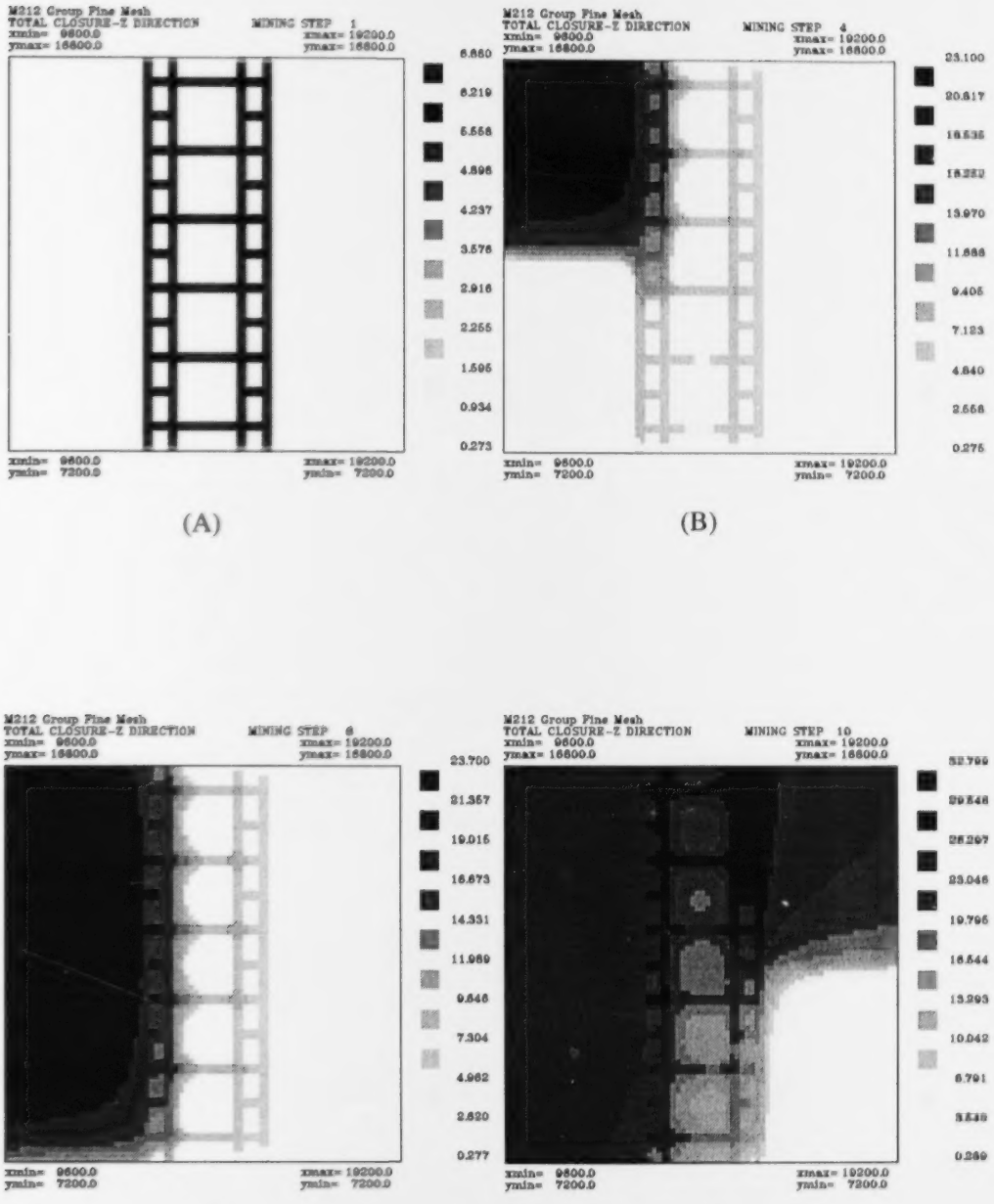

Figure D.12

Vertical closure in the fine mesh zone through the selected mining steps for the four entries with central abutment pillar (YAY) model (1000 ft overburden, strain softening seam, brittle).

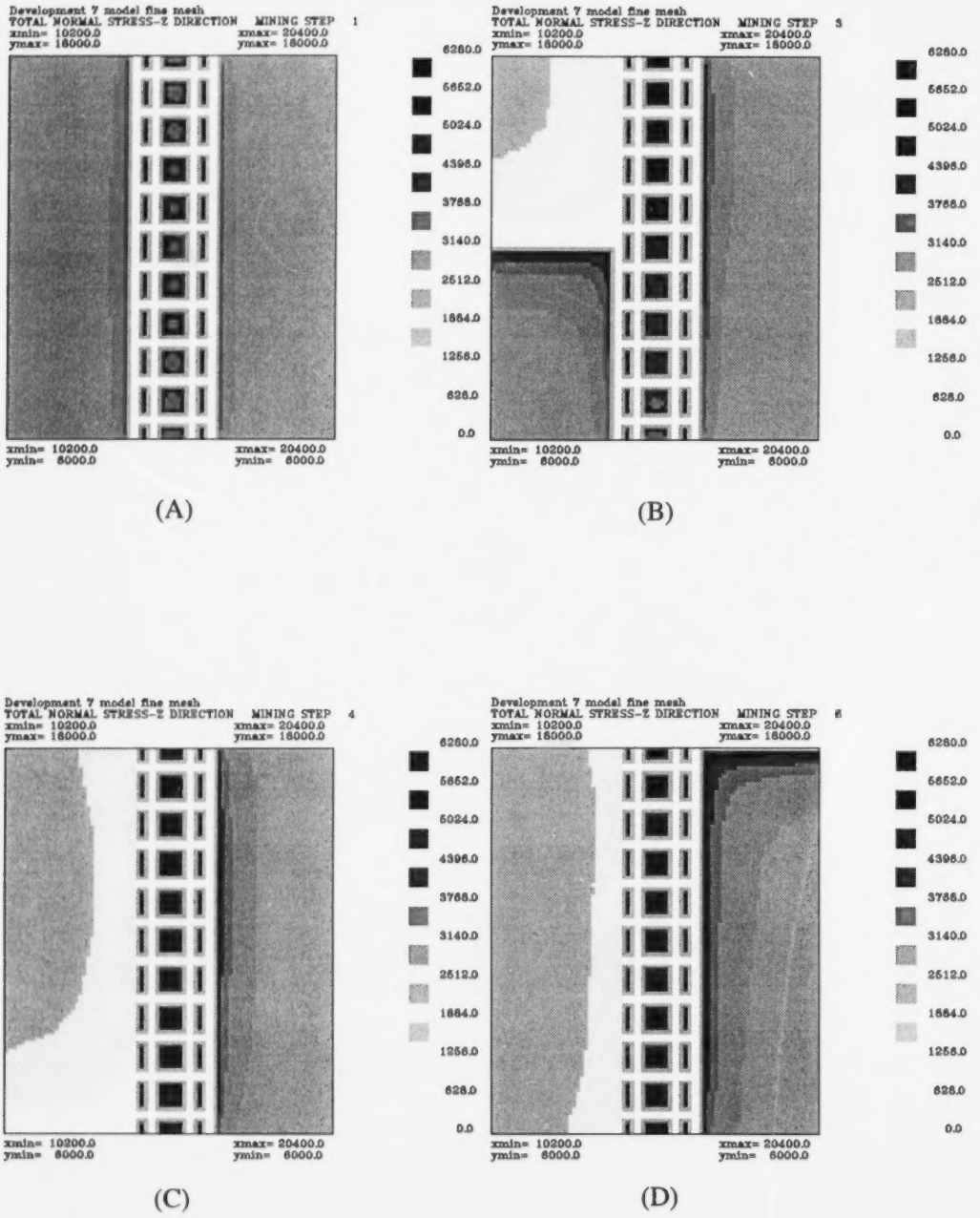

Figure D.13

Vertical stress in the fine mesh zone through the selected mining steps for development 7 model (strain softening seam, 1900 ft overburden).

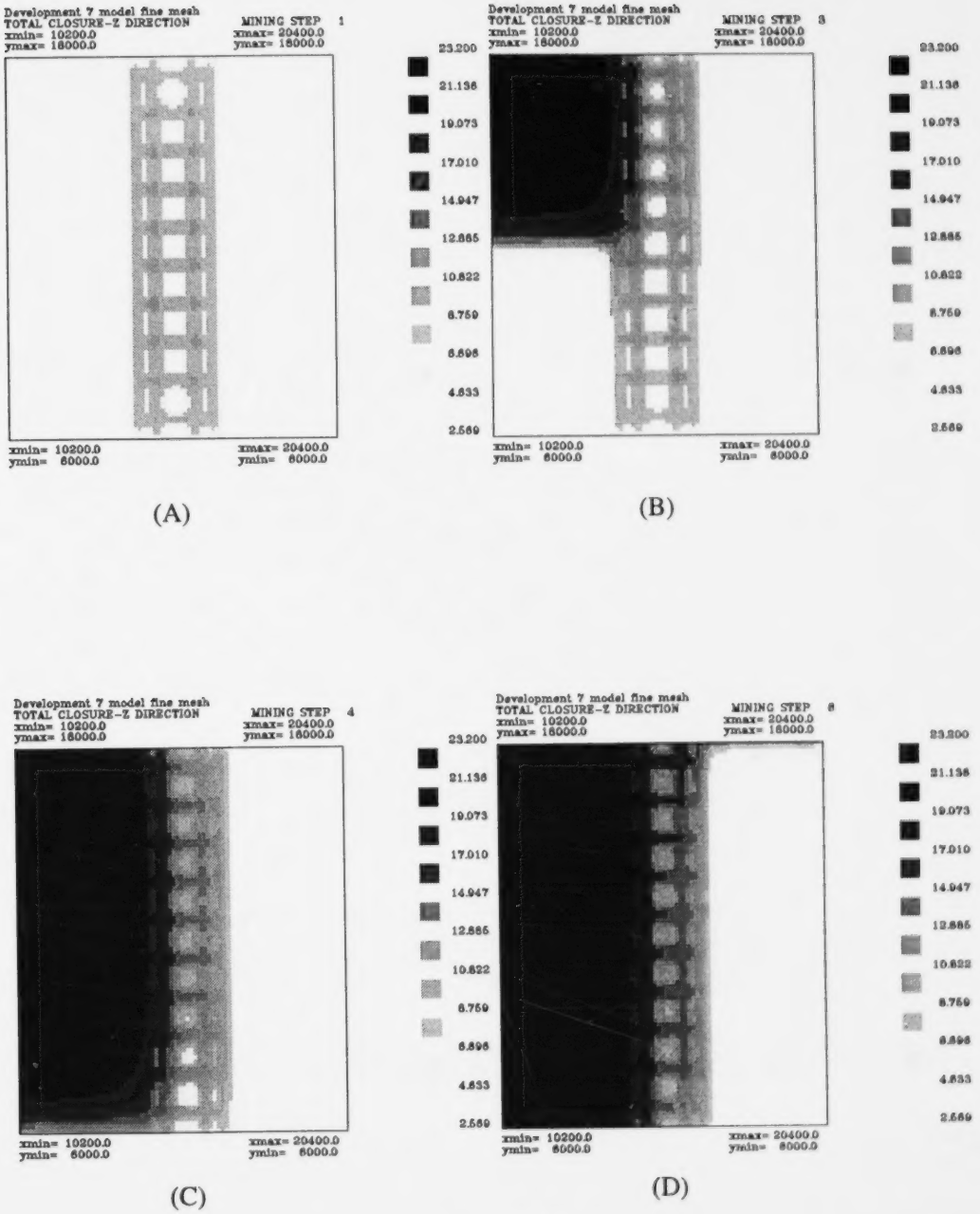

Figure D.14

Vertical closure in the fine mesh zone through the selected mining steps for development 7 model (strain softening seam, 1900 ft overburden).

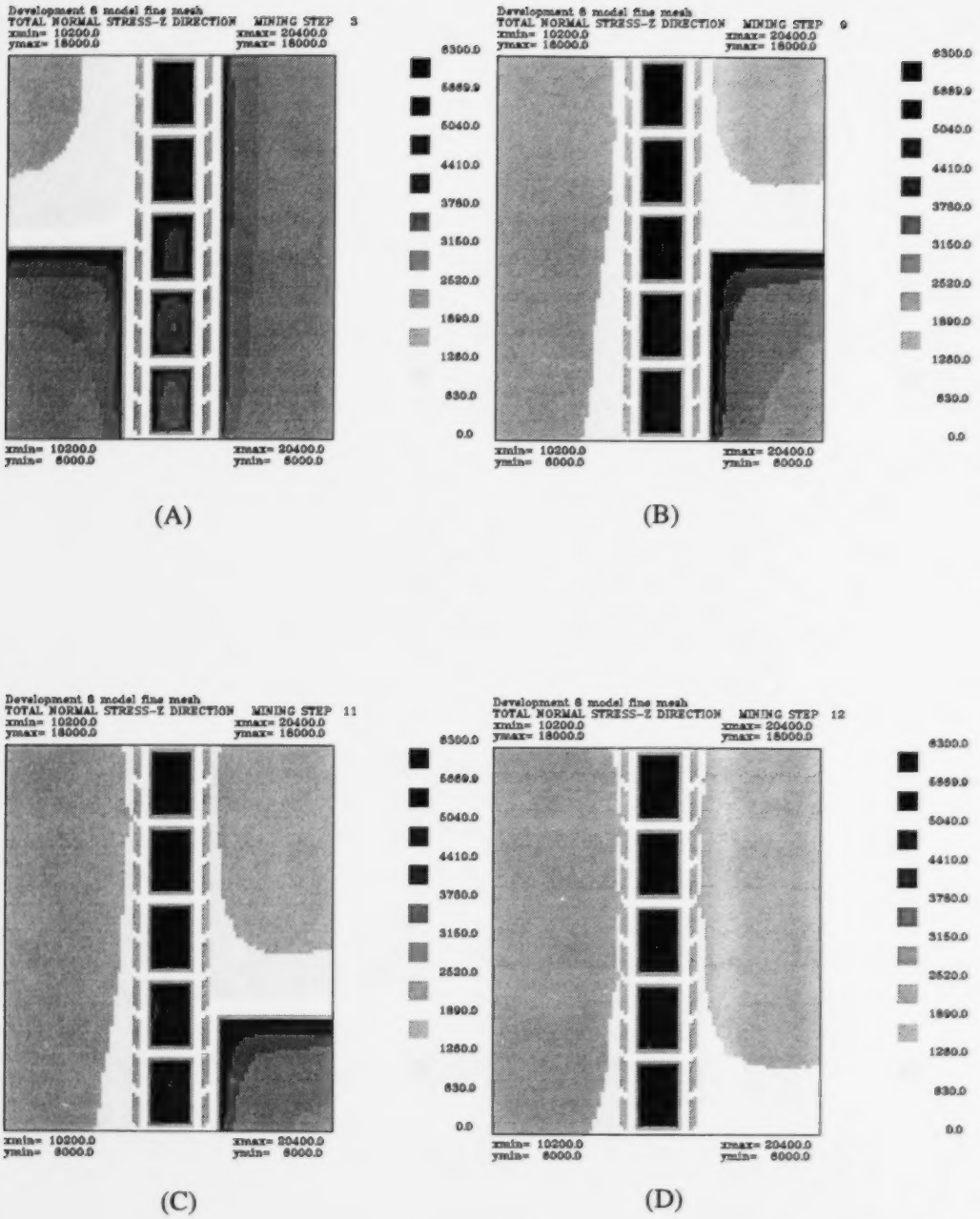

Figure D.15

Vertical stress in the fine mesh zone through the selected mining steps for development 8 model (strain softening seam, 2000 ft overburden).

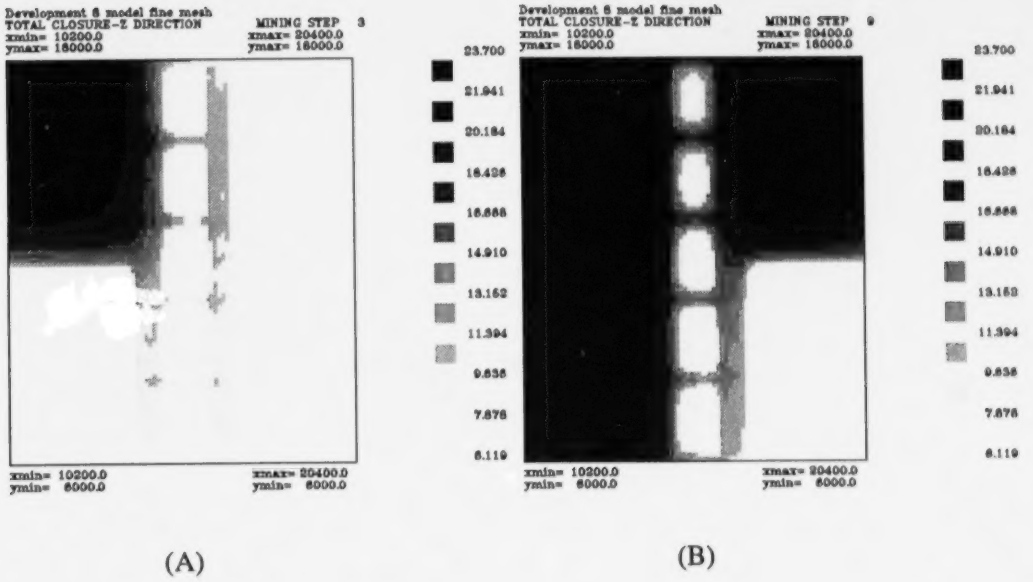

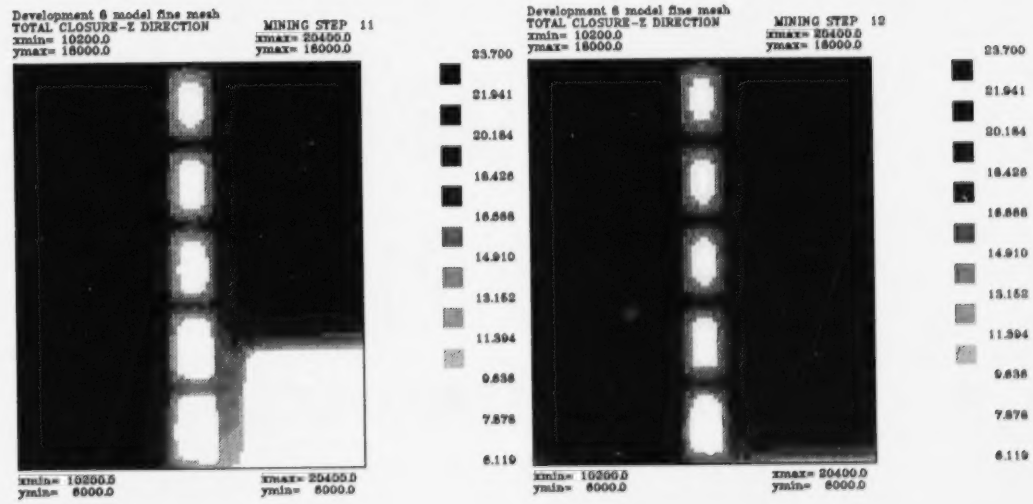

Figure D.16

Vertical closure in the fine mesh zone through the selected mining steps for development 8 model (strain softening seam, 2000 ft overburden).

Appendix E

POST-FAILURE STIFFNESS COMPILATIONS

In all tables and sections of this appendix, except when specified otherwise, Es and Ep denote Young's modulus and post-failure modulus (or post-failure stiffness); W and H denote the width (or diameter) and height of pillars (or specimens), respectively.

E.1 Das's data (1986)

Indian coal, from laboratory tests on the 54 mm diameter core.

Modulus unit: MPa

Coal field	Kenda	Uchitdih	Singhpur	X11	Kargali	Jambad
Es	2667.7	2420	4800	3120	5520	2500

Modulus unit: MPa

Coal field	Kenda	Uchitdih	Singhpur	X11	Kargali	Jambad
W/H	Ep	Ep	Ep	Ep	Ep	Ep
0.5	120000		30000	23100	41600	
1	17000	39000	7200	5800	5250	
2	15000	24500	2650	3600	2250	13950
3	5000	15500	1700	1100	1200	3600
4.5	3500	2300	885	650	500	950
6.75	755	1000	200	500	260	600
9	1067	500	0	450	0	500

E.2 Seedsman's data (1991)

Australian coal; 50 and 25 mm block specimens from Southern, Newcastle, and Bowen Basin coal fields. Ep is the secant post-failure modulus at 1.25 times failure strain.

Modulus unit: GPa

W/H	Ep	Es
1.07	5.2	2.3
1.06	13.8	2.1
1.13	3.1	1.7
1.02	4.5	2.3
0.98	4.3	2.1
1.04	2	2.3
1.01		2.2
1.08	2.7	1.6
1.99	2.35	1.6
1.95	3.01	2.5
2.03	2.17	1.9
2.15	1.54	1.6
2.23	1.57	1.9
2.3	1.15	0.9
2.03	4.6	2.2
2.08	3.8	1.9
1.89	5	2.5
2.68	1	1.2
4.45	3	5
4.16	1.5	5.3
2.12	1.7	2
2.23	2.69	1.6
2.26	4.62	2.8
2.54	0.8	1.1
3.1	0.68	1.3
3.08	1.5	2.2
3.86	0.7	2.9
3.68	1.1	3.1
5.37	1.2	4.5
5.62	0.8	2.7
0.97	1.47	1.6
0.98	12.7	3.1
1.01	2.9	3.5
1	2.15	2.4
1	11	3.5
1	2.38	2
1.02	9.25	3.5
1.04	1.81	1.5
1.04	0.21	0.5
1.12	1.62	1.35
1.99	1.38	1.9
2.01	2.89	2.5
2.04	1.4	1.9
2.05	1.82	2.7
2.14	1.25	1.2
2.29	1.12	3
2.93	1.5	2.3
3.05	0.94	3.1
3.37	0.94	2.8

Continuous table for Seedsman's data

W/H	Ep	Es
3.96		1.9
3.98	2.73	2
3.01		3.8
1.04	3.19	2.3
1	3.14	2.5
1.03	7.13	3.8
1.12	1.13	2
1.11	1.83	2.5
1.03	2.23	1.8
1.04	4.83	2.5
1.01	2.61	2.7
0.99	3.1	2.6
1.05	5.23	2.4
1.08	2.15	1.5
1.04	1.93	2.7

E.3 Heerden's data (1975)

South African coal; field pillars with cross section 1.4×1.4 m.

Modulus unit: GPa

W/H	Ep	Es
1.14	2	3.71
1.15	0.87	4.59
1.28	2.11	4.52
1.31	1.72	3.33
1.87	1.14	3.75
2.13	0.91	4.26
2.79	0.52	3.86
2.79	0.7	3.62
3.28	0.53	3.95
3.39	0.55	4.29

E.4 Cook's data (1971)

South African coal; field pillars with cross section. Average modulus from pillars with cross section up to 2×2 m and height H = 1 - 2 m.

Modulus unit: kPa

W/H	Ep	Es
0.6	5	35

E.5 Wagner's data (1974)

South African coal; field pillars with height H = 1.8 ft.

Modulus unit: Kba (1 Kba = 10 psi)

Average Young's modulus Es = 40 Kba

W/H	Ep
0.8	25.2
0.88	22.4
0.98	20
1.05	16.3
1.59	15
1.75	12
1.82	11.8
1.94	6.6
2	8.71
2.03	7.7
2.09	8.2
2.22	8.71

E.6 Wang's data (1976)

US coal; Pocahontas No.3 seam. Field pillar with width 62 ft and height 5.5 ft

Average Young's modulus Es = 2.38 GPa

W/H = 11.3 Ep = 3.821 GPa

E.7 Pittsburgh Research Center (Iannacchione, 1988)

US coal; Pocahontas No.3 seam, field pillar with width 80 ft and height 70 in.

Modulus unit: GPa

Average Young's modulus Es = 1.63 - 2.47

W/H = 13.7 Ep = 3.14

E.8 Crouch's data (1973)

US coal; came from 2 and 4 in diameter cylinder specimen; mean of post-failure stiffness.

Modulus unit: $\times 10^5$ psi

Average elastic modulus Es = 3.53

Seam	Pocahontas No. 3	Pocahontas No. 4	Geneva	Sunnyside
W/H	Ep	Ep	Ep	Ep
1	7.5	14.37		
2	10.94	4.98	9.05	22.61
3	6	2.49	6.85	6.62
4	2.43	2.16	5.38	6.75
5	2.48	1.48	4.63	3.63
6	2.5	1.46	1.6	3.24
8			0.92	

Appendix F

THREE DIMENSIONAL PRESENTATION OF THE VERTICAL STRESS AND CLOSURE DISTRIBUTIONS FOR DEVELOPMENT 7 AND DEVELOPMENT 8 MODELS AT SELECTED MINING STEPS

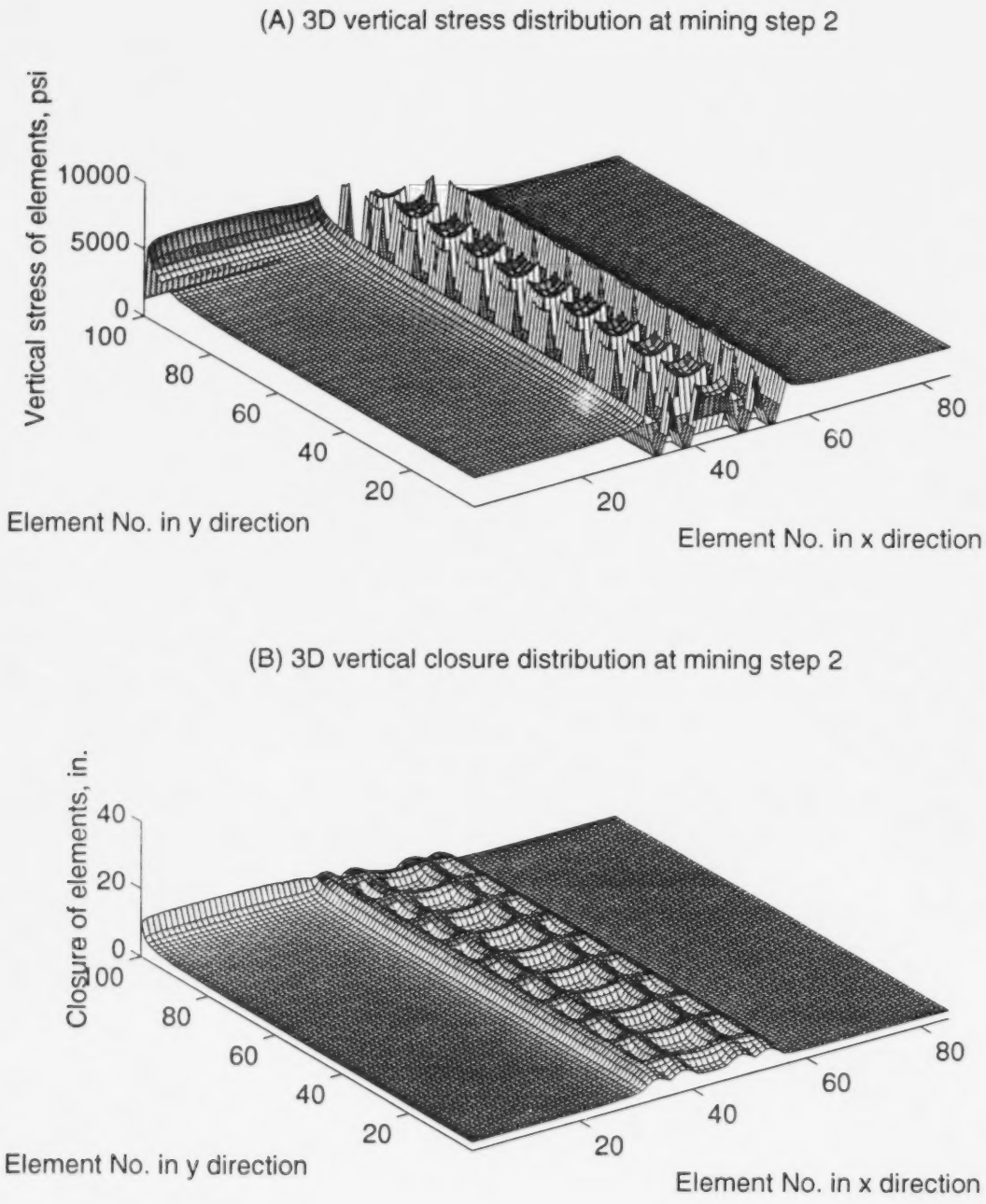

Figure F.1

Vertical stress and closure at mining step 2 for development 7

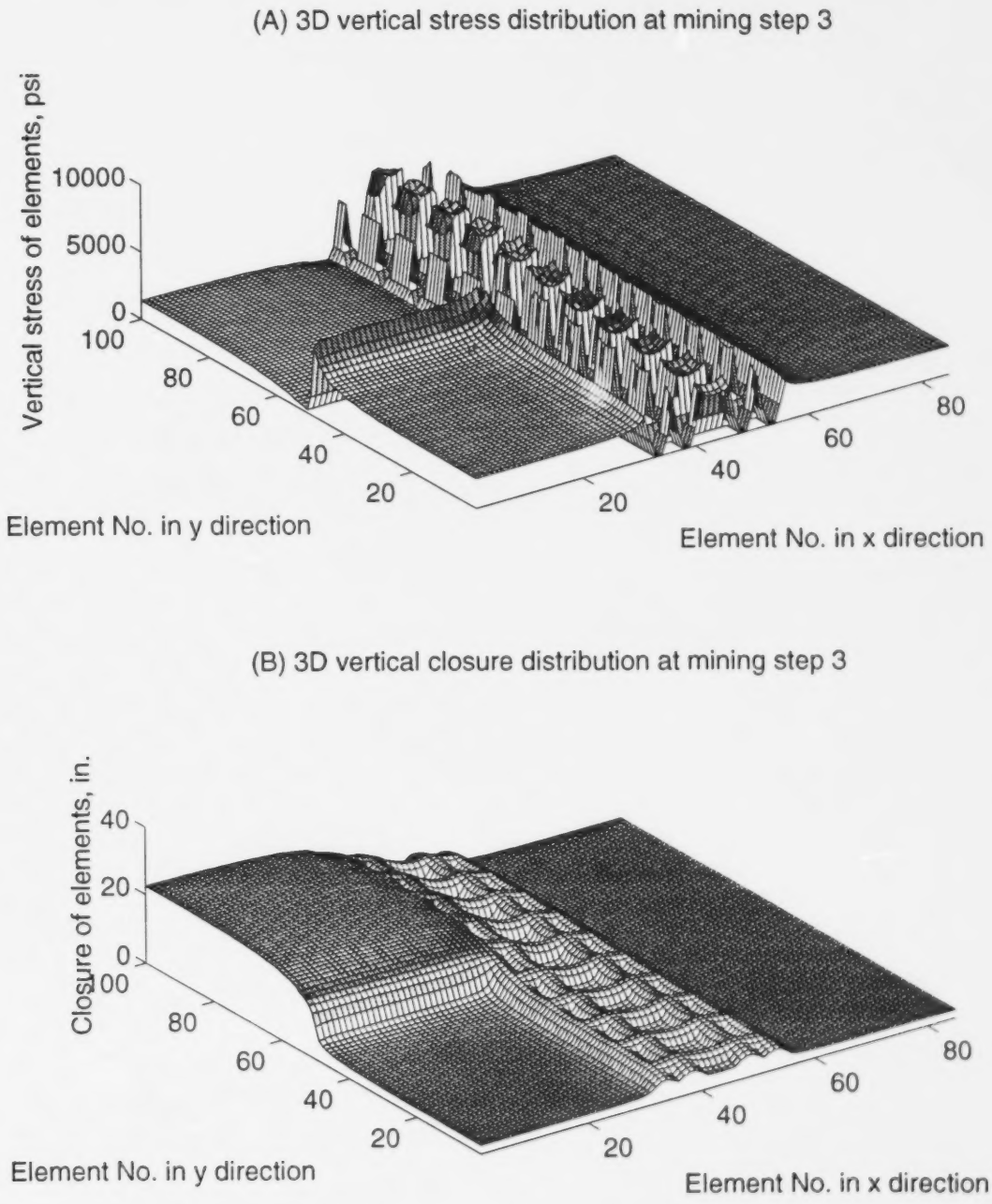

Figure F.2

Vertical stress and closure at mining step 3 for development 7

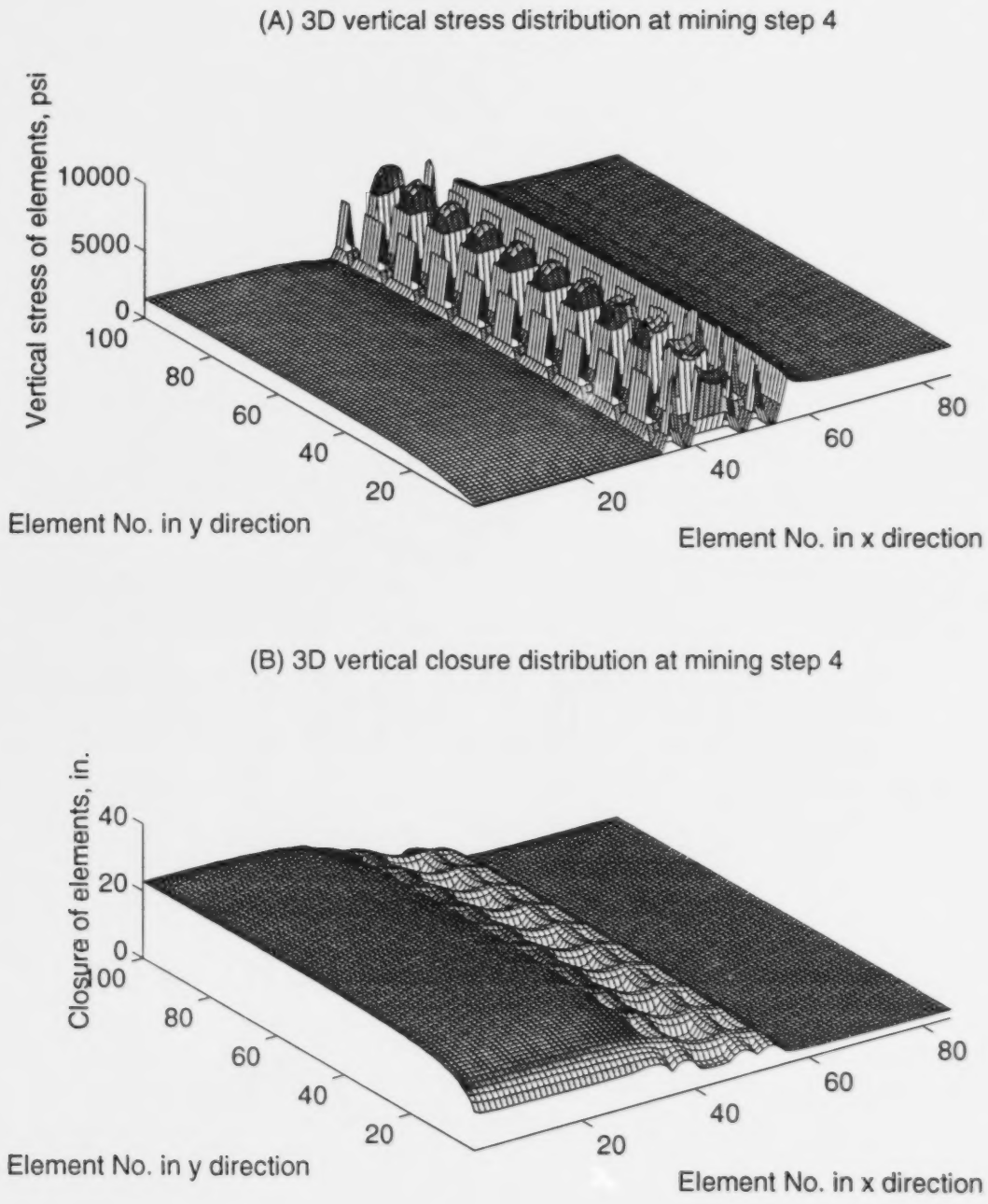

Figure F.3

Vertical stress and closure at mining step 4 for development 7

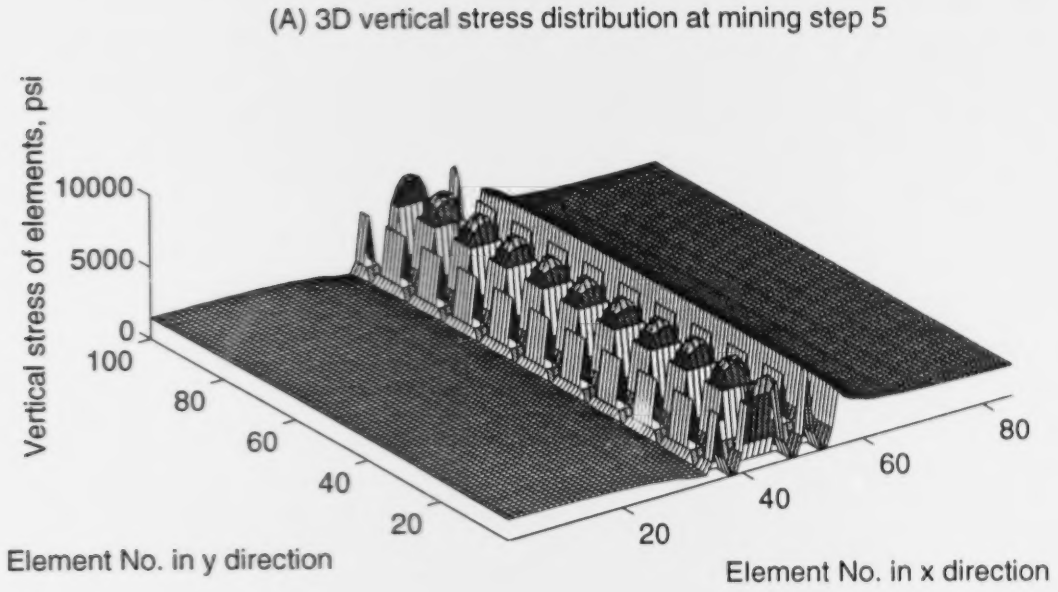

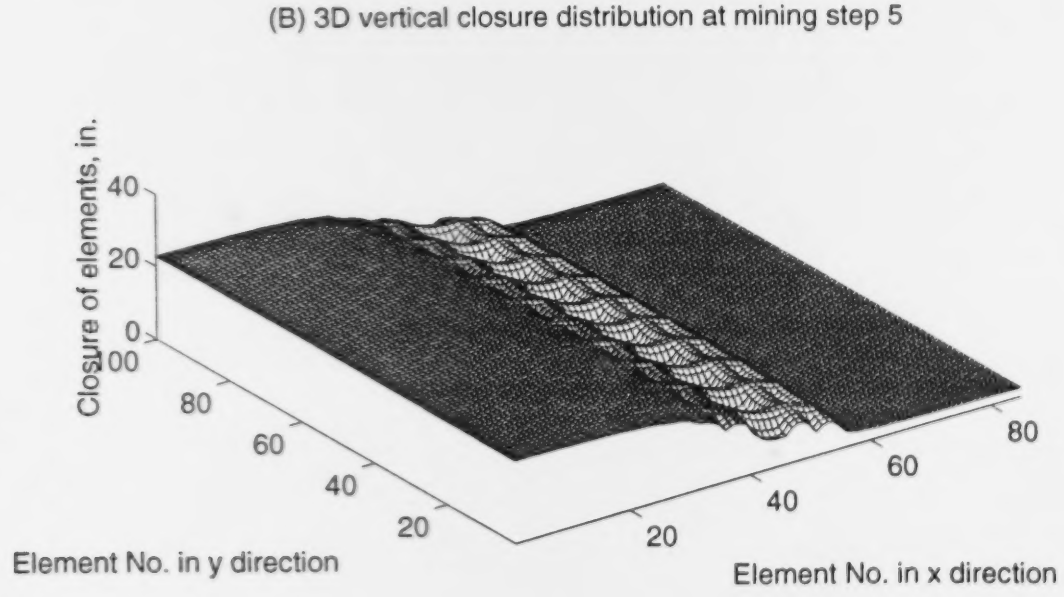

Figure F.4

Vertical stress and closure at mining step 5 for development 7

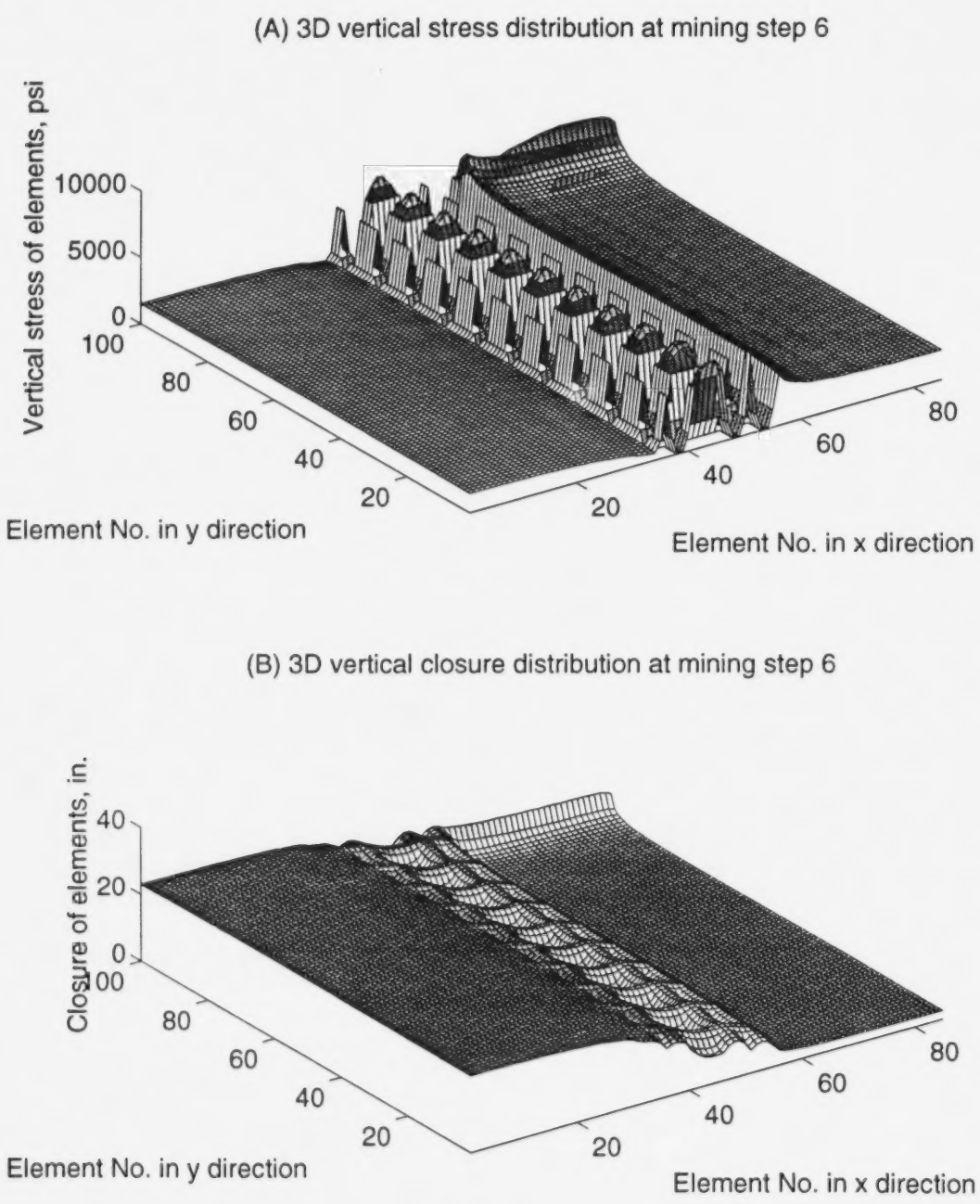

Figure F.5

Vertical stress and closure at mining step 6 for development 7

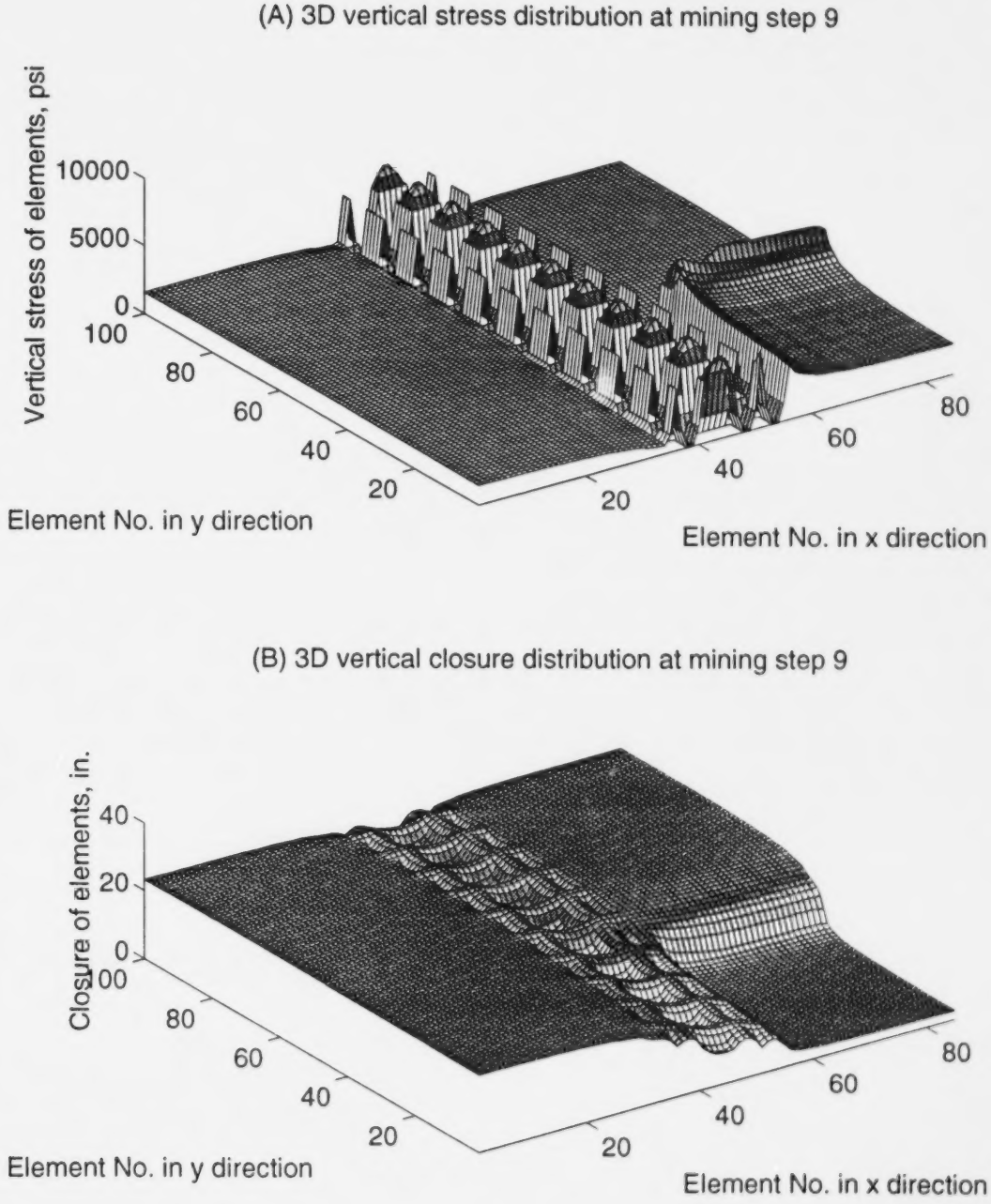

Figure F.6

Vertical stress and closure at mining step 9 for development 7

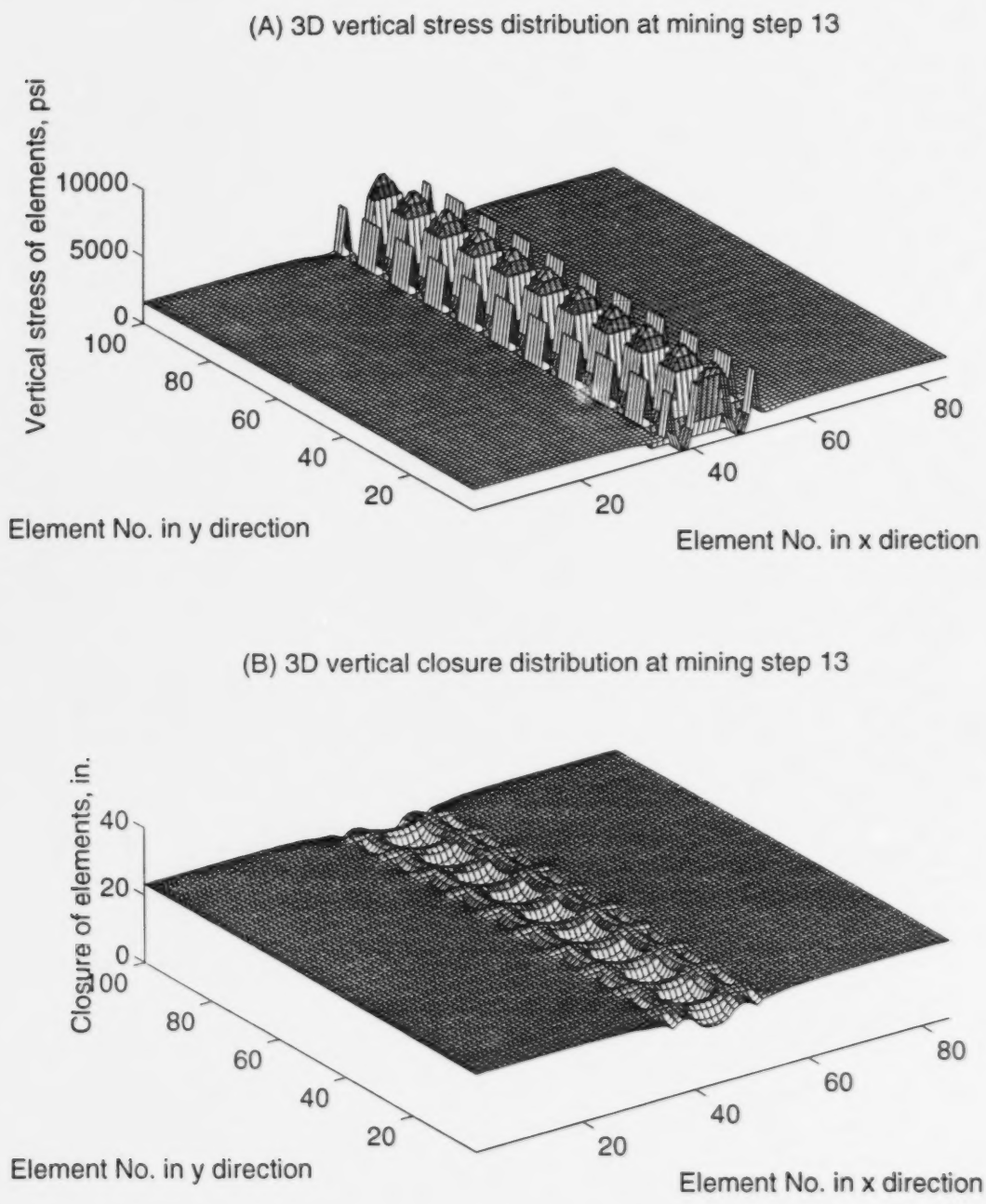

Figure F.7

Vertical stress and closure at mining step 13 for development 7

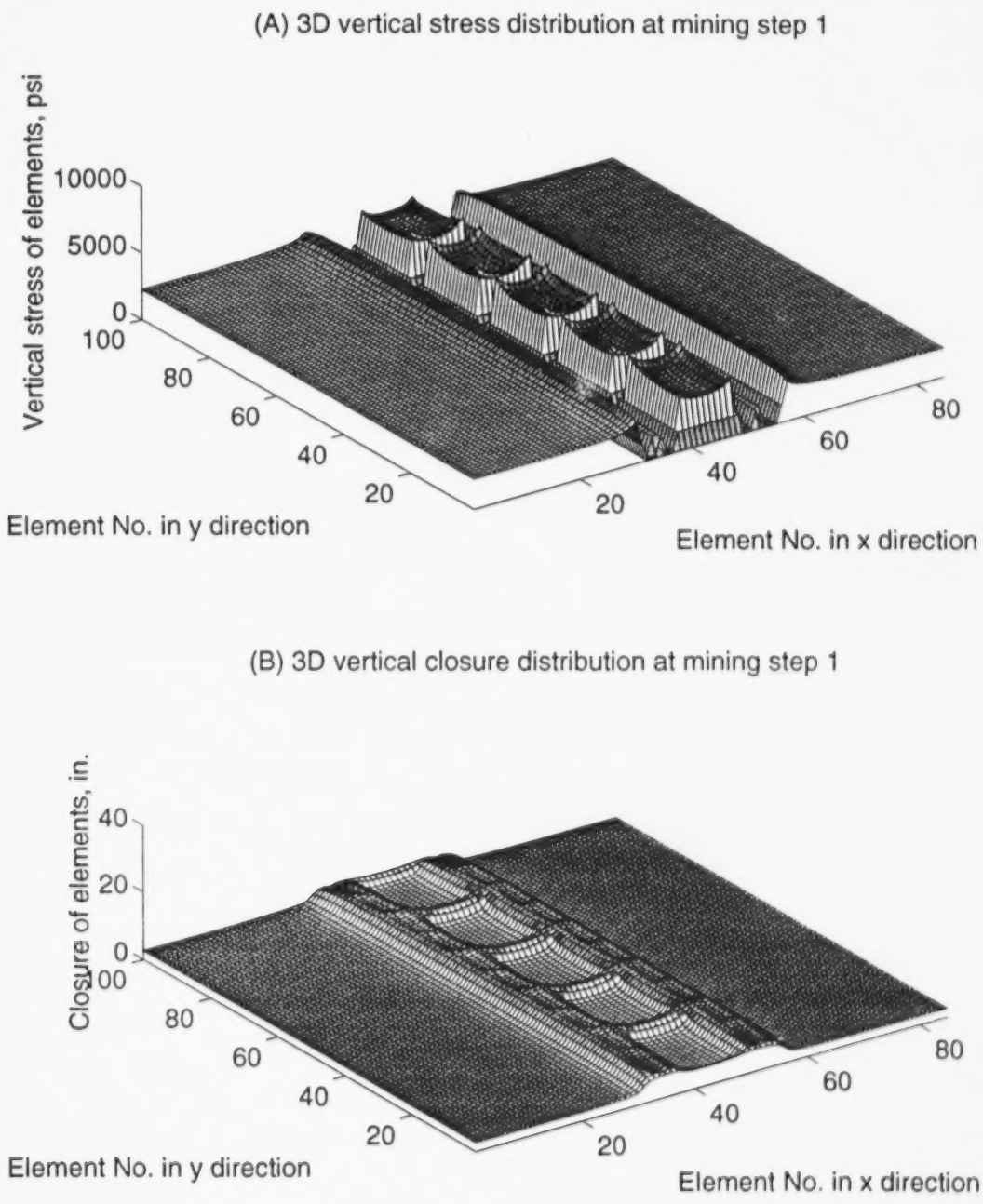

Figure F.8

Vertical stress and closure at mining step 1 for development 8

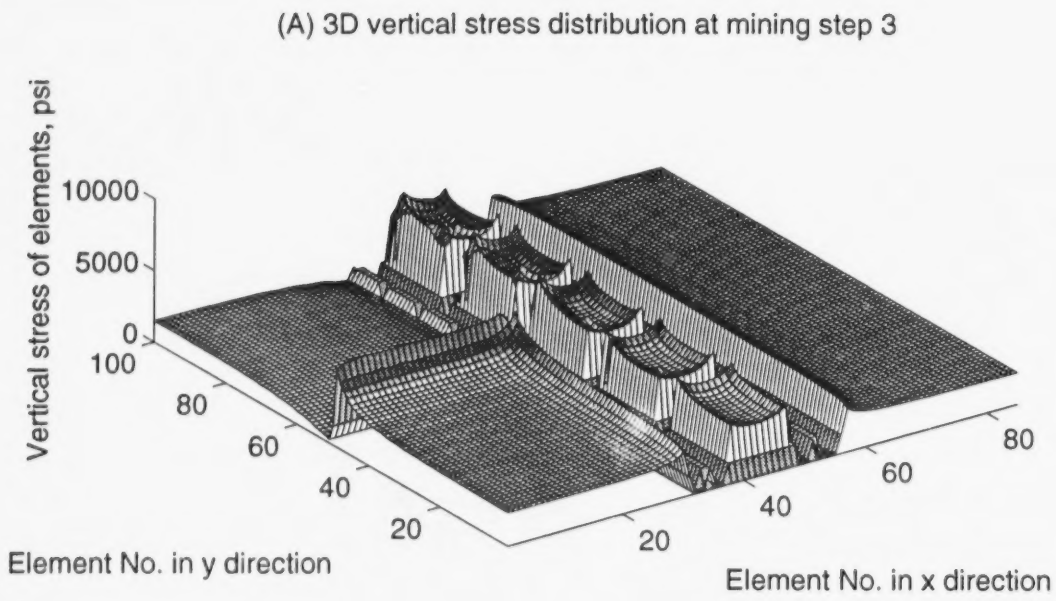

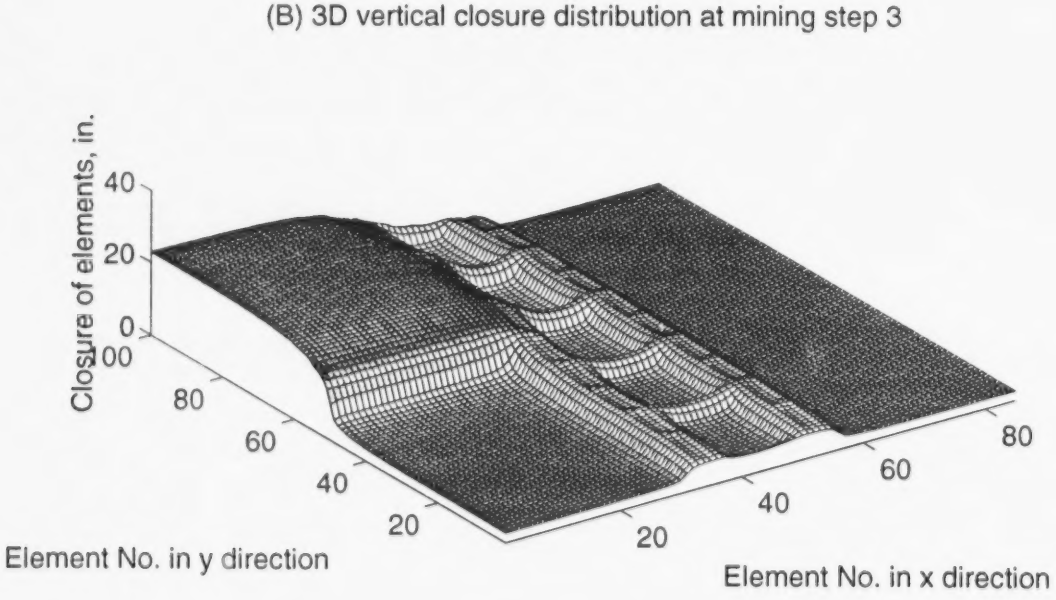

Figure F.9

Vertical stress and closure at mining step 3 for development 8

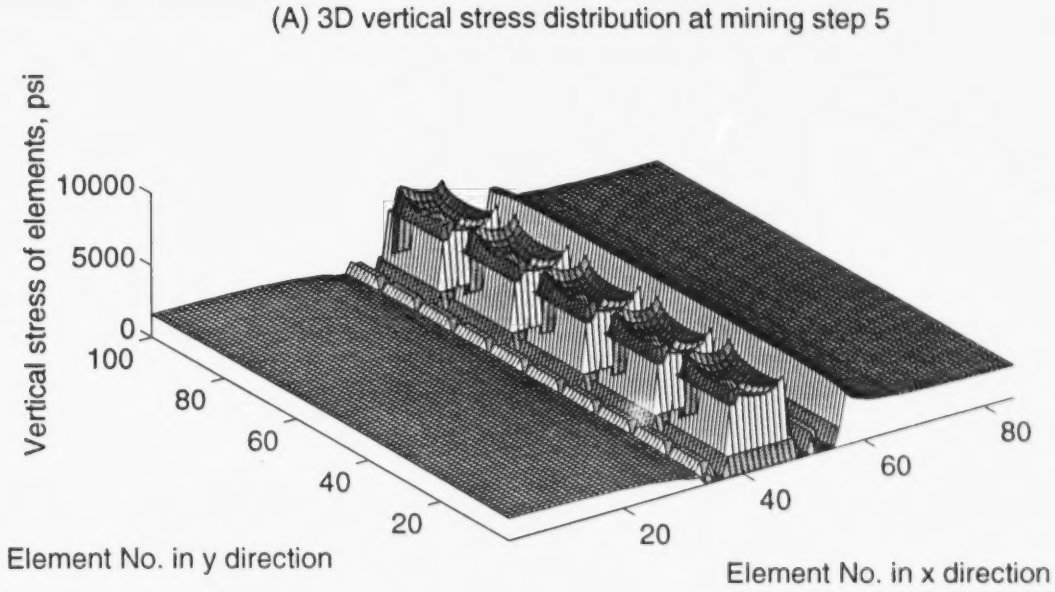

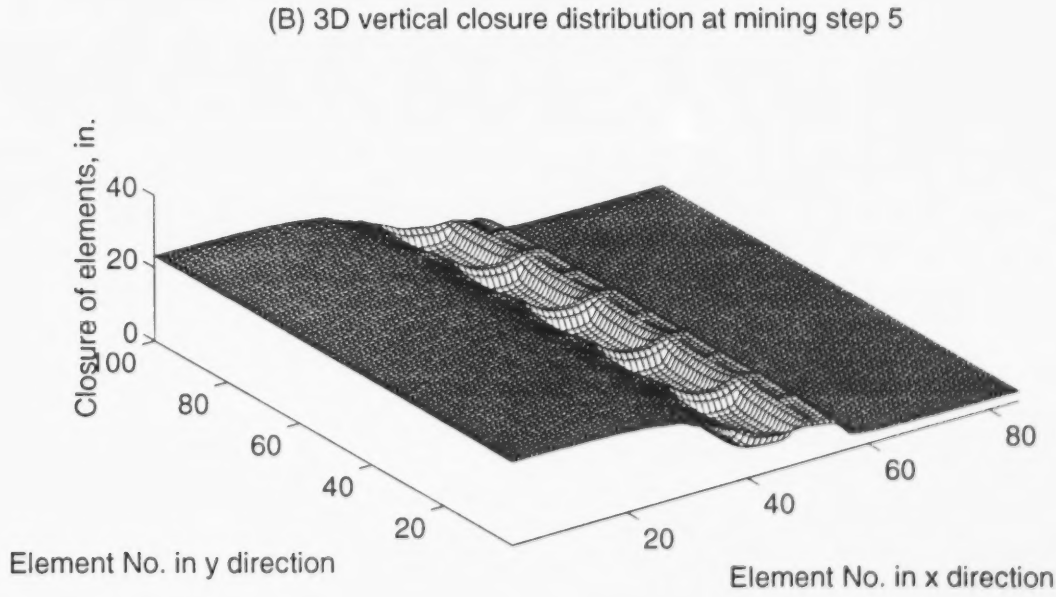

Figure F.10

Vertical stress and closure at mining step 5 for development 8

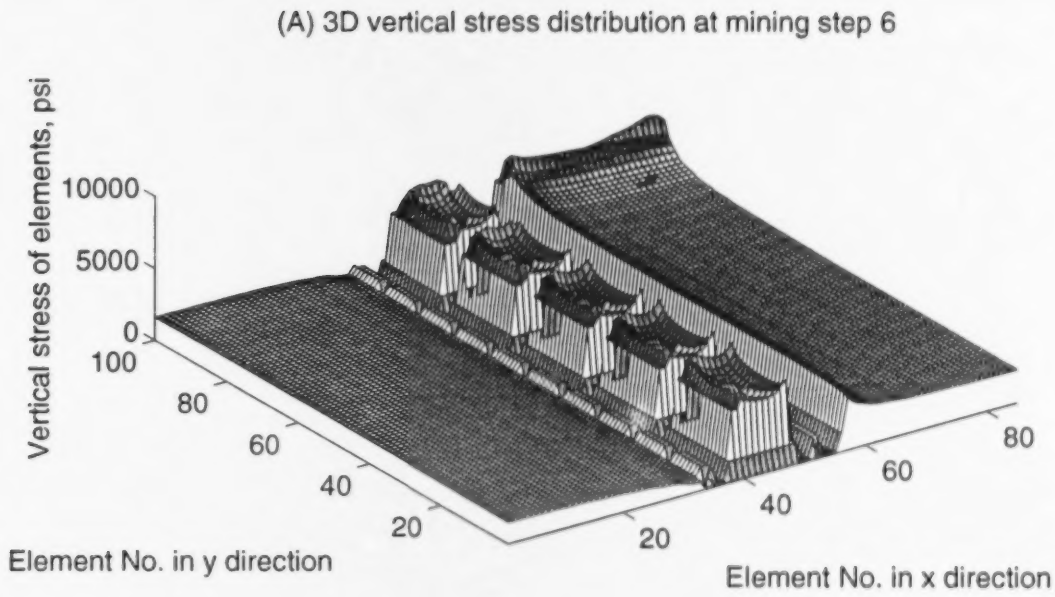

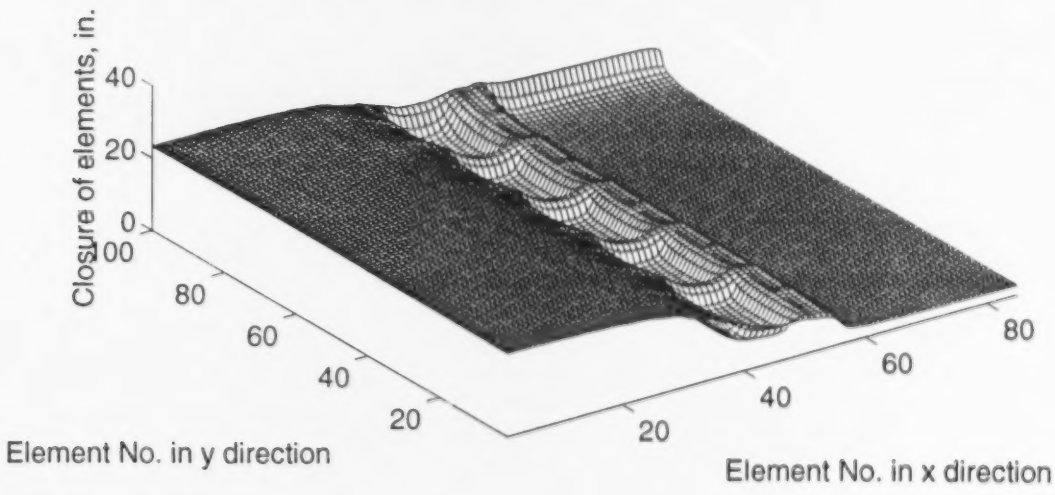

Figure F.11

Vertical stress and closure at mining step 6 for development 8

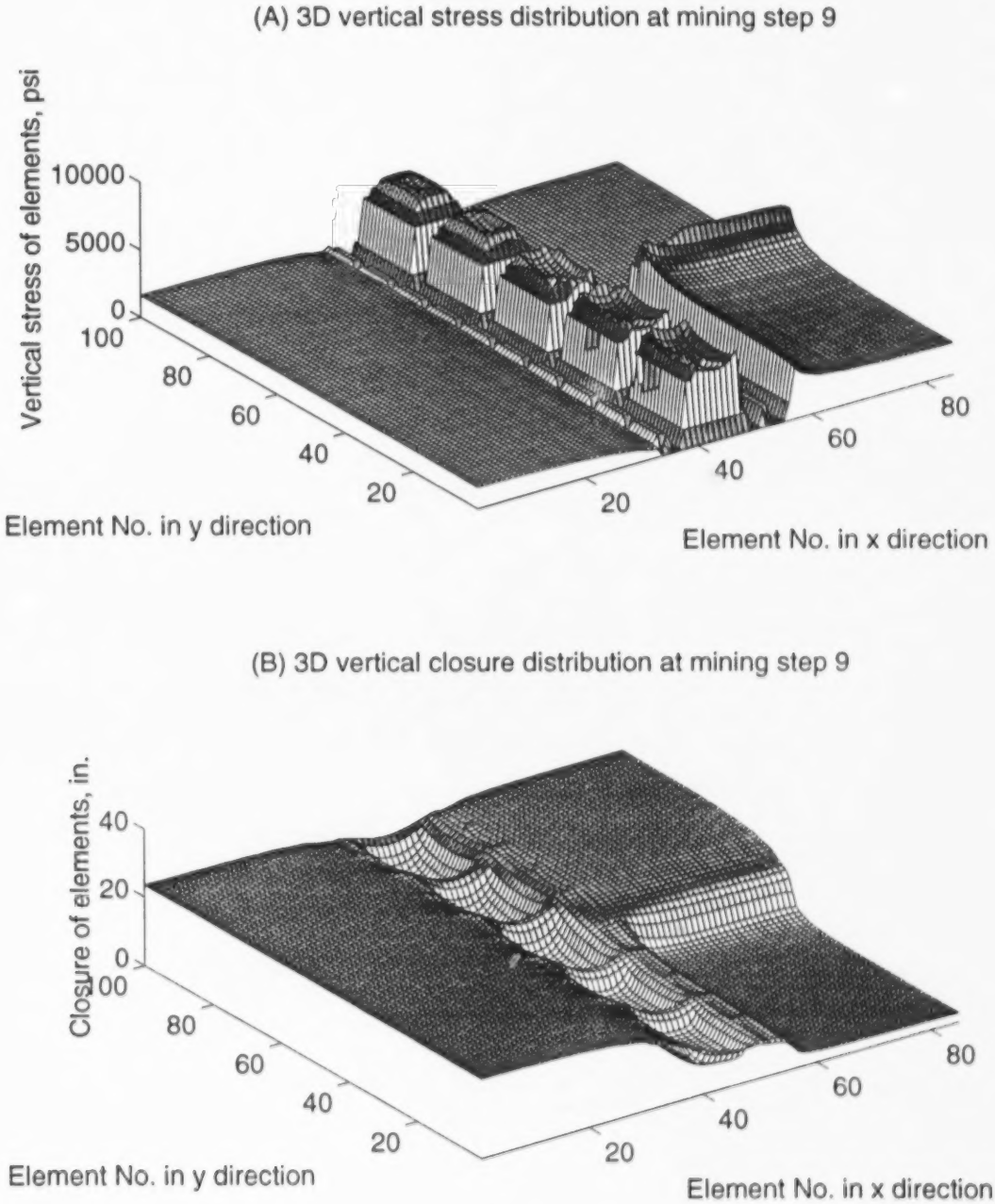

Figure F.12

Vertical stress and closure at mining step 9 for development 8

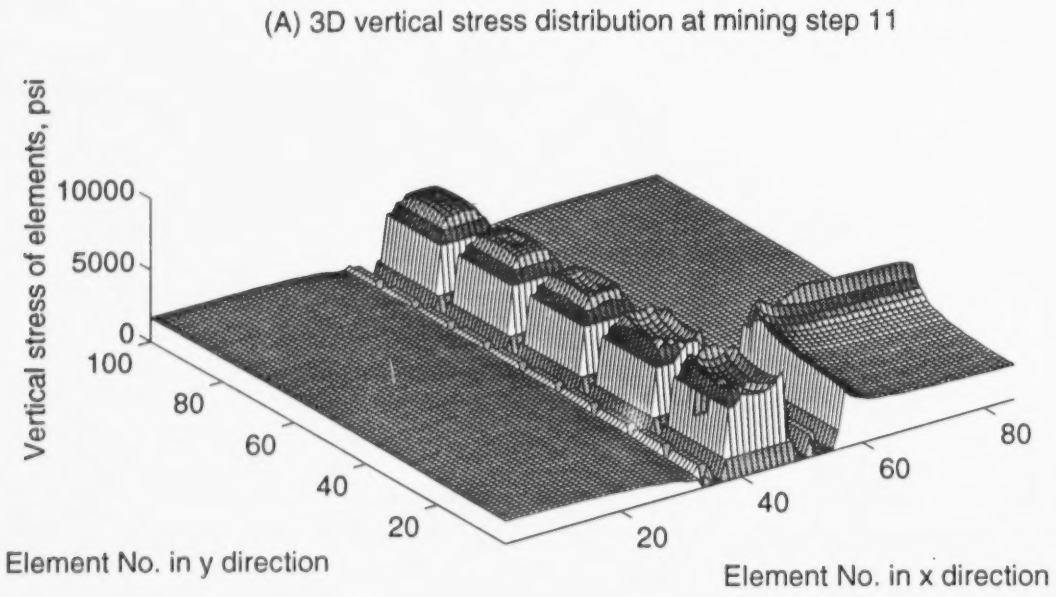

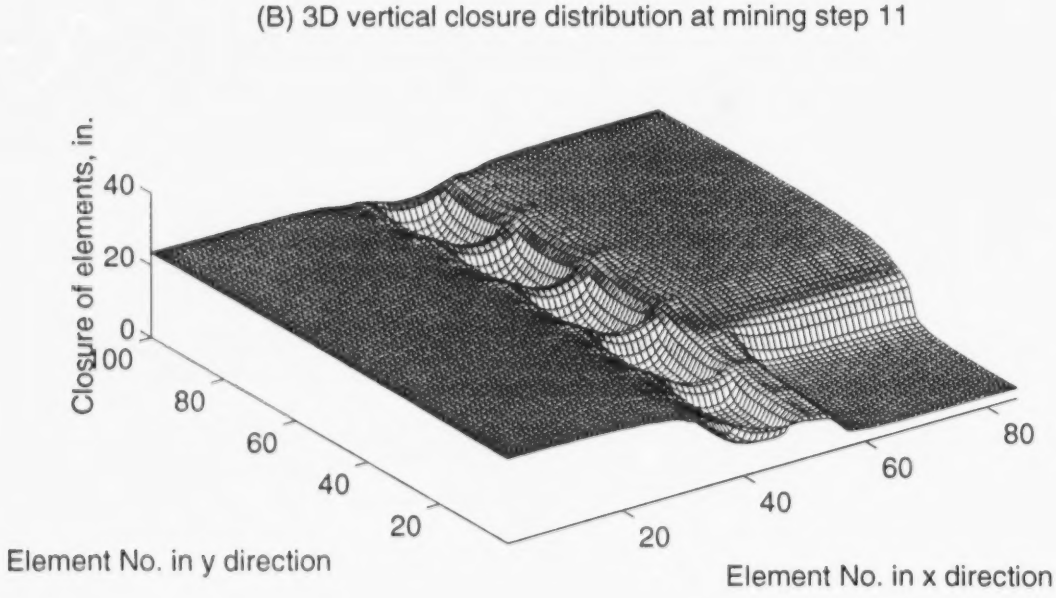

Figure F.13

Vertical stress and closure at mining step 11 for development 8

(A) 3D vertical stress distribution at mining step 12

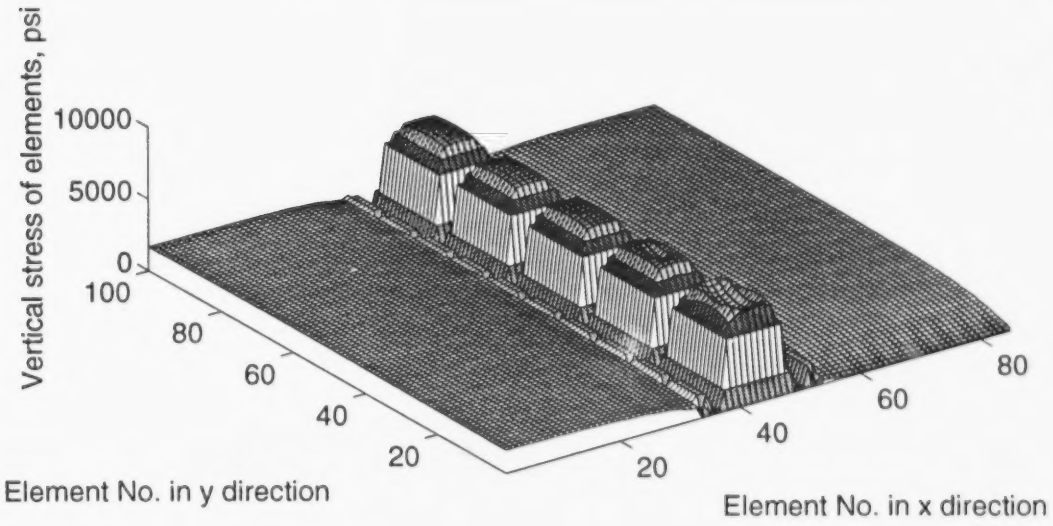

(B) 3D vertical closure distribution at mining step 12

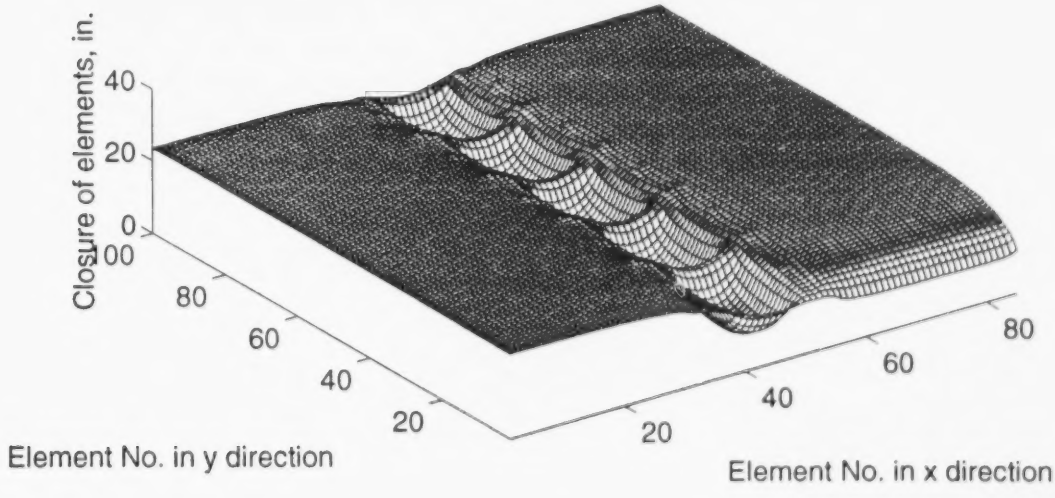

Figure F.14

Vertical stress and closure at mining step 12 for development 8

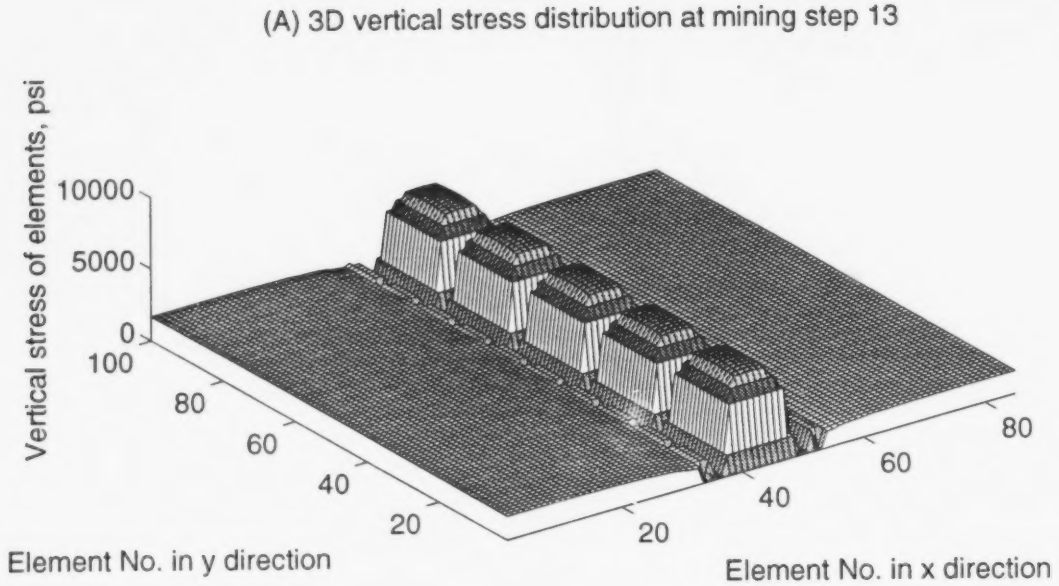

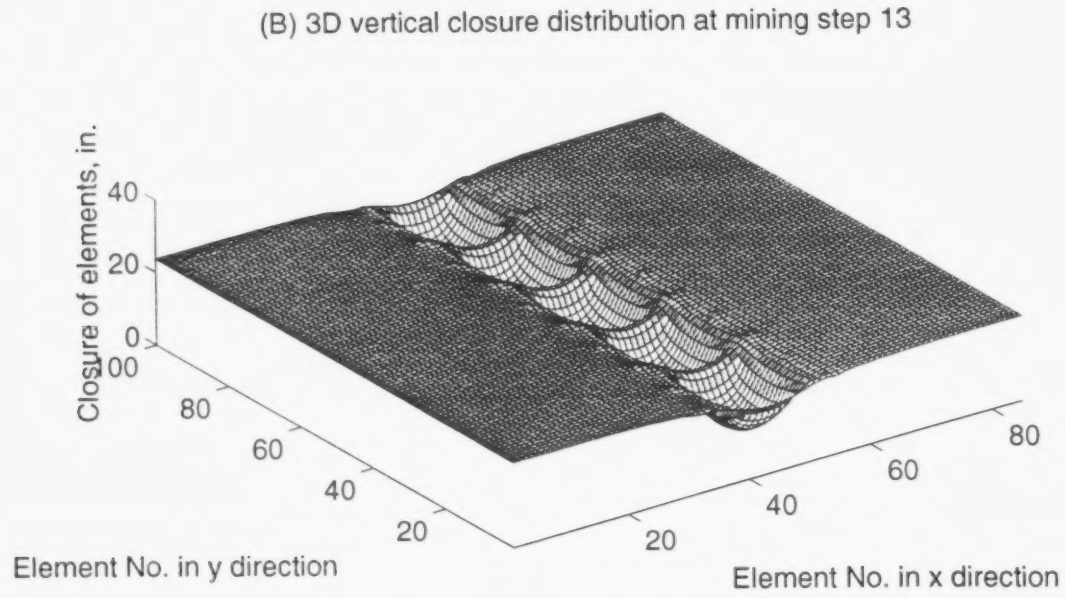

Figure F.15

Vertical stress and closure at mining step 13 for development 8